

Alma Mater Studiorum – Università di Bologna

DOTTORATO DI RICERCA IN

SCIENZE CHIMICHE

Ciclo XXVII

Settore Concorsuale di afferenza: 03/A2

Settore Scientifico Disciplinare: CHIM/02

*Contribution of Non-Covalent Interactions and
Electronic Effects on the Conformational
Landscape and Tautomeric Equilibria of
Molecules and Molecular Complexes:
Structural and Dynamical Data from Rotational
Spectroscopy*

Presentata da:

Camilla Calabrese

Coordinatore Dottorato:
Prof. Aldo Roda

Supervisore:
Prof. Sonia Melandri

Cosupervisore:
Dott. Assimo Maris

Esame finale anno 2015

PREFACE

“[...] Thus it becomes obvious that one must be wary in attributing scientific discovery wholly to anyone person. Almost every discovery has a long and precarious history. Someone finds a bit here, another a bit there. A third step succeeds later and thus onward till a genius pieces the bits together and makes the decisive contribution. Science, like the Mississippi, begins in a tiny rivulet in the distant forest. Gradually other streams swell its volume. And the roaring river that bursts the dikes is formed from countless sources. I cannot deal with this aspect exhaustively, but I may in passing say this: over a period of one or two hundred years the contributions of professional schools to their respective activities will probably be found to lie, not so much in the training of men who may to-morrow become practical engineers or practical lawyers or practical doctors, but rather in the fact that even in the pursuit of strictly practical aims an enormous amount of apparently useless activity goes on. Out of this useless activity there come discoveries which may well prove of infinitely more importance to the human mind and to the human spirit than the accomplishment of the useful ends for which the schools were founded. The considerations upon which I have touched emphasize-if emphasis were needed-the overwhelming importance of spiritual and intellectual freedom. I have spoken of experimental science; I have spoken of mathematics; but what I say is equally true of music and art and of every other expression of the untrammelled human spirit. The mere fact that they bring satisfaction to an individual soul bent upon its own purification and elevation is all the justification that they need. And in justifying these without any reference whatsoever, implied or actual, to usefulness we justify colleges, universities, and institutes of research. An institution which sets free successive generations of human souls is amply justified whether or not this graduate or that makes a so-called useful contribution to human knowledge. A poem, a symphony, a painting, a mathematical truth, a new scientific fact, all bear in themselves all the justification that universities, colleges, and institutes of research need or require.[...]”

Now and then a thoughtless individual in one of the few democracies left in this world will even question the fundamental importance of absolutely untrammelled academic freedom. The real enemy of the human race is not the fearless and irresponsible thinker, be he right or wrong. The real enemy is the man who tries to mold the human spirit so that it will not dare to spread its wings[...].

[...] This is not a new idea. It was the idea which animated von Humboldt when, in the hour of Germany's conquest by Napoleon, he conceived and founded the University of Berlin. It is the idea which animated President Gilman in the founding of the Johns Hopkins University, after which every university in this country has sought in greater or less degree to remake itself. It is the idea to which every individual who values his immortal soul will be true whatever the personal consequences to himself. Justification of spiritual freedom goes,

however, much farther than originality whether in the realm of science or humanism, for it implies tolerance throughout the range of human dissimilarities.[...]”

Abraham Flexner, *The Usefulness of Useless Knowledge*
in “Harper’s Magazine”, October 1939, pp544-552.

The essay of Abraham Flexner is a wonderful text on the relevance of curiosity-driven basic research. For this reason I would like to open my PhD thesis reporting a part of it, suggesting to the reader to deepen his knowledge. Flexner goes through historic examples in which progress came out from scientists not looking for applications but willing to understand nature, which resulted in unforeseen breakthroughs that changed our lives. This is only an input in order to approach my investigations from a different point of view, hoping to suggest some reflections on the reader thinking.

Moving to technical considerations on my PhD activity, the use of rotational spectroscopy allows to reveal a wealth of specified information on molecular structure including many details on molecular dynamics. These precise data on the structure of a molecule are fundamental to define its physical-chemical role that is determined by the conformational arrangement achieved through covalent interactions and non bonding interactions occurring within molecules and different types of environments. An understanding of the forces that drive the stabilization of this conformational arrangement is essential to increase the knowledge on chemical and biological processes.

In this dissertation, the fundamental theories, computational methods and spectroscopic techniques used are briefly reviewed firstly. The pulsed-jet Fourier transform microwave spectroscopy and the free-jet absorption millimeter wave one, have been applied to several single molecules and molecular complexes involving water molecule as partner. The obtained results showcase the suitability of the technique for the study of conformational surfaces and intermolecular interactions.

The advances in the fields of electronics and microwave techniques always had a great impact on the instrumental development in rotational spectroscopy. During my research activity, a lot of time was devoted to improve the setup of the free-jet absorption millimeter wave spectrometer used to perform a part of the experiments here reported.

The possibility to make use of two different setups, sometimes even combining their use in a single experiment, allows to obtain detailed results on the contribution of non-covalent interactions and electronic effects on the conformational landscape of different molecular systems. In particular,

the dissertation starts describing different monomer molecules and follows with the analysis of some molecular 1:1 water adducts.

Regarding monomers, two different molecules are analyzed: anethole and N-methylaminoethanol. These molecular systems are characterized by a high flexibility that affects their conformational landscape and their rotational spectra.

The following chapters examine the changes on the tautomeric equilibria caused by the insertion of a halogen atom in the 2-hydroxypyridine system. In particular the rotational spectra of 6-chloro-2-hydroxypyridine and 5-chloro-2-hydroxypyridine are analyzed with both kind of spectrometers. The use of two rotational spectroscopic setups with different sensitivity and resolution allows a complete investigations of these systems and reveals the influence on the tautomeric equilibrium of halogen substitution in different ring positions.

Pursuing the investigation on the influence of halogenation and microsolvation effects, three different molecular complexes between fluorinated pyridines and a molecule of water are studied. It has been found that, the halogenation of pyridine definitely changes the way in which water links to the partner molecule and if in the monofluorinated pyridines (2-Fluoropyridine and 3-Fluoropyridine) the binding site approached by water moiety remains the nitrogen atom, as in pyridine-water, in the pentafluoropyridine•••water complex the perfluorination effect is clearly observable and the lone pairs of the oxygen atom are directed towards the π -system of the aromatic ring.

The dissertation ends with the study of two other complexes: the cases of benzylamine and acrylic acid complexed with a molecule of water. The study on the benzylamine•••water complex shows that the insertion of a molecule of water alters the conformational preferences of the monomer creating a different conformational arrangement of the complex in which the stabilizing driving force are a delicate balance between intra and intermolecular interactions. Moreover, since the energy differences are very small, the theoretical calculations are not univocal in describing the correct energy sequence of the conformations and only the experimental data can reveal the real conformational landscape.

Regarding the monohydrated acrylic acid system, the rotational spectrum is recorded by the pulsed-jet Fourier transform microwave spectrometer. The structural and dynamical data obtained reveal the complex conformational surface that characterizes this complex, where the water unit approaches the carboxylic acid in order to form a six-membered ring-type structure.

During my PhD activity, I have also spent four months in the Spectroscopy Group of the University of the Basque Country (EHU/UPV) in Bilbao. During my stay there I were able to

PREFACE

record the rotational spectra of two compounds (6-chloro-2-hydroxypyridine and 5-chloro-2-hydroxypyridine) with a higher sensibility and resolution compared to the previous analysis already done in Bologna. More details are described in the related chapters.

Other works have been performed during these three years of PhD activity and they have been already published in international scientific journals of general interests. The details are available in the published papers list at page 243.

TABLE OF CONTENTS

Preface	I-IV
Chapter 1 - Theory of Rotational Spectroscopy	1-14
1.1 Introduction.....	1
1.2 Rigid Rotor Hamiltonian: from Classical to Quantum Mechanical	
Description.....	1
1.3 The Asymmetric-Top Rotor.....	4
1.4 Centrifugal Distortion.....	6
1.5 Quadrupole Coupling Effect.....	7
1.6 Large Amplitude Motions.....	8
1.6.1 Double Minimum Potential.....	9
1.6.2 Internal Rotation.....	9
1.7 Dissociation Energy.....	11
1.8 Evaluation of Molecular Structure.....	11
1.9 References.....	14
Chapter 2 - Computational Methods	15-19
2.1 Theoretical Calculation.....	15
2.2 Computational Programs.....	16
2.3 References.....	18
Chapter 3 - Spectroscopic Techniques	20-33
3.1 Introduction.....	20
3.2 Supersonic Jet Expansion.....	21
3.3 Pulsed-Jet Fourier Transform Microwave Spectrometer.....	23
3.3.1 Resonator Cavity.....	25
3.3.2 Time Domain Technique.....	25

TABLE OF CONTENTS

3.3.3 Pulsed Supersonic Jet Expansion.....	26
3.3.4 Experimental Cycle.....	27
3.4 Free-Jet Absorption MilliMeter Wave Spectrometer.....	28
3.4.1 Absorption Millimeter Wave Line.....	29
3.4.2 Stark Modulation and Detection.....	29
3.4.3 Supersonic Jet Expansion.....	30
3.5 References.....	33
Chapter 4 - Anethole.....	34-49
4.1 Introduction.....	34
4.2 Theoretical Calculations.....	35
4.3 Experimental Results and Analysis.....	37
4.4 Conclusions.....	42
4.5 References.....	43
4.6 Appendix.....	45
Chapter 5 - N-Methylaminoethanol.....	50-76
5.1 Introduction.....	50
5.2 Conformational Overview and Theoretical Calculations.....	52
5.3 Experimental Results and Analysis.....	57
5.4 Conclusions.....	64
5.5 References.....	66
5.6 Appendix.....	67
Chapter 6 - 6-Chloro-2-Hydroxypyridine.....	77-108
6.1 Introduction.....	77
6.2 Theoretical Calculations.....	78
6.3 Experimental Results and Analysis.....	82
6.4 Conclusions.....	88
6.5 References.....	89

TABLE OF CONTENTS

6.6 Appendix.....	91
Chapter 7 - 5-Chloro-2-Hydroxypyridine.....	109-140
7.1 Introduction.....	109
7.2 Theoretical Calculations.....	110
7.3 Experimental Results and Analysis.....	113
7.4 Conclusions.....	119
7.5 References.....	121
7.6 Appendix.....	123
Chapter 8 - 2-Fluoropyridine ··· Water.....	141-164
8.1 Introduction.....	141
8.2 Theoretical Calculations.....	144
8.3 Experimental Results and Analysis.....	147
8.4 Conclusions.....	152
8.5 References.....	154
8.6 Appendix.....	157
Chapter 9 - 3-Fluoropyridine ··· Water.....	165-185
9.1 Introduction.....	165
9.2 Theoretical Calculations.....	166
9.3 Experimental Results and Analysis.....	168
9.4 Dissociation Energy.....	173
9.5 Conclusions.....	175
9.6 References.....	176
9.7 Appendix.....	177
Chapter 10 - Pentafluoropyridine ··· Water.....	186-206
10.1 Introduction.....	186
10.2 Theoretical Calculations.....	187

TABLE OF CONTENTS

10.3	<i>Experimental Results and Analysis</i>	1
10.4	<i>Conclusions</i>	1
10.5	<i>References</i>	1
10.6	<i>Appendix</i>	1
Chapter 11 - Benzylamine ∙∙ Water		207-220
11.1	<i>Introduction</i>	207
11.2	<i>Theoretical Calculations</i>	209
11.3	<i>Experimental Results and Analysis</i>	214
11.4	<i>Conclusions</i>	217
11.5	<i>References</i>	218
11.6	<i>Appendix</i>	219
Chapter 12 - Acrylic acid ∙∙ Water		221-241
12.1	<i>Introduction</i>	221
12.2	<i>Theoretical Calculations</i>	222
12.3	<i>Experimental Results and Analysis</i>	224
12.4	<i>Dissociation Energy</i>	237
12.5	<i>Conclusions</i>	237
12.6	<i>References</i>	239
12.7	<i>Appendix</i>	240
Conclusion		242
Publications		243
Academic Congresses		244
Acknowledgements		245

THEORY OF ROTATIONAL SPECTROSCOPY

1.1 Introduction

Molecular rotational spectroscopy is one of the most powerful sources of precise determinations of chemical structures and physical properties of molecules, holding a prominent role in the field of high-resolution molecular spectroscopy. Over the past 70 years the theoretical analysis of molecular rotational spectroscopy has developed and a thorough description of these theoretical methods can be found in the excellent monograph of Gordy and Cook.^[1] Noteworthy are also the older monographs of Townes and Schawlow^[2] and Kroto^[3] which are valuable sources of information on the early stages of the theoretical and experimental development of microwave (MW) spectroscopy. Moreover the power of this spectroscopic technique is increased even further with the most recent and innovative applications on MW spectroscopy, which are available in some book chapters^[4] and reviews.^[5-7]

In this dissertation, only the key aspects of the theory that are essential for dealing with acquired experimental data are presented.

1.2 Rigid Rotor Hamiltonian: from Classical to Quantum Mechanical Description

In order to describe the rotational spectrum of a molecule, the aid of quantum mechanics is necessary to formulate a mathematical model from which solutions for the quantized energy levels may be obtained. The classical mechanics of a rotating rigid system of particles provides a good starting point for a detailed description of the rotating molecule. In the first approximation the molecule can be regarded as a set of atoms, each of which is taken to be a point mass m_i at coordinates x_i, y_i, z_i . When relative values of these coordinates are fixed, then the rotation of the molecule in space can be described by a rigid rotor Hamiltonian. In classical mechanics the angular momentum of a rigid system of particles is:

$$\mathbf{P} = \mathbf{I} \cdot \boldsymbol{\omega} \quad (1)$$

and the kinetic energy E_r of the rigid-rotor is given by:

$$E_r = \frac{1}{2} \boldsymbol{\omega} \cdot \mathbf{I} \cdot \boldsymbol{\omega} \quad (2)$$

where $\boldsymbol{\omega}$ is the angular velocity vector of the rotating body and \mathbf{I} is the moment of inertia tensor.

The diagonal elements of the moment of inertia tensor in x, y, z axes are given by:

$$I_{\alpha\alpha} = \sum_i m_i (\beta_i^2 + \gamma_i^2) \quad (3)$$

where α, β, γ is a permutation of x, y, z . The off-diagonal elements are:

$$I_{\alpha\beta} = I_{\beta\alpha} = -\sum_i m_i \alpha_i \beta_i \quad (4)$$

where $\alpha \neq \beta$.

The origin of the Cartesian axes system x, y, z is placed at the center of mass of the molecule and the axes are chosen so that all off-diagonal elements of \mathbf{I} vanish. This unique, molecule-fixed axes system is called the principal axes system. The axes are labeled a, b, c and are conventionally chosen to be in the order of increasing values of the principal moments of inertia, such that:

$$I_a \leq I_b \leq I_c \quad (5)$$

The values of the principal moments of inertia and hence those of rotational constants depend only on the molecular geometry (bond lengths and bond angles) and on the atomic masses. The relative values of the elements of the principal moments of inertia allow molecules to be classified into four categories:

1. *Spherical top molecules*, for which all three principal moments of inertia are equal $I_a = I_b = I_c$. Examples of spherical tops are: CH_4 , SF_6 .
2. *Linear molecules*, in which $I_a = 0, I_b = I_c$. Examples of linear tops are: CO_2 , OCS .
3. *Symmetric top molecules*, for which one moment of inertia is unique and two others are equal to each other. If the unique moment is smaller than the other two then the molecule is a prolate symmetric top, $I_a < I_b = I_c$. Examples of prolate symmetric tops are: CH_3D , $\text{CH}_3\text{C}\equiv\text{CH}$. Alternatively, if the unique moment is larger than the other two then the molecule is called an oblate symmetric top, $I_a = I_b < I_c$. Examples of oblate symmetric tops are: NH_3 , benzene.
4. *Asymmetric top molecules*, for which the three moments of inertia are different from each other, $I_a < I_b < I_c$. Examples of asymmetric tops are: H_2O , fluorobenzene. Some molecules, which are strictly asymmetric tops, have two nearly equal moments of inertia. If $I_a < I_b \approx I_c$, then the molecule is a near-prolate asymmetric top, e.g. $\text{CH}_2=\text{CHCN}$, H_2NCN . On the other hand, if $I_a \approx I_b < I_c$ then the molecule is an near-oblate asymmetric top, e.g. pyrazine.

Asymmetric top molecules are by far the most common among molecules studied by rotational spectroscopy.

In the principal axes system the components of angular momentum become:

$$P_x = I_x \omega_x; P_y = I_y \omega_y; P_z = I_z \omega_z \quad (6)$$

where a standard identification between the general principal axes x, y, z and the conventional principal axes a, b, c has been assumed (see page 35 of ref. 3 for a complete table containing all possible identifications).

Rotational kinetic energy in the principal axes system is then:

$$E_r = \frac{1}{2} I_x \omega_x^2 + \frac{1}{2} I_y \omega_y^2 + \frac{1}{2} I_z \omega_z^2 = \frac{1}{2} \left(\frac{P_x^2}{I_x} \right) + \frac{1}{2} \left(\frac{P_y^2}{I_y} \right) + \frac{1}{2} \left(\frac{P_z^2}{I_z} \right) \quad (7)$$

Rotational energy of a molecule is quantized, so the classical angular momentum \mathbf{P} must be replaced by its quantum mechanical equivalent: the angular momentum operator \hat{J} . Rigid rotor Hamiltonian, written in terms of the component angular momentum operators in the principal axes has the form:

$$E_r = \mathcal{H}_{rig} = A \hat{J}_a^2 + B \hat{J}_b^2 + C \hat{J}_c^2 \quad (8)$$

where A, B, C are rotational constants defined by:

$$A = \frac{h}{8\pi^2 I_a}; B = \frac{h}{8\pi^2 I_b}; C = \frac{h}{8\pi^2 I_c} \quad (9)$$

and the operators for momentum about the specific principal axes are related to the total angular momentum of the system by $\hat{J}^2 = \hat{J}_x^2 + \hat{J}_y^2 + \hat{J}_z^2$.

The solution for the energy levels in a quantum mechanical system is obtained from the Schrödinger equation of the rigid rotor:

$$\mathcal{H}_{rig} \psi = E_{rot} \psi \quad (10)$$

where \mathcal{H}_{rig} is the Hamiltonian operator of the rigid rotor system (8), ψ is the wave function describing the system and E_{rot} is the rotational energy. Certain commutation relationships arising from the Heisenberg uncertainty principle between components of angular momentum $\hat{J}_g, g = x, y, z$, suggest that any two components of angular momentum cannot be measured simultaneously. However, by finding the operator for \hat{J}^2 it can be shown that the square of the total angular momentum commutes with components of angular momentum in a molecule-fixed system $\hat{J}_g, g = x, y, z$, and in a space-fixed system $\hat{J}_G, g = X, Y, Z$. This means that there exist simultaneous eigenstates of these three operators defined by independent quantum numbers J, K , and M . The

quantum numbers J , K , M are used to describe wave functions for \hat{J}^2 , \hat{J}_z , and \hat{J}_z , respectively. The matrix elements of these operators are:

$$\langle J, K, M | \hat{J}^2 | J, K, M \rangle = J(J + 1)\hbar^2, \quad (11)$$

$$\langle J, K, M | \hat{J}_z^2 | J, K, M \rangle = K^2\hbar^2, \quad (12)$$

$$\langle J, K, M | \hat{J}_z | J, K, M \rangle = M\hbar. \quad (13)$$

The quantum number J is proportional to the total rotational angular momentum of the molecule. It is called the principal rotational quantum number, and takes on positive integral values $0, 1, 2, \dots$. The quantum number K is associated with angular momentum projection \hat{J}_z along a molecule fixed axis with values $K = -J, -J + 1, \dots, 0, J - 1, J$. In the presence of an external magnetic or electric field the quantum number M describes the component of the total angular momentum along the space-fixed axis Z , with values $M = -J, -J + 1, \dots, 0, J - 1, J$.

The selection rules for allowed transitions between rotational energy levels depend on the type of rotor. For linear and symmetric tops, rotational transitions are only allowed for:

$$\Delta J = \pm 1, \Delta K = 0, \Delta M = 0, \pm 1. \quad (14)$$

For a symmetric top, either a prolate or an oblate one, the quantum number K determines the vector component of the angular momentum about the molecular symmetry axis, which is a -axis for a prolate top or c -axis for an oblate top. The sign of K signifies the direction of the rotation about the z -axis. Energies are degenerated for $+K$ and $-K$, since a simple change of direction does not change the total energy.

The intensity of a rotational transition is governed by the matrix elements of the dipole moment (see Chapter 2 of ref. 1), which are non-zero only for non-zero components of the permanent dipole moment of the molecule. As a consequence, *homo*-nuclear diatomic molecules and molecule with spherical symmetry are not directly observable with rotational spectroscopy.

1.3 The Asymmetric-Top Rotor

When none of the three principal moments of inertia of a molecule is zero and if no two are equal the system is classified as an asymmetric top. Most polyatomic molecules belong to this category that presents considerable complexity in its pure rotational spectrum. As a consequence, the methods for energy level determination of the asymmetric top are more complicate than for symmetric and linear tops. For this reason only a brief outline will be carried out in order to give qualitative characteristics of the asymmetric rotor energy levels.

In an asymmetric rotor there is no internal component of the angular momentum that is a constant of the motion. A given rotational level is no longer labelled only by the J and K quantum numbers as in symmetric tops but involves using a second K quantum number. According to the King-Hainer-Cross notation, a rotational level of asymmetric top is denoted by J_{K_a, K_c} , where K_a and K_c indicate K values at the prolate and oblate symmetric limits respectively, to which the level correlates. Remembering the conventional order, $I_a < I_b < I_c$, then when $I_b \rightarrow I_c$, the prolate symmetric top is approached; and when $I_b \rightarrow I_a$, the oblate symmetric top is approached.

The degree of asymmetry in an asymmetric top is given by the value of Ray's parameter:

$$\kappa = \frac{2B-A-C}{A-C} \quad (15)$$

with A, B, C , the rotational constants with respect to the a, b, c axes. The limiting values for κ , -1 and $+1$, correspond to the prolate and oblate symmetric tops, respectively. The most asymmetric top has $\kappa = 0$. The energy levels of asymmetric rotors ($\kappa \approx -1$ or $\kappa \approx +1$) differ from the limiting symmetric-top ones essentially in that the levels corresponding to $-K$ and $+K$, which are always degenerate in the symmetric rotor, are separated in the asymmetric rotor.

Selection rules for asymmetric rotor transitions with respect to J are $\Delta J = 0, \pm 1$. In the absence of external fields each rotational level is M -fold degenerate, where $M = 2J + 1$.

The condition $\Delta J = 0$ gives rise to Q -branch, $\Delta J = -1$ to P -branch and $\Delta J = +1$ to R -branch transitions. Asymmetric rotors can have three nonzero components of the dipole moment μ_a, μ_b, μ_c giving rise to three types of transitions, called a -, b -, c -type respectively, governed by different ΔK_a and ΔK_c rules, as indicated in the table below.

Table 1.1. - Selection rules for the pseudo-quantum numbers (K_a, K_c) of the asymmetric rotor. Note that larger variations in the indices (in parentheses) produce weak transitions.

Transition type	ΔK_a	ΔK_c
a	$0 (\pm 2, \pm 4)$	$\pm 1 (\pm 3, \pm 5)$
b	$\pm 1 (\pm 3, \dots)$	$\pm 1 (\pm 3, \dots)$
c	$\pm 1 (\pm 3, \dots)$	$0 (\pm 2, \pm 4)$

1.4 Centrifugal Distortion

It's very useful to take molecules as rigid rotors when interpreting the rotational spectra. However, the atomic structure cannot be absolutely rigid. In reality, the nuclei are held together by finite restoring forces. Thus, bond distances and angles will change because of the centrifugal force produced by rotation, which gives rise to a centrifugal distortion. The effects are usually large for light molecules because of the small moments of inertia. Taking into account this distortion, the moments of inertia cannot longer be considered constant and independent of the rotational state. Consequently, the rotational spectrum cannot be just treated as that of a rigid rotor characterized by a sequence of equilibrium moments of inertia, because this centrifugal distortion effect is visible in every rotational spectrum as deviations of rotational line positions from those predicted by the rigid rotor model. The precision of microwave measurements allows determining the centrifugal distortion constants even from the low-lying levels with relatively small rotational energies.

Although we must consider the influence of centrifugal distortion in order to accurately account for the positions of rotational transitions, its effects still represent only a small fraction of the rotational energy which is accounted for mainly by the rigid rotor term. Therefore in many cases this effect can be treated as a perturbation to the rigid rotor Hamiltonian (\mathcal{H}_{rig}).

The theory of the centrifugal distortion was initiated by Wilson,^[8] introducing a series of centrifugal distortion coefficients ($\tau_{\alpha\beta\gamma\delta}$) relating the molecular distortions and force constants. Kivelson and Wilson applied first-order perturbation theory, expressing the Hamiltonian for the semi-rigid rotor as:

$$\mathcal{H} = \mathcal{H}_{rig} + \mathcal{H}_d \quad (16)$$

$$\mathcal{H}_{rig} = A\hat{J}_a^2 + B\hat{J}_b^2 + C\hat{J}_c^2 \quad (17)$$

$$\mathcal{H}_d = \frac{\hbar^4}{4} \sum_{\alpha\beta\gamma\delta} \tau_{\alpha\beta\gamma\delta} \hat{J}_\alpha \hat{J}_\beta \hat{J}_\gamma \hat{J}_\delta \quad (18)$$

where \mathcal{H}_d is the contribution of the centrifugal distortion part. In the expression (18) many of the distortion constants are equivalent and there are only nine different τ coefficients, which can be later reduced to six using the commuting properties of the angular momentum operators. However, only five combinations can be finally determined experimentally. This is the reason to introduce reduced Hamiltonians, which are derived by a succession of contact transformations that preserve the original eigenvalues. Different reductions are possible. One of the most common is the Watson^[9] asymmetric (A) reduction, which, including only quartic terms, is expressed as:

$$\mathcal{H}_{Watson}^{(A)} = \mathcal{H}_{rig}^{(A)} + \mathcal{H}_d^{(A)} \quad (19)$$

$$\mathcal{H}_{rig}^{(A)} = A^{(A)}\hat{J}_a^2 + B^{(A)}\hat{J}_b^2 + C^{(A)}\hat{J}_c^2 \quad (20)$$

$$\mathcal{H}_d^{(A)} = -\Delta_J \hat{J}^4 - \Delta_{JK} \hat{J}^2 \hat{J}_z^2 - \Delta_K \hat{J}_z^4 - 2\delta_J \hat{J}^2 \hat{J}_{xy}^2 - \delta_K (\hat{J}_z^2 \hat{J}_{xy}^2 + \hat{J}_{xy}^2 \hat{J}_z^2) \quad (21)$$

where $J^2 = J \cdot J, J_{xy}^2 = J_x^2 - J_y^2$.

The A-reduction includes the following five centrifugal distortion constants: $\Delta_J, \Delta_K, \Delta_{JK}, \delta_J$ and δ_K . This expression was originally intended for asymmetric rotors and is commonly reported for these molecules. However, the problem of this reduction is that for asymmetric rotors close to the prolate or oblate limits, rotational constants and centrifugal distortion constants are highly correlated. Moreover it should be noted that the centrifugal distortion constant δ_K blows up for near prolates rotor because it contains the rotational constants ($B-C$) in the denominator.

For this reason it is convenient to use the alternative symmetric (S) reduction, which is expressed as

$$\mathcal{H}_d^{(S)} = -D_J \hat{J}^4 - D_{JK} \hat{J}^2 \hat{J}_z^2 - D_K \hat{J}_z^4 - d_1 \hat{J}^2 (\hat{J}_+^2 + \hat{J}_-^2) - d_2 (\hat{J}_+^4 + \hat{J}_-^4) \quad (22)$$

where $\hat{J}_\pm = (\hat{J}_x \pm i\hat{J}_y)$ and the centrifugal distortion constants are $D_J, D_K, D_{JK}, d_1, d_2$.

A least square fitting of the observed frequencies is carried out to obtain the rotational and centrifugal distortion constants. Particularly, the differences between the observed frequencies and the calculated rigid rotor frequencies are taken as the distortion effect. Rotational transitions with high J and K improve the values of the higher order constants, because only rotational energy levels with high quantum numbers depend on higher order centrifugal constants.

1.5 Quadrupole Coupling Effect

Nuclear hyperfine structures in rotational spectra arise from interaction between the electric quadrupole moments of the nuclei and the molecular field gradient. When a nucleus has a spin quantum number, I , greater than 1/2, it has a quadrupole moment. In that case, the coupling of the nuclear spin angular momentum (I) with rotational angular momentum (J) causes splitting of the rotational energy levels described by the new total angular momentum quantum number F . The energies of the sub-levels are proportional to the nuclear quadrupole moment and are a function of F and J , where F takes values according to the Clebsch-Gordan series: $F = J + I, J + I - 1, \dots, 0, \dots, |J - I|$.

If the quantum number J of a rotational level is greater than I , then $2I+1$ levels are produced; but if J is less than I , $2J+1$ levels result. The effect is known as hyperfine splitting and arises from the electric interaction between a quadrupolar atomic nucleus and the molecular electric field gradient at the atomic position.^[1] Isotopes with nuclear spins of 0 and 1/2 have no such interaction because the nuclei are spherically symmetric and have no quadrupole moments. These nuclei

include common isotopes in this work such as ^{12}C and ^1H . The isotope ^{14}N however has a nuclear spin of 1 and thus nuclear hyperfine structure is observed for species containing ^{14}N nuclei. In particular the rotational spectra of the molecules with ^{14}N ($I = 1$), see all levels with $J > 0$ split into 3 components.

Thus, the observation of nuclear quadrupole splitting allows the determination of the magnitude of the nuclear quadrupole moment.^[10]

The selection rule for rotational transitions becomes $\Delta J = \pm 1, \Delta F = 0, \pm 1$.^[11]

The actual fitted parameters of the hyperfine structure are the nuclear quadrupole splitting constants χ defined as:

$$\chi_{\alpha\beta} = eq_{\alpha\beta}Q \quad (23)$$

where Q is the nuclear electric quadrupole moment, and e is the value of the elementary charge. The value of Q has been determined from other experiments and for a given nucleus is a constant. In the general case, the nuclear quadrupole splitting constants in the principal inertial axes are a tensor which has the form:

$$\chi = \begin{pmatrix} \chi_{aa} & \chi_{ab} & \chi_{ac} \\ \chi_{ab} & \chi_{bb} & \chi_{bc} \\ \chi_{ac} & \chi_{bc} & \chi_{cc} \end{pmatrix} \quad (24)$$

The diagonal elements of the tensor represent the electric field gradient in the principal axes of the molecule. These diagonal constants are often satisfactorily determinable from only the first-order nuclear quadrupole splitting Hamiltonian. Owing to the Laplace condition, which restricts the potential in a charge free region, nuclear quadrupole splitting constants are in relationship as below:

$$\chi_{aa} + \chi_{bb} + \chi_{cc} = 0. \quad (25)$$

This condition means that there are only two independent diagonal tensor elements, which can be determined from the analysis of the hyperfine structure of the rotational spectrum.

The coupling constants are very sensitive to the electronic environment in the proximities of the quadrupole and to the orientation of the inertial axes. For this reason the nuclear quadrupole coupling constants are a useful tool for the identification of different chemical species.

1.6 Large Amplitude Motions

Rotational spectroscopy is perhaps most closely associated with the studies of the structures of gas phase molecules, including the determination of molecular structures through the analysis of the rotational spectra of isotopologues. However, it has also played an important role in the area of molecular dynamics especially through studies of internal motions of flexible molecules and clusters.^[12]

For some types of molecules certain vibrational motions are sufficiently large for their displacement vectors to be of the same order of magnitude as the molecular parameters r . These types of motions, called large amplitude motions, are: (i) internal rotation of symmetric (generally methyl) groups; (ii) inversion of amino or imino hydrogens; (iii) internal rotation of light asymmetric groups (OH, SH, NH₂); (iv) ring puckering of (saturated) four- or (near saturated) five membered rings; (v) pseudorotation.

Large amplitude motion within molecules can lead to a fine structure in the rotational spectra. This fine structure results from quantum mechanical tunneling of the molecule from one configuration to another equivalent and indistinguishable configuration. The tunneling splitting depends on the width and height of the barrier and even heavy atoms (or structural groups) can produce large splitting if their motions are characterized by low-barrier potential energy surfaces (PESs) as in many molecular complexes. Below are briefly described some of the most frequent cases.

1.6.1 Double Minimum Potential

The nature of the spectra of molecules with the inversion motion is usually discussed in terms of the double minimum potential. Ring-puckering of cyclic molecules can also be treated in terms of inversion motion.^[13]

The tunneling process through the potential barrier removes the degeneracy resulting in doublets of rotational transitions. Energy splitting between the vibrational substates is a function of the potential barrier height and is reflected in spacing of the observed doublets. The 0^+ , 0^- notation assumes $E(0^-) > E(0^+)$. In the case of strong perturbation it is necessary to carry out simultaneous fit of the data, by taking account for the higher order, Coriolis-type interaction connecting these substates. For correct intensity prediction of rotational transitions in the inversion spectrum it is necessary to take into account the symmetry of the vibrational function, which according to the first notation is symmetric for states denoted by +, and antisymmetric for the - substates. More rigorous details can be found in the Chapter 6.3 of ref. 1.

1.6.2 Internal Rotation

The analysis of the internal rotation is one of the best known applications of rotational spectroscopy and is detectable in the spectrum for moderate barriers below *ca.* 10-15 kJ•mol⁻¹. This phenomenon is a large amplitude motion observed in molecules containing an internal group which rotates

independently from the rest of the molecule.^[14,15] In most cases the internal rotor is symmetric and a periodic variation of the potential energy, with a period determined by the symmetry of the internal rotor, can be observed. The best known case is the internal rotation of a methyl group. The tunneling effect, analogous to the inversion case, splits each torsional level into a non degenerate A component and a doubly degenerate E component. In consequence, each rotational line is a doublet of equal intensity components and this splitting is a sensitive function of the potential barrier of the hindered rotation. If the barrier is very high then the torsional motion corresponds to harmonic oscillation and no splitting of the rotational lines is observed (A and E components are degenerate). For a very low barrier the internal motion can be regarded as a free rotation.

A good starting point for the description of the utilized methods is the model Hamiltonian for an asymmetric rotor with a single methyl internal rotor, which is given in the principal axes system by:

$$\mathcal{H} = \mathcal{H}_R + \mathcal{H}_T + \mathcal{H}_{TR} \quad (26)$$

where \mathcal{H}_R , \mathcal{H}_T and \mathcal{H}_{TR} depend on the reduced angular momentum (P), the internal angular momentum (p), the adimensional moment of inertial rotor (F) and the barrier to internal rotation (V_n), they are described as follows:

$$\mathcal{H}_R = \mathcal{H}_r + F\hat{P}^2 \quad (27)$$

$$\mathcal{H}_T = F\hat{p}^2 + \frac{1}{2}V_n(1 - \cos 3\alpha) \quad (28)$$

$$\mathcal{H}_{TR} = -2F\hat{P}\hat{p} \quad (29)$$

where α is the torsional angle that describes the internal rotation of the two moieties of the molecule relative to each other.

The internal rotation potential function for methyl rotor top has a $2\pi/3$ periodicity and can be expressed by the Fourier series:

$$V(\alpha) = \frac{1}{2}V_3(1 - \cos 3\alpha) + \frac{1}{2}V_6(1 - \cos 6\alpha) + \dots \quad (30)$$

where α denotes the torsional angle, V_3 is the potential barrier height, and usually $V_3 \gg V_6$.

The classification of different methods dealing with internal rotation is correlated with the choice of the coordinate systems (principal inertial axes -PAM method- or the internal rotor axis -IAM method-). A particular selection will produce different coupling terms, and several procedures have been devised to solve the resulting equations, described in great detail in refs. 16 and 17.

1.7 Dissociation Energy

When the intermolecular stretching motion appears to be almost parallel to the a -axis of a complex, it is plausible to estimate its force constant (k_s) within the pseudo diatomic approximation by assuming such a motion to be separated from the other molecular vibrations. For an asymmetric complex, according to:^[18]

$$k_s = 16\pi^4(\mu_D R_{CM})^2[4B^4 + 4C^4 - (B - C)^2(B + C)^2]/(hD_J) \quad (31)$$

while for a symmetric complex, according to:

$$k_s = 128\pi^4(\mu_D R_{CM})^2 B^4 / (hD_J) \quad (32)$$

B and C are the experimental rotational constants. μ_D is the pseudo diatomic reduced mass, for the two subunits 1 and 2:

$$\mu_D = m_1 m_2 / (m_1 + m_2) \quad (33)$$

and R_{CM} is the distance between the centers of the mass of the two subunits; D_J is the experimental centrifugal distortion constant.

The dissociation energy (E_D) can be then evaluated by assuming a Lennard-Jones type potential function and applying the approximate expression:^[19]

$$E_D = \frac{1}{72} k_s R_{CM}^2 \quad (34)$$

1.8 Evaluation of Molecular Structure

It is clear from the definition of the rotational constants, given in equation (9), that rotational spectra are governed by molecular structures. The molecular structure is characterized by the position of each atom determined by the nature of the chemical bonds by which it is connected to its neighboring atoms.

Once a rotational spectrum is obtained and assigned, it yields the rotational constants and from these rotational constants, the moments of inertia and hence the structure of the relative conformation can be obtained.

Different procedures have been introduced which correct various degrees for vibrational effects and which have led to different conceptions of interatomic distance. In particular, three types of structures are frequently used in rotational studies:

- r_e , the equilibrium structure for the hypothetical vibrationless state, evaluated by correction for the effects of vibration including zero-point vibrations. Particularly, in many cases, the geometries from theoretical calculations can be treated as the equilibrium structure.
- r_0 , the effective structure for the ground vibrational state could be calculated from the experimental rotational constants. A least squares fitting procedure has been used to evaluate the r_0 of the studied molecular systems. Several structural parameters could be chosen to fit the differences between experimental and theoretical values of rotational constants. The procedure of the fitting is based on the linearization of the following equation:

$$B_i = B_i^0 + \sum_j (dB_i/dp_j) \Delta p_j \quad (35)$$

where B_i is the i th experimental rotational constant, B_i^0 is the i th rotational constant calculated from the initial assumed structure and p_i is the structural parameter chose for fitting, (dB_i/dp_i) is the changing of B_i^0 with respect to a small changing of p_i while all other structural parameters were kept constant. This procedure is repeated until the convergence has been achieved. However, normally the set of experimental data are not enough to determine the molecular structure completely. Only several bond lengths, valence angles, or valence dihedral angles can be evaluated from the structure fitting and thus only partial r_0 structure can be obtained. For non-covalent interaction bonded molecular complexes, this procedure is adoptable to determine the intermolecular bond length and angles while keeping the geometry of molecular moieties constants.

- r_s , the substitution structure, is derived from the isotopic substitutions. Kraitchman's^[20] method is applied to calculate the position of an atom in a molecule using the changes of moments of inertia resulting from a single isotopic substitution of an atom. Given enough spectroscopic information from the different isotopomers, it is possible to determine the complete structure of a molecule. It should be noted that the rotational constants measured are of the ground state, not equilibrium values, and that the molecular structure is assumed to be identical for all isotopomers.

Regarding the mathematical procedure, the molecule is assumed rigid so that the bond distances and angles are unchanged due to isotopic substitution. The I_x, I_y, I_z and I'_x, I'_y, I'_z are the moments of inertia along the principal axes for the parent and isotopically substituted molecule, respectively. The coordinates are measured from the center of mass of the principal axes system of the parent molecule. The mass of the isotopic atom can be denoted by $m+\Delta m$, with m the original mass of the atom. The moment of inertia in the parent center of mass principal axes system can be expressed as:

$$I'_{xx} = I_x + \Delta m(y^2 + z^2) - \frac{(\Delta m y)^2}{M + \Delta m} - \frac{(\Delta m z)^2}{M + \Delta m} = I_x + \mu(y^2 + z^2) \quad (36)$$

Similarly, that:

$$I'_{yy} = I_y + \mu(z^2 + x^2) \quad (37)$$

$$I'_{zz} = I_z + \mu(x^2 + y^2) \quad (38)$$

where μ is the reduced mass for the isotopic substitution, $\mu = M\Delta m / (M + \Delta m)$ with M is the total mass of the parent molecule. The I_x , I_y , I_z and I'_x , I'_y , I'_z can be determined experimentally, thus the coordinates x , y , and z of the isotopic substituted atom can be obtained.

Others structural parameters that can be easily derived from the rotational constants are the values of the planar moments of inertia, defined as:

$$P_{aa} = \sum_i m_i a_i^2 \quad (39)$$

through the relation:

$$P_{aa} = \frac{1}{2}(-I_a + I_b + I_c) = \frac{h}{16\pi^2} \left(-\frac{1}{A} + \frac{1}{B} + \frac{1}{C} \right) \quad (40)$$

The quantity gives a measure of the mass extension along the a -axis. The same, as well, applies to P_{bb} and P_{cc} .

Moreover an indication of accuracy in the calculated structure is the defect of inertia:

$$\Delta c = I_c - I_a - I_b = -2P_{cc} \quad (41)$$

which should be zero for an absolute planar molecule.

1.9 References

- [1] W. Gordy, R. L. Cook, "Microwave Molecular Spectra", *John Wiley & Sons*, New York, **1984**.
- [2] C. H. Townes, A. L. Schawlow, "Microwave Spectroscopy", *McGraw-Hill Publishing Company Ltd.*, New York, **1955**.
- [3] H. W. Kroto, "Molecular Rotation Spectra", *Dover Publications, Inc.*, Mineola, New York, **1992**.
- [4] W. Caminati, J.-U. Grabow, "Microwave Spectroscopy in Molecular Systems" in "Frontiers of Molecular Spectroscopy", *J. Laane Ed.*, Elsevier, **2009**.
- [5] E. Hirota, *Ann. Rev. Phys. Chem.*, 42, 1-23, **1991**.
- [6] D. W. Pratt, *Ann. Rev. Phys. Chem.*, 49, 481-530, **1998**.
- [7] L. Evangelisti, W. Caminati, *Phys.Chem.Chem.Phys.*, 12, 14433-14441, **2010**.
- [8] E. B. Wilson, J. B. Howard, *J. Chem. Phys.*, 4, 260, **1936**.
- [9] J. K. G. Watson, "Vibrational spectra and structure", Vol. 6, Elsevier, Amsterdam, Oxford & New York, **1977**.
- [10] J. W. Simmons, W. E. Anderson, W. Gordy, *Phys. Rev.*, 77, 77-79, **1950**.
- [11] R. Chang, "Basic Principles of Spectroscopy", *McGraw-Hill*, **1971**.
- [12] B. H. Pate, F. C. De Lucia, *J. Mol. Spectrosc.*, 280, 1-2, **2012**.
- [13] J. Laane, "Vibrational Potential Energy Surfaces in Electronic Excited States" in "Frontiers of Molecular Spectroscopy", *J. Laane Ed.*, Elsevier, **2009**.
- [14] J. M. Brown, A. Carrington, "Rotational spectroscopy of diatomic molecules", *Cambridge University Press*, UK, **2003**.
- [15] D. Lister, J. McDonald, N. Owen, "Internal rotation and inversion", *Academic Press*, New York & San Francisco, **1978**.
- [16] I. Kleiner, *J. Mol. Spectrosc.*, 260, 1-18, **2010**.
- [17] J. T. Hougen, I. Kleiner, M. Godefroid, *J. Mol. Spectrosc.*, 163, 559-586, **1994**
- [18] D. J. Millen, *Can. J. Chem.*, 63, 1477-1479, **1985**.
- [19] S. E. Novick, S. J. Harris, K. C. Janda, W. Klemperer, *Can. J. Phys.*, 53, 2007-2015, **1975**.
- [20] J. Kraitchman, *Am. J. Phys.*, 21, **1953**.

COMPUTATIONAL METHODS

2.1 Theoretical Calculations

Quantum chemistry calculations constitute a valuable and complementary source of information on structural and dynamical properties of molecules and aggregates. Theoretical methods allow to determine structures, stabilization energies, vibrational frequencies and potential energy surfaces of molecules and small clusters.

In this dissertation all the theoretical calculations performed are limited to the electronic and vibrational ground states. The main purposes for which they are used are for setting up the experimental research and for diagnostic comparisons of experimental data with theoretical results.

In particular, geometry optimizations are used to predict molecular equilibrium structures and conformational preferences from the potential energy surface (PES). The resulting information on rotational constants, dipole moment components, relative energies and quadrupole coupling constants are helpful indications for searching for rotational spectra and conformational assignment. In order to obtain reliable conformational energies and molecular properties, *ab initio* and density functional theory (DFT) methods are used to assist the assignment of the rotational spectra.

In the case of the *ab initio* methods, the Møller-Plesset^[1,2] one gives a good balance between accuracy and computational cost for spectroscopic purposes. These calculations are post-Hartree-Fock methods which explicitly introduce electron correlation through perturbation theory, usually, as in our case, up to second order (MP2). In some cases, the computational costs can increase with the MP2 method and for this reason the density functional theory calculations are performed.

Indeed, the methods based in the density functional theory are widely used due to the good efficiency-computational cost ratio compared to the *ab initio* methods. The B3LYP functional^[3] is the one used in our spectroscopic studies, because it reproduces satisfactorily the chemical parameters required.

A comparison between the two methods is reported for some of the studied molecular systems, in order to evaluate which of the two better reproduces the conformational structures.

The *ab initio* and DFT calculations require an adequate selection of a finite set of orbital basis functions. A basis set is a description of the atomic orbitals centered at each nucleus of the molecule, which are commonly described as linear combinations of gaussian orbitals, as suggested

by Pople.^[4] In the present work, the most common basis set employed is the 6-311++G** but in some cases also Peterson and Dunning's correlation-consistent triple-valence polarized basis set (cc-pVTZ) is employed.^[5-7] Frequency calculations are used to calculate the zero point energy and force constants, and to evaluate if the geometry optimized is a real minimum.

In addition, for molecular complexes, a counterpoise correction^[8] is used to remove the well-known basis set superposition error (BSSE).

All theoretical calculations in this dissertation are performed with Gaussian 03^[9] or Gaussian 09^[10] program packages.

2.2 Computational Programs

The majority of computer programs used in the analysis of the spectroscopic data presented in this dissertation, are collected on the PROSPE website.^[11, 12] All programs are freely available. In this section a focus on the AABS package written by Kisiel and Pickett's SPFIT/SPCAT programs is done. These two program packages are the basic tools used for the analysis of all rotational spectra, which are the subject of this dissertation.

The package called AABS, which is an abbreviation of "Assignment and Analysis of Broadband Spectra", is based on a pair of two computer programs: ASCP_L, a graphical program to display spectral predictions from Pickett's program SPCAT, and SVIEW_L, a viewer for frequency domain spectra. In the AABS package these two programs have been synchronized in order to simultaneously display a measured spectrum in one window, and the current predictions in a second window. One of the most important features of the package is a special highlighting option of a predicted transition sequence of interest, by 'cloning' the current line. Frequency regions around successive transitions in this sequence can then be easily inspected in turn, and if there are suitable lines in the spectrum, those can be measured.

The entry for the measured rotational line consisting of quantum numbers from prediction, the measured frequency and measurement error is automatically added to a specified data file for one of several fitting programs. The next step is to fit spectroscopic constants and to make a new prediction from improved constants. The user can visually verify the compatibility of lines added to the fit by a simple refresh option of the prediction window. This graphical process significantly facilitates and accelerates spectral assignment.

This package is successfully used for spectral assignment in the majority of the rotational spectroscopy's laboratories in the world, mainly when a broadband spectrometer is present. More

detailed information on the AABS package is available in ref. 13 and on the PROSPE website (ref. 12).

The SPFIT/SPCAT program package has been written by H. M. Pickett of Jet Propulsion Laboratory. SPFIT is used for fitting the values of constants in a selected Hamiltonian to frequencies of measured transitions, and SPCAT calculates energies and intensities for different transitions. The extensive use of this package by the spectroscopic community results from the extended possibilities for definition of the molecular Hamiltonian required for a particular problem. The fitted parameters can be rotational constants, centrifugal distortion constants in different reductions and representations of the rotational Hamiltonian, nuclear quadrupole coupling constants, spin-spin and spin-rotation constants and a linear combinations of them can be also performed. Spectra calculated with SPCAT can be displayed by the ASCP_L program. Some of the details of the SPFIT/SPCAT package are described in ref. 14 and it is freely available from ref. 15.

2.3 References

- [1] C. Møllert, M. S. Plesset, *Phys. Rev.*, 46, 618, **1934**.
- [2] D. Cremer, *Wiley Interdiscip. Rev. Comput. Mol. Sci.*, 1, 509, **2011**.
- [3] C. Lee, W. Yang, R. G. Parr, *Phys. Rev. B*, 37, 785-789, **1988**.
- [4] W. J. Hehre, L. Radom, J. A. Pople, P. v. R. Schleyer, "Ab initio Molecular Orbital Theory", J. Wiley & Sons, New York, **1986**.
- [5] R. Krishnan, J. S. Binkley, R. Seeger, J. A. Pople, *J. Chem. Phys.*, 71, 650, **1980**.
- [6] T. H. Dunning, Jr., *J. Chem. Phys.*, 90, 1007, **1989**.
- [7] K. A. Peterson, T. H. Dunning, Jr., *J. Chem. Phys.*, 117, 10548, **2002**.
- [8] S. F. Boys, F. Bernardi, *Mol. Phys.*, 19, **1970**.
- [9] M. J. T. Frisch, G. W.; Schlegel, H. B.; Scuseria, G. E.; Robb, M. A.; Cheeseman, J. R.; Montgomery, Jr., J. A.; Vreven, T.; Kudin, K. N.; Burant, J. C.; Millam, J. M.; Iyengar, S. S.; Tomasi, J.; Barone, V.; Mennucci, B.; Cossi, M.; Scalmani, G.; Rega, N.; Petersson, G. A.; Nakatsuji, H.; Hada, M.; Ehara, M.; Toyota, K.; Fukuda, R.; Hasegawa, J.; Ishida, M.; Nakajima, T.; Honda, Y.; Kitao, O.; Nakai, H.; Klene, M.; Li, X.; Knox, J. E.; Hratchian, H. P.; Cross, J. B.; Adamo, C.; Jaramillo, J.; Gomperts, R.; Stratmann, R. E.; Yazyev, O.; Austin, A. J.; Cammi, R.; Pomelli, C.; Ochterski, J. W.; Ayala, P. Y.; Morokuma, K.; Voth, G. A.; Salvador, P.; Dannenberg, J. J.; Zakrzewski, V. G.; Dapprich, S.; Daniels, A. D.; Strain, M. C.; Farkas, O.; Malick, D. K.; Rabuck, A. D.; Raghavachari, K.; Foresman, J. B.; Ortiz, J. V.; Cui, Q.; Baboul, A. G.; Clifford, S.; Cioslowski, J.; Stefanov, B. B.; Liu, G.; Liashenko, A.; Piskorz, P.; Komaromi, I.; Martin, R. L.; Fox, D. J.; Keith, T.; Al-Laham, M. A.; Peng, C. Y.; Nanayakkara, A.; Challacombe, M.; Gill, P. M. W.; Johnson, B.; Chen, W.; Wong, M. W.; Gonzalez, C.; Pople, J. A. , Gaussian 03 (Revision B.01) ed., Gaussian, Inc., Pittsburgh PA, **2003**.
- [10] M. J. Frisch, G. W. Trucks, H. B. Schlegel, G. E. Scuseria, M. A. Robb, J. R. Cheeseman, G. Scalmani, V. Barone, B. Mennucci, G. A. Petersson, H. Nakatsuji, M. L. Caricato, X.; Hratchian, H. P.; Izmaylov, A. F.; Bloino, J.; Zheng, G.; Sonnenberg, J. L.; Hada, M.; Ehara, M.; Toyota, K.; Fukuda, R.; Hasegawa, J.; Ishida, M.; Nakajima, T.; Honda, Y.; Kitao, O.; Nakai, H.; Vreven, T.; Montgomery, J. A.; J. E. J. Peralta, F. B. Ogliaro, M.; Heyd, J. J.; Brothers, E.; Kudin, K. N.; Staroverov, V. N.; Kobayashi, R.; Normand, J.; Raghavachari, K.; Rendell, A.; Burant, J. C.; Iyengar, S. S.; Tomasi, J.; Cossi, M.; Rega, N.; Millam, J. M.; Klene, M.; Knox, J. E.; , J. B. Cross, V. A. Bakken, C.; Jaramillo, J.; Gomperts, R.; Stratmann, R. E.; Yazyev, O.; Austin, A. J.; Cammi, R.; Pomelli, C.; Ochterski, J. W.; Martin, R. L.; Morokuma, K.; Zakrzewski, V. G.; Voth, G. A.;

Salvador, P.; Dannenberg, J. J.; Dapprich, S.; , A. D. Daniels, Ö. F. Farkas, J. B.; Ortiz, J. V.; Cioslowski, J.; Fox, D. J., Gaussian, Inc., Wallingford CT, **2009**.

[11] Z. Kisiel, in: J. Demaison *et al.* (Eds.), *Spectroscopy from Space*, Kluwer Academic Publishers, Dordrecht, 91-106, **2001**.

[12] Z. Kisiel, PROSPE - Programs for ROTational SPEctroscopy, available at <http://www.ifpan.edu.pl/~kisiel/prospe.htm>.

[13] Z. Kisiel, L. Pszczólkowski, I. R. Medvedev, M. Winnewisser, F. C. De Lucia, E. Herbst, *J. Mol. Spectrosc.* 233, 231-243, **2005**.

[14] H. M. Pickett, *J. Mol. Spectrosc.* 148, 371-377, **1991**.

[15] H.M. Pickett, SPFIT/SPCAT package, available from : <http://spec.jpl.nasa.gov>.

SPECTROSCOPIC TECHNIQUES

3.1 Introduction

The wide frequency range (0.3-3000 GHz) in which rotational spectra can be measured leads to the use, in contemporary rotational spectrometers, of many different methods of signal acquisition, microwave radiation sources, detection techniques, and techniques of signal processing.

The rotational spectra in the centimeter-wave region (0.3-30 GHz) are nowadays usually measured at supersonic expansion conditions and the molecular signal is detected in the time domain with Fourier Transform spectrometers. The frequency accuracy of a rotational transition measured in supersonic expansion with these kind of instruments is estimated to be 1-2 kHz. This high accuracy enables precise determination of several essential physical and chemical molecular properties (such as nuclear quadrupole coupling tensor), and allows straightforward observation of hydrogen bonded molecular complexes or van der Waals adducts.

The millimeter-wave (30-3000 GHz) rotational spectra are most efficiently measured in the frequency domain with broadband spectrometers. The expected resolution of the rotational spectrum is determined by the Doppler limited line widths of the absorption lines but sometimes also by the experimental technique used for detection. The frequency measurement accuracy of the rotational transition is specified by a given experimental setup, but it is usually well below 0.1 MHz. Broadband millimeter-wave spectra usually contain many different rotational transitions from R and Q branches up to high values of J and K quantum numbers and in spectra recorded at room temperatures also vibrational satellites are observable.

In this chapter the current configurations of the two spectrometers built at the University of Bologna are described. The spectrometers are a Pulsed-Jet Fourier Transform MicroWave spectrometer (PJ-FTMW), and a Free-Jet Absorption MilliMeter Wave spectrometer (FJAMMW). These spectrometers have been used to record the spectra analysed in this dissertation. Specific experimental conditions for measured species are described in the results chapters of this dissertation.

Before continuing with these descriptions, a brief introduction of supersonic jet expansion will be given in order to point out the characteristics and the capabilities of this procedure.

3.2 Supersonic Jet Expansion

Since different pioneering works^[1,2] on the seeded supersonic jet which revolutionized modern physical chemistry, Balle and Flygare were the first who combined the supersonic jet with high resolution microwave Fourier transform spectroscopy.^[3] The low temperatures (rotational 1-5 K typical and translational 1-2 K typical in the moving frame) in seeded supersonic jets make them particularly attractive as cold sources of large molecules. At room temperature these molecules typically occupy many thousands of rovibrational states, making spectroscopy challenging at best and in many cases impossible; cooling leads to substantial population enhancement of lower rotational states and to a dramatic simplification of the spectrum.^[4] In particular, the effective rotational temperature depends on the carrier gas^[5] and the expansion parameters, but it is usually less than 10 K. In any case, the high degree of rotational cooling considerably simplifies the rotational spectrum since only the low- J rotational transitions for the ground vibrational state are typically observed. This cooling takes place until the expanding gas becomes so rarefied that the collisions stop to occur. From that point on, the system remains as it were, frozen in the situation reached. This phenomenon allows also the observation of unstable species such as ions, radicals and molecular aggregates bonded by weak forces.

A scheme of the essential features of a free jet expansion is shown in Figure 3.1. Its characteristics can be briefly described (more details can be found in the Chapter 2 of ref. 6). The gas source is a converging pinhole nozzle through which the gas is accelerated toward the exit. The gas starts from the stagnation state (P_0 , T_0), and with an imposed pressure difference ($P_0 - P_b$) accelerates, as the area decreases, toward the source exit. The flow may reach sonic speed (that is, mean velocity equal to the local speed of sound or Mach number equal to 1) at the exit, provided the pressure ratio P_0 / P_b exceeds a critical value:

$$G \equiv \left((\gamma + 1) / 2 \right)^{\gamma / (\gamma - 1)}$$

which is less than 2.1 for all gases, (γ represents a property of the fluid species).

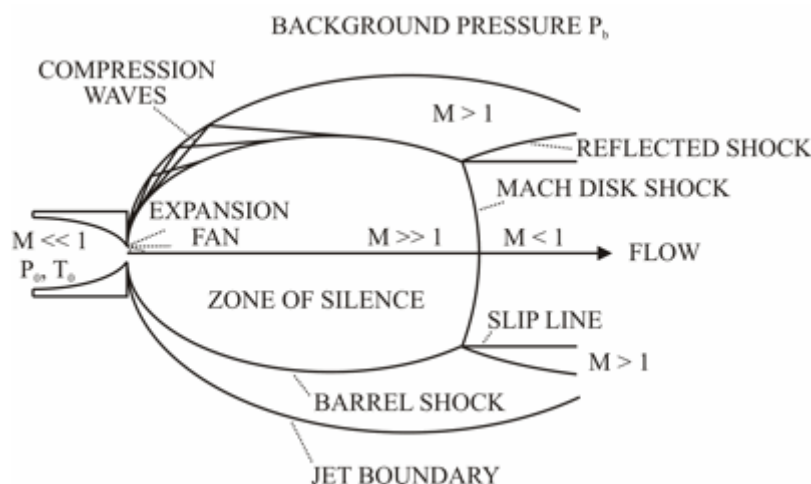


Figure 3.1 - Schematic drawing of the adiabatic gas expansion, which forms a supersonic jet (from ref. 6).

If the pressure ratio is less than this critical value, then the flow will exit subsonically, with exit pressure nearly equal to P_b , without any further expansion.

Typically for this kind of sources, the flow can be considered isentropic and viscous effects and heat conduction can be neglected. At the exit of the nozzle the gas is under-expanded and the expansion really occurs to bring back the gas to environmental conditions determined by the value of P_b . Overflowing the nozzle, the gas can reach higher speeds than the local speed of sound (Mach number $M > 1$) and can expand to much smaller values than the external pressure. The recompression of the fluid and the transition to the environmental conditions takes place by means of the structure of shock, reported in Figure 3.1. The structure of shock is formed by a cylinder (barrel shock) and by a disk perpendicular to the axis of the cylinder called *Mach disk* and this region is a complicated viscous, heat conducting, non-isentropic area.

To simplify the situation and eliminate the presence of the shock structure, a skimmer can be placed inside the isentropic region called the *zone of silence*, or to ensure that the continuum flow does not prevail at the jet boundaries the background pressure P_b should be reduced to low enough values.

These considerations are based on the fact that the behaviour of the gas during the expansion can be described as a continuous flow. This is only true if the density and the velocity of collision are sufficiently high. As the jet expands, the velocities of collision decrease and the kinetic processes, at a certain point, stop. This *frozen point* is the aim for this kind of spectroscopic purposes, and it can be used for creating and observing unstable species during the jet expansion.

A kinetic analysis can be applied to the internal degrees of freedom of the molecules. It is well established that molecules in supersonic beams experience strong translational and rotational

cooling.^[7] Regarding the rotational motions, the cooling is generally extremely efficient, in fact the number of rotational collision needed to achieve relaxation is between 10 and 100 for the lighter molecules, but when the molecular weight increases, it tends to decrease.

Related to rotational cooling, are the jet-cooled abundances of the different conformers. In fact conformational populations may be particularly affected by collisional relaxations. Generally the conformational composition in the vapor, prior to expansion, can remain basically unaltered if conformational relaxation is prevented by a high energy barrier to interconversion and if a large motion takes place. To observe a relaxation phenomenon, the interconversion barrier between conformers must be lower than a threshold value, which empirically depends on the number of structural degrees of freedom and on the energy difference between conformations. For conformational interconversion involving only one degree of freedom several studies^[8] point to a barrier threshold of about $\sim 400\text{ cm}^{-1}$, while this value increases till about 1000 cm^{-1} in the case of conversions in which there are more torsions involved.^[9, 10]

Concluding, the supersonic expansion will preserve the preexisting equilibrium of conformational distribution but this not total conformational relaxation can be an advantage in that observations are not limited to the most stable conformation of a molecule.

3.3 Pulsed-Jet Fourier Transform MicroWave Spectrometer

The Pulsed-Jet Fourier Transform MicroWave spectrometer (PJ-FTMW) covers the frequency range 6.5-18 GHz and presents a Coaxially Oriented Beam Resonator Arrangement (COBRA).^[11] The photo of the spectrometer is shown in Figure 3.2, while the block diagram of this entire



instrument is shown in Figure 3.3. The design of the spectrometer follows the guidelines given by Andresen *et al.*^[12] and Grabow *et al.*^[13] while most of the details are taken from the spectrometer of the group of Prof. Alonso in Valladolid.^[14]

In particular the parts that constitute this device and entails its operation are described below.

Figure 3.2 - Pulsed jet Fourier transform microwave spectrometer built at University of Bologna.

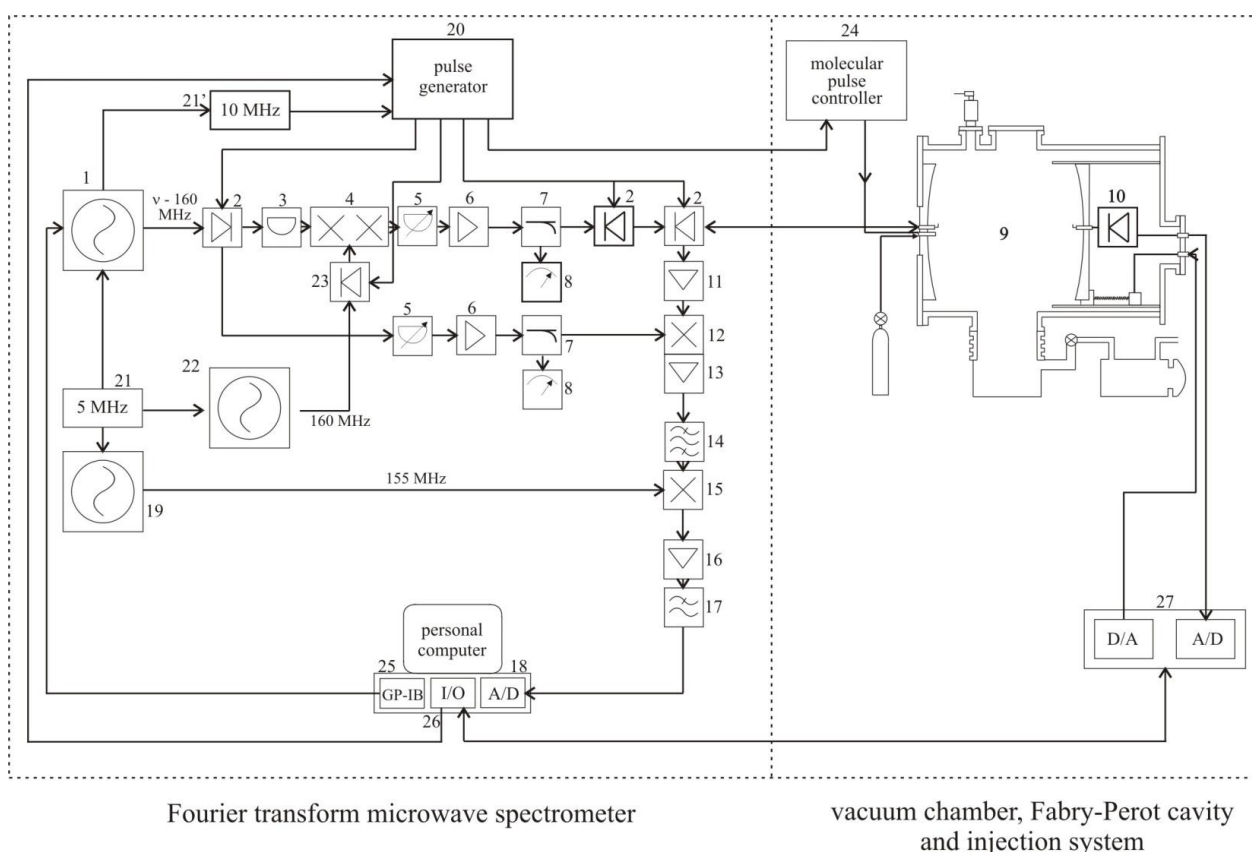


Figure 3.3 - Block diagram of the PJ-FTMW spectrometer.

(MW=Micro Wave; RF=Radio Frequency; P=output power, IF=intermediate frequency, IL=insertion losses, G=gain, NF=noise figure, IS=isolation, IR =image rejection).

1. MW synthesizer, HP 8672 A. 2. MW switch SPDT, SMT SFD0526-001S. 3. Fixed attenuator MCL BW-S3W2. 4. Single side band modulator, MITEQ MN0226LC1C. 5. Variable attenuator, NARDA 4798. 6. MW amplifier ALC Microwave ALS0618-30-20. 7. Directional coupler NARDA 4203-16. 8. Power meter, HP 435 B + Power sensor 8485A. 9. Fabry-Pérot resonator, see text. 10. MW crystal detector HP8470B. 11. MW low noise amplifier, MITEQ JSD4-0600-1800 16-8P. 12. Image rejection mixer, MITEQ IR0226LC1C. 13. 160 MHz RF amplifier, MITEQ AU 1466-140. 14. Bandpass filter, TTE KC6-160M-20M. 15. RF mixer, HP 10514A. 16. RF amplifier, MCL MAN 1LN. 17. Lowpass Filter, TTE LC5-25M-50-7135. 18. Transient recorder, SPECTRUM PAD 82A, modified following the design of the Kiel University. 19. RF synthesizer, PTS 160-M7020. 20. Pulse Sequencer TTL, made at the University of Valladolid, based on a PCB card from the University of Kiel. 21. Reference signal, Rb oscillator 5 MHz , Ball-Efraton FRK LLN. 22. RF synthesizer, MARCONI 2019A. 23. RF switch MCL 7MSW-1111. 24. Pulse controller General Valve IOTA ONE. 25. IEEE 488 interface, NI GP-IB-488 PCII. 26. I/O card, NI PC-DIO-96. 27. A/D and D/A converter for Stepper motor control. Made in Valladolid.

3.3.1 Resonator Cavity

The schematic diagram of the mechanic part is shown in Figure 3.4. The resonator, of the Balle-Flygare type, is made by two aluminum mirrors with a curvature radius of 60 cm and with a diameter of 35 cm and placed in a stainless steel high vacuum chamber of cylindrical shape (built by HVP, Parma, Italy). The diameter of the chamber is 40 cm while the length is 85 cm. The chamber is evacuated with an 8000 s^{-1} diffusion pump driven by a block of two Leybold mechanical pumps (D65B and Ruvac WAU 251, rotary and booster pumps, respectively).

The mirrors are situated in a near-confocal arrangement with one of them fixed in one flange of the vacuum chamber and the other one mounted on a motorized slide rack. A computer program which can control the stepping motor, allows tuning the resonator to the right polarization frequency.

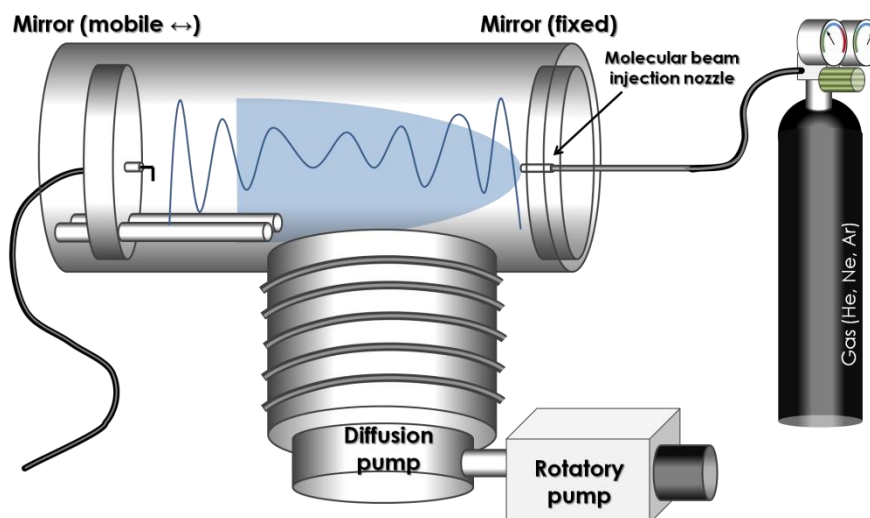


Figure 3.4 - Illustration of the mechanic part of the PJ-FTMW.

3.3.2 Time Domain Technique

Instead of continuously passing monochromatic radiation through the cell and detecting the transmitted signal as a function of frequency, nowadays MW spectrometers apply the radiation for a short period of time. In the presence of a sample, a radiative response is induced. To obtain the spectrum, the response signal is recorded as a function of time and subjected to Fourier transformation (FT). This kind of approach produces a significant improvement in sensitivity.

The time-dependent behavior of absorption and emission of a two-level quantum mechanical systems makes it possible to measure rotational transitions in the time domain. The interaction of

the MW radiation and the molecular beam results in rotational coherence. The molecular signal power is relative to the fraction of the total energy stored by the field within the resonator volume. Due to the fact that the jet expansion and the MW radiation are coaxial, the amplitude of the molecular signal is approximated by:

$$S_{ab}(t) \propto s' \exp(i(\omega_{ab} - kv_{\infty})t + \theta_{ab}') + s'' \exp(i(\omega_{ab} + kv_{\infty})t + \theta_{ab}'')$$

where ω_{ab} is the angular resonance frequency and $k = \omega/c$ is the wavenumber of the radiation. This kind of arrangement produces a significant improvement in frequency resolution (comparable to the sub-Doppler regime at room temperature). The Doppler doublet, consisting of frequency components at $\nu_{ab} (1 - v_{\infty}/c)$ and $\nu_{ab} (1 + v_{\infty}/c)$, is observed in the frequency domain. The molecular resonance frequency is then recovered as the arithmetic mean of the components separated by $\Delta\nu_{ab} = 2\nu_{ab}v_{\infty}/c$. The line width of the individual components is on the order of 1.5 kHz; at an appreciable S/N ratio, a frequency accuracy of 150 Hz, is achieved for unblended lines. The sensitivity allows for the observation of mono-deuterated asymmetric-top molecules in natural abundance (0.015%).

3.3.3 Pulsed Supersonic Jet Expansion

As already said before, the supersonic expansion of molecular systems seeded in rare gas is rich in molecules of low rotational temperature. It is stated that rotational temperature about 1 K can be normally reached. For such low temperatures the maximum in the rotational absorption envelope is usually well below 20 GHz. Thus supersonic expansion provides significantly sensitivity advantage for transitions originating from low energy rotational levels in the vibrational states. Furthermore, due to minimized Doppler broadening effects in the pulsed supersonic expansion the linewidth is significantly reduced when compared to the room temperature static gas experiment.

This expansion can be generated by using an electromagnetic valve and provide a sample of high number density. The COBRA can significantly increase the resolution and sensitivity than the orientation that molecular beam is perpendicular to MW pulsed excitation. In our PJ-FTMW spectrometer, the solenoid valve (General Valve, Series 9) is used to generate the supersonic expansion (nozzle diameter 0.5 mm), which is located above the antenna in the fixed mirror in a coaxial arrangement with the MW radiation.

Typically, ~1% sample seeded in rare gas at a total pressure in range of 0.1~0.6 MPa is expanded into the high evacuated resonator chamber. The process is a rapid adiabatic expansion rather than effusive, which cools the molecular systems to very low vibrational temperature and

generates molecules traveling along radial path without collision. Thus the transition lines are very narrow and the broadening of transitions is only due to that natural line width, which corresponds to a very high resolution.

3.3.4 Experimental Cycle

An experimental cycle (as shown in Figure 3.5) starts with a pulse of a rare gas carrying the sample molecules (the stagnation pressures 0.1~0.6 MPa). Later on, after a certain delay, a MW pulse is applied to produce a macroscopic polarization of the species in the jet. Once the excitation stops with a very short delay, molecular relaxation gives rise to a transient emission signal. Finally, the molecular signal in the time domain (coherent emission) is processed by a fast FT, giving the frequency domain spectrum. A new experimental cycle can start once the vacuum cavity has been evacuated. A repetition rate of 2 Hz is normally employed. For very weak signals thousands of cycles must be added coherently to obtain a better signal-to-noise (S/N) ratio.

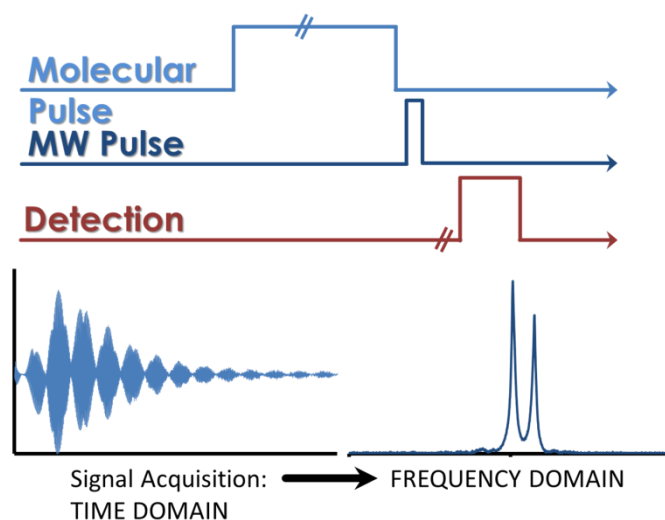


Figure 3.5 - Pulse sequence for a single experimental cycle.

The duration of the pulse, computer controlled, can be optimized depending on the particular molecular systems of interest. The delay between the molecular and MW pulses is critical and must be optimized by taking into account the features of the gas expansion such that the main body of the gas mixture is present in the cavity during the MW pulse. The delay between the MW pulse and the recording of the molecular decay is necessary to allow polarizing radiation to dissipate.

The frequencies were determined after FT of the 8k data points time domain signal, recorded with 100 ns sample interval. The pulsed nozzle valve is mounted near the center of one of the mirrors in such a way that the supersonic beam propagates parallel to the resonator axis. In this setup, all lines appear as enhanced by Doppler effect. The line position is the arithmetic mean of both Doppler component lines. The estimated accuracy of the frequency measurements is better than 3 kHz and the resolution is better than 7 kHz.

3.4 Free-Jet Absorption MilliMeter Wave Spectrometer

The Free-Jet Absorption MilliMeter Wave spectrometer (FJAMMW), Figure 3.6, covers the frequency range 52-74.4 GHz, and the accuracy of the frequency measurements is better than 50 kHz. The scheme of the spectrometer is analogous to that used by Brown *et al.*^[15], although some new features were introduced.

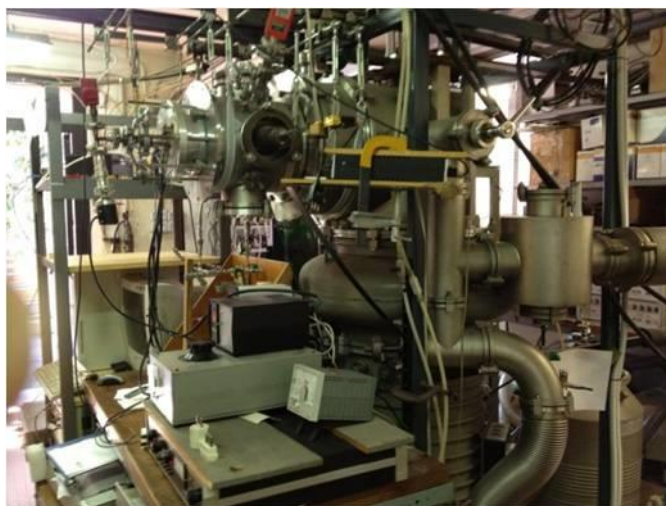


Figure 3.6 - Free-Jet Absorption MilliMeter Wave spectrometer built at University of Bologna.

The early development of the spectrometer can be traced through published papers,^[16, 17] however, since the time of those reports, substantial advances in instrumental configuration have been made and the last published update is reported in the first article of the section “Publications” at page 243.

Below is going to be described the setup containing the VDI multiplier system (see Figure 3.7), that represents the device with which most of the measurements have been carried out.

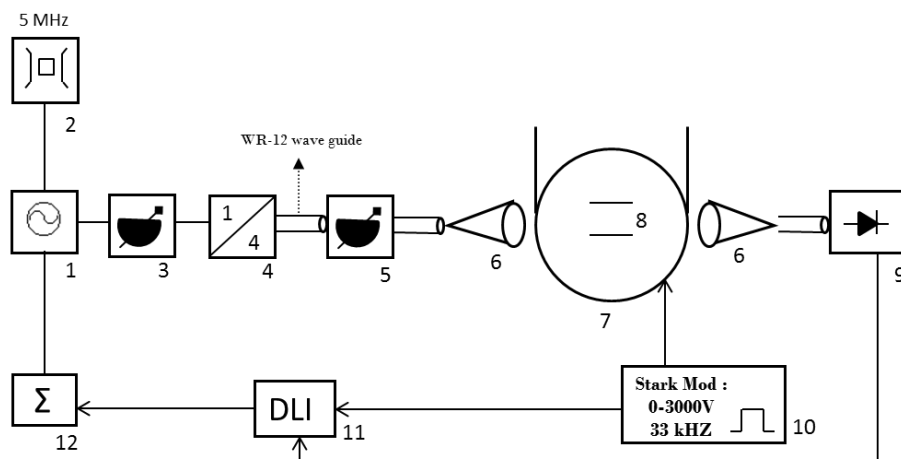


Figure 3.7 - Block diagram of the Free-Jet Absorption Millimeter Wave spectrometer (FJAMMW), with the VDI multiplier system: 1. MicroWave synthesizer - HP8672A 2-18GHz. 2. Reference signal, Rb oscillator 5 MHz, Ball-Efraton FRK-LLN. 3. Variable attenuator, NARDA 10dB. 4. Frequency quadrupler: VDI-AMC WR12 quadrupler 12.5-22 GHz. Output power: +13dBm. 6. Horn-dielectric lens system (Montech-Clayton, Australia). 7. Supersonic-jet expansion chamber. 8. Stark plates. 9. Schottky-diode detector: Millitech DXW10 for frequencies above 60 GHz or a Millitech 4731 4H-1111 for frequencies below 60 GHz. 10. High voltage Stark modulation: electric field up to $750 \text{ V}\cdot\text{cm}^{-1}$ at a frequency of 33 kHz. 11. Digital lock-in amplifier. 12. Experimental control and data acquisition.

3.4.1 Absorption Millimeter Wave Line

As reported in the first article of the section “Publications” at page 243, the millimeter-wave radiation is generated by a radiofrequency source in the 2-18.6 GHz region (HP 8672A) which is fed to an amplifier multiplier chain (Virginia diode AMC WR12 quadrupler). The nominal input frequency range of the multiplier is 12.5-22 GHz (10-16 dBm typical input power), while the nominal output frequency is 50-88 GHz (13 dBm typical output power). Before the microwave radiation enters in the chamber a variable attenuator is present in order to optimize the line’s absorption.

3.4.2 Stark Modulation and Detection

As said above the apparatus consists of the radiation source, the multiplier and a variable attenuator, then a horn-dielectric lens system (Montech-Clayton, Australia) focuses the radiation in the plume

region of the chamber with a waist of about 2 cm, and a Schottky diode allows the detection. Different kind of detectors are used: a Millitech DXW10 for frequencies above 60 GHz or a Millitech 4731 4H-1111 to work below 60 GHz. The MW radiation and the free jet are arranged perpendicularly, and a high voltage Stark modulation (electric field up to 750 V cm^{-1} at a frequency of 33 kHz) is applied to the molecular sample through the presence in the chamber of two plates, where the unearthed one is guarded so the voltage can be applied to the plates without discharges in the chamber. After detection, the modulated signal is fed to a lock-in amplifier. The spectrometer is computer controlled via a National Instrument GPIB board. The GPIB controller communicates with the HP synthesizer in order to guide the frequency scan step by step and with the lock-in amplifier through which the signal provided by the detector is recovered, amplified, and then collected according to the chosen gate time. The control software of the spectrometer has been developed on the LabView graphical programming platform.

3.4.3 Supersonic Jet Expansion

The supersonic beam expands along the axis of a cylindrical vacuum chamber 25 cm in diameter and 25 cm in length, which is evacuated with an effective vacuum yield of around 4000 l s^{-1} . The nozzle used has a diameter of 0.035 cm and the typical range of stagnation pressures is from 10 to 100 KPa, which remains in the background in the region of 10^{-5} Pa . From these data is straightforward to calculate the position of the Mach disk, following the equation below:

$$\frac{x_M}{d} = 0.67 \left(\frac{P_0}{P_b} \right)^{1/2}$$

Using values of $P_0/P_b > 10^5$ and d , diameter of the nozzle, of 0.035 cm the position of the Mach disk obtained is about $x_M = 23 \text{ cm}$. This means that the shock structure is absent in the area where the spectroscopic measurements were done.

A further capability that can be used with the FJAMMW spectrometer is the presence of an efficient heating system, characterized by two resistances that heat at the beginning of the injection part and at the end where is positioned the nozzle (see Figure 3.8). With this electrically controlled heating system, temperatures up to 200°C can be achieved. This possibility opens up the opportunity to study also heavier molecules that usually present a low vapor pressure.

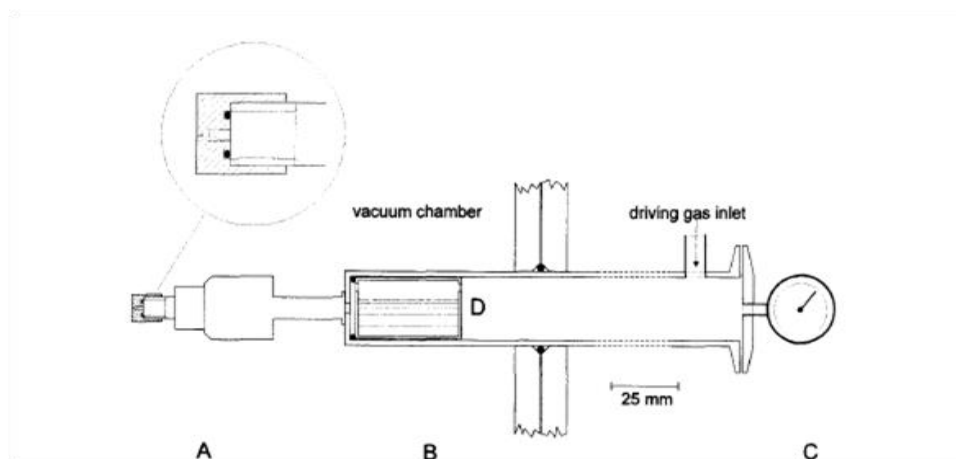


Figure 3.8 - Simplified sketch of the nozzle head: (A) nozzle and modified fuel injector, (B) section where the sample container can be introduced, (C) manometer to measure the stagnation pressure, (D) sample container, from ref. 17.

Even though this last setup, based on the VDI quadrupler (see Figure 3.7), presents quite good performance, during my PhD activity improvements on the signal to noise ratio of this millimeter wave system were developed. In this effort another setup (see Figure 3.9), that can be easily interchanged with the previous one, is under test. It is based on a chain of two multipliers (doublers), the first is active and the second one is passive, separated by an isolator and a low pass filter. The presence of the isolator improves the coupling between adjacent elements of the chain and the filter helps to eliminate unwanted harmonic signals that could be present. In fact the frequency multiplication process is not an ideal one because it introduces some disturbances (phase noise, harmonic frequencies, spurious signals) in the output signal; but, if a high frequency generator is not available, the introduction of *ad hoc* band pass filters placed downstream of the generator and each multiplier, improves the performances of this kind of multiplication system.

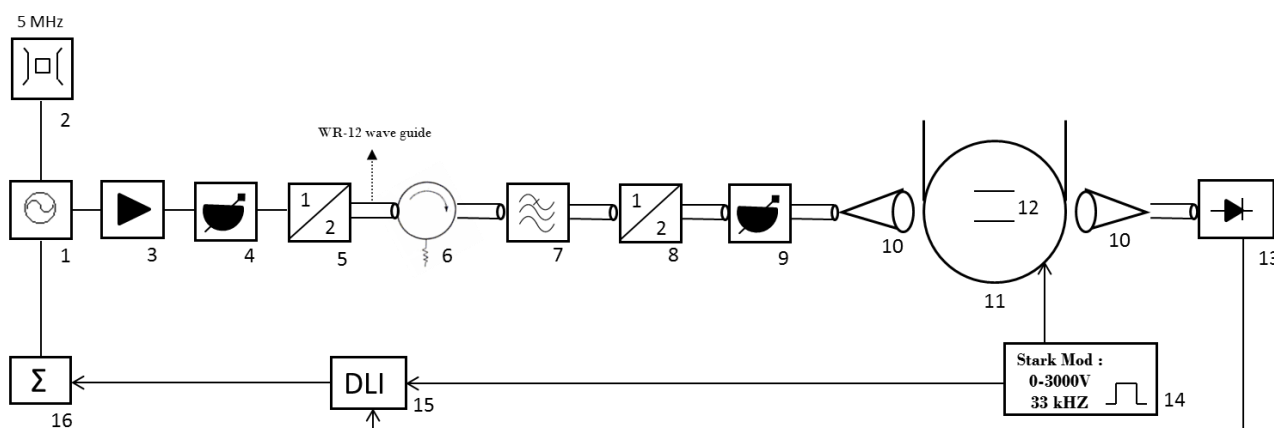


Figure 3.9 - Block diagram of the Free-Jet Absorption Millimeter Wave spectrometer (FJAMMW) with the setup based on a chain of two multipliers (doublers): 1. MicroWave synthesizer - HP8672A 2-18GHz. 2. Reference signal, Rb oscillator 5 MHz , Ball-Efraton FRK-LLN. 3. Hittite Amplifier MW 5-20 GHz Gain : +20dB. 4. Variable attenuator, NARDA 10dB. 5. Frequency doubler Space-labs 26.5-40 GHz. Output power: +17dBm. 6. Dorado Isolator 26.5-40 GHz, 41 GHz. 7. Low pass filter Spacek-labs 41 GHz. 8. Frequency doubler Spacek-labs 53-80 GHz. Output power: -3dBm - 0dBm. 9. Variable attenuator 0-35dB. 10. Horn-dielectric lens system (Montech-Clayton, Australia). 11. Supersonic-jet expansion chamber. 12. Stark plates. 13. Schottky-diode detector: Millitech DXW10 for frequencies above 60 GHz or a Millitech 4731 4H-1111 for frequencies below 60 GHz. 14. High voltage Stark modulation: electric field up to $750 \text{ V}\cdot\text{cm}^{-1}$ at a frequency of 33 kHz. 15. Digital lock-in amplifier. 16. Experimental control and data acquisition.

The new setup allows to observe rotational spectra with a more regular baseline and with a better signal to noise ratio (about twice) rather than the VDI device, which instead produces rotational spectra with some very noisy frequency regions.

The trial period with different setups appears promising to improve the performance of the FJAMMW spectrometer and suggests us to try in the future to introduce this kind of filters also in the millimeter wave line produced with the VDI multiplier, in order to improve its operation.

3.5 References

- [1] R.E. Smalley, L. Wharton and D.H. Levy, *Acc. Chem. Res.*, 10 (4), 139, **1977**.
- [2] A. Kantrowitz and J. Grey, *Rev. Sci. Instrum.*, 22, 328, **1951**.
- [3] T.J. Balle and W.H. Flygare, *Rev. Sci. Instrum.*, 52, 33, **1981**.
- [4] D. Patterson and J.M. Doyle, *Mol. Phys.*, 110, 1757-1766, **2012**.
- [5] O. Desyatnyk, L. Pszczólkowski, S. Thorwith, T. M. Krygowski, Z. Kisiel, *Phys. Chem. Chem. Phys.*, 7, 1708-1715, **2005**; correction *Phys. Chem. Chem. Phys.* 7, 2080, **2005**.
- [6] G. Scoles, "Atomic and Molecular Beam Methods", vol. I, Oxford University Press., **1988**.
- [7] P. Felder, Hs.H. Günthard, *Chem. Phys.*, 71, 9-25, **1982**.
- [8] R. S. Ruoff, T. D. Klots, H. S. Gutowsky, *J. Chem. Phys.*, 93, 3142-3150, **1990**.
- [9] G. M. Florio, R. A. Christie, K. D. Jordan, T. S. Zwier, *J. Am. Chem. Soc.*, 124, 10236-10247, **2002**.
- [10] P. D. Godfrey, R. D. Brown, *J. Am. Chem. Soc.*, 12, 10724-10732, **1998**.
- [11] W. Caminati, A. Millemaggi, J. L. Alonso, A. Lesarri, J. C. Lopez, S. Mata, *Chem. Phys. Lett.*, 392, 1-6, **2004**.
- [12] U. Andresen, H. Dreizler, J. U. Grabow, W. Stahl, *Rev. Sci. Instrum.*, 61, 3694-3699, **1990**.
- [13] J. U. Grabow, W. Stahl, H. Dreizler, *Rev. Sci. Instrum.*, 67, 4072-4084, **1996**.
- [14] J. Alonso, F. J. Lorenzo, J. C. López, A. Lesarri, S. Mata, H. Dreizler, *Chem. Phys.*, 218, 267-275, **1997**.
- [15] R.D. Brown, J.G. Crofts, P.D. Godfrey, D. McNaughton and A.P. Pierlot, *J. Mol. Struct.*, 190, 185, **1988**.
- [16] S. Melandri, W. Caminati, L.B. Favero, A. Millemaggi, P.G. Favero, *J. Mol. Struct.*, 352/353, 253-258, **1995**.
- [17] S. Melandri, G. Maccaferri, A. Maris, A. Millemaggi, W. Caminati, P.G. Favero, *Chem. Phys. Lett.*, 261, 267-271, **1996**.

ANETHOLE

4.1 Introduction

Essential oils are complex mixtures of volatile compounds of low molecular weight extracted from plants by steam distillation and various solvents. They are one of the important products of agriculture based industry and they are commonly used as flavouring agents in food products, drinks, perfumeries, pharmaceuticals and cosmetics.^[1] Concerning pharmaceutical uses, these compounds are prescribed for a variety of health problems by traditional medicine, all over the world. Various pharmaceutical and biological activities like antibacterial, antifungal, anticancer, antimutagenic, antidiabetic, antiviral, antiinflammatory, and antiprotozoal properties are assigned to them.

Anethole (1-methoxy-4-(1-propenyl)benzene) is a natural constituent of essential oils of many plants such as the spice star anise (*Illicium verum* Hook. f., Illiciaceae), see Figure 4.1. This compound was found to have antioxidant, antibacterial, antifungal, and anesthetic properties.^[2-5] Moreover, anethole is able to inhibit pathogens that contaminate food and can be used for food preservation^[6]; it was also reported to be nongenotoxic and noncarcinogenic.^[7]



Figure 4.1 - Sketch of the structure of anethole and on the background images of the seeds of the star anise plant.

Anethole exists in two isomeric forms: *E* and *Z* depending on the relative position of the methyl group about the propenyl C=C bond. The *E* form is the most abundant isomer, indeed plants synthesize this isomer almost exclusively. Therefore, the desired odour and taste of anethole are properties of the *E* isomer, while the *Z* form is toxic and possesses an unpleasant scent and

flavour.^[8] For this reason the current spectroscopic study will focus on the *E* isomer of anethole (*E*-An), in order to analyze structural and dynamical properties of this molecule. Rotational spectroscopy techniques present the necessary high resolution required for identification and characterization of different conformations of this compound and the possible low amplitude motions that can be present.

The *E*-An isomer presents two different possible conformations depending on the orientation of the methyl of the methoxy group, as shown later. The presence of two methyl torsions can arise to different internal rotation motions which could complicate the assignment of the rotational spectrum. Considering the properties of a similar compound, estragole (1-allyl-4-methoxybenzene), studied by P.D. Godfrey *et al.*^[9] with rotational spectroscopy technique, it can be asserted that the methoxy torsion is probably also in our case not noticeable. Estragole in fact presents only the methoxy group that could give rise to internal rotation but its rotational spectrum appears free of internal rotation motions effects.

Taking into consideration other kind of spectroscopic studies, many articles were reported on the anethole compound in recent years. In particular a jet-cooled fluorescence spectroscopy study^[10], a matrix isolation infrared spectra study^[11] and a FT-IR, FT-Raman and UV spectroscopic investigation^[12] published only in the last years. In the first two studies two different conformations of the *E* isomer were observed and in the matrix isolation FT-IR study the isomerization between *E* and *Z* isomers was triggered by irradiation with ultraviolet-tunable laser. In the last study presented by L. Sinha *et al.*, a combined experimental and theoretical spectroscopic analysis of *E*-An was carried out and the authors conclude that the high intramolecular hyper-conjugative interaction around the ring can induce the large bioactivity in the compound. Certainly these studies are evidence that this natural occurring molecule still arouses much interest and the lack of a rotational spectroscopy study moves us to fill this gap.

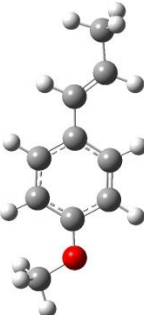
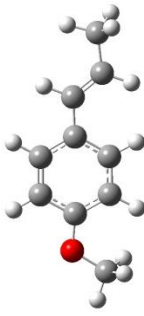
4.2 Theoretical calculations

Based also on the other works (see ref. 10, 11, 12), it is clear that the *E*-An isomer is described by two different conformations: *syn* and *anti* depending on the relative position of the methoxy and the propenyl groups. We can have the *syn* conformation if they lie on the same side with respect to a plane perpendicular to the aromatic ring and the *anti* if they lie on opposite sides (see images in Table 4.1).

In order to obtain a good description of the conformations of *E*-An, different methods and basis sets were used. In particular, calculations were performed with MP2 and B3LYP methods with the 6-

311++G** basis set. In addition, other calculations with the B3LYP method were carried out also with the cc-pVTZ basis set; for the MP2 method this was not possible because of the computational cost.

Table 4.1 - Calculated spectroscopic parameters and shape of the two stable conformations of *E*-An.

	<i>E-anti</i>			<i>E-syn</i>		
						
	MP2	B3LYP	B3LYP	MP2	B3LYP	B3LYP
	6-311++G**	6-311++G**	cc-pVTZ	6-311++G**	6-311++G**	cc-pVTZ
<i>A</i> /MHz	4359.3	4516.3	4539.5	3812.0	3962.0	3985.2
<i>B</i> /MHz	459.1	454.5	456.6	471.0	464.9	467.0
<i>C</i> /MHz	420.4	415.1	417.1	424.4	418.3	420.2
<i>D_K</i> /kHz	3.38	0.61	0.62	3.53	1.92	1.94
μ_a /D	0.39	0.56	0.67	-0.13	-0.31	-0.44
μ_b /D	1.12	1.06	-0.92	-1.43	-1.44	1.31
μ_c /D	-0.15	0.00	0.00	0.02	0.00	0.00
μ_{tot} /D	1.19	1.20	1.14	1.43	1.47	1.38
ΔE /kJ·mol ⁻¹	0.23	0 ^a	0 ^b	0 ^c	0.92	0.75
ΔE_{θ} /kJ·mol ⁻¹	0.25	0 ^d	0 ^e	0 ^f	0.79	0.67
V_3^g /kJ·mol ⁻¹	10.26	8.02	8.05		7.76	8.02

^a Absolute energy value: -463.616631 Hartrees.

^b Absolute energy value: -463.659571 Hartrees.

^c Absolute energy value: -462.223083 Hartrees.

^d Absolute energy value: -463.423821 Hartrees.

^e Absolute energy value: -463.466261 Hartrees.

^f Absolute energy value: -462.029632 Hartrees.

^g Barrier to internal rotation for the methyl propenyl group.

All the spectroscopic parameters useful for the conformational search of the two conformers were obtained from the optimizations and they are reported in Table 4.1. It can be noted that only the distortion constant D_K is given because the values of all the other quartic centrifugal distortion constants were close to zero.

Vibrational frequency calculations of the two optimized structures were performed in the harmonic approximation to check whether all of those are real minima. Moreover, to determine the barrier of the internal rotation of the propenyl methyl group, further calculations on the transition states for both conformers were carried out with the same methods and basis sets used for the minimizations. The values of the V_3 barrier are shown in Table 4.1.

From the data reported, it can be noted that the two different methods give rise to different results about the relative energy of the two conformers *E-syn* and *E-anti*. In fact, if no significant differences appear between DFT calculations made with different bases sets which give the *E-anti* conformer the global minimum, concerning the MP2 ones the situation is reversed: the *E-syn* conformer is predicted to be the most stable one.

Since both *E* conformers of anethole have substantially very close energies, the possibility to observe both is quite real and relaxations effect are not expected because of the high values of the barriers separating the conformers. In particular, as already mentioned in ref. 11, the energy barrier associated with the methoxy torsion is about $10.5 \text{ kJ}\cdot\text{mol}^{-1}$; in turn barrier associated with the changes in the relative orientation of the propenyl moiety (driven by the torsion about the bond between the C of the benzene ring and the first C of the propenyl chain) is predicted to require a relatively higher energy (about $16 \text{ kJ}\cdot\text{mol}^{-1}$).

All calculations were performed with the Gaussian09-D.01 program package.^[13]

4.3 Experimental Results and Analysis

The millimeter-wave spectrum (59.6-74.4 GHz) of *E*-An was recorded using the Free-Jet Absorption MilliMeter Wave spectrometer (FJAMMW - VDI setup), the basic design of which has been described previously (see Chapter 3). *E*-An was purchased from Sigma Aldrich (99%) and used without further purification. The compound was vaporized at a temperature of 80°C in a stream of argon at a pressure of *ca.* 20 kPa and expanded to about 0.05 kPa through a 0.35 mm diameter nozzle, held 5°C above the vaporization temperature. Under these conditions, the post-expansion rotational temperature was about 10 K and no evidence of thermal decomposition was observed. An electric field of 750 V cm^{-1} was used to maximize the degree of Stark modulation.

As already mentioned, theoretical calculations suggest the two conformations of the *E*-An (*E*-*syn* and *E*-*anti*) to be enough populated to allow detection in the jet plume (especially considering their predicted μ_b dipole moment components shown in Table 4.1). For this reason the first search has been targeted to the μ_b -R-branch.

The jet-cooled rotational spectrum showed the presence of a characteristic pattern of lines that formed a triplet: the first line is always more separated from the doublets which consisted of one more intense line (at lower frequencies) and the second one with the same intensity of the first line of the triplet (see Figure 4.2 : the assignment reported in the figures will become clear after the following paragraph). All the transitions observed for *E*-An conformers present this same pattern of lines due to the presence of the internal rotation of the methyl of the propenyl group, as described below.

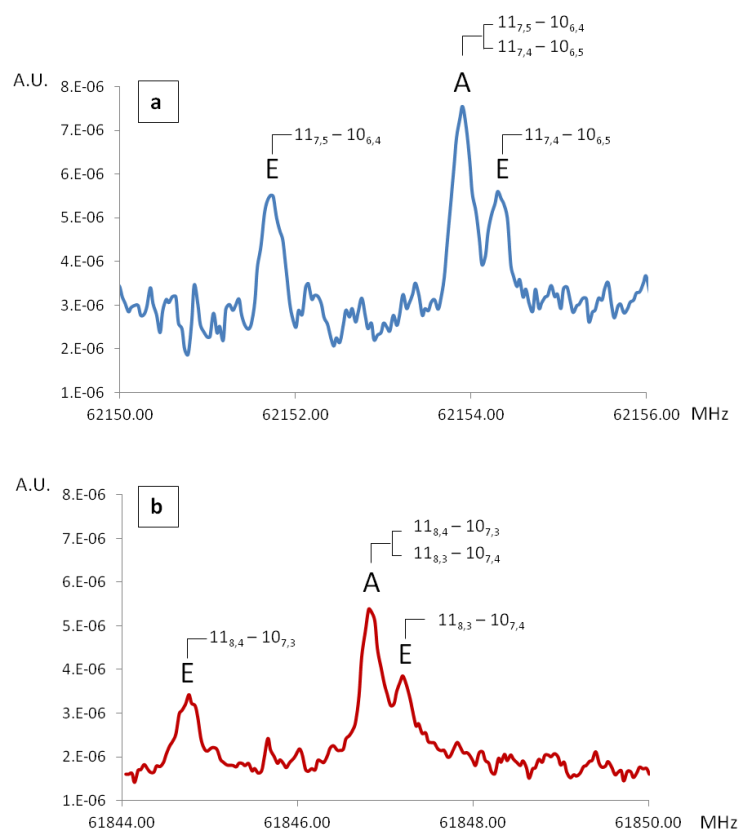


Figure 4.2 - a) The $11_7 - 10_6$ rotational transition of *E*-An *anti* conformer (blue spectrum) showing the splitting for the internal rotation of the propenyl methyl group. The A lines result from the coalescing of two transition: $11_{7,5} - 10_{6,4}$ and $11_{7,4} - 10_{6,5}$. b) The $11_8 - 10_7$ rotational transition of *E*-An *syn* conformer (red spectrum) showing the splitting for the internal rotation of the propenyl methyl group. The A lines result from the coalescing of two transition: $11_{8,4} - 10_{7,3}$ and $11_{8,3} - 10_{7,4}$. From the different signal-to-noise ratio, the intensity difference between the two conformers can also be appreciated.

Preliminary trial predictions of the rotational spectra were based on the rotational constants of Table 4.1 and the assignment of the transitions were carried out starting from the most intense lines appearing in the first scan recorded in a low resolution mode.

More precisely, the first series of assigned lines was the K_a equal 7, starting from J equal 9 up to J 20. As already said, the transition pattern was made of three lines and the assignment was possible looking at the predictions including the internal rotation of the methyl group of the propenyl moiety, performed with the XIAM program.^[14-17]

In this way, as shown in Figure 4.2a for the $11_7 - 10_6$ transition, the assignment was carried out: the most intense line is the result of the coalescing of two μ_b R-type A-symmetry ($11_{7,5}-10_{6,4}$ and $11_{7,4}-10_{6,5}$) overlapped rotational transitions and the other two lines are the corresponding E symmetry transitions (the one at lower frequency is the $11_{7,5}-10_{6,4}$ and the upper one is the corresponding E type $11_{7,4}-10_{6,5}$).

It was then possible to measure transitions with K_a equal 8 (J from 8 to 12) and K_a equal 6 (with J from 27 up to 29, this last transition is the first one that presents the asymmetry splitting). The lines observed in the quick scan were then recorded again at higher resolution.

Subsequently, a more accurate search was performed recording a slower and higher resolution scan. In this way a second series of unassigned lines appears, with the same triplet pattern which were analyzed similarly to the previous one (see Figure 4.2b). Also in this case the first series of μ_b -lines assigned was the K_a equal 7, with high J (from 17 up to 28). It was then possible to measure transitions with K_a equal 6, 8 and 9 (with J from 9 up to 26).

The fits were done using XIAM program in order to analyze the experimental internal rotation splitting. XIAM is a program using the Internal Axis Method (IAM) given by Woods,^[14-17] which treats simultaneously the semi-rigid rotational Hamiltonian and the internal rotation. In cases of sufficient experimental data the analysis of the internal rotation specifically provides the barrier to internal rotation (V_3), the inertial moment of the internal top (I_a) and the orientation of the internal top in the principal inertial axes, given by the three angles between each principal axis and the internal rotation axis ($\alpha(i,g)$, $g=a, b, c$). In this case only the barrier to internal rotation has been obtained and the other structural parameters were derived from the B3LYP calculated structures and maintained fixed (F_0 : 160.234 GHz = $1/I_a$; and δ : 0.26 rad, the angle between internal rotation axis and the principal inertial axis a).

The transition frequencies were fitted using Watson's semirigid Hamiltonian in the "S" reduction and I^r representation,^[18] obtaining the spectroscopic parameters (rotational constants, centrifugal distortion constant D_K and the V_3 barrier) shown in Table 4.2.

Based on the rotational constants obtained from the calculations, the two observed species were assigned to conformer *E-anti* the first one and *E-syn* the last one. All the measured frequencies for the *E-anti* and *E-syn* conformers are listed in Tables 4.3 and 4.4, respectively.

Table 4.2 - Experimental rotational constants (*A*, *B*, *C*), D_K centrifugal distortion constant and barrier V_3 of the internal rotation of the propenyl methyl group for conformers *E-anti* and *E-syn*.

	<i>E-anti</i>	<i>E-syn</i>
<i>A</i> /MHz	4478.059(5) ^a	3915.566(4)
<i>B</i> /MHz	457.668(5)	468.833(4)
<i>C</i> /MHz	417.702(4)	421.288(3)
D_K /kHz	0.80(4)	1.84(2)
V_3 /kJ·mol ⁻¹	7.057(5)	6.952(4)
σ^b /MHz	0.04	0.04
N^c	78	120

^a Error in parentheses in units of the last digit.

^b Root-mean-square deviation of the fit.

^c Number of lines in the fit.

Looking at the experimental values obtained for the V_3 barrier ($V_3^{E-anti} = 7.057(5)$ kJ·mol⁻¹ ; $V_3^{E-syn} = 6.952(4)$ kJ·mol⁻¹), it can be noted that the data are in good agreement with the theoretical ones expressed in Table 4.1, in particular the B3LYP values are closer to the experimental ones. These experimental data can be also compared with other similar compounds presenting the same propenyl group, as *Z*- and *E*-1-Propenyl Isocyanide studied by S. Samdal *et al.*^[19] In this rotational spectroscopy work the V_3 barrier to the internal rotation of the methyl group was observed and fitted for the *Z* isomer (4.0124(12) kJ·mol⁻¹) instead concerning the *E* isomer no internal rotation splitting of the rotational transitions was observed. The authors, knowing the resolution limit of their spectrometer, estimated a lower limit of the internal rotation barrier of about 6 kJ·mol⁻¹. The barrier to internal rotation is therefore much higher in the *E* conformer than in *Z*-1-Propenyl Isocyanide. Looking at the comparison made in this work with other methyl group barriers of *E* and *Z* isomers of some substituted propene's compounds, it can be noted that the values obtained for the *E*-An conformers are in agreement with the experimental values reported for other *E* isomers (the closest value is the one of the *trans* 3-penten-1-yne: 7.96(21) kJ·mol⁻¹).

Regarding *E*-An, V.P. Barber *et al.* in ref. 10 fitted an overall barrier height for both conformers *E-anti* and *E-syn* of 7.45 kJ·mol⁻¹, their value is in agreement with our more precise values obtained from direct measurements of the internal rotation splitting for each conformer.

To obtain information about the relative energies related abundances of the detected conformers in the supersonic jet, relative intensities (I) measurements of the rotational transitions were performed. This can be done because there is a direct relation between the intensities and the population of each conformer in the jet (N_i). The relation between them also includes the square of the values of the dipole moment component involved along each axis (μ_g) according to the following expression:

$$\frac{N_i}{N_0} \propto \frac{I_i \omega_0 \Delta v_i \mu_g^2(0) \lambda_0 v_0^2}{I_0 \omega_i \Delta v_0 \mu_g^2(i) \lambda_i v_i^2} \propto \frac{I_i}{I_0} \cdot \frac{\mu_g^2(0)}{\mu_g^2(i)}$$

where ω is the conformational degeneration, Δv the line width at half height and γ the line strength.^[20] In this way, if the transition intensities are well-known for the different conformers, it is possible to estimate the abundance of each conformer respect to another one or to the most stable one. It is important to remark that this analysis assumes that only the ground vibrational state of each conformer is populated during the supersonic expansion and that there is no conformational relaxation between conformers, as occurs in the present study.

Another important fact is that the calculation of relative intensities strongly depends on several experimental factors, so for sure this is an approximate method.

Because of the low intensity of the lines, mainly for the second assigned species, the *E-syn* conformer, only four μ_b -type transitions could be used for this purpose. For each species two lines lying in the same frequency region, have been recorded in the same experimental conditions in order to minimize the experimental errors. In particular for each pattern of transitions, the area of the closest doublet A-E were considered as intensity value (product of $I_i \Delta v_i$). According to the intensity ratio of the transition lines normalized by the calculated dipole moment components, the population ratio of the *E-syn* conformer to the *E-anti* one in the supersonic expansion is about 0.5. If we assume no conformational cooling effect, the energy difference between them can be estimated to be 2 kJ·mol⁻¹. Although the error on the approximated energies can be estimates to be up to 30% taking into account the uncertainties on the calculated dipole moment components and on the experimental measurements, this value confirms the fact that the *E-anti* conformer is the global minimum. This result is in agreement with the DFT calculations, while the reverse result is obtained from MP2. This order of stability between the two conformer was also evaluated from V.P. Barber *et al.* in ref. 10.

4.4 Conclusions

The rotational spectra of the two conformers of *E*-An have been assigned in the free jet broadband millimeter-wave spectrum (59.6-74.4 GHz). From comparison between the precise sets of spectroscopic data, including rotational constants and the centrifugal distortion constant D_K to the calculated ones, and from relative intensity measurements, it is possible to affirm that the global minimum is the *E-anti* form which the most intense spectrum belongs rather than the lower intensity spectrum that belongs to the less stable *E-syn* conformer, as shown in Figure 4.2. This rotational spectroscopy study allowed us to reach a complete picture of the *E*-An compound, analyzing all its possible stable conformations and obtaining experimental values of the V_3 barrier to the internal rotation of the methyl of the propenyl group, for both conformers. In this way the lack of such a kind of high resolution rotational spectroscopy study for this molecule has been filled. The rotational spectra showed that in the isolated conditions the global minimum is represented by the *E-anti* conformer and this result can be used as benchmark to theoretical calculations. In this case the experimental estimation is consistent with the B3LYP calculations rather than the MP2 ones.

4.5 References

- [1] J. S. Raut, S. M. Karuppaiyil, *Industrial Crops and Product*, 62, 250-264, **2014**, and refs. within.
- [2] R. S. Freire, S. M. Morais, F. E. A. Catunda-Junior, D. C. S. N. Pinheiro, *Bioorg. Med. Chem.*, 13, 4353, **2005**.
- [3] M. J. Mohammed, *J. Pharm. Res.*, 2, 915, **2009**.
- [4] A. A. Shahat, A. Y. Ibrahim, S. F. Hendawy, E. A. Omer, F. M. Hammouda, F. H. Abdel-Rahman, M. A. Saleh, *Molecules*, 16, 1366, **2011**.
- [5] T. P. Domiciano, M. M. D. Dalalio, E. L. Silva, A. M. V. Ritter, C. F. Estevão-Silva, F. S. Ramos, S. M. Caparroz-Assef, R. K. N. Cuman, C. A. Bersani-Amado, *Naunyn-Schmiedeberg's Arch. Pharmacol.*, 386, 331, **2013**.
- [6] O. F. Curtis, K. Shetty, G. Cassagnol, M. Peleg, *Food Biotechnology*, 10(1), 55–73, **1996**.
- [7] S. S. Yea, H. S. Jeong, C. Y. Choi, K. R. Park, S. Oh, J. G. Shin, *et al.*, 20(7), 1098–1105, **2006**.
- [8] R. L. Smith, S. M. Cohen, J. Doull, V. J. Feron, J. I. Goodman, L. J. Marnett, I. C. Munro, P. S. Portoghese, W. J. Waddell, B. M. Wagner, T. B. Adams, *Food Chem. Toxicol.*, 43, 1141, **2005**.
- [9] P. D. Godfrey, D. McNaughton, C. J. Evans, *Chem. Phys. Lett.*, 580, 37-42, **2013**.
- [10] V. P. Barber, J. J. Newby, *J. Phys. Chem. A*, 117, 12831-12841, **2013**.
- [11] J. Krupa, M. Wierzejewska, C. M. Nunes, R. Fausto, *J. Chem. Phys.*, 140, 105102, **2014**.
- [12] L. Sinha, O. Prasad, S. Chand, A. K. Sachan, S. K. Pathak, V. K. Shukla, M. Karabacak, A. M. Asiri, *Spectrochimica Acta A*, 133, 165-177, **2014**.
- [13] M. J. Frisch, G. W. Trucks, H. B. Schlegel, G. E. Scuseria, M. A. Robb, J. R. Cheeseman, G. Scalmani, V. Barone, B. Mennucci, G. A. Petersson, H. Nakatsuji, M. L. Caricato, X.; Hratchian, H. P.; Izmaylov, A. F.; Bloino, J.; Zheng, G.; Sonnenberg, J. L.; Hada, M.; Ehara, M.; Toyota, K.; Fukuda, R.; Hasegawa, J.; Ishida, M.; Nakajima, T.; Honda, Y.; Kitao, O.; Nakai, H.; Vreven, T.; Montgomery, J. A.; J. E. J. Peralta, F. B. Ogliaro, M.; Heyd, J. J.; Brothers, E.; Kudin, K. N.; Staroverov, V. N.; Kobayashi, R.; Normand, J.; Raghavachari, K.; Rendell, A.; Burant, J. C.; Iyengar, S. S.; Tomasi, J.; Cossi, M.; Rega, N.; Millam, J. M.; Klene, M.; Knox, J. E.; J. B. Cross, V. A. Bakken, C.; Jaramillo, J.; Gomperts, R.; Stratmann, R. E.; Yazyev, O.; Austin, A. J.; Cammi, R.; Pomelli, C.; Ochterski, J. W.; Martin, R. L.; Morokuma, K.; Zakrzewski, V. G.; Voth, G. A.; Salvador, P.; Dannenberg, J. J.; Dapprich, S.; A. D. Daniels, Ö. F. Farkas, J. B.; Ortiz, J. V.; Cioslowski, J.; Fox, D. J., Gaussian, Inc., Wallingford CT, **2009**.
- [14] H. Hartwing, H. Dreizler, *Z. Naturforsch., A: Phys. Sci.*, 51, 923, **1996**.
- [15] R. C. Woods, *J. Mol. Spectrosc.*, 21, 4, **1966**.
- [16] R. C. Woods, *J. Mol. Spectrosc.*, 22, 49, **1967**.

- [17] K. N. Rao, C. W. Mathews, in 'Molecular spectroscopy: modern research', New York, **1972**.
- [18] J. K. G. Watson, "Vibrational spectra and structure", Vol. 6, Elsevier, Amsterdam, Oxford & New York, **1977**.
- [19] S. Samdal, H. Møllendal, J. C. Guillemin, *J. Phys. Chem. A*, 116, 8833-8839, **2012**.
- [20] J.-U. Grabow, W. Caminati, *Microwave Spectroscopy: Experimental Techniques*. In *Frontiers of Molecular Spectroscopy*; Laane, J., Ed.; Elsevier: Amsterdam, The Netherlands, , Chapter 14, 383-454, **2008**.

4.6 Appendix

Table 4.3 - Measured frequencies (MHz) for the transitions observed for *E*-An *anti* conformer.

J'	K_a'	K_c'	J''	K_a''	K_c''	Sym.	$\nu_{\text{OBS}}/\text{MHz}$	$\Delta\nu_{\text{OBS-CALC}}/\text{MHz}$
8	8	1	7	7	0	E	67605.74	0.06
						A		
8	8	0	7	7	1	A	67607.89	-0.03
						E	67608.08	-0.11
9	8	2	8	7	1	E	68481.11	-0.03
						A		
9	8	1	8	7	2	A	68483.36	-0.02
						E	68483.71	0.05
10	8	3	9	7	2	E	69356.55	-0.04
						A		
10	8	2	9	7	3	A	69358.86	0.03
						E	69359.10	-0.01
11	8	4	10	7	3	E	70232.04	0.01
						A		
11	8	3	10	7	4	A	70234.30	0.03
						E	70234.52	-0.02
12	8	5	11	7	4	E	71107.43	0.00
						A		
12	8	4	11	7	5	A	71109.70	0.03
						E	71109.99	0.04
9	7	3	8	6	2	E	60400.90	-0.05
						A		
9	7	2	8	6	3	A	60403.10	0.00
						E	60403.53	0.01
10	7	4	9	6	3	E	61276.40	0.03
						A		
10	7	3	9	6	4	A	61278.53	0.01
						E	61278.94	0.00
11	7	5	10	6	4	E	62151.72	-0.03
						A		
11	7	4	10	6	5	A	62153.90	0.01
						E	62154.31	-0.01
12	7	6	11	6	5	E	63027.07	0.00
						A		
12	7	5	11	6	6	A	63029.22	0.01
						E	63029.69	0.05
13	7	7	12	6	6	E	63902.30	-0.01
						A		
13	7	6	12	6	7	A	63904.46	0.01

Chapter 4 - ANETHOLE

J'	K_a'	K_c'	J''	K_a''	K_c''	Sym.	$\nu_{\text{OBS}}/\text{MHz}$	$\Delta\nu_{\text{OBS-CALC}}/\text{MHz}$
						E	63904.88	0.00
14	7	8	13	6	7	E	64777.47	0.02
						A		
14	7	7	13	6	8	A	64779.62	0.02
						E	64780.03	0.01
15	7	9	14	6	8	E	65652.46	-0.01
						A		
15	7	8	14	6	9	A	65654.62	0.00
						E	65655.05	0.01
16	7	10	15	6	9	E	66527.34	0.00
						A		
16	7	9	15	6	10	A	66529.45	-0.04
						E	66529.95	0.04
17	7	11	16	6	10	E	67402.02	-0.01
						A		
17	7	10	16	6	11	A	67404.20	0.02
						E	67404.53	-0.08
18	7	12	17	6	11	E	68276.60	0.08
						A		
18	7	11	17	6	12	A	68278.62	-0.05
						E	68279.07	-0.02
19	7	13	18	6	12	E	69150.73	-0.03
						A		
19	7	12	18	6	13	A	69152.86	-0.05
						E	69153.30	-0.04
20	7	14	19	6	13	E	70024.76	0.03
						A		
20	7	13	19	6	14	A	70026.89	0.01
						E	70027.35	0.04
27	6	22	26	5	21	E	68025.70	-0.01
						A	68027.38	0.05
27	6	21	26	5	22	A	68028.27	0.11
						E		
28	6	23	27	5	22	E	68891.48	-0.02
						A	68892.95	0.03
28	6	22	27	5	23	A	68894.15	0.02
						E		
29	6	24	28	5	24	A	69758.81	-0.05
29	6	23	28	5	23	A	69757.15	-0.08

Table 4.4 - Measured frequencies (MHz) for the transitions observed for *E*-An *syn* conformer.

J'	Ka'	Kc'	J''	Ka''	Kc''	Sym.	$\nu_{\text{OBS}}/\text{MHz}$	$\Delta\nu_{\text{OBS-CALC}}/\text{MHz}$
9	9	1	8	8	0	E	67003.64	-0.05
						A		
9	9	0	8	8	1	A	67005.88	0.02
						E	67006.10	-0.01
10	9	2	9	8	1	E	67893.89	-0.07
						A		
10	9	1	9	8	2	A	67896.16	0.02
11	9	3	10	8	2	E	68784.16	-0.07
						A		
11	9	2	10	8	3	A	68786.42	0.02
12	9	4	11	8	3	E	69674.39	-0.08
						A		
12	9	3	11	8	4	A	69676.59	-0.05
						E	69676.84	-0.05
13	9	5	12	8	4	E	70564.67	0.00
						A		
13	9	4	12	8	5	A	70566.91	0.06
17	7	11	16	6	10	E	60242.31	-0.04
						A		
17	7	10	16	6	11	A	60244.36	0.01
						E	60244.86	-0.01
18	7	12	17	6	11	E	61131.05	0.04
						A		
18	7	11	17	6	12	A	61133.03	0.01
						E	61133.52	-0.01
19	7	13	18	6	12	E	62019.24	-0.04
						A		
19	7	12	18	6	13	A	62021.27	-0.01
						E	62021.77	-0.03
20	7	14	19	6	13	E	62907.07	-0.02
						A		
20	7	13	19	6	14	A	62909.10	0.01
						E	62909.55	-0.06
21	7	15	20	6	14	E	63794.41	0.03
						A		
21	7	14	20	6	15	A	63796.36	-0.03
						E	63796.88	-0.02
22	7	16	21	6	15	E	64681.10	0.01
						A		
22	7	15	21	6	16	A	64683.06	-0.03
						E	64683.58	-0.03

Chapter 4 - ANETHOLE

J'	Ka'	Kc'	J''	Ka''	Kc''	Sym.	V_{OBS}/MHz	$\Delta V_{OBS-CALC}/\text{MHz}$
23	7	17	22	6	16	E	65567.12	-0.02
						A		
23	7	16	22	6	17	A	65569.13	-0.01
						E	65569.66	0.00
24	7	18	23	6	17	E	66452.46	0.00
						A		
24	7	17	23	6	18	A	66454.47	0.01
						E	66454.95	-0.04
25	7	19	24	6	18	E	67337.00	0.03
						A		
25	7	18	24	6	19	A	67338.99	0.02
						E	67339.59	0.09
26	7	20	25	6	19	E	68220.62	0.03
						A		
26	7	19	25	6	20	A	68222.64	0.06
						E	68223.15	0.03
27	7	21	26	6	20	E	69103.26	0.03
						A		
27	7	20	26	6	21	A	69105.28	0.08
						E	69105.76	0.00
28	7	22	27	6	21	A	69986.83	0.09
28	7	21	27	6	22	A	69987.37	0.04
						E		
9	8	2	8	7	1	E	60064.33	0.07
						A		
9	8	1	8	7	2	A	60066.39	0.04
						E	60066.75	0.02
10	8	3	9	7	2	E	60954.52	0.00
						A		
10	8	2	9	7	3	A	60956.63	0.02
						E	60956.95	-0.04
11	8	4	10	7	3	E	61844.75	0.01
						A		
11	8	3	10	7	4	A	61846.84	0.00
						E	61847.20	-0.02
12	8	5	11	7	4	E	62734.90	-0.02
						A		
12	8	4	11	7	5	A	62737.04	0.03
						E	62737.37	-0.02
13	8	6	12	7	5	E	63625.07	0.04
						A		
13	8	5	12	7	6	A	63627.15	0.03
						E	63627.46	-0.05

Chapter 4 - ANETHOLE

J'	Ka'	Kc'	J''	Ka''	Kc''	Sym.	$\nu_{\text{OBS}}/\text{MHz}$	$\Delta\nu_{\text{OBS-CALC}}/\text{MHz}$
14	8	7	13	7	6	E	64515.08	0.03
						A		
14	8	6	13	7	7	A	64517.15	0.00
						E	64517.49	-0.04
15	8	8	14	7	7	E	65405.00	0.04
						A		
15	8	7	14	7	8	A	65407.06	0.00
						E	65407.40	-0.04
16	8	9	15	7	8	E	66294.76	0.03
						A		
16	8	8	15	7	9	A	66296.82	-0.01
						E	66297.19	-0.02
17	8	10	16	7	9	E	67184.35	0.01
						A		
17	8	9	16	7	10	A	67186.44	0.01
						E	67186.85	0.04
18	8	11	17	7	10	E	68073.75	0.01
						A		
18	8	10	17	7	11	A	68075.85	0.01
						E	68076.17	-0.05
19	8	12	18	7	11	E	68962.93	0.01
						A		
19	8	11	18	7	12	A	68965.01	0.00
						E	68965.35	-0.04
20	8	13	19	7	12	E	69851.79	-0.03
						A		
20	8	12	19	7	13	A	69853.95	0.04
						E	69854.30	0.00
25	6	20	24	5	19	E	60367.10	-0.06
						A	60368.24	0.02
25	6	19	24	5	20	A	60369.78	-0.08
						E	60369.61	-0.03
26	6	21	25	5	20	E	61245.12	0.02
						A	61245.69	0.00
26	6	20	25	5	21	A	61248.09	-0.07
						E	61247.47	0.00

N-METHYLAMINOETHANOL

5.1 Introduction

Hydroxy and amino groups rank among the most important hydrogen-bond building blocks in nature.^[1] In particular, if they are separated by a backbone of two sp^3 carbon atoms, an interesting interplay between intra- and intermolecular hydrogen bonding is possible. The competition between these two types of interactions may be investigated in simple molecules bearing several H bonding sites such as aminoalcohols. These family of compounds present several interesting properties: from a biological point of view a lot of natural products contain aminoalcohol functionality, and from an astrochemical sight because the simplest aminoalcohols can be considered a precursors of aminoacids in the interstellar medium.^[2] Moreover, as reported by P. Ehrenfreund and S. B. Charnley^[3], the evaporation on ice mantles containing ammonia, as well as methanol and ethanol, could be the origin of the nitrogen-bearing organics that are seen in star-forming regions and maybe other larger analogs that have not yet been detected.

From the chemical point of view, the combination of donor and acceptor groups in these compounds is very interesting and results in the stabilization of molecular conformations involving intramolecular H bonding either of OH...N or NH...O type. For all the above reasons this family of molecules has been extensively studied both experimentally by microwave and IR spectroscopy as well as theoretically using different levels of calculation.^[4]

In this interesting family of molecules, the simplest prototype is 2-aminoethanol (AE), which has been deeply studied for the past 40 years with different kinds of experimental, theoretical and combined techniques.^[5] Certainly, spectroscopic analysis can lead to explore some of the boundaries and also get to the bottom of the chemical behavior of these compounds.

In this work the investigation on the effect of replacing one amino hydrogen by a methyl group is undertaken, studying the rotational spectrum in supersonic expansion of *N*-methylaminoethanol (MAE).

This molecule was already studied at room temperature by microwave spectroscopy,^[6] and two conformers were observed with a ground-state energy difference of $1.9 \text{ kJ}\cdot\text{mol}^{-1}$, obtained from relative intensity measurements.

The decision to investigate again the rotational spectrum of MAE is twofold: in the first place to extend the measurements to higher frequency values in order to cover the lack of experimental spectra in the millimeter wave region and thus getting closer to the frequencies of common radiotelescopes receivers. Secondly, because MAE is present as a side chain in important biological molecules such as adrenaline, and so a more detailed study can point out results that can better describe the interactions present in the isolated chain which can then be compared to the interactions present when MAE is linked to a catechol ring such as in adrenaline.

MAE is a linear molecule ($\text{CH}_2\text{-NH-CH}_2\text{-CH}_2\text{-OH}$), whose five skeleton atoms are sp^3 hybridized. Its conformation is described by three dihedral angles: $\tau_1 = \text{HOCC}$ that describes the torsion of the hydroxyl group; τ_2 for the OCCN skeletal torsion and τ_3 for the CCNC ones (as shown in Figure 5.1). The presence of all these possible torsions makes MAE a very flexible molecule characterized by a complex conformational landscape.

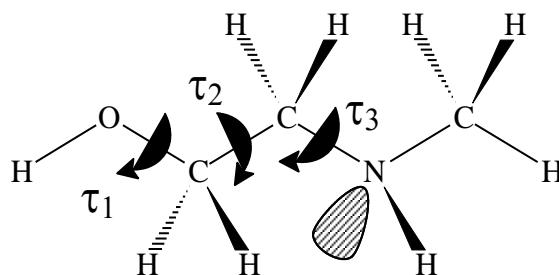


Figure 5.1 - Sketch of *N*-methylaminoethanol and its dihedral angles τ_1 , τ_2 , τ_3 describing its conformational space.

As already cited, various other works on MAE have been performed: in particular a jet-FTIR study,^[1] a fluorescence excitation, UV-UV and IR-UV depletion spectroscopy study^[4] and the previous microwave spectroscopy work.^[6] An initial approach to describe the intricate conformational space of MAE started from these works, where some conformational considerations and theoretical calculations were already done.

As it will be described below, the conformational analysis and the calculations on all the possible conformations were executed again with higher basis sets, in order to obtain all the spectroscopic and energy parameters needed to completely describe this system and drive the rotational spectroscopy search. In addition to the previous rotational study of R. E. Penn and L. W. Buxton^[6], this work improves the spectroscopic results including centrifugal distortion constants and quadrupole coupling constants in the fits and also measuring the rotational transitions for the

deuterated species for the global minimum, resulting in the substituted coordinates for the aminic and hydroxyl hydrogens.

5.2 Conformational Overview and Theoretical Calculations

As said above, the presence of the three dihedral angles τ_1 , τ_2 , τ_3 drive the orientation of the MAE chain to local minima and there is no doubt that intramolecular hydrogen bond interactions dominate the conformational preferences in this aminoalcohol.

Because of steric hindrance there are three possible staggered configurations for each dihedral angle: *gauche* at $\tau \approx 60^\circ$ (*G*), *trans* at $\tau \approx 180^\circ$ (*T*) and *gauche'* at $\tau \approx 300^\circ$ (*G'*).

Three available configurations for each of the three dihedral angles lead to $3^3=27$ different conformations, which can be labelled as $\tau_1\tau_2\tau_3$, where τ can be *G*, *T*, *G'*.

We use upper case letters for the skeletal orientations and lower case letters for the hydroxyl orientation: for each family described by the two skeletal torsion (upper case), three possible orientation of the hydroxyl group (lower case) are available.

In MAE, both the hydroxyl and the amino groups can act as hydrogen donor or hydrogen acceptor, but the preference of the amino group to act as hydrogen acceptor in this molecule is well documented by several studies.^[7-10] For this reason the more stable conformers should be those in which an interaction between the hydroxyl and the amino groups takes place to form an intramolecular hydrogen bond of the O-H...N type. Certainly, looking Table 5.1, it can be seen that when the OCCN frame is in *trans* configuration the hydroxyl and amino groups are too far to interact with each other. The interaction is also forbidden in the *GG'* and *G'G* type conformers, but it may take place in the *G'G'*, *GG*, *GT*, *G'T* forms. In particular, as illustrated in Table 5.1, the relative orientation of the groups allows for a NH...O interaction in the *G'G'* and *GT* forms and for a OH...N interaction in the *GG* and *G'T* conformers.

Table 5.1 - Newman projections of the different possible configurations of MAE respect each dihedral angle.

	T	G	G'
$\tau_1 = \text{HOCC}$			
$\tau_2 = \text{OCCN}$			
$\tau_3 = \text{CCNC}$			

To quantify these considerations free optimizations geometry were run for each of these 27 forms at the B3LYP and MP2/6-311++G** level of calculation but it was possible to optimize only 24 conformers with B3LYP method and 23 with the MP2 one. For all the optimized structures the vibrational frequency calculations were performed in the harmonic approximation to check whether all of those are real minima. All calculations were performed with the Gaussian03-B.01 program package.^[11]

Starting from the first family, $G'T$ (see Figure 5.2), the most stable conformer $gG'T$ represents the global minimum characterized by an intramolecular $\text{OH}\cdots\text{N}$ hydrogen bond. The conformational landscape of each family was explored changing the involved torsional angle (τ_1 in this case), by a step of 15° and all the other coordinates were freely optimized. This kind of scans were performed with the B3LYP method.

From the hydroxyl rotation surface shown in Figure 5.2, it can be seen that if the hydroxyl group is rotated in the *trans* orientation, the *tG'T* conformer is obtained, which lies to higher energy. In fact, depending on the position of the hydroxyl group, attractive interactions can be achieved if the hydroxyl hydrogen is directed towards the lone pair of the nitrogen, like in the global minimum *gG'T*; instead if it is the oxygen which directed towards the lone pair of the nitrogen, the interactions are repulsive like in the *trans* conformer. The conformer *g'G'T* during the optimization collapsed onto the global minimum.

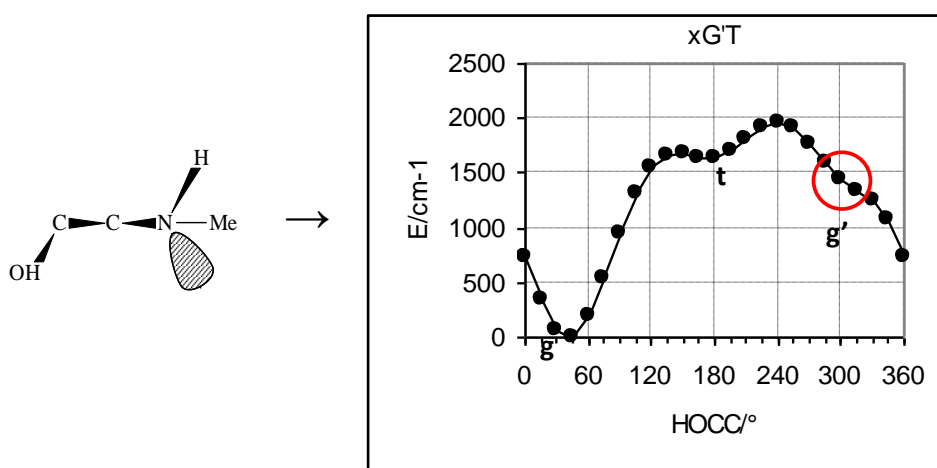


Figure 5.2 - General sketch of the *G'T* family of conformers and energy scan points made to describe the orientation of the hydroxyl group.

The same considerations can be done for the second family of conformers: the *GG* one, see Figure 5.3. The most stable conformation is the *g'GG* in which an intramolecular $\text{OH}\cdots\text{N}$ hydrogen bond can take place. To obtain the *tGG* conformer the hydroxyl group has to be rotated, but also in this *trans*-arrangement one of the oxygen atom lone pairs faces the lone pair of the nitrogen atom giving a repulsive interaction. For this reason the *tGG* conformer lies higher in energy in the B3LYP calculations, while it was not optimized with the MP2.

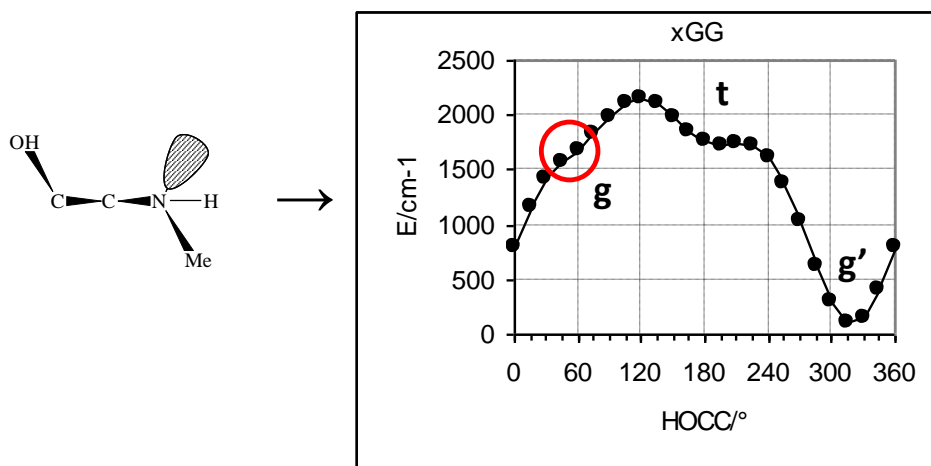


Figure 5.3 - General sketch of the *GG* family of conformers and energy scan points made to describe the orientation of the hydroxyl group.

In Table 5.2, the energy situation for these two family of MAE conformers was summarized. It can be noted that the two most stable conformations are *gG'T* and *g'GG* separated only by 1.22/0.46 kJ·mol⁻¹ for B3LYP/MP2 calculations respectively.

Table 5.2 - Shapes, relative energies (in kJ·mol⁻¹) and intramolecular hydrogen bond distance for the optimized conformers of *G'T* and *GG* families of MAE.

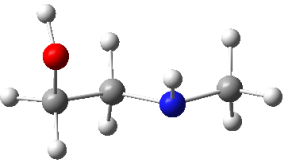
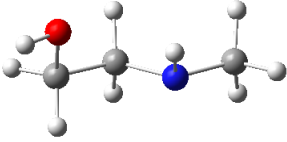
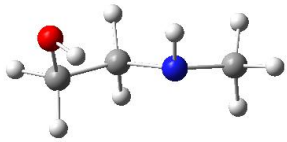
<i>gG'T</i> $d_{\text{OH-N}} = 2.303 \text{ \AA}$ $\Delta E = 0^a$	<i>g'GG</i> $d_{\text{OH-N}} = 2.266 \text{ \AA}$ $\Delta E = 1.22/0.46^b$	<i>tG'T</i> $d_{\text{O-N}} = 3.011 \text{ \AA}$ $\Delta E = 19.67/22.11$	<i>tGG</i> $d_{\text{O-N}} = 3.043 \text{ \AA}$ $\Delta E = 20.77/-$

^a Absolute energy value: B3LYP -249.778776308 Hartrees and MP2 -249.055609722 Hartrees.

^b The first value concerns the B3LYP calculation and the second one the MP2.

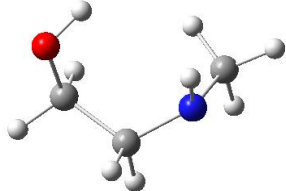
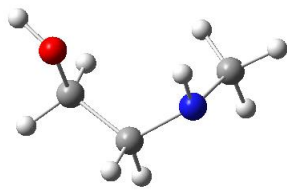
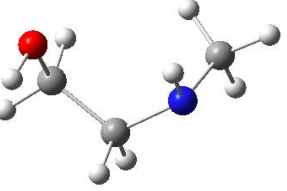
The calculations described above were also performed for all the other families of conformers: *GT*, *G'G'*, *TT*, *G'G*, *TG*, *TG'* and *GG'*. The results have shown that all the other conformations are higher in energy since they are characterized by weaker interactions. In Tables 5.3 and 5.4 the conformers of the families *GT* and *G'G'* are shown. They represent the most stable conformations after the *gG'T* and *g'GG* ones (already listed in Table 5.2).

Table 5.3 - Shapes, relative energies (in $\text{kJ}\cdot\text{mol}^{-1}$) and intramolecular hydrogen bond distance for the optimized conformers of *GT* family of MAE.

<i>gGT</i> $d_{\text{NH}\cdots\text{O}} = 2.515 \text{ \AA}$ $\Delta E = 6.97/7.24^a$	<i>tGT</i> $d_{\text{NH}\cdots\text{O}} = 2.461 \text{ \AA}$ $\Delta E = 5.49/4.57$	<i>g'GT</i> $d_{\text{NH}\cdots\text{O}} = 2.637 \text{ \AA}$ $\Delta E = 8.33/8.42$
		

^aThe first value concerns the B3LYP calculation and the second one the MP2.

Table 5.4 - Shapes, relative energies (in $\text{kJ}\cdot\text{mol}^{-1}$) and intramolecular hydrogen bond distance for the optimized conformers of *G'G'* family of MAE.

<i>gG'G'</i> $d_{\text{OH}\cdots\text{N}} = 2.877 \text{ \AA}$ $\Delta E = 15.19/14.32^a$	<i>tG'G'</i> $d_{\text{OH}\cdots\text{N}} = 2.606 \text{ \AA}$ $\Delta E = 11.35/10.17$	<i>g'G'G'</i> $d_{\text{OH}\cdots\text{N}} = 2.667 \text{ \AA}$ $\Delta E = 12.57/12.26$
		

^aThe first value concerns the B3LYP calculation and the second one the MP2.

Focusing on the data of Table 5.3 for the *GT* family, the relative energy of the three conformers falls in the 4.57-8.42 $\text{kJ}\cdot\text{mol}^{-1}$ range, and they are stabilized by weaker intramolecular $\text{NH}\cdots\text{O}$ hydrogen bonds. Regarding the *G'G'* family, shown in Table 5.4, the relative energy of this three conformations is higher because they are characterized by a longer and weaker $\text{OH}\cdots\text{N}$ hydrogen bond.

All the calculated barriers to the torsion of the $\tau_2=\text{OCCN}$ exceed the 6 $\text{kJ}\cdot\text{mol}^{-1}$ value.

Since the two most stable conformations, as already described in the previous papers,^[1,6] are *gG'T* and *g'GG* the spectroscopic analysis was centered on them and their calculated spectroscopic parameters are reported in Table 5.5.

Table 5.5 - Calculated spectroscopic parameters of the two most stable conformers of MAE (6-311++G**).

MAE	$gG'T$		$g'GG$	
	B3LYP	MP2	B3LYP	MP2
A/MHz	11917	11955	9295	9202
B/MHz	2652	2691	3004	3090
C/MHz	2394	2431	2807	2890
D_J/kHz	1.2	1.17	3.4	4.07
D_{JK}/kHz	-7.0	-8.43	-21.8	-27.07
D_K/kHz	66.0	68.25	68.7	78.44
d_1/kHz	-0.233	-0.22	-0.657	-0.80
d_2/kHz	-0.011	-0.01	-0.008	-0.02
μ_a/D	2.48	2.53	-2.80	-2.86
μ_b/D	1.46	1.60	1.34	1.44
μ_c/D	0.87	0.87	0.09	0.23
μ_{tot}/D	3.00	3.11	3.11	3.21
χ_{aa}/MHz	1.62	1.49	0.56	0.53
χ_{bb}/MHz	-3.86	-3.57	-2.75	-2.32
χ_{cc}/MHz	2.25	2.08	2.19	1.80
$\Delta E/\text{kJ mol}^{-1}$	0 ^a	0 ^b	1.22	0.46
$\Delta E_0/\text{kJ mol}^{-1}$	0 ^c	0 ^d	1.32	0.65

^a Absolute energy value: -249.778776308 Hartrees.

^b Absolute energy value: -249.055609722 Hartrees.

^c Absolute energy value: -249.652558 Hartrees.

^d Absolute energy value: -248.926849 Hartrees.

5.3 Experimental Results and Analysis

The millimeter-wave (59.6-74.4 GHz) spectrum of MAE was recorded using the Free-Jet Absorption MilliMeter Wave spectrometer (FJAMMW - VDI setup), where the basic design has been described previously (see Chapter 3). MAE was purchased from Sigma Aldrich (99%) and used without further purification. The compound was vaporized at a temperature of 40°C in a stream of helium at a pressure of 45 kPa and expanded to about 0.05 kPa through a 0.35mm diameter nozzle, held 5°C above the vaporization temperature. Under these conditions, the post-expansion rotational temperature was about 10 K and no evidence of thermal decomposition was observed. Electric fields of 750 V cm⁻¹ were used to maximize the degree of Stark modulation.

As mentioned before, MAE was already studied by R. E. Penn and L. W. Buxton (see ref. 6) in the 8-32 GHz frequency region with a 25 kHz Stark modulated microwave spectrometer, obtaining the sets of experimental rotational constants and the dipole moments components of the two most stable conformations $gG'T$ and $g'GG$; for convenience these data are reported in Table 5.6, as presented in the published article.

Table 5.6 - Experimental spectroscopic parameters obtained from R. E. Penn and L. W. Buxton^[6] for the two most stable conformers of MAE.

	$gG'T$	$g'GG$
A/MHz	12123.35(31)	8985.12(31)
B/MHz	2653.774(15)	3076.388(14)
C/MHz	2400.756(13)	2868.664(15)
μ_a/D	2.272(8)	2.610(11)
μ_b/D	1.336(20)	1.132(11)
μ_c/D	0.808(18)	0.331(34)
μ_{rot}/D	2.756(13)	2.364(11)

The recorded rotational spectrum showed different type of lines characterized by great intensity. If the prediction for the rotational transitions expected in the 59.6-74.4 GHz frequency range was based on the data already published, then the rotational transitions were fitted independently using Watson's semirigid Hamiltonian in the "S" reduction and I^r representation,^[12] obtaining the spectroscopic parameters (rotational constants, centrifugal distortion constants and quadrupole coupling constants) shown in Table 5.7.

Table 5.7 - Experimental spectroscopic constants of the two observed conformers of MAE obtained in this study.

	$g'T$	$g'GG$
A/MHz	12123.75(1) ^a	9155.319(6)
B/MHz	2653.774(3)	3076.312(4)
C/MHz	2400.772(3)	2868.655(4)
D_j/kHz	1.166(8)	4.36(1)
D_{JK}/kHz	-8.37(1)	-28.86(2)
D_K/kHz	71.0(5)	84.0(1)
d_1/kHz	-0.223(1)	-0.921(3)
d_2/kHz	-0.009(1)	
χ_{aa}/MHz	1.8(4)	[0.53] ^d
χ_{bb}/MHz	-3.48(8)	-2.15(8)
χ_{cc}/MHz	1.68(8)	1.62(8)
σ^b/MHz	0.07	0.06
N^c	121	61

^a Error in parentheses in units of the last digit.

^b Root-mean-square deviation of the fit.

^c Number of lines in the fit.

^d Value fixed to the MP2 calculation.

The rotational spectra showed μ_a -, μ_b - and μ_c -type R-branch transitions and also few μ_b - and μ_c -type Q-branch transitions for the $g'GG$ conformer. Some of these lines presented a resolved ^{14}N quadrupole structure, see Figure 5.4, that allow to determine the values of the quadrupole constants shown in Table 5.7; (Note: because of the lack of transitions resolved for quadrupole for the $g'GG$ conformer, only the quadrupole constants χ_{bb} and χ_{cc} were fitted, the value of χ_{aa} was maintained fixed to the obtained by MP2 calculation). All the new measured frequencies are listed in Tables 5.10 and 5.11. Comparing the results obtained in this work with the older ones, we can see that the centrifugal distortion constants are now determined for both conformers together with the quadrupole coupling constants. Moreover, it is clear that the rotational spectrum of the $g'GG$ conformer has been partly reassigned since the rotational constant A was not correctly fitted. For these reasons, the choice to investigate again this molecule has proved to be interesting and useful. If the assignment of both conformers was straightforward, the measurements and the obtaining of a good fit were more complicated (see standard deviations σ in Table 5.7). The presence of different transitions overlapped due to unresolvable quadrupole splitting and asymmetry splittings causes the lines to be particularly wide, mostly for the $K_a=3$ μ_b - and μ_c -type transitions, as shown and explained in Figure 5.5. Moreover the introduction in this molecule of a methyl group on the amino functionality with respect to AE, gives rise to an internal rotation motion for this CH_3 group, which

is here neglected. Certainly this effect can also contribute to the shape of the lines causing a further increase in the uncertainty of the frequency measurements.

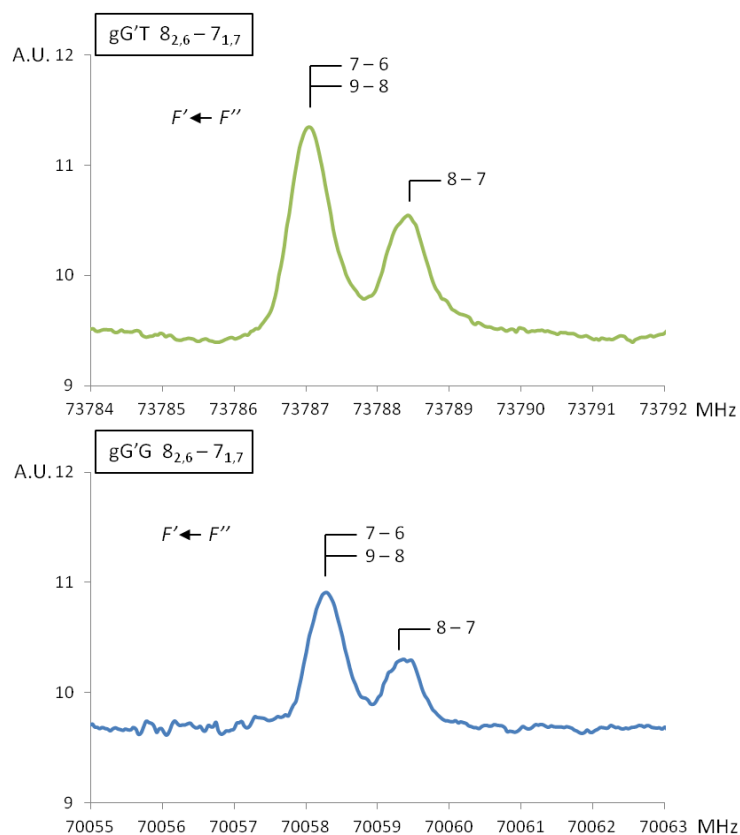


Figure 5.4 - Comparison between the $8_{2,6}-7_{1,7}$ μ_b -type rotational transitions of the two observed rotamers of MAE. In both cases the quadrupole hyperfine structure is resolved in two components because the most intense one results from the coalescing of the two transitions $F' \leftarrow F''$: $7 \leftarrow 6$ and $9 \leftarrow 8$.

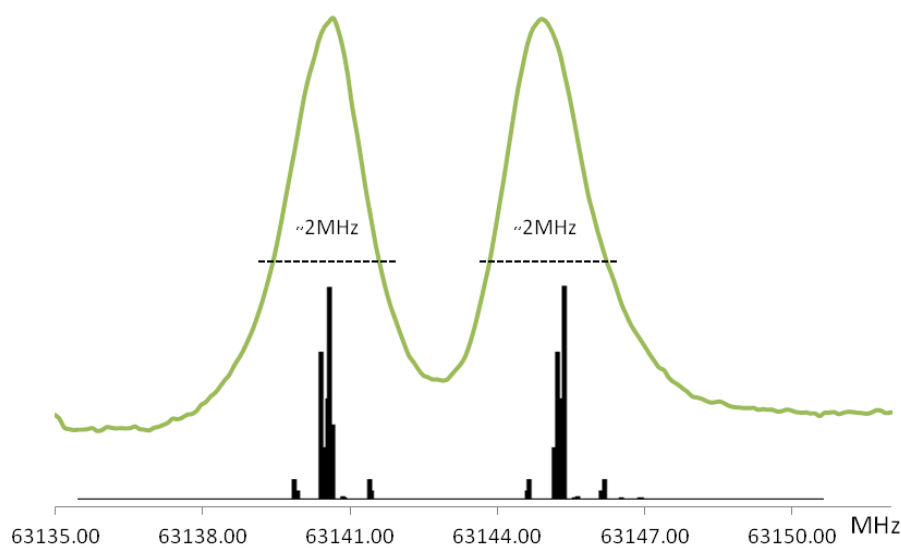


Figure 5.5 - Example of transition with $K_a = 3$ for the $gG'T$ conformer of MAE showing the shape and the FWHM of about 2 MHz of these lines due to the coalescing of many transitions (μ_b and μ_c -type transitions and hyperfine quadrupole splitting) as reported in the simulated spectrum in black, after the fit. The inability to resolve these transitions increases the uncertainty and the error in the fits.

A further study carried out in the present work was the analysis of the hydroxy and amino deuterated species for the global minimum $gG'T$. The bi-deuterated and both monodeuterated species (OD-ND, OH-ND and OD-NH respectively) were formed by fluxing D_2O over the sample. All the spectroscopic parameters fitted using Watson's semirigid Hamiltonian in the "S" reduction and I' representation,^[12] are presented in Table 5.8.

Table 5.8 - Experimental spectroscopic constants of the observed isotopologue of the $gG'T$ conformer of MAE.

$gG'T$	OD-ND	OH-ND	OD-NH
A/MHz	11152.04(1) ^a	11612.78(1)	11622.15(1)
B/MHz	2604.813(6)	2617.3(1)	2642.235(8)
C/MHz	2361.144(7)	2391.7(1)	2371.089(8)
D_J/kHz	1.13(1)	9(1)	1.11(2)
D_{JK}/kHz	-6.04(5)	[-8.37] ^d	-6.1(4)
D_K/kHz	62(1)	[71.0] ^d	[71.0] ^d
d_1/kHz	-0.211(4)	[-0.223] ^d	[-0.223] ^d
d_2/kHz	[-0.009] ^d	[-0.009] ^d	[-0.009] ^d
χ_{aa}/MHz	[1.8] ^d	[1.8] ^d	[1.8] ^d
χ_{bb}/MHz	-3.5(2)	-3.5(4)	-3.2(2)
χ_{cc}/MHz	1.7(2)	1.7(4)	1.4(2)
σ^b/MHz	0.06	0.08	0.07
N^c	44	12	20

^a Error in parentheses in units of the last digit.

^b Root-mean-square deviation of the fit.

^c Number of lines in the fit.

^d Values fixed to the ones of the parent species.

The number of transitions measured, mostly for the OH-ND species, is quite low and for this reason some centrifugal distortion constants and quadrupole coupling constants were impossible to determine and were thus maintained fixed to the parent species' values. All the new measured frequencies are listed for the deuterated isotopologues in Tables 5.12, 5.13 and 5.14.

A comparison of the transitions of the parent species and the bi-deuterated one is presented in Figure 5.6, where the same quartets of μ_b and μ_c -type lines are shown. In the same picture, it can be noted also the decreasing of the asymmetry splitting in going to the bi-deuterated species because of the increase of the involved mass.

From the experimental rotational constants obtained for the different isotopic species a partial experimental r_s -structure using Kraitchman's substitution method^[13] was determined for the global minimum $gG'T$. This analysis leads to the determination of the principal axis coordinates of the substituted atom from the changes in the principal moments of inertia resulting from a single isotopic substitution. As reported in Table 5.9, these coordinates for both the hydroxyl (OH) and aminic (NH) hydrogen atoms of the global minimum were obtained. The hydrogen atom coordinates can be obtained considering the substitution from the hydrogenated to the monodeuterated species and from the bi-deuterated to the monodeuterated one. These values can be compared with the calculated ones (r_e), also listed in Table 5.9.

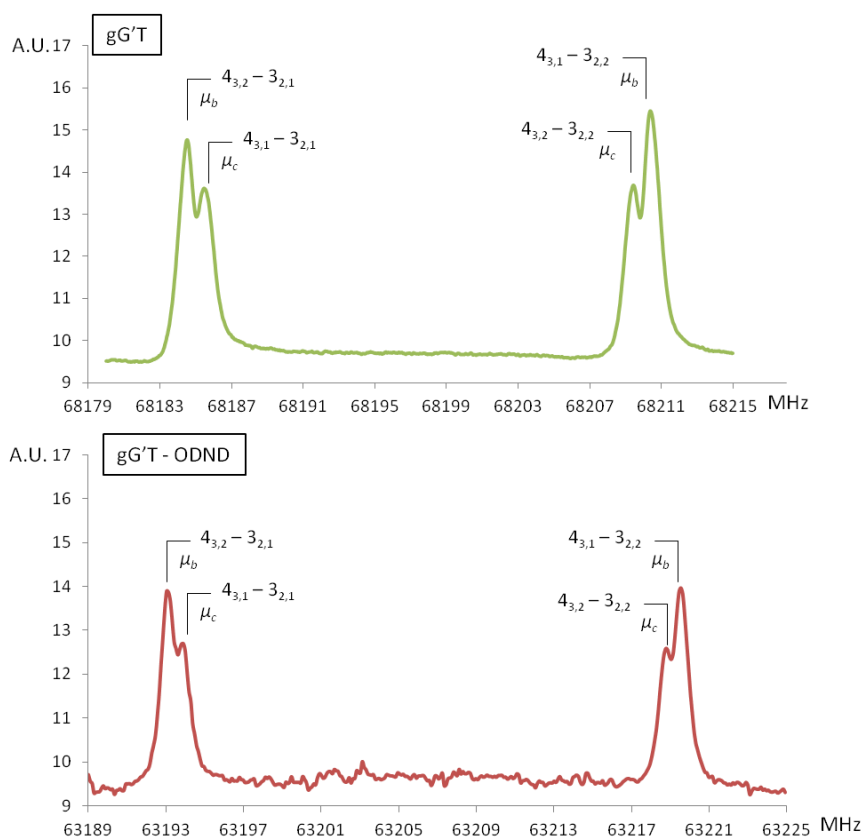


Figure 5.6- Comparison between the parent species $gG'T$ and its bi-deuterated isotopologue OD-ND regarding a rotational transition μ_b and μ_c -quartet split due to asymmetry.

Looking at the values of A , B and C , which reflect the structural distribution about the rotational axes, B3LYP appears to be the method that better reproduces the experimental data. Nevertheless, the comparison between the experimental and theoretical rotational constants regarding the two most stable rotamers of MAE shows that also using a relatively high level of calculations, the results are quite far from describing well the geometries of this small system, characterized by various degrees of freedom.

Regarding the global minimum $gG'T$, a structural fit able to reproduce the experimental rotational constants starting from the calculated geometry is very complicated, since these two sets of rotational constants are quite far from converge and it was not performed yet. In any case some trials were carried out using the experimental rotational constants of the parent species together with those of the deuterated species (OD-ND, OH-ND and OD-NH) with the STRFIT program.^[14] Starting from the B3LYP structure, after many trials on the possible parameters (distances, angles and dihedral angles), it has been surprisingly noticed that the most significant parameter is the O-C distance, that decreasing of about 0.02\AA from the theoretical value of 1.419\AA , improves significantly the difference between the sets of calculated and experimental rotational constants.

Table 5.9 - Comparison between the hydrogen atoms coordinates (\AA) relating to the isotopic substitutions (r_s) and the ones obtained from computational data (r_e).

$gG'T$	r_e^a	r_s
NH	$a/\text{\AA}$ 0.958182/-0.957183	$\pm 0.898(4)^b / \pm 0.948(2)^c$
	$b/\text{\AA}$ -0.055352/0.017340	$[0]^d$
	$c/\text{\AA}$ 1.381401/-1.382514	$\pm 1.366(2) / \pm 1.341(1)$
OH	$a/\text{\AA}$ 1.057412/1.027526	$\pm 0.911(2) / \pm 0.961(3)$
	$b/\text{\AA}$ -1.339336/1.314170	$\pm 1.351(1) / \pm 1.326(2)$
	$c/\text{\AA}$ 0.030420/-0.048444	$[0]^d$

^a The first value refers to B3LYP calculations the second to the MP2 ones.

^b Error expressed in units of the last decimal digit.

^c Two data are calculated. First is monosubstitution from hydrogenated to monodeuterated $-(H \rightarrow D)$. Second number is from di-deuterated species to monodeuterated $(D \rightarrow H)$.

^d Slightly imaginary value has been fixed at zero.

However, this parameter alone is not conclusive and errors are still large. All the trials done on other structural parameters, involving also angles and dihedrals, did not lead to find another parameter as important as the C-O distance and able to reproduce the experimental structure.

Relative intensity measurements on the two different rotamers and estimations of the μ_b/μ_c ratio were not performed for now because of the already reported data in the previous paper, anyway during the current measurements these data were proved and are in agreement with what observed (see for example Figure 5.4 for a qualitative view of the relative intensity between the two observed rotamers and Figure 5.6 where it can be noted the relative smaller intensity of the μ_c -type transitions).

5.4 Conclusions

The analysis of the rotational spectrum of the two most stable conformers of MAE was extended from 59.6 to 74.4 GHz. New sets of spectroscopic constants are now available for both $gG'T$ and $g'GG$ rotamers, including centrifugal distortion constants and quadrupole coupling constants. Moreover for the global minimum $gG'T$ three deuterated species (OD-ND, OH-ND and OD-NH) were analyzed whereas for the $g'GG$ conformer the rotational constants were partially remeasured,

giving in this way more precise data. The stability of the two observed conformers is driven by intramolecular forces that conduct to OH...N hydrogen bond, as depicted in Figure 5.7.

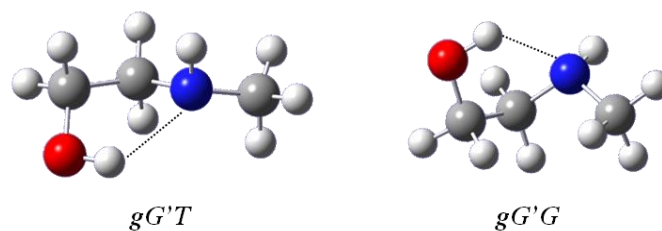


Figure 5.7 - Structural conformations of the two observed conformers of MAE, stabilized by OH...N intramolecular hydrogen bond.

The choice to investigate again this molecule revealed to be interesting and has proved that this kind of flexible systems continue to be a challenge for rotational spectroscopy. For this reason we think that the work on MAE cannot be consider finished but of course the possibility to deepen its structure with higher resolution PJ-FTMW measurements is still opened. This type of research could resolve the internal rotation motion for the methyl group and better fit the ^{14}N quadrupole effect. The isotopomers analysis that can be conducted in natural abundance with this spectrometer could also improve the fittings and complete the study measuring the ^{13}C species. Since many considerations on the structure were done for MAE (and also for AE) during the last years, meaning that their descriptions continue to be stimulating, a complete pattern of rotational constants for all the heavy atoms of the global minimum could help to resolve its effective structure. Furthermore the better sensitivity of the PJ-FTMW spectrometer can lead to observe other rotameric forms. But this is not all about this compound, its astrophysical interest continues to exist and so to further extend the measurements in a higher frequency range can be very interesting to rely on updated data for astronomical observations.

5.5 References

- [1] Y. Liu, C. A. Rice, M. A. Suhm, *Canadian Journal of Chemistry*, 82, 6, **2004**.
- [2] S. Charnley, in *Proceedings of the workshop: The bridge between the Big Bang and Biology*, CNR, Italy 1999.
- [3] P. Ehrenfreund, S. B. Charnley, *Annu. Rev. Astron. Astrophys.*, 38, 427- 483, **2000**.
- [4] N. Seurre, K. Le Barbu-Debus, F. Lahmani, A. Zehnacker-Rentien, J. Sepiol, *J. Mol. Struct.*, 692, 127-137, **2004**, and refs. within.
- [5] I. Vorobyov, M. C. Yappert, D. B. DuPré, *J. Phys. Chem. A*, 106, 668-679, **2002**, and refs. within.
- [6] R. E. Penn, L. W. Buxton, *J. Mol. Spectrosc.*, 56, 229-238, **1975**.
- [7] R. E. Penn, R. F. Curl Jr., *J. Chem. Phys.*, 55, 651, **1971**.
- [8] M. J. Tubergen, C. R. Torok, R. J. Lavrich, *J. Chem. Phys.*, 119, 8397, **2003**.
- [9] S. L. Widicus, B. J. Drouin, K. A. Dyl, G. A. Blake, *J. Mol. Spectrosc.*, 217, 278, **2003**.
- [10] M. Räsänen, A. Aspiala, L. Homanen, J. Murto, *J. Mol. Struct.*, 96, 81, **1982**.
- [11] M. J. T. Frisch, G. W.; Schlegel, H. B.; Scuseria, G. E.; Robb, M. A.; Cheeseman, J. R.; Montgomery, Jr., J. A.; Vreven, T.; Kudin, K. N.; Burant, J. C.; Millam, J. M.; Iyengar, S. S.; Tomasi, J.; Barone, V.; Mennucci, B.; Cossi, M.; Scalmani, G.; Rega, N.; Petersson, G. A.; Nakatsuji, H.; Hada, M.; Ehara, M.; Toyota, K.; Fukuda, R.; Hasegawa, J.; Ishida, M.; Nakajima, T.; Honda, Y.; Kitao, O.; Nakai, H.; Klene, M.; Li, X.; Knox, J. E.; Hratchian, H. P.; Cross, J. B.; Adamo, C.; Jaramillo, J.; Gomperts, R.; Stratmann, R. E.; Yazyev, O.; Austin, A. J.; Cammi, R.; Pomelli, C.; Ochterski, J. W.; Ayala, P. Y.; Morokuma, K.; Voth, G. A.; Salvador, P.; Dannenberg, J. J.; Zakrzewski, V. G.; Dapprich, S.; Daniels, A. D.; Strain, M. C.; Farkas, O.; Malick, D. K.; Rabuck, A. D.; Raghavachari, K.; Foresman, J. B.; Ortiz, J. V.; Cui, Q.; Baboul, A. G.; Clifford, S.; Cioslowski, J.; Stefanov, B. B.; Liu, G.; Liashenko, A.; Piskorz, P.; Komaromi, I.; Martin, R. L.; Fox, D. J.; Keith, T.; Al-Laham, M. A.; Peng, C. Y.; Nanayakkara, A.; Challacombe, M.; Gill, P. M. W.; Johnson, B.; Chen, W.; Wong, M. W.; Gonzalez, C.; Pople, J. A. , Gaussian 03 (Revision B.01) ed., Gaussian, Inc., Pittsburgh PA, **2003**.
- [12] J. K. G. Watson, "Vibrational spectra and structure", Vol. 6, Elsevier, Amsterdam, Oxford & New York, **1977**.
- [13] J. Kraitchman, *Am. J. Phys.*, 21, **1953**.
- [14] Kisiel, Z. PROSPE - Programs for Rotational SPECTroscopy
<http://www.ifpan.edu.pl/~kisiel/prospe.htm>

5.6 Appendix

Table 5.10 - Measured frequencies (MHz) for the transitions observed for conformer *gG'T* of MAE.

<i>J'</i>	<i>Ka'</i>	<i>Kc'</i>	<i>F'</i>	<i>J''</i>	<i>Ka''</i>	<i>Kc''</i>	<i>F''</i>	<i>v</i> _{OBS} /MHz	$\Delta v_{\text{OBS-CALC}}$ /MHz
3	3	1	-	2	2	0	-	63140.24	0.12
3	3	0	-	2	2	0	-		
3	3	0	-	2	2	1	-	63145.11	-0.01
3	3	1	-	2	2	1	-		
4	3	2	-	3	2	1	-	68184.53	-0.19
4	3	1	-	3	2	1	-	68185.49	0.34
4	3	1	-	3	2	2	-	68210.42	0.28
4	3	2	-	3	2	2	-	68209.44	-0.27
5	3	3	-	4	2	2	-	73209.89	-0.13
5	3	2	-	4	2	3	-	73286.68	0.05
5	3	3	-	4	2	3	-	73284.75	-0.15
5	3	2	-	4	2	2	-	73211.85	0.10
6	2	4	5	5	1	5	4	61356.55	0.01
			7				6		
			6				5	61357.69	0.03
6	2	5	5	5	1	5	4	61009.56	0.06
			7				6		
			6				5	61010.40	0.04
7	2	6	6	6	1	5	5	61515.72	0.04
			8				7		
			7				6	61514.66	0.05
7	2	5	6	6	1	5	5	62136.26	-0.09
			8				7		
			7				6	62135.60	-0.02
7	2	5	6	6	1	6	5	67442.76	0.01
			8				7		
			7				6	67443.97	-0.01
7	2	6	6	6	1	6	5	66822.03	-0.05
			8				7		
			7				6	66822.92	-0.05
8	2	7	7	7	1	7	6	72762.26	-0.01
			9				8		
			8				7	72763.16	-0.02
8	2	7	7	7	1	6	6	65693.27	0.06
			9				8		
			8				7	65692.21	0.03
8	2	6	7	7	1	6	6	66717.94	-0.04
			9				8		
			8				7	66717.33	-0.05
8	2	6	7	7	1	7	6	73787.03	-0.01
			9				8		
			8				7	73788.41	0.03
9	2	8	8	8	1	7	7	69753.85	0.05
			10				9		

Chapter 5 - N-METHYLAMINOETHANOL

<i>J'</i>	<i>Ka'</i>	<i>Kc'</i>	<i>F'</i>	<i>J''</i>	<i>Ka''</i>	<i>Kc''</i>	<i>F''</i>	<i>v</i> _{OBS} /MHz	$\Delta v_{\text{OBS-CALC}}$ /MHz
9	2	8	8	8	1	7	7	69753.85	0.05
			10				9		
			9				8	69752.83	0.03
9	2	7	8	8	1	7	7	71343.41	-0.05
			10				9		
			9				8	71342.96	-0.03
9	1	8	8	8	0	8	7	61386.44	0.02
			10				9		
			9				8	61387.67	0.02
10	1	9	9	9	0	9	8	68044.67	-0.02
			11				10		
			10				9	68045.95	-0.04
10	2	9	9	9	1	8	8	73702.75	0.02
			11				10		
			10				9	73701.75	0.00
12	1	12	11	11	0	11	10	62645.68	0.01
			13				12		
			12				11	62645.24	0.03
14	0	14	-	13	1	13	-	66341.39	-0.06
14	1	14	-	13	0	13	-	71218.33	-0.11
15	0	15	-	14	0	14	-	73792.96	0.05
15	0	15	-	14	1	14	-	71590.24	0.01
15	1	15	-	14	1	14	-	73386.40	0.03
15	1	14	14	14	2	13	13	60099.09	0.09
			16				15		
			15				14	60099.81	0.09
12	1	11	-	11	1	10	-	61750.98	-0.07
12	2	11	-	11	2	10	-	60424.22	-0.08
12	2	10	-	11	2	9	-	61631.84	-0.04
12	3	10	-	11	3	9	-	60780.72	0.00
12	3	9	-	11	3	8	-	60900.52	0.04
12	4	9	-	11	4	8	-	60753.92	0.05
12	4	8	-	11	4	7	-	60757.91	0.01
12	5	8	-	11	5	7	-	60721.53	0.04
12	5	7	-	11	5	6	-	60704.91	0.08
12	6	7	-	11	6	6	-	60696.40	0.08
12	6	6	-	11	6	5	-	60692.23	0.03
12	7	6	-	11	7	5	-	60692.23	0.03
12	7	5	-	11	7	4	-	60692.23	0.03
12	8	5	-	11	8	4	-	60692.23	0.03
12	8	4	-	11	8	3	-	60692.23	0.03
13	0	13	-	12	0	12	-	64231.36	0.09
13	0	13	-	12	1	12	-	61020.53	0.02
13	1	13	-	12	1	12	-	63694.82	0.00
13	1	12	-	12	1	11	-	66802.24	-0.09
13	1	13	-	12	0	12	-	66905.58	0.01
13	2	12	-	12	2	11	-	65414.27	-0.03
13	2	11	-	12	2	10	-	66874.54	-0.04
13	3	11	-	12	3	10	-	65855.55	0.00
13	3	10	-	12	3	9	-	66032.94	-0.05
13	4	10	-	12	4	9	-	65831.98	-0.02
13	4	9	-	12	4	8	-	65839.10	-0.03

<i>J'</i>	<i>Ka'</i>	<i>Kc'</i>	<i>F'</i>	<i>J''</i>	<i>Ka''</i>	<i>Kc''</i>	<i>F''</i>	$\nu_{\text{OBS}}/\text{MHz}$	$\Delta\nu_{\text{OBS-CALC}}/\text{MHz}$
13	5	9	-	12	5	8	-	65791.38	0.00
13	5	8	-	12	5	7	-	65791.38	0.00
13	6	8	-	12	6	7	-	65769.76	-0.01

NOTE: the “-“ symbol in the *F* column means that the hyperfine quadrupole effect could not be resolved.

Table 5.11 - Measured frequencies (MHz) for the transitions observed for conformer $g'GG$ of MAE.

J'	Ka'	Kc'	F'	J''	Ka''	Kc''	F''	$\nu_{\text{OBS}}/\text{MHz}$	$\Delta\nu_{\text{OBS-CALC}}/\text{MHz}$
10	2	8	-	9	2	7	-	60053.02	0.04
10	1	9	-	9	1	8	-	60226.55	0.00
5	3	3	-	4	2	2	-	60593.22	-0.08
5	3	2	-	4	2	2	-	60595.81	0.21
5	3	3	-	4	2	3	-	60671.26	-0.20
5	3	2	-	4	2	3	-	60673.82	0.06
10	1	10	10	9	0	9	9	61000.62	-0.07
			11				10		
			9				8	61001.01	-0.06
11	0	11	-	10	1	10	-	62100.97	0.02
7	2	5	6	6	1	6	5	62977.3	0.01
			8				7		
			7				6	62978.3	0.00
8	2	7	8	7	1	6	7	63212.25	-0.01
			9				8		
			7				6	63212.98	0.00
11	1	11	-	10	1	10	-	64004.76	-0.01
11	0	11	-	10	0	10	-	64420.61	-0.01
11	2	10	-	10	2	9	-	65197.77	0.07
11	7	5	-	10	7	4	-		
11	6	6	-	10	6	5	-	65436.74	0.01
11	6	5	-	10	6	4	-		
11	8	3	-	10	8	2	-	65439.98	0.07
11	8	4	-	10	8	3	-		
11	5	7	-	10	5	6	-	65444.85	0.00
11	5	6	-	10	5	5	-		
11	4	8	-	10	4	7	-	65466.37	0.03
11	4	7	-	10	4	6	-	65469.89	-0.06
11	3	9	-	10	3	8	-	65482.21	0.06
11	3	8	-	10	3	7	-	65583.47	-0.05
11	2	9	-	10	2	8	-	66144.82	-0.07
11	1	10	-	10	1	9	-	66177.79	0.03
11	1	11	11	10	0	10	10	66324.26	0.02
			12				11		
			10				9	66324.51	-0.05
6	3	4	-	5	2	3	-	66473.20	-0.05
6	3	4	-	5	2	4	-	66654.77	-0.09
6	3	3	-	5	2	4	-	66661.74	0.00
4	4	1	-	3	3	0	-		
4	4	1	-	3	3	1	-	67050.82	0.02
4	4	0	-	3	3	1	-		
4	4	0	-	3	3	0	-		
12	0	12	-	11	1	11	-	68241.77	0.03

Chapter 5 - N-METHYLAMINOETHANOL

J'	Ka'	Kc'	F'	J''	Ka''	Kc''	F''	ν_{OBS}/MHz	$\Delta\nu_{OBS-CALC}/MHz$
9	2	8	9	8	1	7	8	68347.71	0.03
			10				9	68348.42	0.04
			8				7		
12	1	12	-	11	1	11	-	69781.26	-0.01
8	2	6	7	7	1	7	6	70058.17	-0.02
			9				8		
			8				7	70059.27	-0.01
12	0	12	-	11	0	11	-	70145.69	0.12
12	2	11	-	11	2	10	-	71081.66	0.05
12	7	5	-	11	7	4	-	71384.94	0.03
12	7	6	-	12	7	5	-		
12	6	7	-	11	6	6	-	71387.51	0.05
12	6	6	-	11	6	5	-		
12	8	4	-	11	8	3	-	71387.90	-0.01
12	8	5	-	11	8	4	-		
12	9	3	-	11	9	2	-	71394.67	0.00
12	9	4	-	11	9	3	-		
12	5	8	-	11	5	7	-	71399.45	0.00
12	5	7	-	11	5	6	-		
12	4	9	-	11	4	8	-	71427.53	-0.06
12	4	8	-	11	4	7	-	71434.23	-0.09
12	3	10	-	11	3	9	-	71438.87	-0.05
12	3	9	-	11	3	8	-	71593.89	-0.05
12	1	12	12	11	0	11	11	71684.92	0.00
			13				12	71685.16	-0.02
			11				10		
7	3	5	-	6	2	4	-	72301.04	0.06
7	3	4	-	6	2	5	-	72678.86	0.04
5	4	2	-	4	3	1	-		
5	4	1	-	4	3	2	-	72998.43	0.02
5	4	2	-	4	3	2	-		
5	4	1	-	4	3	1	-		
14	6	9	-	14	5	9	-		
14	6	8	-	14	5	9	-	67889.02	-0.05
14	6	9	-	14	5	10	-		
14	6	8	-	14	5	10	-		
13	6	8	-	13	5	8	-		
13	6	7	-	13	5	8	-		
14	1	13	-	13	2	11	-	67911.36	0.01
13	6	8	-	13	5	9	-		
13	6	7	-	13	5	9	-		
12	6	7	-	12	5	7	-		
12	6	6	-	12	5	7	-	67928.04	0.01
12	6	7	-	12	5	8	-		
12	6	6	-	12	5	8	-		
11	6	6	-	11	5	6	-		
11	6	5	-	11	5	6	-	67940.01	-0.01
11	6	6	-	11	5	7	-		
11	6	5	-	11	5	7	-		
10	6	5	-	10	5	5	-		
10	6	4	-	10	5	6	-	67948.12	-0.02
10	6	4	-	10	5	5	-		
10	6	5	-	10	5	6	-		

<i>J'</i>	<i>Ka'</i>	<i>Kc'</i>	<i>F'</i>	<i>J''</i>	<i>Ka''</i>	<i>Kc''</i>	<i>F''</i>	$\nu_{\text{OBS}}/\text{MHz}$	$\Delta\nu_{\text{OBS-CALC}}/\text{MHz}$
9	6	4	-	9	5	4	-		
9	6	3	-	9	5	4	-	67953.14	0.00
9	6	3	-	9	5	5	-		
9	6	4	-	9	5	5	-		
8	6	2	-	8	5	3	-		
8	6	3	-	8	5	3	-		
8	6	2	-	8	5	4	-		
8	6	3	-	8	5	4	-		
6	6	0	-	6	5	1	-		
6	6	1	-	6	5	2	-	67956.01	0.06
6	6	0	-	6	5	2	-		
6	6	1	-	6	5	1	-		
7	6	1	-	7	5	2	-		
7	6	2	-	7	5	3	-		
7	6	1	-	7	5	3	-		
7	6	2	-	7	5	2	-		

NOTE: the “-” symbol in the *F* column means that the hyperfine quadrupole effect could not be resolved.

Table 5.12 - Measured frequencies (MHz) for the transitions observed for the isotopomer OD-ND of the global minimum $g'GG$ of MAE.

J'	Ka'	Kc'	F'	J''	Ka''	Kc''	F''	ν_{OBS}/MHz	$\Delta\nu_{OBS-CALC}/\text{MHz}$
4	3	2	-	3	2	1	-	63193.14	-0.06
4	3	1	-	3	2	1	-	63193.82	0.14
4	3	1	-	3	2	2	-	63219.51	0.18
4	3	2	-	3	2	2	-	63218.85	-0.01
5	3	3	-	4	2	2	-	68128.88	-0.09
5	3	2	-	4	2	2	-	68130.84	-0.02
5	3	2	-	4	2	3	-	68207.76	0.03
5	3	3	-	4	2	3	-	68205.76	-0.07
6	3	4	-	5	2	3	-	73030.63	-0.08
6	3	3	-	5	2	3	-	73036.38	0.00
6	3	3	-	5	2	4	-	73215.25	0.01
6	3	4	-	5	2	4	-	73209.60	0.03
7	2	5	6	6	1	6	5	63957.26	-0.01
			8				7		
			7				6	63958.53	0.01
7	2	6	6	6	1	6	5	63321.17	-0.03
			8				7		
			7				6	63322.06	-0.03
12	1	11	-	11	1	10	-	60617.05	0.01
12	2	10	-	11	2	9	-	60572.17	0.09
13	0	13	-	12	1	12	-	60378.21	0.02
13	2	12	-	12	2	11	-	64255.32	-0.06
13	3	11	-	12	3	10	-	64702.66	-0.04
13	3	10	-	12	3	9	-	64895.71	-0.09
13	4	10	-	12	4	9	-	64682.73	0.04
13	4	9	-	12	4	8	-	64691.03	0.03
14	0	14	-	13	1	13	-	65555.72	0.06
14	2	12	-	13	2	11	-	70864.72	-0.01
15	0	15	-	14	1	14	-	70664.65	-0.02
4	4	1	-	4	3	2	-		
4	4	0	-	4	3	1	-	60663.91	0.00
4	4	0	-	4	3	2	-		
4	4	1	-	4	3	1	-		
5	4	2	-	5	3	3	-	60658.91	-0.12
5	4	1	-	5	3	3	-		
5	4	2	-	5	3	2	-	60657.17	0.03
5	4	1	-	5	3	2	-		
6	4	3	-	6	3	4	-	60650.54	-0.08
6	4	2	-	6	3	4	-		
6	4	3	-	6	3	3	-	60644.97	0.02
6	4	2	-	6	3	3	-		
7	4	4	-	7	3	4	-	60624.16	0.04
7	4	3	-	7	3	4	-		
7	4	4	-	7	3	5	-	60638.24	-0.03
7	4	3	-	7	3	5	-		

J'	Ka'	Kc'	F'	J''	Ka''	Kc''	F''	$\nu_{\text{OBS}}/\text{MHz}$	$\Delta\nu_{\text{OBS-CALC}}/\text{MHz}$
8	4	5	-	8	3	5	-	60590.68	0.07
8	4	4	-	8	3	5	-		
8	4	5	-	8	3	6	-	60621.70	0.08
8	4	4	-	8	3	6	-		
9	4	6	-	9	3	7	-	60600.58	-0.10
9	4	5	-	9	3	7	-	60601.63	0.01
10	4	7	-	10	3	8	-	60576.53	-0.02
10	4	7	-	10	3	7	-	60462.00	0.06
10	4	6	-	10	3	8	-	60578.78	0.02
10	4	6	-	10	3	7	-	60464.20	0.05
11	4	7	-	11	3	9	-	60555.52	0.00
11	4	7	-	11	3	8	-	60356.01	-0.06

NOTE: the “-“ symbol in the F column means that the hyperfine quadrupole effect could not be resolved.

Table 5.13 - Measured frequencies (MHz) for the transitions observed for the isotopomer OH-ND of the global minimum $g'GG$ of MAE.

J'	Ka'	Kc'	F'	J''	Ka''	Kc''	F''	$\nu_{\text{OBS}}/\text{MHz}$	$\Delta\nu_{\text{OBS-CALC}}/\text{MHz}$
3	3	1	-	2	2	0	-	60562.13	0.07
3	3	0	-	2	2	0	-		
3	3	0	-	2	2	1	-	60566.18	0.07
3	3	1	-	2	2	1	-		
4	3	2	-	3	2	1	-	65561.59	0.09
4	3	1	-	3	2	1	-	65562.11	0.09
4	3	1	-	3	2	2	-	65583.04	0.09
4	3	2	-	3	2	2	-	65582.53	0.08
5	3	3	-	4	2	2	-	70544.28	0.08
5	3	2	-	4	2	2	-	70545.79	0.07
5	3	2	-	4	2	3	-	70608.52	0.09
5	3	3	-	4	2	3	-	70606.98	0.09
7	2	6	6	6	1	5	5	60009.68	0.00
			8				7		
			7				6	60008.54	0.00

NOTE: the “-“ symbol in the F' column means that the hyperfine quadrupole effect could not be resolved.

Table 5.14 - Measured frequencies (MHz) for the transitions observed for the isotopomer OD-NH of the global minimum $g'GG$ of MAE.

J'	Ka'	Kc'	F'	J''	Ka''	Kc''	F''	$\nu_{\text{OBS}}/\text{MHz}$	$\Delta_{\text{VOBS-CALC}}/\text{MHz}$
3	3	1	-	2	2	0	-	60610.91	-0.02
3	3	0	-	2	2	0	-		
3	3	0	-	2	2	1	-	60616.94	-0.04
3	3	1	-	2	2	1	-		
4	3	2	-	3	2	1	-	65611.93	-0.12
4	3	1	-	3	2	1	-	65612.72	0.08
4	3	1	-	3	2	2	-	65642.95	0.10
4	3	2	-	3	2	2	-	65642.14	-0.12
5	3	3	-	4	2	2	-	70589.79	0.00
5	3	2	-	4	2	2	-	70592.27	0.12
5	3	2	-	4	2	3	-	70682.71	0.07
5	3	3	-	4	2	3	-	70680.23	-0.06
8	2	7	7	7	1	6	6	63669.17	0.04
			9				8		
			8				7	63668.11	-0.08
8	2	6	7	7	1	7	6	72473.11	0.05
			9				8		
			8				7	72474.29	-0.04
12	1	11	-	11	1	10	-	61269.91	-0.09
12	2	11	-	11	2	10	-	59883.71	0.09
13	1	13	-	12	0	12	-	65624.99	-0.03
13	2	12	-	12	2	11	-	64819.82	0.01
14	0	14	-	13	0	13	-	68183.34	0.07
14	3	11	-	13	3	10	-	70714.09	-0.05

NOTE: the “-” symbol in the F column means that the hyperfine quadrupole effect could not be resolved.

6-CHLORO-2-HYDROXYPYRIDINE

6.1 Introduction

Studies of prototropic tautomerism in heterocyclic molecules are of continuing interest representing a model for intramolecular proton transfer.^[1] In particular the 2-pyridone/2-hydroxypyridine (2PO/2HP) system represents the smallest model system with biological implications, where the tautomerism plays a significant role as in more complex biological molecules (*e.g.* nucleic acid bases). Similar to α - β -unsaturated carbonyl compounds an equilibrium between an oxo (keto) and hydroxyl (enol) tautomer is established. A great number of theoretical and experimental (see, *e.g.*, refs.2-5 and 6-9, respectively) works has been presented where the study of this tautomeric equilibrium has been explored with different methods and in a variety of conditions, in order to add information on this equilibrium in different chemical environment. These studies show that this tautomeric equilibrium strongly depends on the chemical environment selected and might differ if one changes from the solid state to the aqueous phase or to other solutions or to the gas phase. Moreover the possibility to observe the effect of substitutions, in the 2PO/2HP model system, introducing heteroatoms or functional groups, increases the knowledge on its behavior. Also in this case a lot of spectroscopic studies were performed (see, *e.g.*, refs. 10-13). Regarding halogenation effects and in particular the introduction of chlorine atoms in this keto-enol system, the presence of wide literature demonstrates that this remains an interesting topic. In particular a theoretical analysis,^[14] a UV and vapor-pressure osmometry (VPO) study,^[15] a solid state work,^[16] an IR study^[17] and a FT-IR spectrometric work,^[18] have been performed on 6-chloro-2-hydroxypyridine (6ClHP), the molecule chosen in the present work for studying its rotational spectrum.

As discussed in these cited papers, the substitution at the C-6 (*ortho*) position with chlorine has been shown to have a considerable effect on the 2PO/2HP tautomeric equilibrium, both in the gas phase and in a variety of solvents. Experimentally it is found that the enol form of 6ClHP predominates in the vapour phase, in the solid state and in low polarity solvents (such as carbon tetrachloride), whilst in an aqueous environment the keto form is preferred.

The lack of a high resolution gas phase study induced the choice to investigate, by rotational spectroscopy, the tautomeric equilibrium between enolic and keto form in 6ClHP. Certainly these papers can provide an experimental starting point on what can be expected, nowadays however the most advanced theoretical calculations and higher sensitive and resolved techniques, as microwave spectroscopy, can offer a more complete conformational overview and yield new data.

In this regard, the high interest in this kind of tautomeric equilibria is also due to the fact that theoretical calculations are not able to accurately describe this kind of system, (as will be discussed in the following section). For this reason experimental results and above all gas phase study in isolated conditions, can help to clarify the situation and benchmark the theoretical calculations, as already happened for the case of 2HP/2PO.^[6,8] In fact, for this tautomeric system theoretical calculations were not so univocal to describe the conformational minima: the DFT calculations gave the keto form as the global minimum differently to the MPn methods that evaluated as global minimum the enol tautomer (see ref. 8 for the values). For this reason the experimental rotational study was fundamental to describe the effective situation. Here the 2HP was found to be more abundant about 3 to 1 than the keto form, and the experimental energy difference was estimated to be about 3.2(4) kJ·mol⁻¹.^[6]

The possibility to obtain experimental results that can be directly compared to theoretical ones together with the interest that continues to have the tautomeric equilibrium, lead to the choice of investigating the changes in the same model system with halogen substitution.

This research was performed first with the FJAMW spectrometer of the University of Bologna already illustrated in Chapter 3 and afterwards in the Spectroscopy Group of the University of Basque Country (EHU/UPV), where the presence of a Molecular Beam Fourier Transform MicroWave (MB-FTMW) spectrometer with a heated nozzle^[19,20] allowed to record the rotational spectrum of 6ClHP with a higher sensibility and resolution.

6.2 Theoretical calculations

As already mentioned above, many theoretical investigations were performed in the past years on the keto-enolic tautomerism of 2HP/2PO and derivatives by using different theoretical methods (HF, MPn, DFT) and basis set (see refs. 2-5). As summarized by B. Stanovnik *et al.*,^[1] the calculation results are greatly dependent on the method and the basis set used: in particular the DFT method with the B3LYP functionals overestimate the stability of the keto tautomer whereas the *ab initio* SCF and MPn methods and coupled-cluster method overestimate the stability of the hydroxyl

form. The uncertainties shown by computational calculations indicate that the tautomeric equilibrium continues to represent a challenge from the theoretical point of view.

Although a theoretical study on 6CIHP was already carried out by O. G. Parchment *et al.*^[14] in 1991, a new set of structural optimizations were performed with both MP2 and B3LYP methods with more extended basis set (6-311++G**).

6CIHP presents three different possible forms: 2 enolic conformations (*Z*- or *E*-6CIHP depending on the position of the hydrogen of the hydroxyl group) and one keto form (6CIPO), which are reported in Figure 6.1.

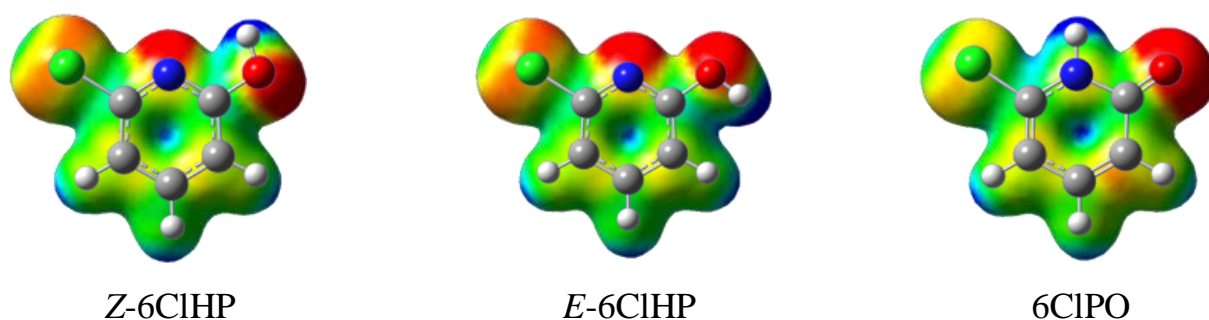


Figure 6.1 - Pictures of the three stable conformers of 6CIHP. For each conformation the electronic distribution surface color coded by the electrostatic potential is also displayed. The red areas identify the most electronegative regions and the blue ones the most electropositive areas.

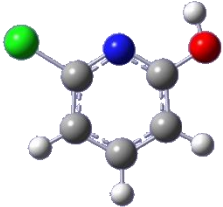
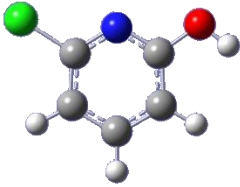
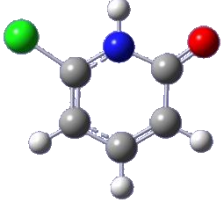
The geometries were fully optimized and subsequently vibrational frequency calculations in the harmonic approximation confirmed that the stationary points were actual minima. All calculations were performed with the Gaussian03-B.01^[21] program package, and all the spectroscopic parameters are shown in Table 6.1.

As expected, the theoretical calculations evaluated without doubts the *Z*-6CIHP conformer as global minimum, whereas the calculated relative ZPE-corrected energies values for the keto form are not so univocal and their values depend on the method used, (ΔE_0 values shown in Table 6.1). The results of the two different methods (B3LYP and MP2) to overestimate or underestimate, respectively, the keto tautomer stability is maintained. In fact, if for the *E*-6CIHP form both methods are in agreement to evaluate its energy, regarding the 6CIPO tautomer the difference between the two methods is about $12 \text{ kJ}\cdot\text{mol}^{-1}$ (B3LYP: $\Delta E_0=9.7 \text{ kJ}\cdot\text{mol}^{-1}$ and MP2: $\Delta E_0=22.5 \text{ kJ}\cdot\text{mol}^{-1}$). For the MPn methods, the same order of magnitude for the ZPE-corrected energies, was obtained also by O. G. Parchment *et al.*^[14], even if a different basis set was used (6-31G**). In particular it seems that the use of this lower basis set increases the stability of the 6CIPO tautomer

for the same MP2 method ($\Delta E_0=18 \text{ kJ}\cdot\text{mol}^{-1}$) and the trend continues in this way going to upper MPn methods (MP3: $\Delta E_0=14.7 \text{ kJ}\cdot\text{mol}^{-1}$ and MP4: $\Delta E_0=9.3 \text{ kJ}\cdot\text{mol}^{-1}$). It can be noted now, that the values of the B3LYP/6-311++G** and MP4/6-31G** calculations converge.

In Table 6.1 also the calculated population ratios between the different species at 373K, temperature estimated and used (see below) to vaporize the sample, are reported. Regarding the possibility to observe the *E*-6CIHP form, looking at these data it is clear that this is unfeasible due to the high energy gap ($> 20 \text{ kJ}\cdot\text{mol}^{-1}$) with respect to the predicted global minimum, whereas regarding 6CIPO, the B3LYP methods together with the high values of the dipole moments components predicted, keep open the chance to detect this tautomer in the rotational spectrum.

Table 6.1 - Comparison between calculated B3LYP/6-311++G** and MP2/6-311++G** spectroscopic parameters for 6-Chloro-2-hydroxypyridine conformers and their shape.

	Z-6CIHP		E-6CIHP		6CIPO	
						
6-311++G**	MP2	B3LYP	MP2	B3LYP	MP2	B3LYP
<i>A</i> / MHz	3409	3418	3418	3434	3417	3441
<i>B</i> / MHz	1279	1274	1276	1269	1270	1263
<i>C</i> / MHz	930	928	929	926	926	924
<i>D_J</i> / kHz	0.033	0.034	0.032	0.034	0.035	0.036
<i>D_{JK}</i> / kHz	0.065	0.065	0.063	0.062	0.047	0.049
<i>D_K</i> / kHz	0.519	0.529	0.537	0.557	0.513	0.516
<i>d₁</i> / kHz	-0.012	-0.012	-0.011	-0.012	-0.013	-0.013
<i>d₂</i> / kHz	-0.002	-0.002	-0.002	-0.002	-0.002	-0.002
<i>μ_a</i> / D	-0.92	-1.16	3.04	3.31	-2.47	-2.53
<i>μ_b</i> / D	1.76	1.68	-3.67	-3.56	-2.44	2.59
<i>μ_c</i> / D	0.00	0.00	0.00	0.00	0.01	0.00
<i>μ_{tot}</i> / D	1.98	2.04	4.77	4.86	3.47	3.62
<i>χ_{aa}</i> / MHz N	1.69	1.96	1.67	1.95	1.41	1.62
<i>χ_{bb}</i> / MHz N	-3.68	-3.93	-4.00	-4.28	1.56	1.72
<i>χ_{cc}</i> / MHz N	1.99	1.96	2.33	2.33	-2.96	-3.34
<i>χ_{ab}</i> / MHz N	1.44	1.53	1.49	1.59	-0.39	-0.39
<i>χ_{aa}</i> / MHz Cl	-58.23	-57.98	-58.05	-57.75	-58.8	-59.6
<i>χ_{bb}</i> / MHz Cl	27.54	28.87	27.76	29.08	25.12	26.94
<i>χ_{cc}</i> / MHz Cl	30.69	29.11	30.29	28.67	33.68	32.65
<i>χ_{ab}</i> / MHz Cl	31.67	31.91	31.67	31.91	-34.24	-34.24
<i>ΔE₀</i> / kJ•mol ⁻¹	0.00 ^a	0.00 ^b	21.09	21.20	23.44	9.56
<i>N_i/N₀</i> % (373K)	100	100	0.117	0.113	0.055	4.689

^a Absolute zero point corrected energy: -781.68474 Hartrees.^b Absolute zero point corrected energy: -783.15481 Hartrees.

6.3 Experimental Results and Analysis

The millimeter-wave spectrum (59.6-74.4 GHz) of 6CIHP was recorded firstly using the free jet absorption millimeter wave spectrometer (FJAMMW - VDI setup), the basic design of which has been described previously (see Chapter 3). After, a second analysis was performed from 4 to 18 GHz with the MB-FTMW at the University of Bilbao, (see ref. 19 for technical details), where the presence of a custom-made heating nozzle^[20] allowed the rotational analysis of this molecule. 6CIHP was purchased from Alfa Aesar (98%) and used without further purification. The sample is a solid with a melting point of about 130°C, so it was vaporized (80-100°C) in both spectrometers. Regarding the experiment with the FJAMMW instrument, the carrier gas was argon at a pressure of 25 kPa and the gas containing the vaporized sample was expanded to about 0.05 kPa through a 0.35 mm diameter nozzle, held at 5°C above the vaporization temperature. Regarding the MB-FTMW experiment, the carrier gas was helium at stagnation pressures of about 200-500 kPa that was expanded through a 0.8 mm nozzle to form a pulsed jet (ca. 200 μ s). In this spectrometer all transitions are observed as split by the Doppler effect, so the rest frequencies are calculated as the average frequency of the two components. Accuracy of the frequency measurements is better than 3 kHz. Transitions separated by less than ca. 10 kHz are resolvable rather than the FJAMMW where the accuracy of the frequency measurements is just under 50 kHz. In both cases no decomposition products were noticeable.

The analysis of the rotational spectrum started in the FJAMMW (59.6-74.4 GHz), where the presence of a series of μ_b -R branch lines with K_a equal 9 allowed a quite straightforward assignment of the rotational spectrum of the Z-6CIHP species, comparing the rotational transitions to the ones predicted by calculations. Moreover it was expected that each transition presented an hyperfine structure as a result of the coupling of the nuclear spin with the overall rotation of the molecule, due to the ³⁵Cl and ³⁷Cl nuclei which have nuclear spins $I=3/2$, and also for the ¹⁴N that present nuclear spins $I=1$. However, the splitting due to the nitrogen atom was not expected to be large enough to be measurable with the resolution of the FJAMMW, while the splitting due to the chlorine atom was predicted to be larger and was observed and partially resolved. As predicted by calculations the highest dipole moment component is μ_b , and in fact 60 lines were measured and assigned as μ_b -R branch rotational transitions for the normal species of the Z-6CIHP, and 32 μ_b -R branch different lines were measured for the isotopologue ³⁷Cl species. These first sets of rotational transitions were fitted using Watson's semirigid Hamiltonian in the "S" reduction and I' representation.^[22] No other lines, attributable to the 6CIPO tautomer, were observed in this recorded spectrum.

The hydroxyl deuterated species of the global minimum *Z*-6ClHP species were also observed with this spectrometer, by fluxing D₂O over the sample. In this way the ³⁵Cl-OD and the ³⁷Cl-OD isotopomers were analyzed, even if the low intensity of the signals did not allow the measurements of many lines. Also these rotational transitions were fitted using Watson's semirigid Hamiltonian in the "S" reduction and I' representation,^[22] and the spectroscopic parameters are shown in Table 6.3 while the frequencies measured are listed in Table 6.7.

Table 6.2 - Experimental spectroscopic parameters of *Z*-6ClHP, for both the chlorine 35 and 37 species.

	Z-6ClHP	
	³⁵ Cl	³⁷ Cl
<i>A</i> /MHz	3422.7097(1) ^a	3414.6413(3)
<i>B</i> /MHz	1286.3294(1)	1251.0313(3)
<i>C</i> /MHz	934.90405(7)	915.5363(1)
<i>D_J</i> /kHz	0.037(1)	0.031(4)
<i>D_{JK}</i> /kHz	0.045(6)	0.06(1)
<i>D_K</i> /kHz	0.555(7)	0.54(1)
<i>d_J</i> /kHz	-0.0135(8)	-0.010(2)
χ_{aa} / MHz Cl	-60.227(4)	-47.8733(8)
χ_{bb} / MHz Cl	29.149(4)	23.379(4)
χ_{cc} / MHz Cl	31.077(4)	24.495(4)
χ_{ab} / MHz Cl	32.83(4)	-25.37(4)
χ_{aa} / MHz N	1.628(4)	1.608(6)
χ_{bb} / MHz N	-3.627(4)	-3.606(6)
χ_{cc} / MHz N	1.999(4)	1.998(6)
χ_{ab} / MHz N	1.37(6)	-1.42(7)
P_{cc} /uÅ ²	-0.014	-0.015
N^b	383	236
σ^c / MHz	0.02	0.02

^a Error in parentheses in units of the last digit.

^b Number of lines in the fit.

^c Root-mean-square deviation of the fit.

Table 6.3 - Experimental spectroscopic constants of the observed monodeuterated species of Z-6CIHP conformer, both for the chlorine 35 and 37.

	Z-6CIHP	
	³⁵ Cl-OD	³⁷ Cl-OD
<i>A</i> /MHz	3308.949(7) ^a	3300.523(8)
<i>B</i> /MHz	1274.05(3)	1238.94(6)
<i>C</i> /MHz	919.79(2)	901.11(6)
<i>D_J</i> /kHz	[0.037] ^b	[0.031] ^b
<i>D_{JK}</i> /kHz	[0.045] ^b	[0.06] ^b
<i>D_K</i> /kHz	0.58(3)	0.63(4)
<i>d_J</i> /kHz	[-0.0135] ^b	[-0.010] ^b
χ_{aa} - Cl	-57.2(4)	-46.3(5)
<i>N</i> ^c	24	26
σ^d / MHz	0.03	0.04

^a Error in parentheses in units of the last digit.

^b Values fixed to the ones of the parent species.

^c Number of lines in the fit.

^d Root-mean-square deviation of the fit.

After this first experimental session, the second investigation was carried out with the MB-FTMW in Bilbao. Starting from the fit already performed, the searching of the lines was straightforward, and the better resolution of this spectrometer allowed the measurement of the most intense hyperfine components for each rotational transition, due to the nuclear quadrupole coupling effects caused by the ¹⁴N, ³⁵Cl and ³⁷Cl nucleus. The assignment of the hyperfine structure was not easy also because in the previous experiment only the χ_{aa} nuclear quadrupole constant of the chlorine atom was fit. Since the quadrupole coupling constants were practically total undetermined, the assignment for both N and Cl atom was started from zero, and the high frequency lines were used to maintain the already fitted rotational constants. A comparison between the predicted and the experimental pattern of the 3₁₂-2₁₁ transition is shown in Figure 6.2, in this figure also the hyperfine quadrupole components can be seen. In contrast with the previous measurements, also 9 μ_a -R-type transitions were observed in the MB-FTMW spectrum and fitted together with 11 μ_b -R-branch and 3 μ_b -Q-branch rotational transitions for the ³⁵Cl species of the Z-6CIHP form, while for the ³⁷Cl species 8 μ_a -R-type transitions and 5 μ_b -R-branch rotational transitions were observed. All the measurements performed for the two isotopologues of chlorine atom were done in natural abundance and in Figure 6.3 the ratio of about 3 to 1 in favour of the ³⁵Cl can be noted. Because of the high number of hyperfine components measured with the MB-FTMW, the non-zero off-

diagonal quadrupole coupling constants χ_{ab} were determined for both Cl and N atoms, giving the complete series of quadrupole constants.

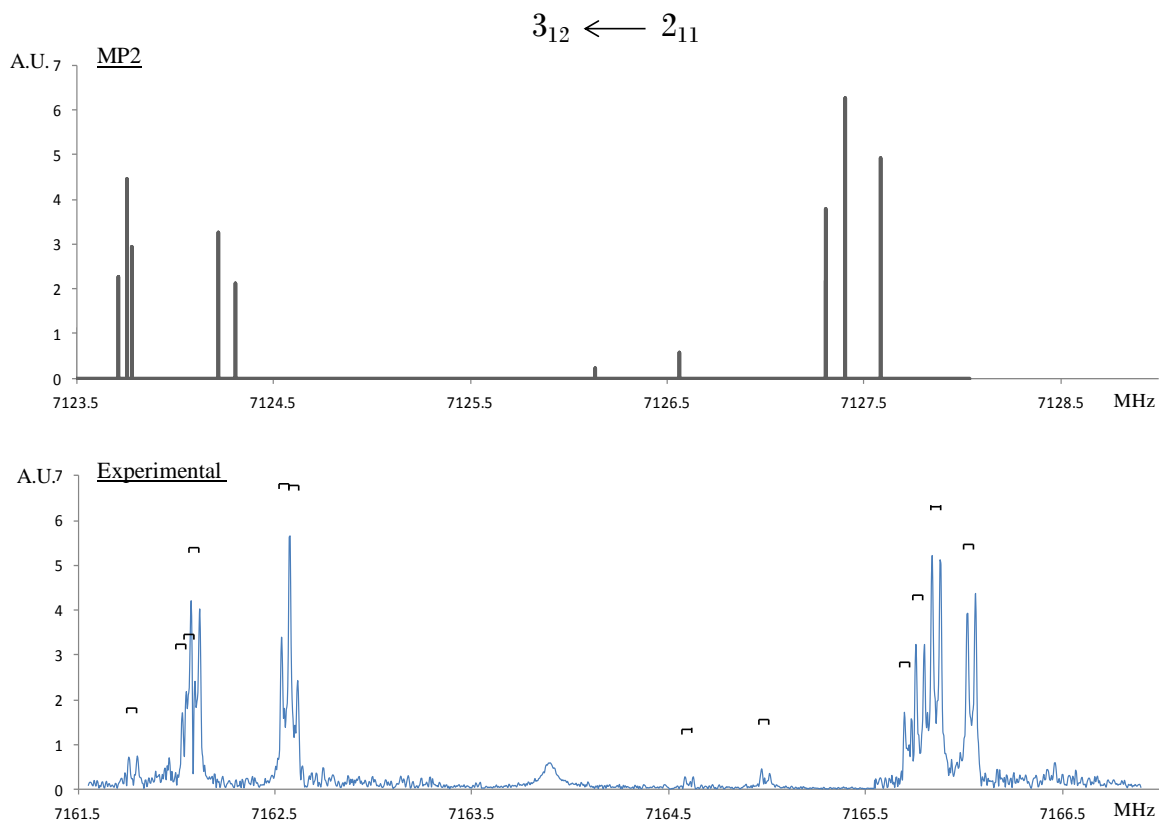


Figure 6.2 - Comparison between the MP2 predicted (black stick spectrum) and MB-FTMW-experimental (blue spectrum) pattern on the transition 3_{12} - 2_{11} . It can be noted how a single rotational transition is composed by different hyperfine quadrupole components. Note also that the experimental lines presented the Doppler splitting.

All the spectroscopic parameters fitted for both isotopomers are reported in Table 6.1 while all the measured transitions are listed in Tables 6.5 and 6.6. The errors of each frequency line used in the fit procedure were of 50 kHz for the FJAMMW measurements and 5 kHz for the MB-FTMW ones.

Because of the higher sensitivity of the MB-FTMW spectrometer, a more accurate search for the 6ClPO tautomer was conducted but no lines were found.

From the experimental rotational constants obtained for the different isotopic species of Z-6ClHP, a partial experimental r_s -structure using Kraitchman's substitution method was determined.^[23] Such analysis leads to the determination of the principal axis coordinates of the

substituted atom from the changes in principal moments of inertia resulting from a single isotopic substitution. As reported in Table 6.4, the coordinates for the chlorine and the hydroxyl (OH) hydrogen atoms were obtained. Each atom coordinate can be obtained considering different kind of mono-substitution: in particular the chlorine's coordinates can be obtained from the hydrogenated species or considering the deuterated ones as the parent species. The same can be done for the hydrogens coordinates: they can be calculated in the ^{35}Cl species but also considering the ^{37}Cl isotopomer.

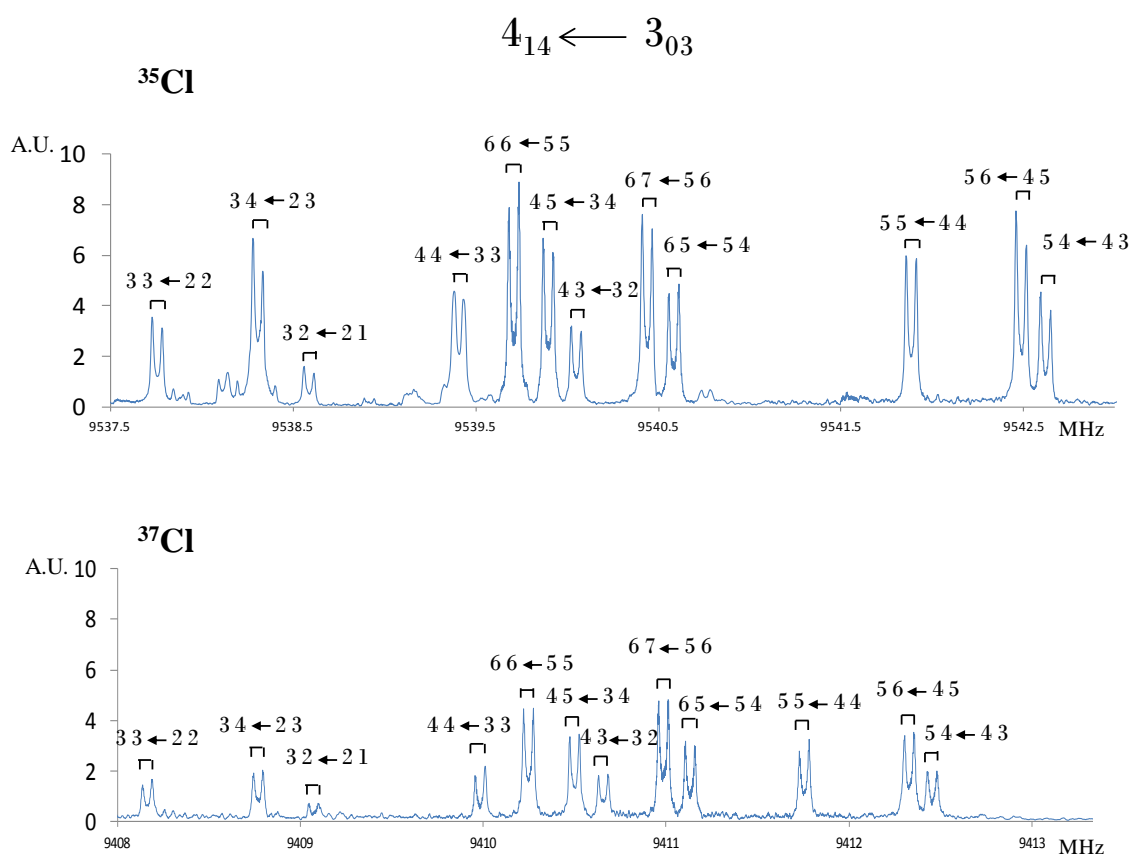


Figure 6.3 - Portion of spectra of Z-6ClHP conformer illustrating the 4_{14} - 3_{03} μ_b -type rotational transition for both the isotopomers of chlorine atom. The spectra were recorded in natural abundances and it can be noted the ratio of about 3 to 1 in favour of the ^{35}Cl species.

Looking Table 6.4, the principal axis coordinates can be compared with the ones calculated with both MP2 and B3LYP methods (r_e) and the ones obtained from the r_0 structure. In fact, to extract information about the structure of observed species, a partial r_0 -structure analysis was performed starting from the MP2 planar geometry and adjusting some structural parameters to

reproduce the observed rotational constants. The choice to use the MP2 planar geometry is due to the closer values of rotational constants to the experimental ones (mostly for B and C) and looking at the planar moment of inertia P_{cc} reported in Table 6.3. This value represents the mass distribution on the c axis and the experimental almost zero values obtained confirm the planarity of the system. In this analysis the experimental rotational constant of the parent species together with those of ^{37}Cl , and the deuterated species ($^{35}\text{Cl-OD}$ and $^{37}\text{Cl-OD}$) were used to fit some structural parameter with the STRFIT program.^[24] in particular the Cl-C and the O-C distances and the NC6C5 angle. The obtained values are respectively: 1.724(2)Å, 1.345(7)Å and 124.28(9)° and with these values the experimental rotational constants are reproduced with an error that falls within unit of MHz. Comparing the values of the structural parameters with the calculated ones (Cl-C = 1.735 Å, O-C = 1.353 Å and NC6C5 = 124.362°) it can be noted that the variation on the angle of the ring is quite small and the distances were reduced of about 0.01 Å with respect to the calculated values.

Table 6.4 - Values of the coordinates (Å) relating to the isotopic substitutions (r_s), obtained from computational data (r_e) and derived from the effective structure (r_0) for the Z-6ClHP conformer.

Cl	r_s^a	r_e B3LYP	r_e MP2	r_0
a	±2.3725(6)/ ±2.389(2)*	2.392	2.380	2.372(2)
b	±0.431(3)/ ±0.455(3)*	-0.429	-0.431	-0.429(2)
H				
a	±1.927(3)/ ±1.967(5)°	-1.940	-1.935	-1.928(7)
b	±2.2721(7)/ ±2.2811(7)°	-2.289	-2.274	-2.2684(4)

^a Error expressed in units of the last decimal digit.

* The first chlorine coordinate value is obtained from the hydrogenated species while the second one is obtained considering the deuterated ones as starting species.

° The first hydrogen coordinate values is obtained from the ^{35}Cl species, instead the second one is obtained considering the ^{37}Cl species.

From this r_0 structure, the coordinates relative to the chlorine atom and the hydroxyl hydrogen were derived and the values are shown in Table 6.4. Here it can be noted how the first set of r_s values (that represent the coordinates obtained from changes on the parent species) and the r_0 coordinates converge with respect to the calculated ones.

6.4 Conclusions

The rotational spectrum of the most stable tautomer of 6ClHP has been assigned in two frequency ranges (4-18 GHz and 59.6-74.4 GHz), with two different spectrometers (FJAMMW and MB-FTMW). Thanks to the higher resolution of the latter one, a complete set of quadrupole coupling constants for both Cl and N nucleus were obtained. In addition all the spectroscopic parameters were fitted also for the isotopomer containing ^{37}Cl in natural abundance, while the enriched monodeuterated species for the hydroxyl hydrogen were analyzed for both ^{35}Cl and ^{37}Cl species, only in the higher frequency range. From the rotational constant of all the isotopologues experimental r_s and r_0 coordinates for the hydroxyl H and the Cl atoms were obtained. A more accurate search was conducted with the more sensitive MB-FTMW, to try to observe lines belonging to the tautomer 6ClPO, but without success.

As mentioned in previous papers,^[17] the increase in the stability of the enol tautomer for the 6ClHP can be correlated to the insertion of the halogen in *ortho* position. The chlorine atom is involved in the inductive effect on the stability of the zwitterionic aromatic resonance form of the keto tautomers. In particular the presence of chlorine in C-6 position destabilizes the aromatic keto form, having a much stronger effect on the equilibrium towards the enolic ones, than other chlorine derivatives (see following chapter).

6.5 References

- [1] B. Stanovnik, M. Tisler, A. R. Katritzky, O. V. Denisko, *Advances in Heterocyclic Chemistry*, 91, **2006**, and refs. within. DOI: 10.1016/S0065-2725(06)91001-0
- [2] M. Piacenza, S. Grimme, *J. Comput. Chem.*, 25, 83-98, **2004**, and refs. within.
- [3] M. B. Messaouda, M. Abderrabba, A. Mahjoub, G. Chambaud, M. Hochlaj, *Comput. and Theor. Chem.*, 990, 94-99, **2012**.
- [4] P. Beak, J. B. Covington, J. M. White, *J. Org. Chem.*, 45, 8, 1347-1353, **1980**.
- [5] J. L. Sonnenberg, K. F. Wong, G. A. Voth, H. B. Schlegel, *J. Chem. Theory Comput.*, 5, 949-961, **2009**.
- [6] L. D. Hatherley, R. D. Brown, P. D. Godfrey, A. P. Pierlot, W. Caminati, D. Damiani, S. Melandri, L. B. Favero, *J. Phys. Chem.*, 97, 46-51, **1993**.
- [7] A. Z. Michelson, A. Petronico, J. K. Lee, *J. Org. Chem.*, 77, 1623-1631, **2012**.
- [8] A. Maris, P. Ottaviani, W. Caminati, *ChemPhysLett*, 360, 155-160, **2002**.
- [9] J. C. Pouilly, J. P. Schermann, N. Nieuwjaer, F. Lecomte, G. Grégoire, C. Descfrancois, G. A. Garcia, L. Nahon, D. Nandi, L. Poisson, M. Hochlaf, *Phys. Chem. Chem. Phys.*, 12, 3566-3572, **2010**.
- [10] R. Sanchez, B. M. Giuliano, S. Melandri, W. Caminati, *ChemPhysLett*, 435, 10-13, **2006**.
- [11] P. Beak, F. S. Fry, Jr., J. Lee, F. Steele, *J. Am. Chem. Soc.*, 98, 171-179, **1976**.
- [12] S. Melandri, L. Evangelisti, A. Maris, W. Caminati, B. M. Giuliano, V. Feyer, K. C. Price, M. Coreno, *J. Am. Chem. Soc.*, 132, 30, 10269-10271, **2010**.
- [13] L. Lapinski, M. J. Nowak, J. Fulara, A. Les, L. Adamowicz, *J. Phys. Chem.*, 96, 6250-6254, **1992**.
- [14] O. G. Parchment, I. H. Hillier, D. V. S. Green, *J. Chem. Soc. Perkin Trans.*, 2, 799-802, **1991**.
- [15] P. Beak, *Acc. Chem. Res.*, 10, 186, **1977**, and refs. within.
- [16] A. Kvik, I. Olovsson, *Ark. Kemi.*, 30, 71, **1968**.
- [17] S. S. T. King, W. L. Dilling, N. B. Tefertiller, *Tetrahedron*, 28, 5859-5863, **1972**.
- [18] M. Takasuka, T. Saito, H. Nakai, *Vibrational Spectroscopy*, 13, 65-74, **1996**.
- [19] E. J. Cocinero, A. Lesarri, P. Ecija, J.-U. Grabow, J. A. Fernandez, F. Castano, *Phys. Chem. Chem. Phys.*, 12, 6076-6083, **2010**.
- [20] R. D. Suenram, F. J. Lovas, D. F. Plusquellic, A. Lesarri, Y. Kawashima, J. O. Jensen, A. C. Samuels, *J. Mol. Spectrosc.*, 211, 110, **2002**.
- [21] M. J. T. Frisch, G. W.; Schlegel, H. B.; Scuseria, G. E.; Robb, M. A.; Cheeseman, J. R.; Montgomery, Jr., J. A.; Vreven, T.; Kudin, K. N.; Burant, J. C.; Millam, J. M.; Iyengar, S. S.;

Tomasi, J.; Barone, V.; Mennucci, B.; Cossi, M.; Scalmani, G.; Rega, N.; Petersson, G. A.; Nakatsuji, H.; Hada, M.; Ehara, M.; Toyota, K.; Fukuda, R.; Hasegawa, J.; Ishida, M.; Nakajima, T.; Honda, Y.; Kitao, O.; Nakai, H.; Klene, M.; Li, X.; Knox, J. E.; Hratchian, H. P.; Cross, J. B.; Adamo, C.; Jaramillo, J.; Gomperts, R.; Stratmann, R. E.; Yazyev, O.; Austin, A. J.; Cammi, R.; Pomelli, C.; Ochterski, J. W.; Ayala, P. Y.; Morokuma, K.; Voth, G. A.; Salvador, P.; Dannenberg, J. J.; Zakrzewski, V. G.; Dapprich, S.; Daniels, A. D.; Strain, M. C.; Farkas, O.; Malick, D. K.; Rabuck, A. D.; Raghavachari, K.; Foresman, J. B.; Ortiz, J. V.; Cui, Q.; Baboul, A. G.; Clifford, S.; Cioslowski, J.; Stefanov, B. B.; Liu, G.; Liashenko, A.; Piskorz, P.; Komaromi, I.; Martin, R. L.; Fox, D. J.; Keith, T.; Al-Laham, M. A.; Peng, C. Y.; Nanayakkara, A.; Challacombe, M.; Gill, P. M. W.; Johnson, B.; Chen, W.; Wong, M. W.; Gonzalez, C.; Pople, J. A. , Gaussian 03 (Revision B.01) ed., Gaussian, Inc., Pittsburgh PA, **2003**.

[22] J. K. G. Watson, "Vibrational spectra and structure", Vol. 6, Elsevier, Amsterdam, Oxford & New York, **1977**.

[23] J. Kraitichman, *Am. J. Phys.*, 21, **1953**.

[24] Kisiel, Z. PROSPE - Programs for Rotational SPECTroscopy
<http://www.ifpan.edu.pl/~kisiel/prospe.htm>

6.6 Appendix

Table 6.5 - Measured frequencies (MHz) for the transitions observed for the parent species of Z-5CIHP conformer.

J'	Ka'	Kc'	F'_N	F'_{Cl}	J''	Ka''	Kc''	F''_N	F''_{Cl}	ν_{OBS}/MHz ^{35}Cl	$\Delta\nu_{OBS-CALC}/MHz$ ^{35}Cl		
3	0	3	4	4	2	0	2	3	3	6508.2308	-0.0015		
			4	5				3	4				
			5	5				4	4			6507.9983	0.0000
			5	6				4	5			6508.1538	0.0004
			5	4				4	3			6508.2082	0.0027
			3	3				2	2			6504.5027	-0.0012
			3	4				2	3			6504.4172	-0.0012
			2	3				1	2			6504.3177	-0.0010
3	1	2	4	4	2	1	1	3	3	7162.5515	0.0000		
			4	5				3	4			7162.0930	-0.0016
			4	3				3	2			7162.0478	-0.0011
			5	5				4	4			7166.0353	0.0002
			5	6				4	5			7165.8566	-0.0004
			5	4				4	3			7165.7746	0.0007
			5	4				4	4			7164.6013	-0.0005
			3	3				2	2			7162.5922	-0.0011
			3	4				2	3			7162.0676	0.0028
			3	2				2	1			7161.7755	-0.0020
4	0	4	6	6	3	0	3	5	5	8513.8125	0.0008		
			6	7				5	6			8514.0349	0.0013
			6	5				5	4			8514.0835	0.0024
			3	4				2	3			8512.2223	-0.0002
			4	4				3	3			8512.3543	0.0008
			4	5				3	4			8512.4042	-0.0007
			4	3				3	2			8513.9762	0.0008
			5	5				4	4			8513.9762	0.0008
			5	4				4	3			8514.1835	0.0011
			5	6				4	5			8514.1348	-0.0018
5	0	5	4	4	4	0	4	3	3	10426.7437	0.0000		
			4	5				3	4			10426.9610	-0.0008
			4	3				3	2			10427.0208	-0.0022
			5	6				4	5			10427.0364	0.0028
			7	8				6	7			10427.9897	0.0017

Chapter 6 - 6-CHLORO-2-HYDROXYPYRIDINE

J'	Ka'	Kc'	F'_N	F'_{Cl}	J''	Ka''	Kc''	F''_N	F''_{Cl}	ν_{OBS}/MHz ^{35}Cl	$\Delta\nu_{OBS-CALC}/\text{MHz}$ ^{35}Cl
			7	6				6	5	10428.0243	0.0002
			7	7				6	6	10427.7587	0.0011
			5	4				4	3	10427.0714	-0.0050
			5	5				4	4	10426.8354	0.0005
			6	6				5	5	10427.8876	0.0014
			6	7				5	6	10428.0883	0.0002
			6	5				5	4	10428.1169	-0.0060
4	1	3	6	6	3	1	2	5	5	9499.7596	0.0025
			6	7				5	6	9499.7257	0.0016
			6	5				5	4	9499.7454	-0.0041
			3	4				2	3	9498.8377	-0.0011
			4	4				3	3	9497.6772	-0.0004
			4	5				3	4	9497.4336	-0.0010
			4	3				3	2	9497.4625	0.0037
			5	5				4	4	9498.4051	0.0000
			5	4				4	3	9498.2518	-0.0027
			5	6				4	5	9498.2194	0.0003
			3	3				2	2	9499.0606	-0.0005
			3	2				2	1	9499.0300	-0.0043
4	1	4	4	4	3	1	3	3	3	8108.7251	0.0005
			4	5				3	4	8108.8417	-0.0004
			4	3				3	2		
			5	5				4	4	8109.7382	0.0009
			5	6				4	5	8109.8484	0.0016
			3	2				2	1	8110.4996	-0.0020
			3	4				2	3	8110.5899	0.0000
			6	6				5	5	8111.0210	0.0019
			6	7				5	6	8111.0498	-0.0023
5	1	5	4	3	4	1	4	3	2	10079.8138	-0.0017
			5	6				4	5	10079.3618	-0.0016
			7	8				6	7	10080.8200	0.0030
			7	6				6	5	10080.8056	-0.0024
			7	7				6	6	10080.7615	0.0013
			5	4				4	3	10079.3618	0.0000
			5	5				4	4	10079.2533	0.0017
5	3	3	6	5	4	3	2	5	4	11211.4602	0.0011
			6	7				5	6	11211.5100	-0.0018
			6	6				5	5	11211.7407	-0.0005
6	0	6	5	5	5	0	5	4	4	12282.8992	0.0013
			5	6				4	5	12283.0922	0.0000
			6	6				5	5	12282.9525	-0.0010
			6	7				5	6	12283.1407	-0.0019
			6	5				5	4	12283.1659	0.0005
			7	7				6	6	12283.6192	-0.0005
			7	8				6	7	12283.8200	0.0036
			7	6				6	5	12283.8339	-0.0022
			8	8				7	7	12283.5887	0.0017

Chapter 6 - 6-CHLORO-2-HYDROXYPYRIDINE

J'	Ka'	Kc'	F'_N	F'_{Cl}	J''	Ka''	Kc''	F''_N	F''_{Cl}	ν_{OBS}/MHz ^{35}Cl	$\Delta\nu_{OBS-CALC}/MHz$ ^{35}Cl
			8	9				7	8	12283.7897	0.0026
			8	7				7	6	12283.8034	-0.0045
2	2	0	4	3	1	1	1	3	2	11591.1519	-0.0004
			4	5				3	4	11591.4076	0.0012
			4	4				3	3	11591.8727	0.0003
			3	3				2	2	11598.3963	-0.0008
			3	4				2	3	11599.3344	0.0002
			3	2				2	1	11599.9909	-0.0005
			2	2				1	2	11601.6858	0.0037
			2	3				1	2		
			3	4				3	4	11606.3461	-0.0007
			3	3				3	3	11607.0139	-0.0014
2	2	1	4	4	1	1	0	3	3	11199.6720	0.0000
			4	5				3	4	11200.5340	0.0017
			4	3				3	2	11200.8225	-0.0001
			2	3				1	2	11210.9154	0.0010
			4	4				3	4	11200.0780	-0.0017
			4	3				3	3	11200.2463	-0.0009
			2	2				1	1	11210.8643	0.0011
			2	1				1	1	11210.8823	0.0042
			2	2				1	2	11210.9018	-0.0040
3	1	3	4	4	2	0	2	3	3	7940.3765	0.0008
			4	5				3	4	7940.8701	0.0004
			4	3				3	2	7941.0225	0.0000
			5	5				4	4	7936.6849	0.0009
			5	6				4	5	7937.5368	0.0009
			5	4				4	3	7937.7523	0.0005
			3	3				2	2	7935.1824	-0.0004
			3	4				2	3	7935.4713	0.0006
			3	2				2	1	7935.5886	0.0005
			2	2				1	1	7931.6865	0.0019
			2	3				1	2	7932.0312	0.0000
			2	1				1	2	7932.3007	-0.0060
			4	4				4	4	7925.2801	0.0000
			4	5				4	5	7925.9819	-0.0004
			4	3				4	3	7926.1674	-0.0009
3	2	1	5	6	2	1	2	4	5	14320.8643	-0.0006
			5	5				4	4	14321.7495	-0.0014
			4	5				3	4	14328.5301	0.0013
			4	4				3	3	14329.1339	-0.0029
3	2	2	4	4	2	1	1	3	3	13077.7737	0.0000
			4	5				3	4	13078.1077	0.0012
			4	3				3	2	13078.3632	-0.0003
			5	5				4	4	13069.7800	0.0006
			5	6				4	5	13070.7797	0.0005
			5	4				4	3	13070.9279	-0.0006
			3	3				2	2	13072.4103	-0.0010

Chapter 6 - 6-CHLORO-2-HYDROXYPYRIDINE

J'	Ka'	Kc'	F'_N	F'_{Cl}	J''	Ka''	Kc''	F''_N	F''_{Cl}	ν_{OBS}/MHz ^{35}Cl	$\Delta\nu_{OBS-CALC}/\text{MHz}$ ^{35}Cl
			3	4				2	3	13072.5754	0.0004
			3	2				2	1	13072.6435	-0.0009
			2	2				1	1	13065.4400	0.0023
			2	3				1	2		
			2	1				1	2	13065.5188	-0.0023
4	1	4	4	4	3	0	3	3	3	9539.4046	0.0011
			4	5				3	4	9539.8945	0.0006
			4	3				3	2	9540.0468	0.0005
			5	5				4	4	9541.8825	0.0010
			5	4				4	3	9542.6184	0.0013
			5	6				4	5	9542.4852	0.0018
			3	3				2	2	9537.7514	0.0014
			3	2				2	1	9538.5825	-0.0005
			3	4				2	3	9538.3034	0.0009
			6	6				5	5	9539.7059	0.0011
			6	5				5	4	9540.5814	0.0011
			6	7				5	6	9540.4359	0.0012
5	0	5	4	5	4	1	4	3	4	9400.8796	-0.0010
			4	3				3	2	9400.7686	-0.0008
			7	8				6	7	9401.5839	-0.0028
			7	6				6	5	9401.5293	0.0044
			7	7				6	6	9401.8653	0.0008
			5	6				4	5	9399.4924	-0.0007
			5	4				4	3	9399.4363	0.0012
			5	5				4	4	9399.6571	0.0019
			6	6				5	5	9399.9802	0.0001
			6	7				5	6	9399.7411	-0.0002
			6	5				5	4	9399.6867	-0.0016
5	1	5	4	4	4	0	4	3	3	11105.4070	0.0001
			4	5				3	4	11105.9216	0.0000
			4	3				3	2	11106.0690	-0.0001
			7	8				6	7	11107.2189	0.0007
			7	6				6	5	11107.3086	0.0013
			7	7				6	6	11106.6542	0.0009
			5	6				4	5	11106.9041	0.0001
			5	4				4	3	11107.0039	0.0006
			5	5				4	4	11106.4318	0.0005
			6	6				5	5	11107.7181	0.0007
			6	7				5	6	11108.2236	0.0003
			6	5				5	4	11108.3059	0.0017
6	0	6	6	5	5	1	5	5	4	11603.2407	0.0020
			6	7				5	6	11603.2700	-0.0024
			6	6				5	5	11603.3582	0.0010
			7	6				6	5	11603.6527	-0.0021
			7	8				6	7	11603.6833	0.0007
			5	5				4	5		
			7	7				6	6	11603.7897	0.0011

Chapter 6 - 6-CHLORO-2-HYDROXYPYRIDINE

J'	Ka'	Kc'	F'_N	F'_{Cl}	J''	Ka''	Kc''	F''_N	F''_{Cl}	ν_{OBS}/MHz ^{35}Cl	$\Delta\nu_{OBS-CALC}/MHz$ ^{35}Cl
			5	4				4	3	11604.0710	-0.0008
			5	6				4	5	11604.1333	0.0008
			5	5				4	4	11604.2352	0.0004
			8	7				7	6	11604.5246	-0.0002
			8	9				7	8	11604.5587	0.0018
			8	8				7	7	11604.6923	0.0009
6	1	6	5	5	5	0	5	4	4	12702.5139	-0.0004
			5	6				4	5	12702.8948	0.0002
			5	4				4	3	12702.9601	-0.0017
			6	6				5	5	12703.0546	0.0004
			6	7				5	6	12703.4180	0.0008
			6	5				5	4	12703.4672	-0.0017
			7	7				6	6	12703.8239	0.0016
			7	8				6	7	12704.2073	0.0007
			7	6				6	5	12704.2480	-0.0008
			8	8				7	7	12703.3050	0.0005
			8	9				7	8	12703.7061	0.0013
			8	7				7	6	12703.7514	-0.0016
7	1	7	6	6	6	0	6	5	5	14364.6080	-0.0009
			6	7				5	6	14364.8723	0.0000
			6	5				5	4	14364.8987	-0.0023
			7	7				6	6	14364.8485	-0.0015
			7	8				6	7	14365.1024	-0.0028
			7	6				6	5	14365.1344	0.0046
			8	8				7	7	14365.3680	0.0019
			8	9				7	8	14365.6289	-0.0015
			8	7				7	6	14365.6511	0.0018
			9	9				8	8	14365.1344	0.0000
			9	10				8	9	14365.3998	-0.0018
			9	8				8	7	14365.4259	0.0000
3	2	2	5	4	3	1	3	5	4	8009.8521	-0.0018
			5	4				5	5		
			5	6				5	5	8010.5224	0.0125
			5	5				5	5		
			5	6				5	6	8009.9811	-0.0008
			2	2				2	3		
			2	3				2	3	8004.9572	0.0004
			2	2				2	2		
			2	3				2	2	8005.2991	-0.0003
			2	1				2	2		
			3	2				2	1	8004.3429	-0.0008
			3	4				2	3	8004.6048	-0.0005
			2	2				2	1		
			2	1				2	1	8004.6800	-0.0020
			4	3				4	3		
			4	4				4	3	8021.6559	0.0057

Chapter 6 - 6-CHLORO-2-HYDROXYPYRIDINE

J'	Ka'	Kc'	F'_N	F'_{Cl}	J''	Ka''	Kc''	F''_N	F''_{Cl}	ν_{OBS}/MHz ^{35}Cl	$\Delta\nu_{OBS-CALC}/MHz$ ^{35}Cl
			4	5				4	5	8021.7488	0.0050
			4	4				4	5		
3	3	1	4	5	3	2	2	4	4	11596.7671	-0.0052
			4	5				4	5		
			4	3				4	4	11596.8930	-0.0081
			4	3				4	3		
7	1	6	8	8	7	0	7	8	8	9540.7561	0.0018
10	9	1	12	13	9	8	2	11	12		
			9	10				8	9	61535.23	-0.01
10	9	2	12	13	9	8	1	11	12		
			9	10				8	9		
10	9	1	11	12	9	8	2	10	11		
			10	11				9	10	61536.37	-0.02
10	9	2	11	12	9	8	1	10	11		
			10	11				9	10		
11	9	3	10	11	10	8	2	9	10		
			13	14				12	13	63768.05	0.02
11	9	2	10	11	10	8	3	9	10		
			13	14				12	13		
11	9	3	11	12	10	8	2	10	11		
			12	13				11	12	63769.48	0.01
11	9	2	11	12	10	8	3	10	11		
			12	13				11	12		
12	9	4	11	12	11	8	3	10	11		
			14	15				13	14	65998.94	0.01
12	9	3	11	12	11	8	4	10	11		
			14	15				13	14		
12	9	4	12	13	11	8	3	11	12		
			13	14				12	13	66000.50	0.01
12	9	3	12	13	11	8	4	11	12		
			13	14				12	13		
13	9	5	12	13	12	8	4	11	12		
			15	16				14	15	68226.86	-0.02
13	9	4	12	13	12	8	5	11	12		
			15	16				14	15		
13	9	5	13	14	12	8	4	12	13		
			14	15				13	14	68228.45	-0.01
13	9	4	13	14	12	8	5	12	13		
			14	15				13	14		
14	9	6	13	14	13	8	5	12	13		
			16	17				15	16	70450.68	0.02
14	9	5	13	14	13	8	6	12	13		
			16	17				15	16		
14	9	6	14	15	13	8	5	13	14		
			15	16				14	15	70452.21	0.00
14	9	5	14	15	13	8	6	13	14		
			15	16				14	15		

Chapter 6 - 6-CHLORO-2-HYDROXYPYRIDINE

J'	Ka'	Kc'	F'_N	F'_{Cl}	J''	Ka''	Kc''	F''_N	F''_{Cl}	ν_{OBS}/MHz ^{35}Cl	$\Delta\nu_{OBS-CALC}/\text{MHz}$ ^{35}Cl
10	10	0	12	13	9	9	1	11	12	66146.20	0.01
10	10	1	12	13	9	9	0	11	12		
10	10	0	9	10	9	9	1	8	9	66146.57	0.00
			11	12				10	11		
10	10	1	9	10	9	9	0	8	9		
			11	12				10	11		
10	10	0	10	11	9	9	1	9	10	66146.96	0.02
10	10	1	10	11	9	9	0	9	10		
11	10	1	13	14	10	9	2	12	13	68380.23	0.00
			10	11				9	10		
11	10	2	13	14	10	9	1	12	13		
			10	11				9	10		
11	10	1	12	13	10	9	2	11	12	68381.18	-0.01
			11	12				10	11		
11	10	2	12	13	10	9	1	11	12		
			11	12				10	11		
12	10	2	11	12	11	9	3	10	11	70613.39	0.02
			14	15				13	14		
12	10	3	11	12	11	9	2	10	11		
			14	15				13	14		
12	10	2	12	13	11	9	3	11	12	70614.60	-0.01
			13	14				12	13		
12	10	3	12	13	11	9	2	11	12		
			13	14				12	13		
12	8	5	11	12	11	7	4	10	11	61377.68	0.01
			14	15				13	14		
12	8	4	11	12	11	7	5	10	11		
			14	15				13	14		
12	8	5	12	13	11	7	4	11	12	61379.42	-0.02
			13	14				12	13		
12	8	4	12	13	11	7	5	11	12		
			13	14				12	13		
13	8	6	12	13	12	7	5	11	12	63597.56	-0.02
			15	16				14	15		
13	8	5	12	13	12	7	6	11	12		
			15	16				14	15		
13	8	6	13	14	12	7	5	12	13	63599.28	0.01
			14	15				13	14		
13	8	5	13	14	12	7	6	12	13		
			14	15				13	14		
14	8	7	13	14	13	7	6	12	13	65809.53	0.06
			16	17				15	16		
14	8	6	13	14	13	7	7	12	13	65810.32	-0.03
			16	17				15	16		
14	8	7	14	15	13	7	6	13	14	65811.14	0.05
			15	16				14	15		
14	8	6	14	15	13	7	7	13	14	65812.00	0.02
			15	16				14	15		

Chapter 6 - 6-CHLORO-2-HYDROXYPYRIDINE

J'	Ka'	Kc'	F'_N	F'_{Cl}	J''	Ka''	Kc''	F''_N	F''_{Cl}	ν_{OBS}/MHz ^{35}Cl	$\Delta\nu_{OBS-CALC}/\text{MHz}$ ^{35}Cl
15	8	8	14	15	14	7	7	13	14	68010.84	0.03
			17	18				16	17		
15	8	7	14	15	14	7	8	13	14	68013.63	0.19
			17	18				16	17		
15	8	8	15	16	14	7	7	14	15	68012.22	-0.09
			16	17				15	16		
15	8	7	15	16	14	7	8	14	15	68015.01	0.06
			16	17				15	16		
16	8	9	15	16	15	7	8	14	15	70198.09	-0.06
			18	19				17	18		
16	8	9	16	17	15	7	8	15	16	70199.43	-0.15
			17	18				16	17		
16	8	8	15	16	15	7	9	14	15	70205.28	-0.03
			18	19				17	18		
16	8	8	16	17	15	7	9	15	16	70206.69	-0.04
			17	18				16	17		
14	7	8	13	14	13	6	7	12	13	61116.65	-0.01
			16	17				15	16		
14	7	8	14	15	13	6	7	13	14	61118.17	0.02
			15	16				14	15	61118.42	-0.02
14	7	7	13	14	13	6	8	12	13	61140.31	0.04
			16	17				15	16		
14	7	7	14	15	13	6	8	13	14	61141.76	0.02
14	7	7	15	16	13	6	8	14	15	61142.03	0.00
15	7	9	14	15	14	6	8	13	14	63266.57	-0.15
			17	18				16	17		
15	7	9	15	16	14	6	8	14	15	63268.25	0.01
			16	17				15	16		
15	7	8	14	15	14	6	9	13	14	63324.82	0.07
			17	18				16	17		
15	7	8	15	16	14	6	9	14	15	63326.26	0.01
			16	17				15	16		
16	7	10	15	16	15	6	9	14	15	65371.58	-0.02
			18	19				17	18		
16	7	10	16	17	15	6	9	15	16	65372.99	-0.02
			17	18				16	17		
16	7	9	15	16	15	6	10	14	15	65503.87	-0.02
			18	19				17	18		
16	7	9	16	17	15	6	10	15	16	65505.27	0.00
			17	18				16	17		
17	7	11	16	17	16	6	10	15	16	67405.96	-0.02
			19	20				18	19		
17	7	11	17	18	16	6	10	16	17	67407.31	0.00
			18	19				17	18		
17	7	10	16	17	16	6	11	15	16	67688.09	0.00
			19	20				18	19		

Chapter 6 - 6-CHLORO-2-HYDROXYPYRIDINE

J'	Ka'	Kc'	F'_N	F'_{Cl}	J''	Ka''	Kc''	F''_N	F''_{Cl}	ν_{OBS}/MHz ^{35}Cl	$\Delta\nu_{OBS-CALC}/\text{MHz}$ ^{35}Cl
17	7	10	17	18	16	6	11	16	17	67689.36	0.01
			18	19				17	18		
18	7	12	17	18	17	6	11	16	17	69331.60	0.01
			20	21				19	20		
18	7	12	18	19	17	6	11	17	18	69332.87	-0.05
			19	20				18	19		
18	7	11	17	18	17	6	12	16	17	69897.71	0.01
			20	21				19	20		
18	7	11	18	19	17	6	12	17	18	69898.86	0.01
			19	20				18	19		
19	7	13	18	19	18	6	12	17	18	71093.94	0.05
			21	22				20	21		
19	7	13	19	20	18	6	12	18	19	71095.17	0.04
			20	21				19	20		
16	6	10	15	16	15	5	11	14	15	61184.92	0.01
			18	19				17	18		
16	6	10	16	17	15	5	11	15	16	61186.11	0.02
			17	18				16	17	65811.14	0.05

Table 6.6 - Measured frequencies (MHz) for the transitions observed for the ^{37}Cl isotopomer of Z-6CIHP conformer.

J'	Ka'	Kc'	F'_N	F'_{Cl}	J''	Ka''	Kc''	F''_N	F''_{Cl}	$\nu_{\text{OBS}}/\text{MHz}$ ^{35}Cl	$\Delta\nu_{\text{OBS-CALC}}/\text{MHz}$ ^{35}Cl
3	0	3	2	1	2	0	2	1	1	6355.5119	-0.0015
			2	3				1	2	6355.6191	0.0006
			3	3				2	2	6355.7934	-0.0009
			3	4				2	3	6355.7039	0.0003
			5	5				4	4	6358.5332	0.0011
			5	6				4	5	6358.6770	-0.0002
			4	4				3	3	6358.7424	0.0019
3	1	2	3	3	2	1	1	2	2	6977.7502	-0.0035
			3	4				2	3	6977.2651	0.0013
			5	5				4	4	6980.4373	0.0010
			5	6				4	5	6980.2606	0.0011
			5	4				4	3	6980.1422	0.0003
			4	4				3	3	6977.7248	0.0020
			4	5				3	4	6977.2651	-0.0001
			3	2				3	2	6981.3898	0.0006
3	4	3	4	6981.4744	-0.0003						
4	0	4	4	4	3	0	3	3	3	8327.0728	-0.0038
			4	5				3	4	8327.1982	0.0010
			4	3				3	2	8327.2460	-0.0013
			3	3				2	2	8326.9471	-0.0005
			3	4				2	3	8327.0943	0.0032
			3	2				2	1	8327.1982	0.0000
			5	5				4	4	8328.4667	-0.0005
			5	6				4	5	8328.6154	-0.0028
			5	4				4	3	8328.6609	-0.0019
			6	6				5	5	8328.3234	0.0006
			6	7				5	6	8328.5362	0.0013
6	5	5	4	8328.5837	0.0028						
4	1	3	4	4	3	1	2	3	3	9256.3993	0.0001
			4	5				3	4	9256.1617	0.0010
			4	3				3	2	9256.1780	-0.0067
			3	3				2	2	9257.4861	-0.0004
			3	4				2	3	9257.2654	0.0003
			3	2				2	1	9257.4599	-0.0006
			5	5				4	4	9256.9801	0.0005
			5	6				4	5	9256.7910	0.0021
			5	4				4	3	9256.8235	-0.0031
			6	6				5	5	9258.0306	-0.0026
6	7	5	6	9257.9973	0.0005						
4	1	4	4	4	3	1	3	3	3	7928.6399	-0.0001
			4	5				3	4	7928.7789	-0.0047
			4	3				3	2		

Chapter 6 - 6-CHLORO-2-HYDROXYPYRIDINE

J'	Ka'	Kc'	F'_N	F'_{Cl}	J''	Ka''	Kc''	F''_N	F''_{Cl}	ν_{OBS}/MHz ^{35}Cl	$\Delta\nu_{OBS-CALC}/MHz$ ^{35}Cl
			3	3				2	2	7929.6093	-0.0011
			3	4				2	3	7929.7551	0.0013
			5	5				4	4	7929.2472	-0.0012
			5	6				4	5	7929.3218	0.0021
			5	4				4	3		
			6	6				5	5	7930.5711	-0.0013
			6	7				5	6	7930.6015	-0.0026
			6	5				5	4	7930.5895	0.0061
5	0	5	5	5	4	0	4	4	4	10209.8385	0.0002
			5	6				4	5	10210.0313	0.0008
			5	4				4	3	10210.0691	-0.0041
			4	4				3	3	10209.7525	-0.0011
			4	5				3	4	10209.9654	0.0000
			4	3				3	2	10210.0313	0.0040
			6	6				5	5	10210.6759	0.0008
			6	7				5	6	10210.8701	-0.0010
			6	5				5	4	10210.9019	-0.0041
			7	8				6	7	10210.7863	0.0016
			7	6				6	5	10210.8223	0.0012
			7	7				6	6	10210.5606	0.0008
5	1	5	5	5	4	1	4	4	4	9858.9747	-0.0004
			5	6				4	5	9859.0623	0.0008
			4	4				3	3	9859.7879	0.0016
			4	5				3	4	9859.8458	-0.0036
			6	6				5	5	9859.6152	0.0001
			6	7				5	6		
			6	5				5	4	9859.7108	0.0004
			7	8				6	7	9860.1334	0.0021
			7	7				6	6	9860.0791	0.0015
6	0	6	6	6	5	0	5	5	5	12033.3620	-0.0003
			6	7				5	6	12033.5472	-0.0025
			6	5				5	4	12033.5731	0.0007
			5	5				4	4	12033.3024	0.0013
			5	6				4	5	12033.4940	0.0002
			7	7				6	6	12033.8893	0.0012
			7	8				6	7	12034.0879	0.0024
			7	6				6	5	12034.1090	0.0041
			8	9				7	8	12034.0520	-0.0006
			8	7				7	6	12034.0721	-0.0017
			8	8				7	7	12033.8527	0.0005
2	2	1	4	4	1	1	0	3	3	11156.6428	0.0003
			4	5				3	4	11157.4959	0.0012
			4	3				3	2	11157.7779	0.0012
			3	2				2	1	11162.8699	-0.0004
			3	4				2	3	11163.0964	0.0007
			3	3				2	2	11163.2997	-0.0001
			2	3				1	2	11165.6794	-0.0010

Chapter 6 - 6-CHLORO-2-HYDROXYPYRIDINE

J'	Ka'	Kc'	F'_N	F'_{Cl}	J''	Ka''	Kc''	F''_N	F''_{Cl}	ν_{OBS}/MHz ^{35}Cl	$\Delta\nu_{OBS-CALC}/MHz$ ^{35}Cl
			2	2				1	1	11165.6084	-0.0053
			2	1				1	1	11165.6372	0.0031
3	1	3	3	2	2	0	2	2	1	7837.5352	0.0003
			3	3				2	2	7837.1343	-0.0015
			3	4				2	3	7837.4217	0.0007
			5	5				4	4	7838.2046	0.0002
			5	6				4	5	7839.0572	0.0007
			5	4				4	3	7839.2721	0.0000
			4	4				3	3	7841.2461	0.0000
			4	5				3	4	7841.7419	-0.0002
			4	3				3	2	7841.8925	-0.0002
4	1	4	4	4	3	0	3	3	3	9409.9818	0.0001
			4	5				3	4	9410.4972	0.0001
			4	3				3	2	9410.6548	-0.0004
			3	3				2	2	9408.1599	0.0005
			3	4				2	3	9408.7660	0.0005
			3	2				2	1	9409.0688	-0.0003
			5	5				4	4	9411.7548	0.0007
			5	6				4	5	9412.3303	0.0005
			5	4				4	3	9412.4565	0.0002
			6	6				5	5	9410.2452	0.0005
			6	7				5	6	9410.9823	-0.0011
			6	5				5	4	9411.1306	0.0008
5	0	5	5	5	4	1	4	4	4	9126.9333	0.0000
			5	6				4	5	9126.7312	0.0007
			5	4				4	3	9126.6653	0.0001
			4	4				3	3	9128.5421	0.0001
			4	5				3	4	9128.2950	0.0039
			4	3				3	2	9128.1553	-0.0009
			6	6				5	5	9127.3883	0.0000
			6	7				5	6	9127.1604	0.0008
			6	5				5	4	9127.1114	-0.0012
			7	8				6	7	9128.3379	0.0017
			7	6				6	5	9128.2707	-0.0014
			7	7				6	6	9128.6383	0.0006
6	1	6	6	6	5	0	5	5	5	12496.3743	0.0030
			6	7				5	6	12496.7478	0.0008
			6	5				5	4	12496.7973	-0.0031
			5	5				4	4	12495.8841	-0.0020
			5	6				4	5	12496.2806	-0.0012
			5	4				4	3	12496.3509	-0.0027
			7	7				6	6	12496.9743	-0.0046
			7	8				6	7	12497.3820	0.0004
			7	6				6	5	12497.4210	-0.0022
			8	9				7	8	12496.9453	0.0022
			8	7				7	6	12496.9961	0.0016
			8	8				7	7	12496.5246	0.0005

Chapter 6 - 6-CHLORO-2-HYDROXYPYRIDINE

J'	Ka'	Kc'	F'_N	F'_{Cl}	J''	Ka''	Kc''	F''_N	F''_{Cl}	ν_{OBS}/MHz ^{35}Cl	$\Delta\nu_{OBS-CALC}/MHz$ ^{35}Cl
10	9	1	12	13	9	8	2	11	12	61314.34	0.00
			9	10				8	9		
10	9	2	12	13	9	8	1	11	12	61315.25	0.00
			9	10				8	9		
10	9	1	11	12	9	8	2	10	11	63491.37	0.01
			10	11				9	10		
10	9	2	11	12	9	8	1	10	11	63492.50	-0.01
			10	11				9	10		
11	9	3	10	11	10	8	2	9	10	65666.70	0.03
			13	14				12	13		
11	9	2	10	11	10	8	3	9	10	65667.92	0.01
			13	14				12	13		
11	9	3	11	12	10	8	2	10	11	67839.30	-0.01
			12	13				11	12		
11	9	2	11	12	10	8	3	10	11	67840.54	-0.02
			12	13				11	12		
12	9	4	11	12	11	8	3	10	11	70008.20	0.01
			14	15				13	14		
12	9	3	11	12	11	8	4	10	11	70009.46	0.04
			14	15				13	14		
12	9	4	12	13	11	8	3	11	12	68143.18	0.01
			13	14				12	13		
12	9	3	12	13	11	8	4	11	12	68143.95	0.02
			13	14				12	13		
13	9	5	12	13	12	8	4	11	12	68143.18	0.01
			15	16				14	15		
13	9	4	12	13	12	8	5	11	12	68143.95	0.02
			15	16				14	15		
13	9	5	13	14	12	8	4	12	13	70008.20	0.01
			14	15				13	14		
13	9	4	13	14	12	8	5	12	13	70009.46	0.04
			14	15				13	14		
14	9	6	13	14	13	8	5	12	13	68143.18	0.01
			16	17				15	16		
14	9	5	13	14	13	8	6	12	13	68143.95	0.02
			16	17				15	16		
14	9	6	14	15	13	8	5	13	14	68143.18	0.01
			15	16				14	15		
14	9	5	14	15	13	8	6	13	14	68143.95	0.02
			15	16				14	15		
11	10	1	13	14	10	9	2	12	13	68143.18	0.01
			10	11				9	10		
11	10	2	13	14	10	9	1	12	13	68143.95	0.02
			10	11				9	10		
11	10	1	12	13	10	9	2	11	12	68143.18	0.01
			11	12				10	11		
11	10	2	12	13	10	9	1	11	12	68143.95	0.02
			11	12				10	11		

Chapter 6 - 6-CHLORO-2-HYDROXYPYRIDINE

J'	Ka'	Kc'	F'_N	F'_{Cl}	J''	Ka''	Kc''	F''_N	F''_{Cl}	ν_{OBS}/MHz ^{35}Cl	$\Delta\nu_{OBS-CALC}/MHz$ ^{35}Cl
12	10	2	11	12	11	9	3	10	11	70320.46	-0.05
			14	15				13	14		
12	10	3	11	12	11	9	2	10	11	70321.46	-0.03
			14	15				13	14		
12	10	2	12	13	11	9	3	11	12	61006.72	0.05
			13	14				12	13		
12	10	3	12	13	11	9	2	11	12	61008.11	0.03
			13	14				12	13		
12	8	5	11	12	11	7	4	10	11	63172.10	0.00
			14	15				13	14		
12	8	4	11	12	11	7	5	10	11	63173.48	0.02
			14	15				13	14		
12	8	5	12	13	11	7	4	11	12	67479.31	0.04
			13	14				12	13		
12	8	4	12	13	11	7	5	11	12	67480.99	-0.09
			13	14				12	13		
13	8	6	12	13	12	7	5	11	12	67480.52	0.03
			15	16				14	15		
13	8	5	12	13	12	7	6	11	12	67482.22	-0.09
			15	16				14	15		
13	8	6	13	14	12	7	5	12	13	69615.87	-0.08
			14	15				13	14		
13	8	5	13	14	12	7	6	12	13	69617.04	-0.01
			14	15				13	14		
15	8	8	14	15	14	7	7	13	14	69620.90	0.02
			17	18				16	17		
15	8	7	14	15	14	7	8	13	14	69622.04	0.06
			17	18				16	17		
15	8	8	15	16	14	7	7	14	15	60608.09	-0.01
			16	17				15	16		
15	8	7	15	16	14	7	8	14	15	60609.36	-0.01
			16	17				15	16		
16	8	9	15	16	15	7	8	14	15	60625.31	0.03
			18	19				17	18		
16	8	9	16	17	15	7	8	15	16	60626.59	0.05
			17	18				16	17		
16	8	8	15	16	15	7	9	14	15		
			18	19				17	18		
16	8	8	16	17	15	7	9	15	16		
			17	18				16	17		
14	7	8	13	14	13	6	7	12	13		
			16	17				15	16		
14	7	8	14	15	13	6	7	13	14		
			15	16				14	15		
14	7	7	13	14	13	6	8	12	13		
			16	17				15	16		
14	7	7	14	15	13	6	8	13	14		
			15	16				14	15		

Chapter 6 - 6-CHLORO-2-HYDROXYPYRIDINE

J'	Ka'	Kc'	F'_N	F'_{Cl}	J''	Ka''	Kc''	F''_N	F''_{Cl}	ν_{OBS}/MHz ^{35}Cl	$\Delta\nu_{OBS-CALC}/MHz$ ^{35}Cl
15	7	9	14	15	14	6	8	13	14	62714.15	0.09
			17	18				16	17		
15	7	9	15	16	14	6	8	14	15	62715.18	-0.08
			16	17				15	16		

Table 6.7 - Measured frequencies in MHz for the transitions observed for deuterated species of conformer Z-6CIHP.

J'	Ka'	Kc'	F'	J''	Ka''	Kc''	F''	$\nu_{\text{OBS}}/\text{MHz}$ $^{35}\text{Cl-OD}$	$\Delta\nu_{\text{OBS-CALC}}/\text{MHz}$ $^{35}\text{Cl-OD}$	$\nu_{\text{OBS}}/\text{MHz}$ $^{37}\text{Cl-OD}$	$\Delta\nu_{\text{OBS-CALC}}/\text{MHz}$ $^{37}\text{Cl-OD}$																																																																																																																																																																																																																																																																																																																																																																				
10	10	0	-	9	9	1	-	63971.76	0.02	63783.89	0.03																																																																																																																																																																																																																																																																																																																																																																				
10	10	1	-	9	9	0	-					11	10	1	13	10	9	2	12	66178.86	0.01	65935.80	-0.11				10				9	11	10	2	10	10	9	1	9				13				12					11	10	1	12	10	9	2	11	66179.77	0.00	65936.64	-0.01				11				10	11	10	2	11	10	9	1	10				12				11					12	10	2	11	11	9	3	10	68385.36	-0.02	68087.39	-0.01				14				13	12	10	3	11	11	9	2	10				14				13					12	10	2	12	11	9	3	11	68386.59	0.03	68088.39	0.03				13				12	12	10	3	12	11	9	2	11				13				12					13	10	3	12	12	9	4	11	70590.31	-0.03	70237.47	-0.01				15				14	13	10	4	12	12	9	3	11				15				14					13	10	3	13	12	9	4	12	70591.67	0.02	70238.56	0.02				14				13	13	10	4	13	12	9	3	12				14				13					11	9	3	10	10	8	2	9	61767.51	-0.05	61486.56	0.01				13				12	11	9	2	10	10	8	3	9				13				12					11	9	3	11	10	8	2	10	61768.91	-0.02	61487.73	0.07				12				11	11	9	2	11	10	8	3	10				12				11					12	9	4	11	11	8	3	10	63971.76	0.07	63635.85	-0.03				14				13	12	9	3	11	11	8	4	10				14				13
11	10	1	13	10	9	2	12	66178.86	0.01	65935.80	-0.11																																																																																																																																																																																																																																																																																																																																																																				
			10				9																																																																																																																																																																																																																																																																																																																																																																								
11	10	2	10	10	9	1	9																																																																																																																																																																																																																																																																																																																																																																								
			13				12																																																																																																																																																																																																																																																																																																																																																																								
11	10	1	12	10	9	2	11	66179.77	0.00	65936.64	-0.01																																																																																																																																																																																																																																																																																																																																																																				
			11				10																																																																																																																																																																																																																																																																																																																																																																								
11	10	2	11	10	9	1	10																																																																																																																																																																																																																																																																																																																																																																								
			12				11																																																																																																																																																																																																																																																																																																																																																																								
12	10	2	11	11	9	3	10	68385.36	-0.02	68087.39	-0.01																																																																																																																																																																																																																																																																																																																																																																				
			14				13																																																																																																																																																																																																																																																																																																																																																																								
12	10	3	11	11	9	2	10																																																																																																																																																																																																																																																																																																																																																																								
			14				13																																																																																																																																																																																																																																																																																																																																																																								
12	10	2	12	11	9	3	11	68386.59	0.03	68088.39	0.03																																																																																																																																																																																																																																																																																																																																																																				
			13				12																																																																																																																																																																																																																																																																																																																																																																								
12	10	3	12	11	9	2	11																																																																																																																																																																																																																																																																																																																																																																								
			13				12																																																																																																																																																																																																																																																																																																																																																																								
13	10	3	12	12	9	4	11	70590.31	-0.03	70237.47	-0.01																																																																																																																																																																																																																																																																																																																																																																				
			15				14																																																																																																																																																																																																																																																																																																																																																																								
13	10	4	12	12	9	3	11																																																																																																																																																																																																																																																																																																																																																																								
			15				14																																																																																																																																																																																																																																																																																																																																																																								
13	10	3	13	12	9	4	12	70591.67	0.02	70238.56	0.02																																																																																																																																																																																																																																																																																																																																																																				
			14				13																																																																																																																																																																																																																																																																																																																																																																								
13	10	4	13	12	9	3	12																																																																																																																																																																																																																																																																																																																																																																								
			14				13																																																																																																																																																																																																																																																																																																																																																																								
11	9	3	10	10	8	2	9	61767.51	-0.05	61486.56	0.01																																																																																																																																																																																																																																																																																																																																																																				
			13				12																																																																																																																																																																																																																																																																																																																																																																								
11	9	2	10	10	8	3	9																																																																																																																																																																																																																																																																																																																																																																								
			13				12																																																																																																																																																																																																																																																																																																																																																																								
11	9	3	11	10	8	2	10	61768.91	-0.02	61487.73	0.07																																																																																																																																																																																																																																																																																																																																																																				
			12				11																																																																																																																																																																																																																																																																																																																																																																								
11	9	2	11	10	8	3	10																																																																																																																																																																																																																																																																																																																																																																								
			12				11																																																																																																																																																																																																																																																																																																																																																																								
12	9	4	11	11	8	3	10	63971.76	0.07	63635.85	-0.03																																																																																																																																																																																																																																																																																																																																																																				
			14				13																																																																																																																																																																																																																																																																																																																																																																								
12	9	3	11	11	8	4	10																																																																																																																																																																																																																																																																																																																																																																								
			14				13																																																																																																																																																																																																																																																																																																																																																																								

Chapter 6 - 6-CHLORO-2-HYDROXYPYRIDINE

J'	Ka'	Kc'	F'	J''	Ka''	Kc''	F''	ν_{OBS}/MHz $^{35}Cl-OD$	$\Delta\nu_{OBS-CALC}/MHz$ $^{35}Cl-OD$	ν_{OBS}/MHz $^{37}Cl-OD$	$\Delta\nu_{OBS-CALC}/MHz$ $^{37}Cl-OD$
12	9	4	12	11	8	3	11				
			13				12				
12	9	3	12	11	8	4	11	63973.14	-0.03	63637.14	0.06
			13				12				
13	9	5	12	12	8	4	11				
			15				14				
13	9	4	12	12	8	5	11	66172.63	-0.03	65782.40	0.03
			15				14				
13	9	5	13	12	8	4	12				
			14				13				
13	9	4	13	12	8	5	12	66174.17	0.00	65783.57	-0.01
			14				13				
14	9	6	13	13	8	5	12				
			16				15				
14	9	5	13	13	8	6	12	68369.14	-0.06	67924.87	0.01
			16				15				
14	9	6	14	13	8	5	13				
			15				14				
14	9	5	14	13	8	6	13	68370.71	0.03	67926.03	-0.02
			15				14				
15	9	7	14	14	8	6	13				
			17				16				
15	9	6	14	14	8	7	13	x	x	70062.04	0.00
			17				16				
15	9	7	15	14	8	6	14				
			16				15				
15	9	6	15	14	8	7	14	x	x	70063.21	0.02
			16				15				
13	8	6	12	12	7	5	11				
			15				14				
13	8	5	12	12	7	6	11	61743.18	0.02	61316.58	-0.03
			15				14				
13	8	6	13	12	7	5	12				
			14				13				
13	8	5	13	12	7	6	12	61744.81	0.02	61317.84	-0.09
			14				13				
14	8	7	13	13	7	6	12				
			16				15				
14	8	6	13	13	7	7	12				
			16				15				
14	8	7	14	13	7	6	13	63928.21	0.06	63448.73	0.05
			15				14				
14	8	6	14	13	7	7	13				
			15				14				
14	8	6	14	13	7	7	13	63929.49	-0.04	63449.67	-0.05
			15				14				
15	8	8	14	14	7	7	13				
			17				16	x	x	65568.67	-0.03

Chapter 6 - 6-CHLORO-2-HYDROXYPYRIDINE

J'	Ka'	Kc'	F'	J''	Ka''	Kc''	F''	ν_{OBS}/MHz $^{35}\text{Cl-OD}$	$\Delta\nu_{OBS-CALC}/\text{MHz}$ $^{35}\text{Cl-OD}$	ν_{OBS}/MHz $^{37}\text{Cl-OD}$	$\Delta\nu_{OBS-CALC}/\text{MHz}$ $^{37}\text{Cl-OD}$
15	8	8	15	14	7	7	14	x	x	65569.89	0.02
			16				15				
15	8	7	14	14	7	8	13	x	x	65571.25	0.08
			17				16				
15	8	7	15	14	7	8	14	x	x	65572.30	-0.05
			16				15				
16	8	9	15	15	7	8	14	68255.81	0.02	x	x
			18				17				
16	8	9	16	15	7	8	15	68257.11	-0.05	x	x
			17				16				
16	8	8	15	15	7	9	14	68265.67	0.03	x	x
			18				17				
16	8	8	16	15	7	9	15	68267.00	0.00	x	x
			17				16				

NOTE: the “-“ symbol in the F column means that the hyperfine quadrupole effect was not resolved; the “x” symbol in the frequency column means that the corresponding line was not measured.

5-CHLORO-2-HYDROXYPYRIDINE

7.1 Introduction

The choice to continue the study of prototropic heterocyclic tautomerism in heterocyclic molecules in order to deepen the role of halogen substitution in the model system 2-pyridone/2-hydroxypyridine (2PO/2HP) was followed, analyzing the rotational spectrum of 5-chloro-2-hydroxypyridine (5ClHP). The importance of this systems was explained in the previous chapter, but some more considerations can be made regarding the substitution effect. Several papers regarded studies on the 2HP/2PO tautomeric system and its derivatives, in order to understand the behavior of the substituent and evaluate the changes produced on this tautomeric equilibrium.

For example, moving from 2HP to 3HP and 4HP the rotational spectrum presents different features: in particular the extent of the tautomeric equilibrium is determined in the first system,^[1] where the rotational spectrum contains information about both 2HP and 2PO, with the enol form being the more stable by 3.2(4) kJ·mol⁻¹. Regarding 3HP, its rotational spectrum is characterized by the presence of two enol conformers with a relatively small energy difference: the *cis* enol conformer is more stable by *ca.* 4(1) kJ·mol⁻¹ than the *trans* enol one.^[2] Instead for the last isomer, 4HP, the rotational spectrum displayed only the enol form, where an internal rotation of the hydroxyl group splits all the μ_c -type-transitions.^[3] In this last study the keto-enolic equilibrium is strongly shifted, with respect to 2HP/2PO, towards the enolic form. This can be attributed to a much higher dipole-dipole interaction energy in the case of 2PO with respect to 4PO. In the former case the C=O and N-H bond electric dipole moment are, indeed, quite anti-parallel, while in the latter one they are exactly parallel, as explained by authors in ref. 3. In these different systems the closeness of the hydroxyl group to the nitrogen atom seems fundamental to stabilize the presence of both tautomers.

On the other hand, the case of 2-mercaptopyridine (2MP), where the oxygen atom is replaced by sulfur, was interesting from the tautomeric and conformational point of view. 2MP was analyzed by microwave spectroscopy and core level photoemission spectroscopy,^[4] and all the three stable conformations were detected. In particular the *anti* enol conformer was easily observed but

also the *syn* enol one and the thione tautomer were found, confirming also in this case the overestimation by MP2 theoretical calculations regarding the energy of the thione tautomer.

Beak *et al.* studied hydroxypyridines, mercaptopyridines and also hydroxypyrimidines with UV spectroscopy,^[5] and they conclude that for this family of compounds the equilibria are different in the vapor and in polar solvents, demonstrating that the environment can have a dominant effect on the stabilities of these system. In particular regarding solvent effects, the authors conclude that as solvent polarity increases, the more polar isomer is stabilized relative to the less polar isomer and that the equilibrium of chloropyridines is least sensitive and that of the thiopyridines most sensitive to the polarity of the medium. The ultraviolet spectra in the gas phase are predominated by the presence of the enol forms for these families of compounds.

Regarding chlorination effect, King *et al.* in their IR work^[6] carried out in isolated argon matrix, studied a lot of mono or trisubstituted chloro-2HP (as already mentioned in Chapter 6), and conclude that the concentration ratio for the keto-enol equilibrium depends on the position of the chlorine atom which has an inductive effect on the ring: progressing from 3-chloro-2-hydroxypyridine to the 4-, 5- and 6- monosubstituted 2HP species, the increase in the enol-keto ratio is observed. Another UV-IR spectroscopic study on 5CIHP was performed by Spinner^[7] in 1986, where it was observed the presence of mainly the keto form in solution of carbon tetrachloride, chloroform and cyclohexane, with extensive NH...O=C intermolecular association; while the energetic balance favoring the keto over the enol tautomer is not very great in water. In this paper it is also explained that at the concentrations required for IR spectroscopy, the proportion of unassociated 5CIHP is too low to obtain information about the equilibrium of single monomers of 5CIHP/5CIPO, because of the large presence of dimers. For this reason a gas phase spectroscopic study can be interesting to give precise and unambiguous information on this equilibrium.

It can be noted that the panorama on analogous systems of 2HP is very rich and also in this case the lack of high resolution molecular spectroscopic studies on 5CIHP encourage to fill this gap.

The experimental investigation was carried out with the same procedure already described in Chapter 6 for 6CIHP. Two different spectrometers were used to record the rotational spectra: the FJAMMW in the University of Bologna (see Chapter 3 for more details) and the MB-FTMW in the University of Bilbao.^[8]

7.2 Theoretical calculations

Unlike the analogous 6CIHP, to the best of my knowledge, for 5CIHP no theoretical calculations were performed earlier. For this reason structural optimizations were carried out with both MP2 and

B3LYP methods at 6-311++G** level of calculation. The same level of theory was used for 6CIHP, in order to compare the computational results.

Similarly to 6CIHP, also 5CIHP presents three different stable forms: 2 enolic conformations (*Z*- or *E*-5CIHP depending on the position of the hydrogen of the hydroxyl group) and one keto form (5CIPO). All three forms are reported in Figure 7.1.

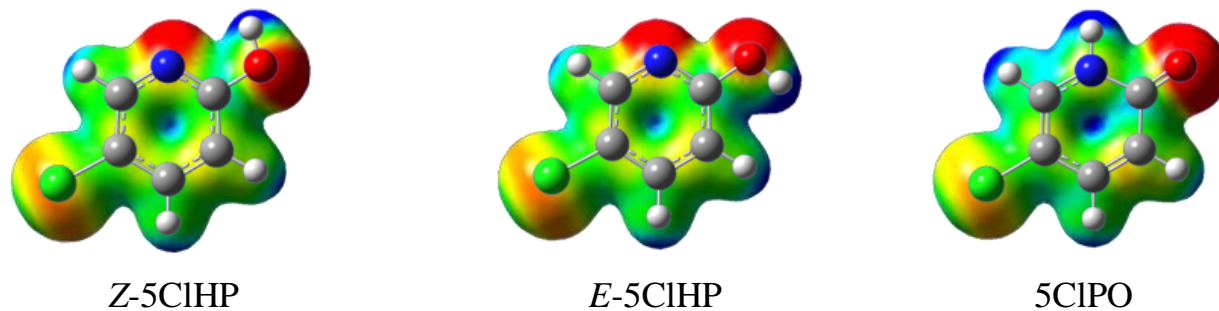


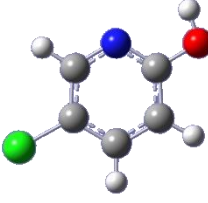
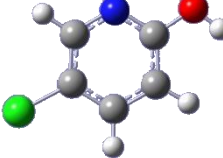
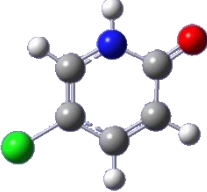
Figure 7.1 - Pictures of the three conformers of 5CIHP. For each conformation the electronic distribution surface color coded with respect to the electrostatic potential is also displayed. The red areas identify the most electronegative regions and the blue ones the most electropositive areas.

The geometries were fully optimized and subsequently vibrational frequency calculations in the harmonic approximation confirmed that the stationary points were actual minima. All calculations were performed with the Gaussian03-B.01^[9] program package, and all the spectroscopic parameters are shown in Table 7.1.

Looking the results, it can be noted that the theoretical calculations show the same trend than in the 6CIHP case. The *Z*-5CIHP conformer is predicted as global minimum, the *E*-5CIHP conformer is evaluated to be very high in energy, more than 20 kJ·mol⁻¹ above the global minimum and concerning the keto tautomer the results are quite different using the two different methods. In fact, looking at the ZPE-corrected energies values for the keto form reported in Table 7.1, the B3LYP method also in this case predicts 5CIPO quite stable (B3LYP: $\Delta E_0=3.95$ kJ·mol⁻¹) while the MP2 method continues to estimate a high energy value for this tautomer (MP2: $\Delta E_0=18.94$ kJ·mol⁻¹). Because of the very large difference of this values, further MP4/6-311++G** calculations were performed on this system. The relative ZPE-corrected energies values obtained for the *Z*-5CIHP, *E*-5CIHP and 5CIPO are respectively: 0 (absolute energy value:-781.855908 Hartrees), 22.68 and 10.06 kJ·mol⁻¹. The trend already observed for 6CIHP is confirmed also in this case from the results obtained with the MP4 method: the stability of the keto tautomer is increased using this method and falls between that predicted by B3LYP and MP2.

All the spectroscopic parameters useful for the rotational investigation together with the population ratios values between the different species at 413K, temperature estimated and used (see below) to vaporize the sample, are listed in Table 7.1.

Table 7.1 - Theoretical (B3LYP/6-311++G** and MP2/6-311++G**) spectroscopic parameters for 5CIHP stable conformers and their shape.

	Z-5CIHP		E-5CIHP		5CIPO	
						
6-311++G**	MP2	B3LYP	MP2	B3LYP	MP2	B3LYP
<i>A</i> / MHz	5772	5810	5794	5835	5639	5638
<i>B</i> / MHz	1001	997	997	993	1000	999
<i>C</i> / MHz	853	851	850	848	850	848
<i>D_J</i> / kHz	0.0184	0.019	0.0182	0.0188	0.0186	0.019
<i>D_{JK}</i> / kHz	0.0738	0.076	0.0737	0.0757	0.0658	0.0761
<i>D_K</i> / kHz	1.1315	1.1496	1.148	1.1639	1.2727	1.2268
<i>d₁</i> / kHz	-0.0033	-0.0033	-0.0032	-0.0033	-0.0033	-0.0035
<i>d₂</i> / kHz	-0.0004	-0.0004	-0.0004	-0.0004	-0.0004	-0.0004
<i>μ_a</i> / D	-0.14	-0.47	-0.28	-0.64	-2.52	-2.53
<i>μ_b</i> / D	0.65	0.59	3.50	3.43	1.16	1.24
<i>μ_c</i> / D	0.00	0.00	0.00	0.00	-0.01	0.00
<i>μ_{tot}</i> / D	0.67	0.75	3.51	3.50	2.78	2.82
<i>χ_{aa}</i> / MHz N	0.27	0.4	0.19	0.35	1.59	1.75
<i>χ_{bb}</i> / MHz N	-2.68	-2.77	-2.97	-3.11	1.15	1.34
<i>χ_{cc}</i> / MHz N	2.41	2.37	2.78	2.77	-2.74	-3.09
<i>χ_{ab}</i> / MHz N	-2.62	-2.84	-2.75	-2.98	0.05	0.06
<i>χ_{aa}</i> / MHz Cl	-71.12	-70.53	-71.07	-70.49	-72.37	-72.21
<i>χ_{bb}</i> / MHz Cl	36.88	37.39	36.89	37.42	36.71	37.44
<i>χ_{cc}</i> / MHz Cl	34.24	33.14	34.19	33.07	35.66	34.77
<i>χ_{ab}</i> / MHz Cl	3.2	3.22	3.32	3.19	0.81	0.57
ΔE_0 / kJ•mol ⁻¹	0.00 ^a	0.00 ^b	21.78	22.00	18.94	3.95
N _i /N ₀ % (413K)	100	100	0.184	0.173	0.419	31.923

^a Absolute zero point corrected energy: -781.680008 Hartrees.

^b Absolute zero point corrected energy: -783.150143 Hartrees.

If the possibility to observe the *E*-5CIHP form remains precluded because of its high energy, as in the analogous 6CIHP, instead, regarding the 5CIPO tautomer, the B3LYP method predicts an energy value that produces an estimated population ratio for this species to be a third compared to the global minimum and this together with the relatively high calculated values of the dipole moments components ($\mu_a=2.5$ Debye and $\mu_b=1.2$ Debye) supports its possible detection.

7.3 Experimental Results and Analysis

The millimeter-wave spectrum (59.6-74.4 GHz) of 5CIHP was recorded using the free jet absorption millimeter wave spectrometer (FJAMMW - VDI setup), the basic details of which have been reported previously (see Chapter 3). A subsequent analysis was performed from 4 to 18 GHz with the MB-FTMW at the University of Bilbao, (see ref. 8 for technical details), where the presence of an efficient custom-made heating nozzle^[10] allowed the recording and analysis of the rotational spectrum of this molecule. 5CIHP was purchased from Alfa Aesar (98+%) and used without further purification. The sample is solid at room temperature with a melting point of about 165°C, so it was necessary to heat it at 120-140°C, to obtain the vapor pressure suitable for the experiment in both spectrometers. Regarding the experiment with the FJAMMW, the carrier gas was argon at a pressure of 25 kPa above the sample and the mixture containing the vaporized sample was expanded to about 0.05 kPa through a 0.35 mm diameter nozzle, held at 5°C above the vaporization temperature. Regarding the MB-FTMW experiment, the carrier gas was helium at stagnation pressures of about 200-500 kPa that was expanded through a 0.8 mm nozzle to form a pulsed jet (*ca.* 200 μ s). Due to the parallel arrangement of the jet and the radiation, in this spectrometer all transitions are split by the Doppler effect, so that the rest frequencies are calculated as the average frequency of the two components. With the MB-FTMW instrument the accuracy of the frequency measurements is better than 3 kHz and transitions separated less than *ca.* 10 kHz are resolvable while for the FJAMMW spectrometer the accuracy of the frequency measurements is just under 50 kHz. In both cases no decomposition products were noticeable.

The analysis of the rotational spectrum started with the FJAMMW spectrometer (59.6-74.4 GHz), and similarly to the previous analysis on 6CIHP, the predictions based on calculation allowed a straightforward assignment regarding the *Z*-5CIHP conformer. Even if the rotational parameters between the two tautomers are very close (see Table 7.1), the assignment of only μ_b -R-type rotational transitions without the observation of any μ_a -type lines confirmed the presence of the *Z*-5CIHP tautomer in the jet plume. Also in this case, the presence of two nuclei with nuclear spin $I > 1/2$, Cl and N, causes the splitting of each rotational transition in a hyperfine structure as a result of

the coupling of nuclear spin with the overall rotation of the molecule. However, the nitrogen splitting was not expected to be large enough to be measurable with the resolution of the FJAMMW; instead it was possible to observe and partially resolve, the splitting due to the chlorine atom. In this spectrum, 65 different lines were measured and fitted as μ_b -R-type rotational transitions for the parent species, and it was possible to measure only 20 different lines for the ^{37}Cl isotopologue because of the low intensity of the observations performed in natural abundance. These first sets of rotational transitions were fitted using Watson's semirigid Hamiltonian in the "S" reduction and I^r representation.^[11] Based on the relative energy values obtained with B3LYP calculations, an accurate search for the keto tautomer was conducted, accumulating the signal in areas where the calculations predicted the most intense lines. Unfortunately no other lines were observed which could be attributed to the 5CIPO tautomer.

In the same way as it was done for 6CIHP, also for Z-5CIHP the hydroxyl deuterated species were analyzed fluxing D_2O over the sample. In this way the spectra of the ^{35}Cl -OD and the ^{37}Cl -OD isotopomers were observed and analyzed, even if the low intensity of the signals did not allow the measurement of many lines. Also these rotational transitions were fitted using Watson's semirigid Hamiltonian in the "S" reduction and I^r representation,^[11] and the spectroscopic parameters are shown in Table 7.3 while the list of measured frequencies is reported in Table 7.8.

After this first experimental research, a second investigation was carried out with the MB-FTMW in Bilbao. Starting from the fit already performed, the search for the lines was straightforward. Since the high resolution of this spectrometer allowed the observation of more 12 hyperfine components (attributed to the nuclear quadrupole coupling effects caused by the ^{14}N , ^{35}Cl and ^{37}Cl nuclei) for each rotational transition, the assignment of each quadrupole components of Z-5CIHP was challenging. 173 different lines were measured for the parent species, and they were fitted as different quadrupole components of 7 μ_a -R-type transitions, 6 μ_b -R-type transitions and 1 μ_b -Q-type transition. The high sensitivity of this spectrometer allowed us also to observe μ_a -type lines that were undetectable with the FJAMMW. Regarding the ^{37}Cl isotopomer 127 lines were measured as components of 7 different μ_a -R-type transitions and 5 μ_b -R-type transitions. All the spectroscopic parameters fitted for both isotopomers are reported in Table 7.1. The errors assigned to each frequency line used in the fit procedure were of 50 kHz for the FJAMMW measurements and 5 kHz for the MB-FTMW ones. All the measured transitions are listed in Tables 7.5 and 7.6.

Even if the search for the keto tautomer was vain with the other spectrometer, the chance to observe it in the MB-FTMW was still real, being confident of the B3LYP energy results and the values of the dipole moments components that would help its possible detection.

Starting from the prediction of the rotational constants, the most intense μ_a -type lines were searched for the keto tautomer, using high sensitivity conditions. Finally some new lines were observed and the 5CIPO was detected. 76 different lines were measured, fitted as 90 different quadrupole components of 5 μ_a -R-type transitions and 2 μ_b -R-type transitions. Because of the very low intensity of the lines, the spectrum of the ^{37}Cl isotopomer could not be observed. The rotational transitions were fitted using Watson's semirigid Hamiltonian in the "S" reduction and I' representation,^[11] and the spectroscopic parameters are shown in Table 7.2 while the measured frequencies are listed in Table 7.7.

Table 7.2 - Experimental spectroscopic parameters of the observed tautomers Z-5CIHP (for ^{35}Cl and ^{37}Cl isotopologues) and 5CIPO (only ^{35}Cl parent species).

	Z-5CIHP		5CIPO
	^{35}Cl	^{37}Cl	^{35}Cl
<i>A</i> /MHz	5785.0267(5) ^a	5784.848(1)	5612.110(1)
<i>B</i> /MHz	1006.60906(7)	980.2862(4)	1009.4284(2)
<i>C</i> /MHz	857.47814(9)	838.2986(2)	855.6732(2)
<i>D_J</i> /kHz	0.018(1)	0.025(4)	0.021(3)
<i>D_{JK}</i> /kHz	0.07(1)	0.05(2)	
<i>D_K</i> /kHz	1.19(2)	1.19(3)	
<i>d_J</i> /kHz	-0.005(3)	-0.008(3)	
χ_{aa} / MHz Cl	-72.772(4)	-57.363(4)	-74.30(2)
χ_{bb} / MHz Cl	37.949(4)	29.916(5)	37.991(9)
χ_{cc} / MHz Cl	34.823(4)	27.4478(5)	36.312(9)
χ_{aa} / MHz N	0.282(5)	0.281(4)	1.636(5)
χ_{bb} / MHz N	-2.635(4)	-2.637(5)	1.241(7)
χ_{cc} / MHz N	2.352(4)	2.356(5)	-2.876(7)
<i>P_{cc}</i> /uÅ ²	0.021	0.021	0.044
<i>N</i> ^b	286	187	90
σ^c / MHz	0.02	0.01	0.003

^a Error in parentheses in units of the last digit.

^b Number of lines in the fit.

^c Root-mean-square deviation of the fit.

Table 7.3 - Experimental spectroscopic constants of the observed monodeuterated species of Z-5CIHP conformer, both for the ^{35}Cl and ^{37}Cl isotopologues.

Z-5CIHP		
	$^{35}\text{Cl-OD}$	$^{37}\text{Cl-OD}$
<i>A</i> /MHz	5728.720(1) ^a	5728.45(1)
<i>B</i> /MHz	983.675(3)	958.22(9)
<i>C</i> /MHz	839.595(3)	820.62(8)
<i>D_J</i> /Hz	0.020(5)	[0.025] ^b
<i>D_{JK}</i> /Hz	[0.07] ^b	[0.05] ^b
<i>D_K</i> /Hz	[1.19] ^b	1.6(2)
<i>d_J</i> /kHz	[-0.005] ^b	[-0.008] ^b
χ_{aa} - Cl	-73.5(3)	-58.0(4)
<i>N</i> ^c	49	28
σ^d / MHz	0.05	0.04

^a Error in parentheses in units of the last digit.

^b Values fixed to the ones of the parent species.

^c Number of lines in the fit.

^d Root-mean-square deviation of the fit.

To achieve information about the abundances of the detected conformers in the supersonic jet, relative intensities (*I*) measurements of the rotational transitions were performed. The information on the abundances can be obtained because there is a direct relation between the intensities and the population of each conformer in the jet (*N_i*). The relation between them also includes the component of the dipole moment involved along each axis (μ_g) according to the following expression:

$$\frac{N_i}{N_0} \propto \frac{I_i \omega_0 \Delta v_i \mu_g^2(0) \lambda_0 v_0^2}{I_0 \omega_i \Delta v_0 \mu_g^2(i) \lambda_i v_i^2} \propto \frac{I_i}{I_0} \cdot \frac{\mu_g^2(0)}{\mu_g^2(i)}$$

where ω is the conformational degeneration, Δv the line width at half height and γ the line strength.^[12] In this way, if the transition intensities are well-known for the different conformers, it is possible to estimate the abundance of each conformer respect to the most stable one. It is important to remark that this analysis assumes that only the ground vibrational state of each conformer is populated during the supersonic expansion and that there is no conformational relaxation between conformers, as occurs in the present study for the two tautomers observed due to the high barrier to interconversion between the enol and keto form.

Another important fact is that the calculation of relative intensities strongly depends on several experimental factors, so for sure this is an approximate method.

Because of the very low intensity of the lines, above all for the 5CIPO tautomer, only the most intense μ_a -type transitions were taken into account for the relative intensity measurements. Lines that lie in the same frequency region have been recorded in the same conditions in order to minimize the experimental errors. Moreover the presence of the hyperfine quadrupole splitting increase the difficulty for this kind of measurements and the most separated components were considered for this abundance estimation.

The measured intensity ratio between equivalent lines of the two tautomers normalized for the calculated dipole moment component (*Z*-5CIHP: $\mu_a = -0.47/-0.14$ D and 5CIPO: $\mu_a = -2.53/-2.52$ D; B3LYP/MP2 respectively) suggests that the global minimum is the *Z*-5CIHP enolic form and that the relative abundance in the supersonic expansion is about 5 to 1. Assuming that no relaxation occurs in the jet, the derived relative energy is about $14 \text{ kJ}\cdot\text{mol}^{-1}$. Although the error on the approximated energies can be estimates to be up to 40%, taking also into account that the dipole moments components are the predicted ones and that the intensity measurements are affected by the partial overlapping of different quadrupole transitions, this value points out that the MP2 and MP4 calculated relative energy is closer to the experimental one than the B3LYP results. In Figure 7.2 the comparison between the two tautomers for an equivalent transitions recorded for this intensity measurements, is reported.

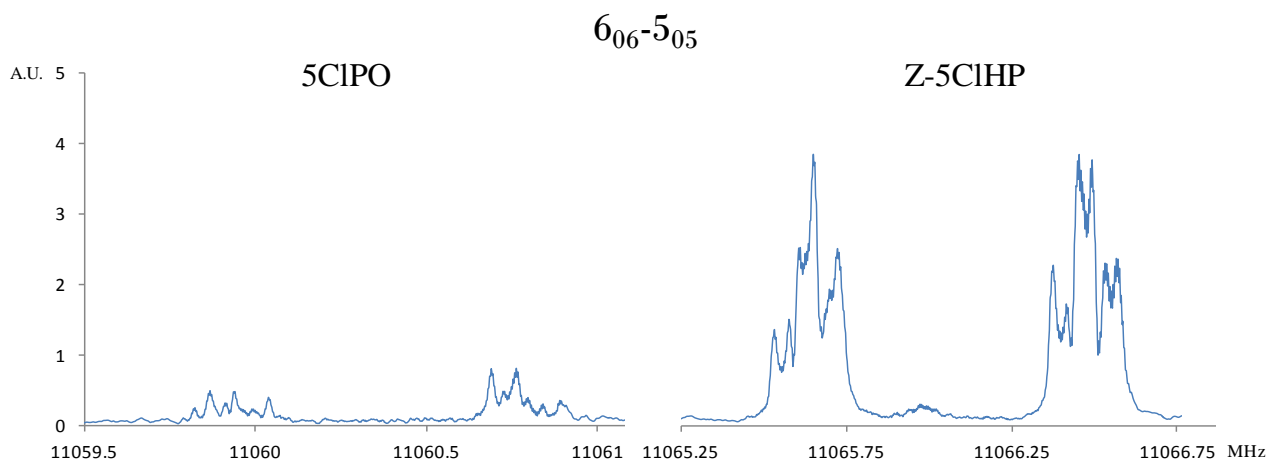


Figure 7.2 - Portion of the $6_{06}-5_{05}$ μ_a -type transition recorded for intensity measurement for both tautomers of 5CIHP.

From the experimental rotational constants obtained for the different isotopic species of Z-5ClHP, a partial experimental r_s -structure using Kraitchman's substitution method was determined.^[13] Such analysis leads to the determination of the absolute value of the principal axis coordinates of the substituted atom from the changes in principal moments of inertia resulting from a single isotopic substitution. As reported in Table 7.4, the coordinates for the chlorine and the hydroxyl (OH) hydrogen atoms were obtained. Also for 5ClHP, as already explained in the previous chapter for 6ClHP, each atom coordinates can be obtained considering different kind of mono-substitution: in particular the chlorines coordinates can be obtained considering the hydrogenated species as parent or considering the deuterated ones. The same can be done for the hydrogens coordinates: they can be calculated from the ^{35}Cl species but also considering the ^{37}Cl isotopomer as the parent species. Looking at Table 7.4, these values can be compared to the calculated ones (r_e), both with MP2 and B3LYP methods, and also to the ones obtained from the r_0 structure.

In fact, to extract information about the structure of the global minimum observed, a partial r_0 -structure analysis was performed starting from the MP2 planar structure and adjusting some structural parameters to reproduce the observed rotational constants. The choice to use the MP2 planar geometry is due to the closer values of rotational constants to the experimental ones (mostly for B and C) and looking at the planar moment of inertia P_{cc} reported in Table 7.3. This value represents the mass distribution on the c axis and the experimental almost zero values obtained confirm the planarity of the system, as occurred also for the 6ClHP molecule. In this analysis the experimental rotational constants of the parent species together with those of ^{37}Cl , and of the deuterated species ($^{35}\text{Cl-OD}$ and $^{37}\text{Cl-OD}$) were used to fit some structural parameter with the STRFIT program.^[14] The similarity with the analogous 6ClHP lead to fit also in this case the same structural parameters: in particular the Cl-C and the O-C distances and the NC6C5 angle. The obtained values are respectively: 1.722(4)Å, 1.349(7)Å and 122.32(3)° and the experimental rotational constants are reproduced with an error that falls within unit of MHz. Comparing these values with the calculated ones (Cl-C =1.731 Å, O-C =1.355 Å and NC6C5 =122.535°) and with the ones obtained from the same procedure for the 6ClHP (Cl-C =1.724(2)Å, O-C =1.345(7)Å and NC6C5 =124.28(9)°), it can be noted again that if the variation on the angle of the ring is quite small, the distances were reduced of about 0.01 Å respect to the calculated values, and that these distances converge to the same values obtained for the 6ClHP.

From this r_0 structure, the coordinates relative to the chlorine atom and the hydroxyl hydrogen were derived resulting in the values shown in Table 7.4.

Table 7.4 - Values of the coordinates (\AA) relating to the isotopic substitutions (r_s), obtained from computational data (r_e) and derived from the effective structure (r_0) for Z-5CIHP.

Cl	r_s^a	r_e	r_e	r_0
		B3LYP	MP2	
a	± 2.6182 (3)/ ± 2.635 (5)*	2.638	2.626	2.618(2)
b	± 0.04 (4)/ ± 0.05 (3)*	-0.037	-0.037	-0.0337(4)
H				
a	± 3.4204 (5)/ ± 3.446 (8) ^o	-3.446	-3.431	-3.421(5)
b	± 0.940 (2)/ ± 0.941 (2) ^o	-0.941	-0.938	-0.9348(4)

^a Error expressed in units of the last decimal digit.

* The first chlorine coordinate value is obtained from the hydrogenated species while the second one is obtained considering the deuterated ones as starting species.

^o The first hydrogen coordinate values is obtained from the ³⁵Cl species, instead the second one is obtained considering the ³⁷Cl species.

7.4 Conclusions

The rotational spectrum of the most stable Z-enol tautomer of 5CIHP have been assigned in two frequency ranges (4-18 GHz and 59.6-74.4 GHz), with two different spectrometers (FJAMMW and MB-FTMW), while the keto tautomer 5CIPO was observed only with the more sensitive MB-FTMW instrument. Thanks to the higher resolution of the latter one, the quadrupole nuclear splittings for both Cl and N nucleus were resolved. In addition all the spectroscopic parameters were fitted also for the ³⁷Cl isotopologue of the global minimum Z-5CIHP, in natural abundance. Moreover for this conformer the enriched hydroxyl monodeuterated species for both ³⁵Cl and ³⁷Cl species, in the higher frequency range, were analyzed. From these rotational constants, experimental r_s and r_0 coordinates for the hydroxyl H and the Cl atoms were obtained.

The fact that the keto tautomer was observed only in the more sensitive MB-FTMW spectrometer, even if it has got relatively high dipole moment components, already suggests that the global minimum is for sure the Z-5CIHP enol conformer. To support this conclusion, relative intensity measurements were carried out and resulting in a 5 to 1 relative abundance in favor of the Z-5CIHP, with an estimated relative energy of about 14 kJ·mol⁻¹. This result points out the considerable underestimation performed by DFT calculations in describing this kind of tautomeric systems.

The most important conclusion that can be drawn from this work on chlorine substituted 2-hydroxypyridines is that chlorination in C-5 position induces an increase in the stability of the

5CIPO form rather than in the analogue 6CIHP studied previously, where the keto tautomer was not observed with the same experimental setup and similar calculated dipole moments components. This is in agreement with some older observations,^[6] where the stability in the keto/enol ratio increases moving the substituents towards the hydroxyl group.

7.5 References

- [1] L. D. Hatherley, R. D. Brown, P. D. Godfrey, A. P. Pierlot, W. Caminati, D. Damiani, S. Melandri, L. B. Favero, *J. Phys. Chem.*, 97, 46-51, **1993**.
- [2] R. Sanchez, B. M. Giuliano, S. Melandri, W. Caminati, *ChemPhysLett*, 435, 10-13, **2007**.
- [3] R. Sanchez, B. M. Giuliano, S. Melandri, W. Caminati, *ChemPhysLett*, 425, 6, **2006**.
- [4] S. Melandri, L. Evangelisti, A. Maris, W. Caminati, B. M. Giuliano, V. Feyer, K. C. Price, M. Coreno, *J. Am. Chem. Soc.*, 132, 30, 10269-10271, **2010**.
- [5] P. Beak, F. S. Fry, Jr., J. Lee, F. Steele, *J. Am. Chem. Soc.*, 98, 171-179, **1976**.
- [6] S. S. T. King, W. L. Dilling, N. B. Tefertiller, *Tetrahedron*, 28, 5859-5863, **1972**.
- [7] E. Spinner, *Spectrochim. Acta*, 42A, 11, 1289-1293, **1986**.
- [8] E. J. Cocinero, A. Lesarri, P. Ecija, J.-U. Grabow, J. A. Fernandez, F. Castano, *Phys. Chem. Chem. Phys.*, 12, 6076–6083, **2010**.
- [9] M. J. T. Frisch, G. W.; Schlegel, H. B.; Scuseria, G. E.; Robb, M. A.; Cheeseman, J. R.; Montgomery, Jr., J. A.; Vreven, T.; Kudin, K. N.; Burant, J. C.; Millam, J. M.; Iyengar, S. S.; Tomasi, J.; Barone, V.; Mennucci, B.; Cossi, M.; Scalmani, G.; Rega, N.; Petersson, G. A.; Nakatsuji, H.; Hada, M.; Ehara, M.; Toyota, K.; Fukuda, R.; Hasegawa, J.; Ishida, M.; Nakajima, T.; Honda, Y.; Kitao, O.; Nakai, H.; Klene, M.; Li, X.; Knox, J. E.; Hratchian, H. P.; Cross, J. B.; Adamo, C.; Jaramillo, J.; Gomperts, R.; Stratmann, R. E.; Yazyev, O.; Austin, A. J.; Cammi, R.; Pomelli, C.; Ochterski, J. W.; Ayala, P. Y.; Morokuma, K.; Voth, G. A.; Salvador, P.; Dannenberg, J. J.; Zakrzewski, V. G.; Dapprich, S.; Daniels, A. D.; Strain, M. C.; Farkas, O.; Malick, D. K.; Rabuck, A. D.; Raghavachari, K.; Foresman, J. B.; Ortiz, J. V.; Cui, Q.; Baboul, A. G.; Clifford, S.; Cioslowski, J.; Stefanov, B. B.; Liu, G.; Liashenko, A.; Piskorz, P.; Komaromi, I.; Martin, R. L.; Fox, D. J.; Keith, T.; Al-Laham, M. A.; Peng, C. Y.; Nanayakkara, A.; Challacombe, M.; Gill, P. M. W.; Johnson, B.; Chen, W.; Wong, M. W.; Gonzalez, C.; Pople, J. A. , Gaussian 03 (Revision B.01) ed., Gaussian, Inc., Pittsburgh PA, **2003**.
- [10] R. D. Suenram, F. J. Lovas, D. F. Plusquellic, A. Lesarri, Y. Kawashima, J. O. Jensen, A. C. Samuels, *J. Mol. Spectrosc.*, 211, 110, **2002**.
- [11] J. K. G. Watson, "Vibrational spectra and structure", Vol. 6, Elsevier, Amsterdam, Oxford & New York, **1977**.
- [12] J.-U. Grabow, W. Caminati, *Microwave Spectroscopy: Experimental Techniques*. In *Frontiers of Molecular Spectroscopy*; Laane, J., Ed.; Elsevier: Amsterdam, The Netherlands, , Chapter 14, 383-454, **2008**.
- [13] J. Kraitchman, *Am. J. Phys.*, 21, **1953**.

[14] Kisiel, Z. PROSPE - Programs for Rotational SPECTroscopy
<http://www.ifpan.edu.pl/~kisiel/prospe.htm>

7.6 Appendix

Table 7.5 - Measured frequencies (MHz) for the transitions observed for the parent species of Z-5CIHP conformer.

J'	Ka'	Kc'	F'_N	F'_{Cl}	J''	Ka''	Kc''	F''_N	F''_{Cl}	ν_{OBS}/MHz ^{35}Cl	$\Delta\nu_{OBS-CALC}/\text{MHz}$ ^{35}Cl
4	0	4	4	4	3	0	3	3	3	7420.5147	0.0015
			3	4				2	3		
			4	5				3	4		
			3	2				2	1		
			4	3				3	2		
			3	3				2	2		
			5	5				4	4		
			6	7				5	6		
			5	6				4	5		
			5	4				4	3		
4	1	3	4	4	3	1	2	3	3	7745.9871	-0.0006
			4	5				3	4		
			4	3				3	2		
			3	3				2	2		
			3	4				2	3		
			3	2				2	1		
			5	5				4	4		
			5	6				4	5		
			5	4				4	3		
			3	2				2	2		
4	1	4	5	4	3	1	3	5	4	7137.3052	0.0014
			5	6				5	6		
			5	5				5	5		
			4	4				3	3		
			4	5				3	4		
			4	3				3	2		
			3	4				2	3		
			5	5				4	4		
			5	6				4	5		
			5	4				4	3		
4	1	4	6	6	3	1	3	5	5	7152.3980	0.0004
			6	7				5	6		
			6	5				5	4		
			4	4				4	4		
			4	4				4	4		
			4	4				4	4		
			4	4				4	4		
			4	4				4	4		
			4	4				4	4		
			4	4				4	4		

Chapter 7 - 5-CHLORO-2-HYDROXYPYRIDINE

J'	Ka'	Kc'	F'_N	F'_{Cl}	J''	Ka''	Kc''	F''_N	F''_{Cl}	ν_{OBS}/MHz ^{35}Cl	$\Delta\nu_{OBS-CALC}/MHz$ ^{35}Cl
			4	5				4	5	7155.9288	0.0009
			4	3				4	3	7155.9528	-0.0008
5	0	5	5	5	4	0	4	4	4	9251.3488	-0.0033
			5	6				4	5	9251.4046	-0.0019
			5	4				4	3	9251.4227	0.0048
			4	4				3	3	9251.3104	0.0022
			4	5				3	4	9251.3685	0.0021
			6	6				5	5	9252.6090	-0.0036
			6	7				5	6	9252.6665	-0.0031
			7	8				6	7	9252.6286	0.0004
			7	6				6	5	9252.6432	0.0058
			7	7				6	6	9252.5690	0.0039
5	1	4	5	6	4	1	3	4	5	9676.5969	-0.0024
			5	4				4	3	9676.6272	0.0013
			5	5				4	4	9676.6892	-0.0010
			6	7				5	6	9677.4457	0.0019
			4	5				3	4	9677.4846	-0.0082
			6	6				5	5	9677.5092	-0.0025
			4	4				3	3	9677.5662	-0.0001
			4	3				3	2	9677.5662	-0.0001
			7	8				6	7	9678.3560	-0.0036
			7	7				6	6	9678.3806	0.0031
			7	6				6	5	9678.3806	0.0031
5	1	5	5	5	4	1	4	4	4	8931.9935	0.0010
			5	6				4	5	8932.0945	0.0022
			5	4				4	3	8932.0767	-0.0030
			4	5				3	4	8932.9884	-0.0003
			6	6				5	5	8932.7932	-0.0003
			4	4				3	3	8932.8992	-0.0047
			6	7				5	6	8932.8701	0.0030
			6	5				5	4	8932.8565	-0.0008
			7	8				6	7	8933.7601	0.0011
			7	7				6	6	8933.7265	0.0025
6	0	6	6	6	5	0	5	5	5	11065.6182	-0.0025
			6	7				5	6	11065.6902	-0.0022
			5	5				4	4	11065.5664	-0.0014
			5	6				4	5	11065.6428	0.0006
			5	4				4	3	11065.6594	0.0055
			7	7				6	6	11066.4574	-0.0035
			7	8				6	7	11066.5315	-0.0024
			8	9				7	8	11066.4865	0.0026
			8	7				7	6	11066.4965	0.0039
			8	8				7	7	11066.4085	0.0009
			6	5				5	4	11065.7049	0.0022
6	1	5	6	6	5	1	4	5	5	11602.3295	0.0024
			6	7				5	6	11602.2827	-0.0010
			6	5				5	4	11602.3061	-0.0030

Chapter 7 - 5-CHLORO-2-HYDROXYPYRIDINE

J'	Ka'	Kc'	F'_N	F'_{Cl}	J''	Ka''	Kc''	F''_N	F''_{Cl}	ν_{OBS}/MHz ^{35}Cl	$\Delta\nu_{OBS-CALC}/MHz$ ^{35}Cl
			5	5				4	4	11602.8142	-0.0033
			5	6				4	5	11602.7897	0.0018
			5	4				4	3	11602.8380	0.0016
			7	7				6	6	11602.9710	0.0019
			7	8				6	7	11602.9369	-0.0003
			7	6				6	5	11602.9531	-0.0046
			8	9				7	8	11603.4527	-0.0005
			8	8				7	7	11603.4527	-0.0005
			8	7				7	6	11603.4750	0.0044
2	1	2	2	1	1	0	1	1	1	8339.2762	0.0058
			2	3				1	2	8339.3032	0.0007
			2	2				1	2	8339.3322	-0.0031
			2	2				1	1	8339.3322	-0.0031
			3	3				3	3	8347.3889	-0.0011
			3	4				3	4	8347.7190	-0.0001
			3	2				3	3	8347.7358	0.0028
			3	2				3	2	8347.8160	-0.0016
			1	2				1	2	8348.0562	0.0008
			1	2				1	1	8348.0562	0.0008
			1	1				1	2	8348.0767	-0.0092
			1	1				1	1	8348.0767	-0.0092
			4	4				3	3	8355.7997	0.0049
			4	5				3	4	8356.4935	0.0008
			4	3				3	3	8356.6584	0.0003
			4	3				3	2	8356.7436	0.0008
			3	3				2	3	8365.5995	0.0038
			3	3				2	2	8365.6522	-0.0002
			3	4				2	3	8365.8652	-0.0002
			2	3				2	3	8372.0496	-0.0022
3	1	3	2	3	2	0	2	1	2	9991.7218	0.0018
			3	3				2	2	9996.2057	-0.0009
			3	3				2	3	9996.2057	-0.0009
			3	4				2	3	9996.5755	0.0003
			3	2				2	2	9996.7180	0.0005
			5	5				4	4	9997.8366	0.0001
			5	6				4	5	9998.5933	-0.0002
			5	4				4	3	9998.7791	0.0009
			4	4				3	3	10002.9322	0.0020
			4	5				3	4	10003.4564	0.0000
			4	3				3	2	10003.5872	-0.0031
4	1	4	4	4	3	0	3	3	3	11570.8998	0.0008
			4	5				3	4	11571.4577	0.0000
			4	3				3	2	11571.6161	0.0018
			3	4				2	3	11568.3952	-0.0009
			3	2				2	1	11568.6696	-0.0043
			3	3				2	2	11567.7600	-0.0013
			5	5				4	4	11574.0420	-0.0030

Chapter 7 - 5-CHLORO-2-HYDROXYPYRIDINE

J'	Ka'	Kc'	F'_N	F'_{Cl}	J''	Ka''	Kc''	F''_N	F''_{Cl}	ν_{OBS}/MHz ^{35}Cl	$\Delta\nu_{OBS-CALC}/MHz$ ^{35}Cl
			5	6				4	5	11574.6862	0.0003
			5	4				4	3	11574.8117	-0.0021
			6	6				5	5	11570.8676	-0.0001
			6	7				5	6	11571.6401	0.0017
			6	5				5	4	11571.7849	-0.0013
5	1	5	5	5	4	0	4	4	4	13082.3808	0.0006
			5	6				4	5	13083.0093	0.0003
			5	4				4	3	13083.1414	-0.0009
			4	4				3	3	13080.1853	0.0004
			4	5				3	4	13080.8690	-0.0008
			4	3				3	2	13081.0672	-0.0021
			6	6				5	5	13084.2005	-0.0003
			6	7				5	6	13084.8788	-0.0006
			6	5				5	4	13084.9887	0.0003
			7	8				6	7	13082.7554	0.0008
			7	6				6	5	13082.8788	0.0041
			7	7				6	6	13081.9964	0.0000
6	1	6	6	7	5	0	5	5	6	14541.9402	-0.0027
			6	5				5	4	14542.0480	-0.0035
			5	5				4	4	14539.6658	-0.0005
			5	6				4	5	14540.3500	-0.0001
			5	4				4	3	14540.4998	0.0004
			7	7				6	6	14542.4803	-0.0012
			7	8				6	7	14543.1570	-0.0009
			7	6				6	5	14543.2459	-0.0012
			8	9				7	8	14541.5751	-0.0017
			6	6				5	5	14541.3005	0.0001
			8	8				7	7	14540.8492	-0.0005
			8	7				7	6	14541.6781	0.0032
6	0	6	6	7	5	1	5	5	6	7234.0897	-0.0004
			6	5				5	4	7233.9776	-0.0005
			5	5				4	4	7236.6904	-0.0007
			5	6				4	5	7236.1370	-0.0016
			5	4				4	3	7235.9658	-0.0002
			7	7				6	6	7234.8737	0.0008
			7	8				6	7	7234.3240	0.0000
			7	6				6	5	7234.2340	0.0001
			8	9				7	8	7236.3569	-0.0006
			6	6				5	5	7234.5925	-0.0001
			8	8				7	7	7236.9768	0.0005
			8	7				7	6	7236.2553	0.0000
7	1	6	6	5	7	0	7	6	5	7262.7482	-0.0004
			9	8				9	8	7262.8633	-0.0007
			6	7				6	7	7262.9471	0.0011
			9	10				9	10	7262.9928	-0.0015
			7	6				7	6	7263.1922	-0.0005
			8	7				8	7	7263.2813	0.0001

Chapter 7 - 5-CHLORO-2-HYDROXYPYRIDINE

J'	Ka'	Kc'	F'_N	F'_{Cl}	J''	Ka''	Kc''	F''_N	F''_{Cl}	ν_{OBS}/MHz ^{35}Cl	$\Delta\nu_{OBS-CALC}/MHz$ ^{35}Cl
			7	8				7	8	7263.3609	0.0000
			8	9				8	9	7263.4276	-0.0001
			6	6				6	6	7264.0099	0.0003
			9	9				9	9	7264.1080	-0.0001
			7	7				7	7	7264.3786	-0.0002
			8	8				8	8	7264.4645	0.0021
6	6	0	8	9	5	5	1	7	8	64566.12	0.02
6	6	1	8	9	5	5	0	7	8		
6	6	0	5	6	5	5	1	4	5	64567.03	0.00
6	6	1	5	6	5	5	0	4	5		
6	6	0	7	8	5	5	1	6	7	64567.40	0.01
6	6	1	7	8	5	5	0	6	7		
6	6	0	6	7	5	5	1	5	6	64568.36	0.02
6	6	1	6	7	5	5	0	5	6		
8	6	3	7	8	7	5	2	6	7	68295.26	-0.03
8	6	2	7	8	7	5	3	6	7		
8	6	3	10	11	7	5	2	9	10	68295.64	-0.03
8	6	2	10	11	7	5	3	9	10		
8	6	3	8	9	7	5	2	7	8	68298.25	0.03
8	6	2	8	9	7	5	3	7	8		
8	6	3	9	10	7	5	2	8	9	68298.61	0.02
8	6	2	9	10	7	5	3	8	9		
9	6	4	8	9	8	5	3	7	8	70159.60	0.00
9	6	3	8	9	8	5	4	7	8		
9	6	4	11	12	8	5	3	10	11	70160.05	0.00
9	6	3	11	12	8	5	4	10	11		
9	6	4	9	10	8	5	3	8	9	70162.46	-0.03
9	6	3	9	10	8	5	4	8	9		
9	6	4	10	11	8	5	3	9	10	70162.92	-0.01
9	6	3	10	11	8	5	4	9	10		
10	6	5	9	10	9	5	4	8	9	72023.27	-0.01
10	6	4	9	10	9	5	5	8	9		
10	6	5	12	13	9	5	4	11	12	72023.70	-0.02
10	6	4	12	13	9	5	5	11	12		
10	6	5	10	11	9	5	4	9	10	72025.98	-0.01
10	6	4	10	11	9	5	5	9	10		
10	6	5	11	12	9	5	4	10	11	72026.38	-0.05
10	6	4	11	12	9	5	5	10	11		
9	5	5	8	9	8	4	4	7	8	60451.43	0.10
9	5	4	8	9	8	4	5	7	8		
9	5	5	11	12	8	4	4	10	11	60451.98	0.05
9	5	4	11	12	8	4	5	10	11		
9	5	5	10	11	8	4	4	9	10	60454.97	0.00
9	5	4	10	11	8	4	5	9	10		
10	5	6	9	10	9	4	5	8	9	62311.83	0.04
			12	13				11	12		
10	5	5	9	10	9	4	6	8	9	62312.37	-0.07

Chapter 7 - 5-CHLORO-2-HYDROXYPYRIDINE

J'	Ka'	Kc'	F'_N	F'_{Cl}	J''	Ka''	Kc''	F''_N	F''_{Cl}	ν_{OBS}/MHz ^{35}Cl	$\Delta\nu_{OBS-CALC}/MHz$ ^{35}Cl
			12	13				11	12	62313.01	-0.08
10	5	6	10	11	9	4	5	9	10	62314.57	0.08
			11	12				10	11	62315.14	-0.01
10	5	5	10	11	9	4	6	9	10	62315.82	0.02
			11	12				10	11	64169.61	0.00
11	5	7	10	11	10	4	6	9	10	64170.08	0.02
			13	14				12	13	64171.47	0.04
11	5	6	10	11	10	4	7	9	10	64171.97	0.02
			13	14				12	13	64172.45	-0.02
11	5	6	11	12	10	4	7	10	11	64173.84	0.00
			12	13				11	12	64174.32	0.03
13	5	9	12	13	12	4	8	11	12	67872.67	-0.06
			15	16				14	15	67873.04	-0.02
			13	14				12	13	67874.64	-0.01
			14	15				13	14	67874.97	-0.01
13	5	8	12	13	12	4	9	11	12	67880.56	0.01
			15	16				14	15	67880.89	0.01
			13	14				12	13	67882.49	0.03
			14	15				13	14	67882.79	0.00
14	5	10	13	14	13	4	9	12	13	69715.29	-0.08
			16	17				15	16	69716.96	0.02
			14	15				13	14	69717.23	0.00
			15	16				14	15	69730.03	0.02
14	5	9	13	14	13	4	10	12	13	69730.29	0.00
			16	17				15	16	69731.71	-0.01
			14	15				13	14	69732.04	0.03
			15	16				14	15	60097.04	0.02
14	4	10	16	17	13	3	11	15	16	60098.20	0.01
			14	15				13	14	60098.48	0.01
			15	16				14	15	61374.80	-0.05
15	4	12	14	15	14	3	11	13	14	61376.33	0.05
			15	16				14	15	61376.58	0.05
			16	17				15	16	62000.41	-0.09
15	4	11	15	16	14	3	12	14	15	62000.73	0.00
			16	17				15	16	62997.98	0.02
16	4	13	15	16	15	3	12	14	15	62998.18	0.01
			18	19				17	18	62999.36	-0.03
			16	17				15	16	63926.46	0.07
			17	18				16	17	63927.60	0.08
17	4	14	16	17	16	3	13	15	16	64546.85	0.01
			19	20				18	19		

Chapter 7 - 5-CHLORO-2-HYDROXYPYRIDINE

J'	Ka'	Kc'	F'_N	F'_{Cl}	J''	Ka''	Kc''	F''_N	F''_{Cl}	ν_{OBS}/MHz ^{35}Cl	$\Delta\nu_{OBS-CALC}/MHz$ ^{35}Cl
17	4	13	16	17	16	3	14	15	16	65887.11	-0.06
			19	20				18	19	65887.31	-0.03
			17	18				16	17	65888.23	-0.01
			18	19				17	18		
17	3	14	16	17	16	2	15	15	16		
			19	20				18	19	60221.31	0.02
			17	18				16	17		
			18	19				17	18		
18	3	15	17	18	17	2	16	16	17		
			20	21				19	20	63257.69	-0.01
			18	19				17	18		
			19	20				18	19		

Table 7.6 - Measured frequencies (MHz) for the transitions observed for the ^{37}Cl isotopomer of Z-5CIHP conformer.

J'	Ka'	Kc'	F'_N	F'_{Cl}	J''	Ka''	Kc''	F''_N	F''_{Cl}	$\nu_{\text{OBS}}/\text{MHz}$ ^{37}Cl	$\Delta\nu_{\text{OBS-CALC}}/\text{MHz}$ ^{37}Cl
4	0	4	3	3	3	0	3	2	2	7242.1446	0.0007
			3	4				2	3	7242.1757	0.0034
			4	4				3	3		
			4	5				3	4		
			3	2				2	1	7242.1937	-0.0059
			4	3				3	2		
			5	6				4	5	7243.8714	-0.0035
			5	4				4	3	7243.8899	0.0059
			6	7				5	6	7243.8506	-0.0025
			6	6				5	5	7243.8081	-0.0001
4	1	3	4	4	3	1	2	3	3	7550.7456	-0.0008
			4	5				3	4	7550.5582	-0.0021
			4	3				3	2	7550.5702	0.0006
			3	3				2	2	7552.1466	0.0001
			3	4				2	3	7551.9718	-0.0022
			3	2				2	1	7552.1002	0.0002
			5	5				4	4	7551.4953	-0.0005
			5	6				4	5	7551.3557	-0.0017
			5	4				4	3	7551.3787	0.0037
			6	6				5	5	7552.8536	-0.0007
			6	7				5	6	7552.8133	-0.0002
5	0	5	5	6	4	0	4	4	5	9030.6810	-0.0015
			5	4				4	3	9030.6947	0.0013
			4	4				3	3	9030.5992	0.0016
			6	5				5	4	9031.6898	0.0036
			6	6				5	5	9031.6176	-0.0055
			6	7				5	6	9031.6748	-0.0020
			7	8				6	7	9031.6440	-0.0028
			7	6				6	5	9031.6609	0.0052
			7	7				6	6	9031.5891	0.0021
			5	4				4	4	9030.7147	0.0073
			6	5				5	5	9031.6951	-0.0059
5	1	4	4	4	4	1	3	3	3	9433.7737	0.0020
			4	5				3	4	9433.6979	-0.0003
			4	3				3	2	9433.7737	0.0014
			6	6				5	5	9433.7324	0.0019
			6	7				5	6	9433.6601	-0.0010
			6	5				5	4	9433.6773	-0.0068
			7	8				6	7	9434.3848	-0.0011
			7	6				6	5	9434.4057	0.0020
			7	7				6	6		
5	1	5	5	5	4	1	4	4	4	8723.9489	0.0002

Chapter 7 - 5-CHLORO-2-HYDROXYPYRIDINE

J'	Ka'	Kc'	F'_{N}	F'_{Cl}	J''	Ka''	Kc''	F''_{N}	F''_{Cl}	ν_{OBS}/MHz ^{37}Cl	$\Delta\nu_{OBS-CALC}/MHz$ ^{37}Cl
			5	6				4	5	8724.0498	0.0014
			5	4				4	3	8724.0330	-0.0036
			4	5				3	4	8724.7565	0.0005
			4	4				3	3	8724.6798	0.0086
			4	3				3	2	8724.6955	-0.0038
			6	6				5	5	8724.5831	-0.0020
			6	7				5	6	8724.6587	0.0009
			7	8				6	7	8725.3611	0.0034
			7	7				6	6	8725.3173	-0.0058
			7	6				6	5	8725.3392	-0.0001
5	2	4	6	5	4	2	3	5	4	9084.3689	-0.0011
			6	7				5	6		
			6	6				5	5	9084.3849	0.0030
			5	4				4	3		
			5	6				4	5	9084.7898	-0.0018
			5	5				4	4	9084.8074	0.0033
6	1	6	6	6	5	1	5	5	5	10461.3187	0.0008
			6	7				5	6	10461.3853	0.0000
			6	5				5	4	10461.3682	-0.0041
			5	5				4	4	10461.7260	-0.0025
			5	6				4	5	10461.7831	-0.0020
			7	7				6	6	10461.8160	0.0061
			7	8				6	7	10461.8673	0.0039
			7	6				6	5	10461.8530	-0.0005
			8	9				7	8	10462.2614	0.0033
			8	8				7	7	10462.2231	-0.0035
			8	7				7	6	10462.2443	-0.0004
2	1	2	2	3	1	0	1	1	2	8285.4260	0.0030
			2	2				1	2		
			2	2				1	1	8285.4641	-0.0019
			3	3				3	3	8291.7332	-0.0003
			3	4				3	4		
			3	2				3	3	8292.0682	-0.0024
			1	2				1	2		
			1	2				1	1	8292.3236	0.0016
			1	1				1	2		
			1	1				1	1	8292.3572	-0.0034
			4	4				3	3	8298.3225	0.0004
			4	5				3	4	8299.0181	-0.0002
			3	3				2	2	8306.1494	-0.0015
			3	4				2	3	8306.3627	-0.0075
			2	3				2	3	8311.2313	-0.0027
			3	2				2	1	8306.3946	0.0054
			2	1				2	1	8311.1427	-0.0022
			2	2				2	3	8311.2811	0.0042
			2	3				2	2	8311.2951	0.0045
			2	2				2	2	8311.3330	-0.0002

Chapter 7 - 5-CHLORO-2-HYDROXYPYRIDINE

J'	Ka'	Kc'	F'_N	F'_{Cl}	J''	Ka''	Kc''	F''_N	F''_{Cl}	ν_{OBS}/MHz ^{37}Cl	$\Delta\nu_{OBS-CALC}/MHz$ ^{37}Cl
3	1	3	4	4	2	0	2	4	4	9895.0621	0.0000
			4	5				4	5	9895.6285	0.0010
			2	2				1	1	9900.2270	0.0019
			2	2				1	2	9900.6772	0.0005
			2	3				1	2	9900.6772	0.0005
			3	3				2	2	9904.1540	0.0010
			3	3				2	3	9904.1540	0.0010
			3	4				2	3	9904.5184	0.0014
			3	2				2	2	9904.6586	0.0050
			5	5				4	4	9905.3668	0.0010
			5	6				4	5	9906.1243	0.0008
			5	4				4	3	9906.3122	0.0017
			4	4				3	3	9909.4081	0.0000
			4	5				3	4	9909.9379	-0.0004
4	3	3	2	9910.0673	0.0014						
4	1	4	4	4	3	0	3	3	3	11446.5119	-0.0002
			4	5				3	4	11447.0677	-0.0006
			4	3				3	2	11447.2204	-0.0004
			6	7				5	6	11447.2204	-0.0004
			3	4				2	3	11444.6469	-0.0010
			3	2				2	1	11444.9193	-0.0070
			3	3				2	2	11444.0124	0.0000
			5	5				4	4	11448.9637	-0.0029
			5	6				4	5	11449.6121	0.0003
			5	4				4	3	11449.7331	-0.0016
			6	6				5	5	11446.4452	-0.0012
			6	5				5	4	11447.3678	-0.0011
5	1	5	5	5	4	0	4	4	4	12928.2922	0.0000
			5	6				4	5	12928.9218	0.0009
			5	4				4	3	12929.0531	0.0004
			4	4				3	3	12926.5407	0.0009
			4	5				3	4	12927.2287	0.0007
			4	3				3	2	12927.4286	-0.0001
			6	6				5	5	12929.7100	0.0000
			6	7				5	6	12930.3945	0.0000
			6	5				5	4	12930.5005	0.0013
			7	8				6	7	12928.7252	0.0012
6	1	6	6	7	5	0	5	5	6	14359.6226	-0.0009
			6	5				5	4	14359.7325	0.0008
			5	5				4	4	14357.6711	0.0003
			5	6				4	5	14358.3583	-0.0023
			7	7				6	6	14359.8966	-0.0001
			7	8				6	7	14360.5801	-0.0009
			7	6				6	5	14360.6672	0.0007
			8	9				7	8	14359.3347	-0.0004

Chapter 7 - 5-CHLORO-2-HYDROXYPYRIDINE

J'	Ka'	Kc'	F'_N	F'_{Cl}	J''	Ka''	Kc''	F''_N	F''_{Cl}	ν_{OBS}/MHz ^{37}Cl	$\Delta\nu_{OBS-CALC}/MHz$ ^{37}Cl
			6	6				5	5	14358.9782	-0.0005
			8	8				7	7	14358.6008	0.0000
			8	7				7	6	14359.4355	0.0007
6	6	0	8	9	5	5	1	7	8	64541.53	0.00
6	6	1	8	9	5	5	0	7	8		
6	6	0	5	6	5	5	1	4	5	64542.28	0.01
6	6	1	5	6	5	5	0	4	5		
6	6	0	7	8	5	5	1	6	7	64542.53	-0.03
6	6	1	7	8	5	5	0	6	7		
6	6	0	6	7	5	5	1	5	6	64543.31	0.01
6	6	1	6	7	5	5	0	5	6		
8	6	3	7	8	7	5	2	6	7	68179.79	0.09
8	6	2	7	8	7	5	3	6	7		
8	6	3	10	11	7	5	2	9	10	68179.99	-0.01
8	6	2	10	11	7	5	3	9	10		
8	6	3	8	9	7	5	2	7	8	68181.99	-0.02
8	6	2	8	9	7	5	3	7	8		
8	6	3	9	10	7	5	2	8	9	68182.26	-0.04
8	6	2	9	10	7	5	3	8	9		
9	6	4	8	9	8	5	3	7	8	69998.50	0.01
9	6	3	8	9	8	5	4	7	8		
9	6	4	11	12	8	5	3	10	11	69998.82	-0.02
9	6	3	11	12	8	5	4	10	11		
9	6	4	9	10	8	5	3	8	9	70000.76	0.00
9	6	3	9	10	8	5	4	8	9		
9	6	4	10	11	8	5	3	9	10	70001.08	-0.03
9	6	3	10	11	8	5	4	9	10		
10	6	5	9	10	9	5	4	8	9	71816.76	0.07
10	6	4	9	10	9	5	5	8	9		
10	6	5	12	13	9	5	4	11	12	71817.04	0.01
10	6	4	12	13	9	5	5	11	12		
10	6	5	10	11	9	5	4	9	10	71818.80	-0.02
10	6	4	10	11	9	5	5	9	10		
10	6	5	11	12	9	5	4	10	11	71819.14	-0.03
10	6	4	11	12	9	5	5	10	11		
9	5	5	8	9	8	4	4	7	8		
			11	12				10	11		
9	5	4	8	9	8	4	5	7	8	60245.57	-0.01
			11	12				10	11		
9	5	5	9	10	8	4	4	8	9		
			10	11				9	10		
9	5	4	9	10	8	4	5	8	9	60248.02	0.04
			10	11				9	10		

Chapter 7 - 5-CHLORO-2-HYDROXYPYRIDINE

J'	Ka'	Kc'	F'_N	F'_{Cl}	J''	Ka''	Kc''	F''_N	F''_{Cl}	ν_{OBS}/MHz ^{37}Cl	$\Delta\nu_{OBS-CALC}/MHz$ ^{37}Cl
11	5	7	10	11	10	4	6	9	10	63873.78	-0.02
			13	14				12	13		
11	5	6	10	11	10	4	7	9	10	63875.44	-0.04
			13	14				12	13		
11	5	7	11	12	10	4	6	10	11	63877.21	0.04
			12	13				11	12		
11	5	6	11	12	10	4	7	10	11	63877.21	0.04
			12	13				11	12		

Table 7.7 - Measured frequencies in MHz for the transitions observed for the parent species of 5CIPO conformer.

J'	Ka'	Kc'	F'_N	F'_{Cl}	J''	Ka''	Kc''	F''_N	F''_{Cl}	ν_{OBS}/MHz ^{35}Cl	$\Delta\nu_{OBS-CALC}/MHz$ ^{35}Cl
4	0	4	3	3	3	0	3	2	2	7421.1553	0.0036
			3	4				2	3	7421.0007	-0.0017
			4	3				3	2	7421.0193	0.0015
			4	5				3	4	7421.1786	-0.0013
			4	4				3	3	7423.3244	-0.0012
			5	5				4	4	7423.1991	0.0017
			5	6				4	5	7423.1840	-0.0028
			5	4				4	3	7423.2618	0.0022
			6	5				5	4	9249.4749	0.0000
			6	6				5	5	9249.5085	-0.0013
5	0	5	4	5	4	0	4	3	4	9249.5900	0.0048
			5	6				4	5	9249.6256	-0.0008
			5	4				4	3	9249.6256	-0.0008
			4	3				3	2	9250.7729	0.0000
			4	4				3	3	9250.8038	0.0037
			5	5				4	4	9250.9018	0.0006
			7	8				6	7	11060.0020	0.0019
			6	7				5	6	11060.0252	-0.0022
			6	5				5	4	11059.8991	0.0015
			6	6				5	5	11059.9228	0.0048
6	0	6	6	6	5	0	5	5	5	11059.9525	-0.0012
			7	6				6	6	11059.8559	0.0003
			6	7				5	6	11059.8711	-0.0056
			6	5				5	4	11060.8500	-0.0008
			8	7				7	7	11060.7566	0.0001
			5	5				4	4	11060.7240	0.0017
			5	6				4	5	11060.8019	0.0019
			5	4				4	3	9691.6340	0.0036
			5	6				4	5	9691.6181	-0.0014
			4	5				3	4	9691.6028	-0.0044
5	1	4	5	5	4	1	3	4	4	9692.5332	-0.0024
			4	5				3	4	9692.4765	0.0020
			6	6				5	5	9692.4570	0.0019
			6	7				5	6	9692.4429	-0.0022
			6	5				5	4		

Chapter 7 - 5-CHLORO-2-HYDROXYPYRIDINE

J'	Ka'	Kc'	F'_N	F'_{Cl}	J''	Ka''	Kc''	F''_N	F''_{Cl}	ν_{OBS}/MHz ^{35}Cl	$\Delta\nu_{OBS-CALC}/MHz$ ^{35}Cl
5	1	5	5	5	4	1	4	4	4	8924.1950	0.0007
			5	6				4	5	8924.0297	-0.0007
			5	4				4	3	8924.0561	0.0029
			4	5				3	4	8924.9448	0.0008
			4	4				3	3	8925.0874	-0.0020
			4	3				3	2	8925.0174	-0.0085
			6	6				5	5	8924.9878	0.0009
			6	7				5	6	8924.8530	0.0023
			7	8				6	7	8925.7885	-0.0039
			7	7				6	6	8925.8678	-0.0004
7	6	6	5	8925.8093	-0.0003						
4	1	4	4	4	3	1	3	3	3	7143.9716	-0.0008
			4	5				3	4	7143.6959	0.0050
			4	3				3	2	7144.8721	0.0000
			5	5				4	4	7144.6502	-0.0042
			5	6				4	5	7146.6552	0.0010
			5	4				4	3	7146.5363	-0.0014
			6	6				5	5	7146.5540	0.0034
			6	7				5	6		
4	1	3	4	4	3	1	2	3	3	7758.4048	-0.0024
			4	3				3	2	7758.4228	0.0025
			4	5				3	4	7760.2612	-0.0001
			3	3				2	2	7759.4193	0.0045
			3	4				2	3	7759.4033	-0.0005
			5	5				4	4	7759.3844	-0.0065
			5	6				4	5		
3	1	3	3	3	2	0	2	2	2	9812.7020	0.0004
			3	4				2	3	9812.1525	0.0000
			5	5				4	4	9814.7045	-0.0023
			5	6				4	5	9814.1642	0.0022
			5	4				4	3	9814.0798	-0.0002
			4	4				3	3	9819.5402	0.0068
			4	5				3	4	9819.0293	0.0000
2	1	2	4	4	1	0	1	3	3	8178.3425	0.0000
			4	5				3	4	8177.8893	0.0028
			3	2				2	1	8186.9446	-0.0020
			4	3				3	2	8177.8639	-0.0037
			3	4				2	3	8187.3899	0.0008
4	1	4	4	4	3	0	3	3	3	11380.0173	-0.0007
			4	5				3	4	11379.4804	0.0000
			5	5				4	4	11383.1915	-0.0016
			5	6				4	5	11382.6718	0.0000
			5	4				4	3	11382.5528	-0.0043
			6	6				5	5	11380.2598	-0.0007
			6	7				5	6	11379.6819	0.0013

Chapter 7 - 5-CHLORO-2-HYDROXYPYRIDINE

J'	Ka'	Kc'	F'_N	F'_{Cl}	J''	Ka''	Kc''	F''_N	F''_{Cl}	ν_{OBS}/MHz ^{35}Cl	$\Delta\nu_{OBS-CALC}/MHz$ ^{35}Cl
			6	5				5	4	11379.6046	0.0007

Table 7.8 - Measured frequencies in MHz for the transitions observed for deuterated species of conformer Z-5CIHP.

J'	Ka'	Kc'	F'	J''	Ka''	Kc''	F''	$\nu_{\text{OBS}}/\text{MHz}$ $^{35}\text{Cl-OD}$	$\Delta\nu_{\text{OBS-CALC}}/\text{MHz}$ $^{35}\text{Cl-OD}$	$\nu_{\text{OBS}}/\text{MHz}$ $^{37}\text{Cl-OD}$	$\Delta\nu_{\text{OBS-CALC}}/\text{MHz}$ $^{37}\text{Cl-OD}$
6	6	0	8	5	5	1	7	63926.47	0.01	63901.02	0.02
6	6	1	8	5	5	0	7				
6	6	0	5	5	5	1	4	63927.45	0.04		
6	6	1	5	5	5	0	4			63901.83	-0.06
6	6	0	7	5	5	1	6	63927.74	-0.03		
6	6	1	7	5	5	0	6				
6	6	0	6	5	5	1	5	63928.72	0.00	63902.74	-0.05
6	6	1	6	5	5	0	5				
7	6	2	6	6	5	1	5				
			9				8				
7	6	1	6	6	5	2	5	65750.35	0.01	65680.54	0.10
			9				8				
7	6	1	7	6	5	2	6				
			8				7				
7	6	2	7	6	5	1	6	65752.95	-0.02	65682.52	0.01
			8				7				
8	6	3	7	7	5	2	6			67459.57	-0.03
8	6	2	7	7	5	3	6	67574.12	0.02		
8	6	3	10	7	5	2	9			67459.87	-0.03
8	6	2	10	7	5	3	9				
8	6	3	8	7	5	2	7				
			9				8				
8	6	2	8	7	5	3	7	67577.00	-0.05	67462.16	0.08
			9				8				
9	6	4	8	8	5	3	7	69397.41	0.03	69238.66	0.03
9	6	3	8	8	5	4	7				
9	6	4	11	8	5	3	10	69397.80	-0.04	69239.02	0.03
9	6	3	11	8	5	4	10				
9	6	4	9	8	5	3	8	69400.31	0.02	69240.92	-0.01
9	6	3	9	8	5	4	8				
9	6	4	10	8	5	3	9	69400.70	-0.05	69241.27	-0.02
9	6	3	10	8	5	4	9				
10	6	5	9	9	5	4	8	71220.31	0.04		
10	6	4	9	9	5	5	8			71017.26	-0.04
10	6	5	12	9	5	4	11	71220.70	-0.02		
10	6	4	12	9	5	5	11				
10	6	5	10	9	5	4	9	71223.03	0.03	71019.28	0.00
10	6	4	10	9	5	5	9				
10	6	5	11	9	5	4	10	71223.43	-0.02	71019.60	-0.03
10	6	4	11	9	5	5	10				
10	5	6	9	9	4	5	8	61580.84	-0.02	61334.67	0.09

Chapter 7 - 5-CHLORO-2-HYDROXYPYRIDINE

J'	Ka'	Kc'	F'	J''	Ka''	Kc''	F''	$\nu_{\text{OBS}}/\text{MHz}$ $^{35}\text{Cl-OD}$	$\Delta\nu_{\text{OBS-CALC}}/\text{MHz}$ $^{35}\text{Cl-OD}$	$\nu_{\text{OBS}}/\text{MHz}$ $^{37}\text{Cl-OD}$	$\Delta\nu_{\text{OBS-CALC}}/\text{MHz}$ $^{37}\text{Cl-OD}$
10	5	6	12	9	4	5	11	61581.44	-0.03	61335.00	-0.08
10	5	5	9	9	4	6	8				
10	5	5	12	9	4	6	11	61582.10	0.02	61335.49	-0.08
10	5	6	10	9	4	5	9	61583.59	0.00	61336.68	-0.06
10	5	6	11	9	4	5	10	61584.19	-0.01	61337.44	0.04
10	5	5	10	9	4	6	9				
10	5	5	11	9	4	6	10	61584.88	0.07		
11	5	7	10	10	4	6	9	63398.32	0.04	63108.41	0.09
11	5	7	13	10	4	6	12	63398.74	0.01		
11	5	6	10	10	4	7	9	63399.92	0.02		
11	5	6	13	10	4	7	12	63400.54	0.01	63110.00	0.06
11	5	7	11	10	4	6	10				
11	5	7	12	10	4	6	11	63401.12	-0.04		
11	5	6	11	10	4	7	10	63402.29	-0.04	63111.37	-0.01
11	5	6	12	10	4	7	11	63402.73	-0.05	63111.73	-0.01
12	5	8	11	11	4	7	10	65212.28	-0.10	64878.65	-0.05
			14				13				
12	5	8	12	11	4	7	11	65214.50	-0.04	64880.41	0.01
			13				12				
12	5	7	11	11	4	8	10	65215.83	-0.03	64881.47	-0.08
			14				13				
12	5	7	12	11	4	8	11	65218.00	-0.01	64883.33	0.07
			13				12				
13	5	9	12	12	4	8	11	67021.67	0.07		
			15				14				
			13				12	67023.58	0.06		
			14				13				
13	5	8	12	12	4	9	11	67028.55	-0.01		
			15				14				
			13				12	67030.57	0.08		
			14				13				
14	5	10	13	13	4	9	12	68824.71	-0.02		
			16				15				
			14				13	68826.47	0.01		
			15				14				
14	5	9	13	13	4	10	12	68837.94	0.04		
			16				15				
			14				13	68839.68	0.06		
			15				14				
15	4	12	14	14	3	11	13	60552.31	-0.06		
			17				16				
			15				14	60553.81	0.08		
			16				15				

Chapter 7 - 5-CHLORO-2-HYDROXYPYRIDINE

J'	Ka'	Kc'	F'	J''	Ka''	Kc''	F''	$\nu_{\text{OBS}}/\text{MHz}$ $^{35}\text{Cl-OD}$	$\Delta\nu_{\text{OBS-CALC}}/\text{MHz}$ $^{35}\text{Cl-OD}$	$\nu_{\text{OBS}}/\text{MHz}$ $^{37}\text{Cl-OD}$	$\Delta\nu_{\text{OBS-CALC}}/\text{MHz}$ $^{37}\text{Cl-OD}$
15	4	11	14	14	3	12	13	61124.42	0.00		
			17				16				
			15				14	61125.72	0.01		
			16				15				
16	4	13	15	15	3	12	14	62152.26	-0.04		
			18				17				
			16				15	62153.55	0.01		
			17				16				
16	4	12	15	15	3	13	14	63003.37	-0.05		
			18				17				
			16				15	63004.57	-0.01		
			17				16				

2-FLUOROPYRIDINE ... WATER**8.1 Introduction**

Pyridine (PY) is one of the most important heterocyclic aromatic molecule and it continues to be an important topic of research in all the areas of chemistry and biochemistry-related journal with more than 30000 publications in the last five years. PY and a large number of its derivatives are used extensively in coordination and surface chemistry, and for this reason, as described by Q. Gou and co-workers,^[1] many of its molecular adducts have been studied using high resolution molecular spectroscopy.

On the other hand water is ubiquitous in chemical, physical and biological systems and the knowledge of the ways it interacts with the various kinds of molecules would be helpful to understand the solvation processes in aqueous environments and its effects on gas-phase reactions.^[2-5] The type of the complexes of water with organic molecules has been described and classified in a recent paper.^[6] Depending on the nature of the partner molecules, water can act as a proton donor or a proton acceptor, or with a double role. In several cases, it has been shown that halogenations affects the way in which organic molecules interact with water. For instance, water generally acts as a proton donor to form relative strong (15-25 kJ·mol⁻¹) hydrogen bonds with ethers.^[7-10] Regarding instead the 1:1 adduct of a halogenated ether (the anesthetic isoflurane) with water, the conformation stabilized by a O-H...O interaction through the ether oxygen, expected to be the global minimum, has not been observed. The water subunit is found to link isoflurane as a proton acceptor, through an almost linear C-H...O weak hydrogen bond.^[11] In trifluoroanisole-H₂O, the triple fluorination of the methyl group greatly affects the features of the rotational spectrum of the complex with water,^[12] with respect to the related complex anisole-water.^[13] From these features, the shape, the internal dynamics and the isotopic effects turned out to be quite different with respect to those of the anisole-water adduct. The configurations observed in adducts of water with molecules containing a π -electrons system, such as ethylene-water^[14] and benzene-water^[15], have been found to be stabilized by OH... π interactions. However, an O-lone pair... π (Bürgi-Dunitz

$n-\pi^*$) interaction where the oxygen lone pairs are directed towards the π -system is the driving force found to stabilize the water adduct of a perhalogenated ethylene, the chlorotrifluoroethylene.^[16]

Regarding the interaction of PY with solvent molecules, a recent paper by P. Nieto *et al.*,^[17] in which the authors characterize the formation of the pyridine-water heterodimer with IR spectroscopy performed in helium nanodroplets, indicates that the most stable structure is the O-H...N bonded one. Similar results were obtained by rotational spectroscopy performed on the 1:1 adducts of water with pyrazine,^[18] pyrimidine,^[19] pyridazine^[20] and 1,3,5,-triazine.^[21] In all of these cases the water molecule is linked to the heterocyclic nitrogen atom with a O-H...N angle between 152-166° and binding energies around 20 kJ·mol⁻¹. As reported in ref. 21, the observed structures and binding energies are in good agreement with the results of *ab initio* calculations and those obtained by an electrostatic model based on the Distributed Multiple Analysis^[22] extended to the hexadecapole level.

Among all possibilities, the exploitation of fluorine chemistry in all fields of science, opens up many new opportunities to modify molecules which is not offered by other substituents. In fact the substitution of a hydrogen atom with fluorine can profoundly change the conformational preferences of a molecule because of size and stereo-electronic effects and it can have a strong influence on the properties of pharmaceutical compounds^[23] and novel materials.^[24] Seeking information about the fluorination effect, a comparison among different van der Waals complexes between PY and fluorinated-PY with an argon atom can be done.^[25, 26] For the PY monomer, which presents a symmetry plane perpendicular to the ring plane, the adduct is always found to have the equilibrium position of the rare gas atom in that symmetry plane. When fluorine is substituted in the *meta* position the intermolecular interaction that occurs is weaker. The relative force constant k_s becomes smaller in going from the un-substituted PY to 2FPY to 3FPY. This suggests that the interaction is stronger between 2FPY and argon than in 3FPY...Ar adduct. This can be explained by the hyperconjugation effect that for 3FPY produces two resonance structures with similar energies, adding the negative charge on the carbons adjacent to the site of fluorination and in this way the charge is more delocalized than in 2FPY, where the negative charge is on the nitrogen atom resulting in a most stable hyperconjugated resonance structure. This smaller density of charge causes the decreasing of the intermolecular bond strength in the 3FPY...Ar adduct with respect to 2FPY...Ar and PY...Ar.

Other complexes of PY with weaker hydrogen bond donors are reported. For example, investigating the interactions of pyridine with a fluorinated probe, we can consider the cases of PY-CHF₃^[27], PY-CH₃F^[28] and PY-CH₂F₂^[29] adducts. In the case of PY-CHF₃ and PY-CH₃F the small fluorine-organic molecule points toward the nitrogen atom of the PY with the hydrogen atom

forming a C-H...N weak hydrogen bond while one of the fluorine atom is oriented toward a hydrogen atom adjacent to the nitrogen of the pyridine ring to form another intermolecular interaction. Besides the presence of multiple hydrogen bonds, the adduct shows some internal motion of the fluorinated molecule rotating around its symmetry axis. Differently from the previous cases, in PY-CH₂F₂ the two subunits are linked to each other through a bifurcated CH...N and a CH...F weak hydrogen bonds. The σ -type bonds observed in the complexes of PY with freons differ from the one observed in benzene-CHF₃,^[30] demonstrating the greater preference to create an intermolecular hydrogen bond with the high electronic density site presented by the nitrogen atom, instead of the weaker C-H... π linkage.

Concerning the microsolvation effect on fluorinated aromatic compounds, the cases of fluorobenzene and *p*-difluorobenzene complexed with a molecule of water were studied by rotational spectroscopy.^[31] The results indicate a planar (or nearly planar) structure for both complexes, where water links one of its hydrogen atom toward a fluorine atom of the fluorobenzene species forming a O-H...F hydrogen bond and a weaker C-H...O interaction (about 2.50Å) takes place between the lone pair of the oxygen of the water moiety and the closest hydrogen of the benzene ring. The introduction of fluorine atoms in these cases clearly show the difference between the same adduct with the simple benzene,^[32] where the water molecule is positioned above the benzene ring plane undergoing nearly free internal rotation.

Inspired by the results reported above we decided to pursue the study of the water adducts of halogen substituted pyridines. The rotational spectrum of the complex pyridine-water (PY-W) is rather complicated, due to the ¹⁴N quadrupole coupling splittings and the internal motions of the water moiety connecting two equivalent configurations. For this reason its full assignment has not yet been completed.^[33] The fluorination in *ortho* position of the PY ring will break the symmetry and therefore simplify the internal motion pathway of water. Herein, the rotational spectrum of the complex 2-fluoropyridine-water (2FPY-W) has been studied with Pulsed-Jet Fourier Transform MicroWave technique.

From spectroscopic studies conducted on the 2FPY monomer,^[34, 35] some changes at the structural level, with respect to pyridine itself, have been observed: in particular the N-C2 bond length results to be appreciable shortened (~-0.028Å) in the case of 2FPY than the other bond involving the substituted carbon (C2-C3 ~-0.006Å), suggesting that any perturbation of the π -system by fluorine and its lone pair is more pronounced in the region between C2 and N than toward C₃. In support of this, the electrostatic potential surface displayed by van Dijk *et al.*,^[34] for

2FPY shows a noticeable increase in the electron density shared between N and C2, which is consistent with the observation of substantial shortening of the N-C2 bond.

In this work the microsolvation effect on the 2FPY monomer is evaluated studying its rotational spectrum in the 1:1 water complex. Moreover the spectra of the isotopologue species of the water molecule (D_2O and $H^{18}O$) were also recorded in order to increase information about the position of the water with respect to the fluoro-substituted pyridine.

8.2 Theoretical calculations

The approach used to explore the conformational space of the complex 2FPY-W was twofold: from one side a molecular mechanics procedure based on conformational search algorithms implemented in MacroModel 9.2 within the MMFFs force field,^[36] was used and at the same time different kind of possible structures were directly optimized with *ab initio* MP2 method.

From the molecular mechanics approach 49 different geometries were found within an energy window of $21 \text{ kJ}\cdot\text{mol}^{-1}$ which, at the MP2/6-311++G** level of calculation, converged to four plausible conformers. Further vibrational frequency calculations in the harmonic approximation at the same level proved that these four conformers were real minima, providing the zero-point corrected energies (ZPE) and additional centrifugal distortion constants.

Concerning the second procedure, two different geometries were found to be real minima directly optimizing their structures with the same type of calculation mentioned above.

Comparing all these results, as shown in Table 8.1, the global minimum (2FPY-W1) was identified by both procedures to be the one where the water links one of its hydrogen atom toward the lone pair of the nitrogen atom forming a O-H...N hydrogen bond and with the oxygen points toward the closest hydrogen of the pyridine ring, maintaining an almost planar arrangement.

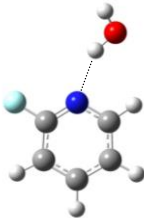
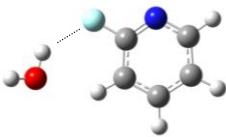
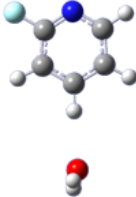
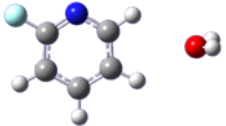
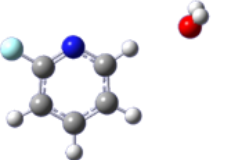
The second conformer (2FPY-W2) in order of energy, is the one characterized by an O-H...F intermolecular interaction with the oxygen of the water pointing towards the hydrogen atom in the *meta* position. It is interesting to note that this conformer was “missed” by the molecular mechanics approach but it was found to be a real minimum optimizing directly some different hypothetical arrangements for the complex based on “chemical intuition”.

Then, at higher energy, three more different conformers (2FPY-W3, 2FPY-W4 and 2FPY-W5) were found by molecular mechanics procedure, and all of them are characterized by a C-H...O weak hydrogen bond where the water moiety acts this time as a proton acceptor.

In order to have a better estimation of the energy differences, all intermolecular binding energy values were counterpoise corrected for basis set superposition error (BSSE).^[37] All the theoretical parameters are reported in Table 8.1.

The Gaussian 09 program package was used to carry out all the calculations.^[38]

Table 8.1 - Calculated spectroscopic parameters, relative energies and shape of the 2FPY-W adduct conformers (MP2/6-311++G**).

	2FPY-W1	2FPY-W2	2FPY-W3	2FPY-W4	2FPY-W5
					
A/MHz	2704	3984	3483	4684	3437
B/MHz	1475	1227	944	950	968
C/MHz	956	939	745	793	758
μ_a/D	-3.70	-0.40	5.95	4.64	2.77
μ_b/D	-0.82	1.88	-0.58	2.17	1.84
μ_c/D	0.79	0.83	0.01	0.02	0.00
χ_{aa}/MHz	-3.49	1.69	-4.17	1.53	1.35
χ_{bb}/MHz	0.93	-4.46	1.40	-2.80	-4.17
χ_{cc}/MHz	2.56	2.77	2.77	4.33	2.82
$\Delta_c/\text{u}\text{\AA}^2$	-0.88	-0.48	-2.10	-2.57	-2.40
$\Delta E_0/\text{kJ}\cdot\text{mol}^{-1}$	0 ^a	7.6	11.2	11.8	13.2
$\Delta E_{0-BSSSE}/\text{kJ}\cdot\text{mol}^{-1}$	0 ^b	7.0	11.1	11.5	13.1

^aAbsolute energies value: -422.876692 Hartrees.

^bAbsolute energies value: -422.874699 Hartrees.

8.3 Experimental Results and Analysis

Molecular clusters of 2FPY-W were generated in a supersonic expansion, under conditions optimized for the molecular 1:1 adduct formation. The rotational spectra of 2FPY-W in the 6-18.5 GHz frequency region were recorded using the COBRA-type PJ-FTMW spectrometer at the University of Bologna, already described in Chapter 3.

2FPY (99%) was purchased from Alfa Aesar and used without further purification. The measurements were carried out using helium as the carrier gas at a stagnation pressure of ~ 0.5 MPa passed over the samples of water and 2FPY (at 0°C), in two separated containers, and expanded through a solenoid valve (General Valve, Series 9, nozzle diameter 0.5 mm) into the Fabry-Perot cavity. The spectral line positions were determined after Fourier transformation of the time domain signal with 8k data points, recorded with 100 ns sample intervals. Each rotational transition displays a Doppler splitting, enhanced by the coaxial arrangement of the spectrometer. The rest frequency was calculated as the arithmetic mean of the frequencies of the two Doppler components. The estimated accuracy of the frequency measurements is better than 3 kHz, resolution is better than 7 kHz.

The search was started with frequency scans based on the predicted rotational constants and aimed at finding some μ_a -type *R*-branch transitions belonging to the 2FPY-W1 conformer, which, according to the theoretical calculations, is the most stable species. Firstly it was possible to identify the $J = 4 \leftarrow 3$, $K_a = 0$ and $K_a = 1$ transitions, shown in Figure 8.1. Each transition (see, for example, the $4_{04} \leftarrow 3_{03}$ transition in Figure 8.1) appeared split due to the ^{14}N (which has a nuclear spin quantum number $I = 1$) quadrupole effect. Then the assignment was extended to many *R*-type transitions with J from 3 up to 8 and with K_a up to 4. Later on, some much weaker μ_b *R*-type transitions could be measured.

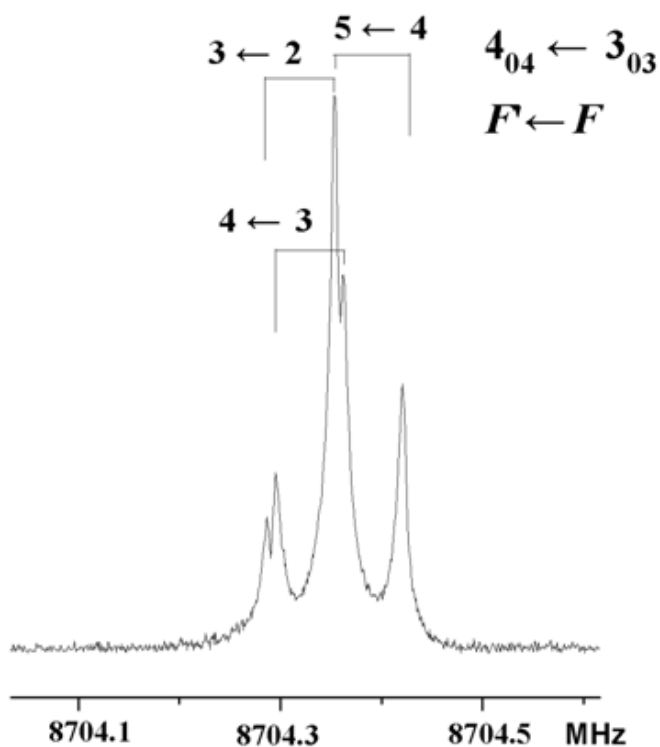


Figure 8.1 - $4_{04} \leftarrow 3_{03}$ transition of the observed 2FPY-W1 conformer. Each rotational line is split by Doppler effect and the nuclear quadrupole hyperfine effect (quantum numbers $F' \leftarrow F$ are shown).

No μ_c type transition neither the further splitting, contributable to a possible internal motion of water, has been observed. Using Pickett's SPFIT program,^[39] the 105 rotational transition frequencies were fitted and all the spectroscopic parameters (rotational constants, centrifugal distortion constants and quadrupole coupling constants) are reported in the first column of Table 8.2. The fit was carried out using the S reduction and I^r representation.^[40]

Table 8.2 - Experimental spectroscopic constants of the parent species and the observed isotopologues of 2FPY-W1 conformation.

2FPY-W1	HOH [*]	H ¹⁸ OH	DOH	HOD	DOD
<i>A</i> /MHz	2738.178(1) ^a	2734.370(3)	2739.991(7)	2733.389(8)	2735.235(9)
<i>B</i> /MHz	1462.5220(4)	1369.5790(4)	1436.4306(5)	1397.4350(5)	1374.2071(5)
<i>C</i> /MHz	953.0579(2)	912.2303(2)	942.1317(2)	924.6688(2)	914.6656(3)
<i>D_J</i> /kHz	0.034(3)	0.039(2)	0.122(5)	0.122(4)	0.116(4)
<i>D_{JK}</i> /kHz	11.24(2)	11.95(6)	[11.24] ^b	[11.24] ^b	[11.24] ^b
<i>D_K</i> /kHz	9.6 (1)	[9.6] ^b	[9.6] ^b	[9.6] ^b	[9.6] ^b
<i>d₁</i> /kHz	-0.178(2)	[-0.178] ^b	[-0.178] ^b	[-0.178] ^b	[-0.178] ^b
<i>d₂</i> /kHz	-0.223(2)	[-0.223] ^b	[-0.223] ^b	[-0.223] ^b	[-0.223] ^b
χ_{aa} /MHz	-3.570 (6)	-3.51(6)	-3.65(6)	-3.55(7)	-3.77(6)
χ_{bb} /MHz	1.00 (2)	0.94(5)	1.03(6)	0.97(7)	1.10(6)
χ_{cc} /MHz	2.57 (2)	2.57(5)	2.63(6)	2.58(7)	2.68(6)
Δ_c^c / uÅ ²	0.15	0.18	0.15	0.01	0.02
<i>N</i> ^d	105	61	29	27	27
σ^e / kHz	3	4	3	3	5

^{*} In the HOH notation, the first hydrogen is referred to the H₁₄ and the second one to the H₁₃ (see Figure 8.2).

^a Error in parentheses in units of the last digit.

^b Fixed at the values of the parent species.

^c Evaluated according to Pickett, see text.

^d Number of lines in the fit.

^e Root-mean-square deviation of the fit.

After the empirical adjustment of the molecular structure to reproduce the experimental rotational constants, the spectra of four additional water isotopologues, the ones containing H₂¹⁸O, DOH, HOD and D₂O, have been assigned. The spectrum of 2FPY-H₂¹⁸O was obtained using 98% enriched H₂¹⁸O (Sigma Aldrich) and all the spectroscopic parameters fitted are reported in the second column of Table 8.2. Its centrifugal distortion constants *D_k*, *d₁* and *d₂* have been fixed at the corresponding values of the parent species, due to the smaller number of transitions measured. The deuterated species were prepared using a mixture of H₂O/D₂O = 1/1. The spectra become much weaker due to the simultaneous presence of different partially deuterated species and for this reason it was possible to observe only some strong μ_a transitions, thus all five centrifugal distortion constants have been fixed at the corresponding values of the parent species. In the HOH notation, the first hydrogen is referred to the H₁₄ and the second one to the H₁₃ (see Figure 8.2 for the complete numbering used for the complex). All the results are listed in the following columns of

Table 8.2, where also the inertial defects Δ_c of the five isotopologues are reported. The latter values are very close to zero (the *ab initio* value is $-0.88 \text{ u}\text{\AA}^2$, see Table 8.1), suggesting a planar arrangement of the complex which is in agreement with the fact that no μ_c -type transitions have been observed. All the measured transition frequencies for the parent species and the water isotopologues are available in Tables 8.5, 8.6, 8.7, 8.8 and 8.9.

From a comparison of Table 8.1 and Table 8.2 it can be seen that the obtained rotational constants and quadrupole coupling constants match only the calculated values of species 2FPY-W1, making the conformational assignment straightforward. No lines belonging to the other conformers could be identified in the spectra, as expected looking at the calculated energy and dipole moment components of the other minimized conformations. This can also be due to the conformational relaxation of the higher energy conformers to the global minimum upon supersonic expansion.

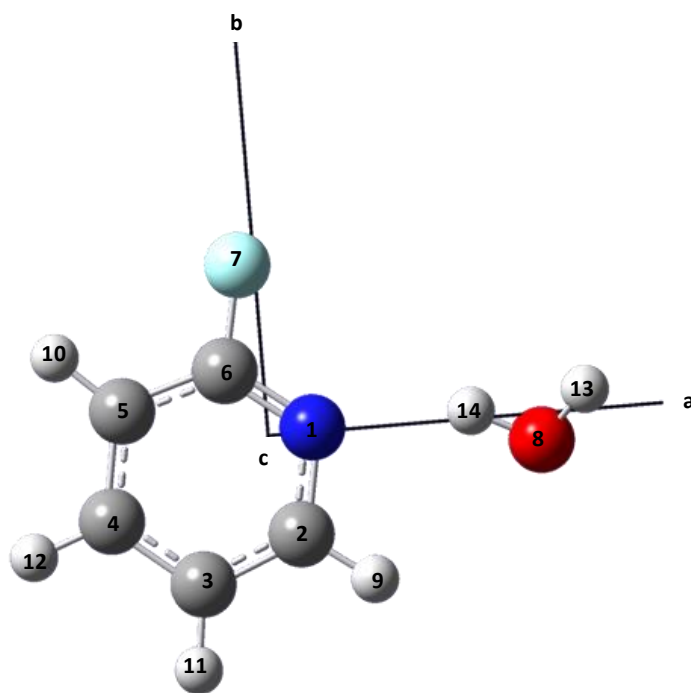


Figure 8.2 - Image of the observed conformer 2FPY-W1 with the atom numbering used in the text and the principal axes system.

In 2FPY-W1 (the observed conformer shown in Figure 8.2 where the principle axes and atom numbering are given), an $\text{OH}\cdots\text{N}$ hydrogen bond holds the two subunits together. In addition, the weak hydrogen bond $\text{CH}\cdots\text{O}$ also contributes to the stability of this complex. From the rotational constants of the first four isotopologues, it is possible to calculate the substitution coordinates, r_s , of the three substituted atoms belonging to the water moiety in the principal axes of

the parent species.^[41] The obtained values are summarized in Table 8.3 where the values of a partial r_0 structure is also given. The c -coordinates have been set to zero by symmetry (because of the indication given by the inertial defect) while the b -coordinate of the H atom involving in hydrogen bond results from the calculations to be small and imaginary, as usual for values of coordinates close to zero. The partial r_0 structure, was obtained by adjusting three structural parameters (R_{N1O8} , $\angle N1\cdots O8C2$ and $\angle H13O8\cdots N1$), while keeping the remaining parameters fixed to their *ab initio* values (coplanar), in order to reproduce the experimental rotational constants of the five isotopologues. The fitted and derived hydrogen bond parameters are reported in Table 8.4, where they are also compared to the *ab initio* values.

Table 8.3 - Values of the coordinates (\AA) relating to the isotopic substitutions (r_s), obtained from computational data (r_e) and derived from the effective structure (r_0).

		r_e^a	r_0	r_s
O	a	3.440	3.442 ^b	$\pm 3.4474(4)^c$
	b	0.341	0.448	$\pm 0.387(4)$
H ₁₃	a	4.038	3.985	$\pm 4.0127(4)/\pm 3.9652(4)$
	b	0.265	-0.343	$\pm 0.597(3)/\pm 0.537(3)$
H ₁₄	a	2.579	2.552	$\pm 2.5094(6)/\pm 2.4532(6)$
	b	0.097	0.067	$[0]^d$

^a MP2/6-311++G**.

^b Calculated with the r_0 structure in Table 8.4.

^c Error in parentheses in units of the last digit.

^d Slightly imaginary value has been fixed at zero.

The value obtained for the intermolecular hydrogen bond is in accord with other values obtained for this kind of interactions between the nitrogen of the PY ring and the water unit, as will be seen also in the next chapter where a comparison with other complexes is made.

Regarding the dissociation energy of 2FPY-W complex, for the global minimum arrangement the pseudo-diatomic approximation cannot hold because of the spatial distribution of the masses: in this case the intermolecular stretching motion is not parallel to the *a*-axis of the complex.

Table 8.4 - r_0 and r_e hydrogen bond parameters of 2FPY-W1.

Fitted parameters			
	$R_{N1O8}/\text{\AA}$	$\angle N1\cdots O8C2/^\circ$	$\angle H13O8\cdots N1/^\circ$
r_0	2.910(5) ^a	96.7(1)	116(4)
r_e	2.906	93.1	120
Derived parameters			
	$R_{N1H14}/\text{\AA}$	$\angle N1\cdots H14O8/^\circ$	$R_{H9O8}/\text{\AA}$
r_0	1.988(5)	158(4)	2.877(5)
r_e	2.015	152	2.753

^aUncertainties (in parentheses) are expressed in units of the last digit.

8.4 Conclusions

The analysis of the Fourier transform microwave spectra of five isotopologues of 2FPY-W points out that water has the double role of proton donor and proton acceptor. The observed conformer is characterized, indeed, by an O-H...N interaction, while a weaker C-H...O hydrogen bond plausibly contributes to the stability of the complex, maintaining an almost planar arrangement of the system.

The electron distribution surface of the assigned conformation is shown in Figure 8.3. Looking this surface it seems possible that another conformational arrangement could be probable where the water moiety creates a “bridge” between the fluorine atom and the nitrogen one of the 2FPY unit, donating both hydrogen atoms for two different intermolecular hydrogen bonds. Since this structure was not found to be a minimum by calculations (although it was tried to be optimized), the preference of the water to bind the lone pair of nitrogen instead of fluorine and to act both as proton donor and proton acceptor is here proved.

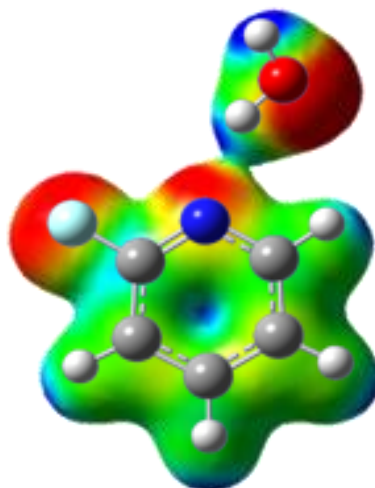


Figure 8.3 - Picture of the observed 2FPY-W1 conformation, where the electronic distribution surface colored by the electrostatic potential is displayed. The red areas identify the most electronegative regions and the blue ones the most electropositive areas.

In going from PYR to 2FPYR, the feature of the rotational spectrum becomes quite different. It seems that the replacement of the H atom in *ortho* position of the PYR ring with F, makes the molecule asymmetric enough to quench any tunneling detectable with our instrumental resolving power.

8.5 References

- [1] Q. Gou, L. Spada, M. Vallejo-López, A. Lesarri, E. J. Cocinero, W. Caminati, *Phys. Chem. Chem. Phys.*, 16, 13041, **2014**, and refs. within.
- [2] E. Vçhringer-Martinez, B. Hansmann, H. Hernandez-Soto, J. S. Francisco, J. Troe, B. Abel, *Science*, 315, 497-501, **2007**.
- [3] M. L. Chabiny c, S. L. Craig, C. K. Regan, J. L. Brauman, *Science*, 279, 1882-1886, **1998**.
- [4] M. J. Tait, F. Franks, *Nature*, 230, 91-94, **1971**.
- [5] B. C. Garrett, *Science*, 303, 1146-1147, **2004**.
- [6] L. Evangelisti, W. Caminati, *Phys. Chem. Chem. Phys.*, 12, 14433-14441, **2010**.
- [7] W. Caminati, A. Dell'Erba, S. Melandri, P. G. Favero, *J. Am. Chem. Soc.*, 120, 5555-5558, **1998**.
- [8] U. Spoerel, W. Stahl, W. Caminati, P. G. Favero, *Chem. Eur. J.*, 4, 1974-1981, **1998**.
- [9] W. Caminati, P. Moreschini, I. Rossi, P. G. Favero, *J. Am. Chem. Soc.*, 120, 11144-11148, **1998**.
- [10] Z. Su, Q. Wen, Y. Xu, *J. Am. Chem. Soc.*, 128, 6755-6760, **2006**.
- [11] Q. Gou, G. Feng, L. Evangelisti, M. Vallejo-López, L. Spada, A. Lesarri, E. J. Cocinero, W. Caminati, *Chem. Eur. J.*, 20, 1980-1984, **2014**.
- [12] Q. Gou, L. Spada, M. Vallejo-López, L. Kang, S. E. Novick, W. Caminati, *J. Phys. Chem. A*, 118, 1047-1051, **2014**.
- [13] B. M. Giuliano, W. Caminati, *Angew. Chem. Int. Ed.*, 44, 603-606, **2005**.
- [14] A. M. Andrews, R. L. Kuczkowski, *J. Chem. Phys.*, 98, 791-795, **1993**.
- [15] H. S. Gutowsky, T. Emilsson, E. Arunan, *J. Chem. Phys.*, 99, 4883-4893, **1993**.
- [16] Q. Gou, G. Feng, L. Evangelisti, W. Caminati, *Angew. Chem. Int. Ed.*, 52, 11888-11891, **2013**.
- [17] P. Nieto, M. Letzner, T. Endres, G. Schwaab, M. Havenith, *Phys. Chem. Chem. Phys.*, 16, 8384-8391, **2014**.
- [18] W. Caminati, L. B. Favero, P. G. Favero, A. Maris, S. Melandri, *Angew. Chem. Int. Ed.*, 37, 6, **1998**.
- [19] S. Melandri, M. E. Sanz, W. Caminati, P. G. Favero, Z. Kisiel, *J. Am. Chem. Soc.*, 120, 11504-11509, **1998**.
- [20] W. Caminati, P. Moreschini, P. G. Favero, *J. Phys. Chem. A*, 102, 8097-8100, **1998**.
- [21] A. Maris, S. Melandri, M. Miazzi, F. Zerbetto, *Chem. Phys. Chem.*, 9, 1303-1308, **2008**.
- [22] A. J. Stone, *Chem. Phys. Lett.*, 83, 233, **1981**; A. J. Stone, A. Alderton, *Mol. Phys.*, 56, 1047, **1985**; A. J. Stone, S. L. Price, *Phys. Chem.*, 92, 3325, **1988**.
- [23] K. Müller, C. Faeh, F. Diederich, *Science*, 317, 1881, **2007**.

- [24] R. Berger, G. Resnati, P. Metrangolo, E. Weberd, J. Hulliger, *Chem. Soc. Rev.*, 40, 3496-3508, **2011**.
- [25] R. M. Spycher, D. Petitprez, F. L. Bettens, A. Bauder, *J. Phys. Chem.*, 98, 11863-11869, **1994**.
- [26] M. Sun, M. Kamaee, J. van Wijngaarden, *J. Phys. Chem. A*, 117, 13429-13434, **2013**.
- [27] L. B. Favero, B. M. Giuliano, A. Maris, S. Melandri, P. Ottaviani, B. Velino, W. Caminati, *Chem. Eur. J.*, 16, 1761-1764, **2010**.
- [28] L. Spada, Q. Gou, M. Vallejo-López, A. Lesarri, E. J. Cocinero, W. Caminati, *Phys. Chem. Chem. Phys.*, 16, 2149-2153, **2014**.
- [29] M. Vallejo-López, L. Spada, Q. Gou, A. Lesarri, E. J. Cocinero, W. Caminati, *Chem. Phys. Lett.*, 591, 216-219, **2014**.
- [30] J. C. López, W. Caminati, J. L. Alonso, *Angew. Chem. Int. Ed.*, 118, 2, **2005**.
- [31] K. Brendel, H. Mäder, Y. Xu, W. Jäger, *J. Mol. Spectr.*, 268, 47–52, **2011**.
- [32] S. Suzuki, P.G. Green, R.E. Bumgarner, S. Dasgupta, W.A. Goddard III, G.A. Blake, *Science*, 257, 942–945, **1992**.
- [33] W. Caminati, *et al.* Pyridine-water. Private communication.
- [34] C. W. van Dijk, M. Sun, J. van Wijngaarden, *J. Phys. Chem. A*, 116, 4082-4088, **2012**, and refs. within.
- [35] P. Boopalachandran, J. Laane, *Spectrochimica Acta A*, 79, 1191-1195, **2011**.
- [36] MASTRO, version 9.2, Schrödinger, LLC, New York, NY, **2012**.
- [37] S. F. Boys, F. Bernardi, *Mol. Phys.*, 19, 553, **1970**.
- [38] M. J. Frisch, G. W. Trucks, H. B. Schlegel, G. E. Scuseria, M. A. Robb, J. R. Cheeseman, G. Scalmani, V. Barone, B. Mennucci, G. A. Petersson, H. Nakatsuji, M. L. Caricato, X.; Hratchian, H. P.; Izmaylov, A. F.; Bloino, J.; Zheng, G.; Sonnenberg, J. L.; Hada, M.; Ehara, M.; Toyota, K.; Fukuda, R.; Hasegawa, J.; Ishida, M.; Nakajima, T.; Honda, Y.; Kitao, O.; Nakai, H.; Vreven, T.; Montgomery, J. A.; J. E. J. Peralta, F. B. Ogliaro, M.; Heyd, J. J.; Brothers, E.; Kudin, K. N.; Staroverov, V. N.; Kobayashi, R.; Normand, J.; Raghavachari, K.; Rendell, A.; Burant, J. C.; Iyengar, S. S.; Tomasi, J.; Cossi, M.; Rega, N.; Millam, J. M.; Klene, M.; Knox, J. E.; J. B. Cross, V. A. Bakken, C.; Jaramillo, J.; Gomperts, R.; Stratmann, R. E.; Yazyev, O.; Austin, A. J.; Cammi, R.; Pomelli, C.; Ochterski, J. W.; Martin, R. L.; Morokuma, K.; Zakrzewski, V. G.; Voth, G. A.; Salvador, P.; Dannenberg, J. J.; Dapprich, S.; A. D. Daniels, Ö. F. Farkas, J. B.; Ortiz, J. V.; Cioslowski, J.; Fox, D. J., Gaussian, Inc., Wallingford CT, **2009**.
- [39] M. H. Pickett, *J. Mol. Spectrosc.*, 148, 371-377, **1991**.
- [40] J. K. G. Watson, "Vibrational spectra and structure", Vol. 6, Elsevier, Amsterdam, Oxford & New York, **1977**.

[41] J. Kraitchman, *Am. J. Phys.*, 21, **1953**.

8.6 Appendix

Table 8.5 - Measured frequencies (MHz) for the transitions observed for the parent species of 2FPY-W1 conformation.

J'	K'_a	K'_c	J''	K''_a	K''_c	F'	F''	ν_{OBS}/MHz	$\Delta\nu_{OBS-CALC}/\text{kHz}$
3	1	2	2	1	1	4	3	7920.8592	2.2
						3	2	7920.5319	-2.6
						2	1	7920.8960	-7.5
3	2	2	2	2	1	4	3	7246.7460	2.9
						3	2	7245.5945	-1.8
						2	1	7247.3765	-3.8
3	2	1	2	2	0	4	3	7702.9236	4.7
						3	2	7701.8262	1.4
						2	1	7703.5456	0.3
4	0	4	3	0	3	3	2	8704.3269	-0.7
						4	3	8704.3380	-0.4
						5	4	8704.4250	0.6
4	1	4	3	1	3	4	3	8442.1218	-1.3
						3	2	8442.2204	0.9
						5	4	8442.2847	-1.1
4	1	3	3	1	2	4	3	10366.3591	-0.4
						3	2	10366.5005	1.1
						5	4	10366.5152	-3.1
4	2	3	3	2	2	4	3	9563.2399	0.9
						3	2	9563.8629	1.1
						5	4	9563.7334	-1.0
4	2	2	3	2	1	4	3	10518.5227	0.7
						5	4	10518.9627	3.8
						3	2	10519.0852	5.9
4	3	2	3	3	1	4	3	9861.8269	1.0
						3	2	9863.2790	-0.9
						5	4	9862.8736	1.8
4	3	1	3	3	0	4	3	9975.3531	-1.3
						3	2	9976.7965	-2.2
						5	4	9976.3917	-0.7
5	0	5	4	0	4	5	4	10561.8157	1.3
						4	3	10561.8278	-2.3
						6	5	10561.8876	-0.4
5	1	5	4	1	4	4	3	10420.7241	-1.0
						5	4	10420.6755	-2.0
						6	5	10420.7771	1.0
5	1	4	4	1	3	4	3	12606.8432	6.1
						5	4	12606.7547	3.3
						6	5	12606.8600	1.8

Chapter 8 - 2-FLUOROPYRIDINE...WATER

J'	K'_a	K'_c	J''	K''_a	K''_c	F'	F''	ν_{OBS}/MHz	$\Delta\nu_{OBS-CALC}/\text{kHz}$
5	2	4	4	2	3	5	4	11801.7618	-2.4
						6	5	11802.0364	3.3
						4	3	11802.0580	-3.2
5	2	3	4	2	2	4	3	13297.7422	-7.3
						5	4	13297.5069	-2.9
						6	5	13297.7219	-2.5
5	3	3	4	3	2	4	3	12340.6542	3.7
						5	4	12339.9744	-2.1
						6	5	12340.5158	-0.6
5	3	2	4	3	1	4	3	12701.3968	2.2
						5	4	12700.7469	6.9
						6	5	12701.2690	5.7
5	4	2	4	4	1	5	4	12350.9699	0.5
						4	3	12352.1992	-2.2
						6	5	12351.9176	0.7
6	0	6	5	0	5	7	6	12428.8336	1.3
						5	4	12428.7933	0.9
						6	5	12428.7644	-7.7
6	1	6	5	1	5	7	6	12363.9338	-0.5
						6	5	12363.8661	-0.2
						5	4	12363.8949	-1.1
6	1	5	5	1	4	7	6	14613.6649	5.0
						6	5	14613.5712	-0.1
						5	4	14613.6385	-4.6
6	2	5	5	2	4	7	6	13954.1892	2.3
						6	5	13954.0177	-0.1
						5	4	13954.1892	0.5
6	2	4	5	2	3	7	6	15932.4423	0.3
						6	5	15932.3239	6.9
						5	4	15932.4423	-0.9
6	3	4	5	3	3	7	6	14774.2528	-2.8
						5	4	14774.3117	5.5
						6	5	14773.9269	-11.0
6	3	3	5	3	2	7	6	15578.0139	-2.3
						6	5	15577.7217	-3.2
8	0	8	7	0	7	9	8	16210.5452	1.6
						8	7	16210.4995	-4.9
						7	6	16210.5193	-0.8
8	1	8	7	1	7	9	8	16199.8160	-1.0
						8	7	16199.7770	-0.1
						7	6	16199.7994	5.6
3	3	0	2	2	1	4	3	14988.3109	1.2
						3	2	14988.6591	-3.5
						2	1	14988.4283	6.5
3	2	2	2	1	1	4	3	11073.3355	-1.9
						3	2	11073.6612	3.0
						2	1	11073.1597	0.5

Chapter 8 - 2-FLUOROPYRIDINE...WATER

J'	K'_a	K'_c	J''	K''_a	K''_c	F'	F''	ν_{OBS}/MHz	$\Delta\nu_{OBS-CALC}/\text{kHz}$
3	2	1	2	1	2	4	3	13182.4247	0.9
						3	2	13183.3360	-2.4
						2	1	13181.9304	-3.3
4	0	4	3	1	3	3	2	8191.9242	-1.2
						4	3	8191.7841	0.5
						5	4	8191.9807	-1.7
4	1	4	3	0	3	3	2	8954.6250	3.2
						4	3	8954.6774	-0.6
						5	4	8954.7269	-0.8
4	3	2	3	2	1	5	4	17003.8596	-2.3
						4	3	17004.2211	-3.5
						3	2	17003.7792	2.4
5	0	5	4	1	4	6	5	10311.5850	0.3
						5	4	10311.4746	-0.2
						4	3	10311.5329	-3.1
5	1	5	4	0	4	6	5	10671.0799	0.4
						5	4	10671.0186	1.4
						4	3	10671.0186	-0.6
6	1	6	5	0	5	7	6	12473.1252	-0.5
						6	5	12473.0704	1.3
						5	4	12473.0928	7.6

Table 8.6 - Measured frequencies (MHz) for the transitions observed for the isotopologue species H¹⁸OH of 2FPY-W1 conformation.

<i>J'</i>	<i>K'_a</i>	<i>K'_c</i>	<i>J''</i>	<i>K''_a</i>	<i>K''_c</i>	<i>F'</i>	<i>F''</i>	<i>v</i> _{OBS} /MHz	$\Delta v_{\text{OBS-CALC}}$ /kHz
4	0	4	3	0	3	4	3	8341.8384	-3.5
						3	2	8341.8384	4.7
						5	4	8341.9313	-1.1
4	1	4	3	1	3	4	3	8051.6816	0.6
						3	2	8051.7739	1.8
						5	4	8051.8470	-2.1
4	1	3	3	1	2	4	3	9804.2508	-16.1
						3	2	9804.4139	3.3
5	0	5	4	0	4	5	4	10128.1789	4.7
						4	3	10128.1903	-2.1
						6	5	10128.2486	-1.8
5	1	5	4	1	4	5	4	9953.8874	0.4
						4	3	9953.9334	-2.1
						6	5	9953.9852	-1.6
5	1	4	4	1	3	5	4	11989.9875	-4.6
						4	3	11990.0806	-1.8
						6	5	11990.0950	-7.4
6	0	6	5	0	5	6	5	11911.0618	0.3
						5	4	11911.0824	-0.8
						7	6	11911.1215	-1.9
6	1	6	5	1	5	6	5	11821.9388	-0.1
						5	4	11821.9701	0.6
						7	6	11822.0081	0.0
6	1	5	5	1	4	6	5	13980.2158	3.3
						5	4	13980.2812	-7.9
						7	6	13980.3112	6.2
7	0	7	6	0	6	7	6	13709.6321	-0.8
						6	5	13709.6522	-0.2
						8	7	13709.6841	1.6
7	1	7	6	1	6	7	6	13668.3668	2.5
						6	5	13668.3861	-0.4
						8	7	13668.4121	-4.1
7	1	6	6	1	5	7	6	15801.1395	12.7
						6	5	15801.1971	-1.2
						8	7	15801.2249	14.13
8	0	8	7	0	7	8	7	15520.7984	-2.3
						7	6	15520.8229	5.8
						9	8	15520.8361	-4.6
8	1	8	7	1	7	8	7	15502.8530	0.8
						7	6	15502.8752	5.8
						9	8	15502.8901	-2.8
8	1	7	7	1	6	8	7	17543.3689	5.9
						7	6	17543.4256	-2.9

Chapter 8 - 2-FLUOROPYRIDINE...WATER

J'	K'_a	K'_c	J''	K''_a	K''_c	F'	F''	ν_{OBS}/MHz	$\Delta\nu_{OBS-CALC}/\text{kHz}$
8	1	7	7	1	6	8	7	17543.3689	5.9
						7	6	17543.4256	-2.9
						9	8	17543.4448	6.1
9	0	9	8	0	8	9	8	17338.9112	-3.6
						10	9	17338.9457	-1.8
4	0	4	3	1	3	4	3	7716.6135	5.9
						3	2	7716.7472	-0.6
						5	4	7716.8088	2.7
4	1	4	3	0	3	3	2	8676.8637	-0.3
						4	3	8676.9086	-6.7
						5	4	8676.9651	-6.4
5	0	5	4	1	4	5	4	9793.1046	3.8
						4	3	9793.1642	2.1
						6	5	9793.2132	1.9
5	1	5	4	0	4	5	4	10288.9528	-7.6
						6	5	10289.0232	-2.8
6	0	6	5	1	5	6	5	11750.2745	-0.8
						5	4	11750.3070	-2.8
						7	6	11750.3489	1.1
6	1	6	5	1	5	6	5	11982.7288	3.7
						5	4	11982.7388	-4.1
						7	6	11982.7802	-3.5

Table 8.7 - Measured frequencies (MHz) for the transitions observed for the DOH monodeuterated isotopologue species of 2FPY-W1 conformation.

J'	K'_a	K'_c	J''	K''_a	K''_c	F'	F''	ν_{OBS}/MHz	$\Delta\nu_{OBS-CALC}/\text{kHz}$
3	1	2	2	1	1	3	2	7793.5645	-2.3
						4	3	7793.8919	2.6
						2	1	7793.9389	2.8
4	0	4	3	0	3	3	2	8608.2054	-6.6
						4	3	8608.2204	-2.4
						5	4	8608.3178	9.1
4	1	4	3	1	3	4	3	8336.8211	1.4
						3	2	8336.9128	-3.4
						5	4	8336.9836	1.0
4	1	3	3	1	2	4	3	10212.5092	-5.1
						3	2	10212.6568	2.2
						5	4	10212.6745	1.0
5	0	5	4	0	4	5	4	10446.3541	2.4
						4	3	10446.3648	-2.5
						6	5	10446.4251	-0.2
5	1	5	4	1	4	5	4	10295.3529	-1.5
						4	3	10295.3984	-3.6
						6	5	10295.4581	5.2
5	1	4	4	1	3	5	4	12441.3998	-0.1
						4	3	12441.4875	1.4
						6	5	12441.5054	-1.7
6	1	6	5	1	5	6	5	12218.7111	0.5
						5	4	12218.7407	0.3
						7	6	12218.7829	4.3
7	0	7	6	0	6	7	6	14152.2439	-2.0
						8	7	14152.2941	-0.2
4	0	4	3	1	3	4	3	8062.8019	0.8
						3	2	8062.9431	-0.5
						5	4	8062.9989	-1.7
4	1	4	3	0	3	3	2	8882.1819	-2.6
						4	3	8882.2399	-1.5
						5	4	8882.2945	3.8

Table 8.8 - Measured frequencies (MHz) for the transitions observed for the HOD monodeuterated isotopologue species of 2FPY-W1 conformation.

J'	K'_a	K'_c	J''	K''_a	K''_c	F'	F''	ν_{OBS} / MHz	$\Delta\nu_{OBS-CALC}$ / kHz
3	1	2	2	1	1	3	2	7600.5404	1.2
						4	3	7600.8614	-0.4
						2	1	7600.9128	4.2
4	0	4	3	0	3	3	2	8452.2423	9.6
						4	3	8452.2423	-1.3
						5	4	8452.3262	-3.3
4	1	4	3	1	3	4	3	8170.3535	0.2
						3	2	8170.4454	-4.4
						5	4	8170.5182	2.0
4	1	3	3	1	2	4	3	9974.5919	-0.5
						3	2	9974.7376	4.7
						5	4	9974.7480	-3.7
5	0	5	4	0	4	5	4	10259.6709	1.0
						4	3	10259.6855	0.2
						6	5	10259.7423	-1.0
5	1	5	4	1	4	5	4	10095.9056	-2.9
						4	3	10095.9584	2.2
						6	5	10096.0079	0.8
5	1	4	4	1	3	5	4	12178.4925	-2.6
						4	3	12178.5841	2.5
						6	5	12178.5988	-3.8
6	0	6	5	0	5	6	5	12067.8968	4.1
						5	4	12067.9082	-4.4
						7	6	12067.9530	0.3
6	1	6	5	1	5	6	5	11986.8328	-0.7
						5	4	11986.8662	3.0
						7	6	11986.9041	2.6
4	0	4	3	1	3	4	3	7863.6085	0.4
						3	2	7863.7484	-2.7
						5	4	7863.8087	0.8

Table 8.9 - Measured frequencies (MHz) for the transitions observed for the DOD bi-deuterated isotopologue species of 2FPY-W1 conformation.

J'	K'_a	K'_c	J''	K''_a	K''_c	F'	F''	ν_{OBS} / MHz	$\Delta\nu_{OBS-CALC}$ / kHz
3	1	2	2	1	1	3	2	7486.2365	-1.4
						4	3	7486.5787	1.9
						2	1	7486.6207	-4.2
4	0	4	3	0	3	3	2	8363.0493	7.3
						4	3	8363.0662	10.5
						5	4	8363.1362	-8.6
4	1	4	3	1	3	4	3	8073.9435	-0.2
						3	2	8074.0360	-9.0
						5	4	8074.1132	-1.2
4	1	3	3	1	2	4	3	9833.9536	-5.1
						3	2	9834.1154	10.4
						5	4	9834.1266	1.2
5	0	5	4	0	4	5	4	10153.7020	-1.4
						4	3	10153.7120	-6.4
						6	5	10153.7752	-4.2
5	1	5	4	1	4	5	4	9980.8335	-7.1
						4	3	9980.8923	2.0
						6	5	9980.9535	9.8
5	1	4	4	1	3	5	4	12023.8055	-2.5
						4	3	12023.9011	3.9
						6	5	12023.9153	-4.4
6	0	6	5	0	5	6	5	11941.5084	5.6
						5	4	11941.5157	-7.4
						7	6	11941.5667	1.6
6	1	6	5	1	5	6	5	11853.5079	3.0
						5	4	11853.5385	2.6
						7	6	11853.5781	2.1
4	0	4	3	1	3	4	3	7742.8315	1.5
						3	2	7742.9780	-3.4
						5	4	7743.0414	0.8

3-FLUOROPYRIDINE ... WATER**9.1 Introduction**

In order to give more information on the study of fluorine substitution effects on microsolvation, another adduct of water with a different fluorinated derivative of pyridine has been investigated with rotational spectroscopy in order to study the intermolecular interactions that govern the structure and binding and the effect caused by halogenations; in particular in this work the 3-fluoropyridine-water (3FPY-W) adduct is analyzed.

An overview of the behaviour of this kind of molecules during complexation with different partners was already realized in the previous chapter. In particular it has been shown how the rotational spectroscopy technique is a fundamental tool to obtain structural information and describe intermolecular interactions, like the hydrogen bond, that characterize molecular complexes.

The monomer of 3-fluoropyridine (3FPY) has already been characterized spectroscopically both with rotational^[1] and vibrational techniques.^[2] In particular regarding rotational spectroscopy in supersonic expansion, the most recent work presented by van Dijk *et al.*,^[1] reported the analysis of the spectra of the 3FPY parent species and its six heavy atom isotopologues. The data show that the localized structural changes in 3FPY can be explained also by a simple inductive effect due to the electron withdrawing nature of fluorine and that the nitrogen atom is too far away to have a significant effect on any π -donation from fluorine atom with respect to the case of 2-fluoropyridine (2FPY). In fact, as explained also by Boopalachandran *et al.*,^[2] the changes at the structural level, with respect to pyridine itself, concern the ring bond distances and most notably the N-C(F) bond length that results to be appreciable shortened only in the case of 2FPY, due to π interactions; as already mentioned in the previous chapter. The data thus suggest that fluorination in the *meta* position has a smaller effect on the geometry of the pyridine ring backbone than the introduction of fluorine in *ortho* position.

In the present work the observation and analysis of the pure rotational spectrum of the 3FPY-W complex is reported. Pulsed-Jet Fourier Transform MicroWave (PJ-FTMW) spectroscopy was used to obtain information about the conformational preferences of this system in its ground vibrational state. The spectra of the isotopologue species of the water molecule (D₂O and H¹⁸O)

were also recorded in order to add information about the position of the water respect the fluoro-substituted pyridine.

9.2 Theoretical calculations

Geometry optimization of different structures of 3FPY-W has been performed using the MP2 method with the 6-311++G** basis set and using also the counterpoise procedure with basis set superposition error (BSSE).^[3] Vibrational frequency calculations of all the optimized structures were carried out in the harmonic approximation to check whether all of those are real minima. The Gaussian 09 program package was used to perform all the calculations.^[4]

The possible starting geometries can be divided into four types: first of all the water moiety could be linked to 3FPY *via* an O-H...N or an O-H...F interaction and secondly due to the symmetry of 3FPY different conformation can be achieved if the O atom is on one side or on the other of a plane perpendicular to the ring. This means that when the O-H...N interaction is present, the O atom can be towards the F atom (3FPY-W2) or opposite to it (3FPY-W1) while when a O-H...F interaction is formed, the O atom can point towards the N atom (3FPY-W4) or in opposite direction (3FPY-W3). The results of the theoretical calculations for the four conformations are reported in Table 9.1.

The global minimum is represented by the 3FPY-W1 species which presents an intermolecular O-H...N hydrogen bond; the oxygen atom lies on the pyridine plane and it is oriented opposite to the fluorine atom. The arrangement is such that one of the oxygen's lone pairs point towards the closest C-H group.

From Table 9.1, it can also be seen that in some cases the two different type of calculations minimize different kind of conformations. In particular, looking at the data shown, it can be noted that the species named 3FPY-W2 achieves a different optimized structure with and without BSSE correction. Starting from the 3FPY-W2 the MP2 method alone optimizes the structure reported to the left while the MP2-BSSE method is able to locate the planar minimum similar to the other conformations (the data are reported on the right side).

The relative energies' sequence for the optimized minima is the same with the two methods used and in both cases the most stable conformation is 3FPY-W1.

Table 9.1 - Calculated spectroscopic parameters, relative energies and shape of the 3FPY-W adduct conformers.

6-311++G**	3FPY-W1		3FPY-W2*		3FPY-W3		3FPY-W4	
	MP2	MP2-BSSE	MP2	MP2-BSSE	MP2	MP2-BSSE	MP2	MP2-BSSE
A/MHz	4159	4096	3390	2900	3989	4017	3892	3936
B/MHz	1067	1046	1129	1254	1200	1168	1213	1174
C/MHz	852	835	852	877	923	905	925	904
μ_a/D	-2.36	-2.24	3.25	-2.60	2.03	1.98	-0.34	-0.42
μ_b/D	0.98	1.02	2.31	3.46	0.74	0.68	2.81	3.02
μ_c/D	1.15	1.14	1.59	1.25	0.84	0.00	0.88	0.03
χ_{aa}/MHz	-2.96	-3.74	-4.07	-5.49	-3.39	-4.03	1.54	1.62
χ_{bb}/MHz	-0.11	-0.10	1.04	1.65	0.05	-0.09	-4.94	-5.81
χ_{cc}/MHz	3.08	3.84	3.04	3.84	3.34	4.13	3.4	4.20
$\Delta_c/\text{u}\text{\AA}^2$	-1.96	-1.04	-3.94	-1.21	-0.47	-0.01	-0.51	0.00
$\Delta E_0/\text{kJ}\cdot\text{mol}^{-1}$	0 ^a	0 ^b	0.50	0.34	9.04	8.21	12.18	11

* The structure to the right can be optimized only using BSSE correction. Starting from the same geometry with MP2 it is possible only to obtain the structure to the left.

^a Absolute energy: -422.866522 Hartrees. ^b Absolute energy: -422.86633 Hartrees.

9.3 Experimental Results and Analysis

Molecular clusters of 3FPY-W were generated in a supersonic expansion, under conditions optimized for the 1:1 molecular adduct formation. The rotational spectra of 3FPY-W in the 6-18.5 GHz frequency region were recorded using the COBRA-type PJ-FTMW spectrometer at the University of Bologna, already described in Chapter 3.

3FPY (98%) was purchased from Alfa Aesar and used without further purification. The measurements were carried out using helium as the carrier gas at a stagnation pressure of ~ 0.5 MPa passed over the samples of water and 3FPY (at 0°C), in two separated containers, and expanded through a solenoid valve (General Valve, Series 9, nozzle diameter 0.5 mm) into the Fabry–Perot cavity. The spectral line positions were determined after Fourier transformation of the time domain signal with 8k data points, recorded with 100 ns sample intervals. Each rotational transition displays a Doppler splitting, enhanced by the coaxial arrangement of the spectrometer. The rest frequency was calculated as the arithmetic mean of the frequencies of the two Doppler components. The estimated accuracy of the frequency measurements is better than 3 kHz, resolution is better than 7 kHz.

Preliminary trial predictions of the rotational spectra were based on the rotational constants of Table 9.1. It was possible to assign only one rotational spectrum, that of the species 3FPY-W1 and according to the theoretical values of the dipole moment components, the first search has been targeted to the μ_a -R band. The $J = 4 \leftarrow 3$ was observed first (see Figure 9.1) and then the assignment was extended to higher J , up to $J = 9$. After that, it was possible to measure some μ_b -type transitions, with rotational quantum number J ranging from 3 to 7 for a total of 41 measured rotational transitions. In addition also some μ_b -Q branch transitions were measured. All the measured transitions showed a nuclear-quadrupole hyperfine structure due to the presence of the nitrogen ^{14}N nucleus. The S -reduction of Watson's semirigid rotational Hamiltonian in the I' representation^[5] was fitted to the experimental frequencies, giving the spectroscopic constants reported in Table 9.2 while the measured frequencies are listed in Table 9.5.

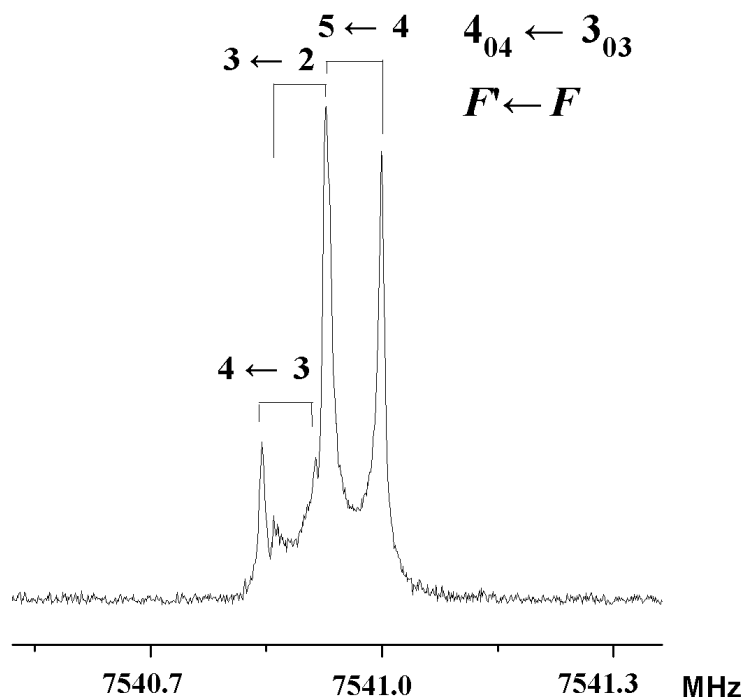


Figure 9.1 - $4_{04} \leftarrow 3_{03}$ transition of the observed 3FPY-W1 conformer. Each rotational line is split by Doppler effect and the nuclear quadrupole hyperfine effect (quantum numbers $F' \leftarrow F$ are shown).

The rotational spectrum of some water isotopologues were also investigated. These species were generated by adding D_2O or $H_2^{18}O$ to the system and observing the rotational spectrum in the same conditions as for the normal species. The experimental spectroscopic parameters of the two mono-deuterated species (3FPY-HOD and 3FPY-DOH), the bi-deuterated species (3FPY-DOD) and the isotopologue with $H^{18}OH$ are also reported in Table 9.2 and they were obtained using the same fitting procedure as for the normal species. In the HOH notation, the first hydrogen is referred to the H_{12} and the second one to the H_{14} (see Figure 9.2 for the complete numbering used for the complex). The measured frequencies of all the isotopologue species are listed in Tables 9.6, 9.7, 9.8, 9.9.

The search for the 3FPY-W2 conformer was also performed but without success. This conformer presents an energy very close to the global minimum (see Table 9.1) and sizable values of the dipole moment components but it is possible that this conformation is not a real minimum or that it relaxes in the jet expansion.

Table 9.2 - Experimental spectroscopic constants of the parent species and the observed isotopologues of 3FPY-W1 conformation.

3FPY-W1	HOH*	H ¹⁸ OH	DOH	HOD	DOD
<i>A</i> /MHz	4163.0585(9) ^a	4148.419(2)	4136.381(3)	4123.842(3)	4098.341(3)
<i>B</i> /MHz	1064.3651(1)	1003.1465(2)	1047.8077(4)	1024.6943(4)	1009.6845(4)
<i>C</i> /MHz	847.8457(1)	807.9682(2)	836.2324(5)	821.3607(4)	810.7445(4)
<i>D_J</i> /kHz	0.1309(9)	0.126(2)	0.122(5)	0.122(4)	0.116(4)
<i>D_{JK}</i> /kHz	4.90(1)	[4.90] ^d	[4.90] ^d	[4.90] ^d	[4.90] ^d
<i>D_K</i> /kHz	21.03(9)	[21.03] ^d	[21.03] ^d	[21.03] ^d	[21.03] ^d
<i>d₁</i> /kHz	-0.0413(8)	[-0.0413] ^d	[-0.0413] ^d	[-0.0413] ^d	[-0.0413] ^d
<i>d₂</i> /kHz	-0.0254(6)	[-0.0254] ^d	[-0.0254] ^d	[-0.0254] ^d	[-0.0254] ^d
<i>χ_{aa}</i> /MHz	-3.085(8)	-3.12(3)	-3.04(7)	-3.15(7)	-3.08(7)
<i>χ_{bb}</i> /MHz	-0.119(5)	-0.086(1)	-0.097(3)	-0.106(3)	-0.099(3)
<i>χ_{cc}</i> /MHz	3.204(5)	3.204(1)	3.135(3)	3.255(3)	3.182(3)
<i>Δ_c^c</i> /uÅ ²	-0.14	-0.12	-0.15	-0.46	-0.49
<i>N^b</i>	135	66	30	33	33
<i>σ^c</i> /kHz	3	3	3	4	4

*NOTE: in the HOH notation, the first hydrogen is referred to the H₁₂ and the second one to the H₁₄ (see Figure 9.2).

^a Error in parentheses are in units of the last digit.

^b Number of lines in the fit.

^c Root-mean-square deviation of the fit.

^d In the fit the quartic centrifugal distortion constants have been kept fixed to the corresponding values of the parent species.

The experimental rotational constants of the 3FPY-W1 complex are in good agreement with the calculated values reported in Table 9.1. The value determined for the inertial defects Δ_c (see Table 9.2), of the observed parent species, which is a measure of the mass distribution out of the *ab*-plane (see Chapter 1 for more details), is almost zero (-0.14 uÅ²), as expected for a planar system. The overall planarity is in accord also with the observation of μ_a and μ_b , but no μ_c -type transitions. Moreover, the isotopic substitutions of ¹⁶O by ¹⁸O as well as the replacement of the bonded hydrogen in the intermolecular hydrogen bond (number 12, as denoted in Figure 9.2) by deuterium affect Δ_c only very little (-0.12 and -0.15 uÅ² respectively, see Table 9.2). It may thus be concluded that both H₁₂ and the O atoms of the water molecule are localized in the plane of the aromatic ring. Regarding the other mono-deuterated species and the bi-deuterated one, it can be noted that substitution with the heavier deuterium atom of the hydrogen atom not involved in the intermolecular interaction (number 14, as showed in Figure 9.2) causes an increment of the Δ_c values. This increment is not to be imputed to the fact that this free hydrogen does not lie perfectly

on the *ab*-plane, but to the fact that the hydrogen atom is involved in very large amplitude vibrational motions through the aromatic plane. Based on this evidence it can be asserted that the water molecule lies in the aromatic plane at equilibrium because no tunneling splittings related to the motion of this free hydrogen through the aromatic ring were observed in the rotational spectrum. This conclusion is also in accord with the very small barrier calculated for the planar structure, which is estimated to be $0.61 \text{ kJ}\cdot\text{mol}^{-1}$.

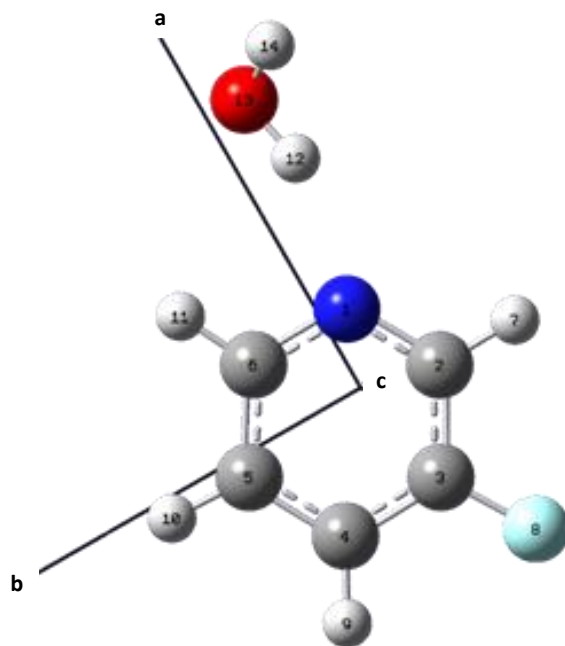


Figure 9.2 - Image of the observed conformer 3FPY-W1 with the atom numbering used in the text and the principal axes system.

For all of the above reasons the structure analyses of the complex were performed assuming planarity. A partial experimental r_s -structure using Kraitchman's substitution method was determined.^[6] Such analysis leads to the determination of the absolute values of the principal axis coordinates of the substituted atom from the changes in principal moments of inertia resulting from a single isotopic substitution. As reported in Table 9.3, these coordinates for the oxygen and hydrogen atoms of the water molecule were obtained. The hydrogen atom coordinates can be calculated considering the substitution from the hydrogenated to the monodeuterated species and from the bi-deuterated to the monodeuterated one. Looking at Table 9.3, these values can be compared with the calculated ones (r_e) and the ones obtained from the r_0 structure (see below).

Table 9.3 - Values of the coordinates (\AA) relating to the isotopic substitutions (r_s), obtained from computational data (r_e) and derived from the effective structure (r_0).

		r_0	r_e^a	r_s
O	a	-3.826375	3.811619	$\pm 3.8330(4)^b$
	b	-0.506048	-0.522264	$\pm 0.485(3)$
H ₁₂	a	-2.876067	2.866375	$\pm 2.7395(6)/ \pm 2.6904(6)^c$
	b	-0.702495	-0.714481	$\pm 0.895(2)/ \pm 0.858(2)$
H ₁₄	a	-4.238597	4.237858	$\pm 4.2857(4)/ \pm 4.2422(4)$
	b	-1.371820	-1.131966	$\pm 1.103(1)/ \pm 1.031(1)$

^a MP2/6-311++G**^b Error expressed in units of the last decimal digit.^c Two data are calculated. First is monosubstitution from hydrogenated to monodeuterated ($\text{H} \rightarrow \text{D}$). Second number is from di-deuterated species to monodeuterated ($\text{D} \rightarrow \text{H}$).

In fact, to extract information about the relative orientation of the two subunits, partial r_0 -structure analysis for the observed complex was performed starting from the MP2 planar structure and adjusting some structural parameters to reproduce the observed rotational constants. In this analysis the rotational constants of the deuterated species were not taken into account to obtain structural information on the location of the hydrogen atom involved in the hydrogen bond, because affected by the Ubbelohde effect, which is related to the increase of the distance upon $\text{H} \rightarrow \text{D}$ substitution. Nevertheless using the experimental rotational constant of the parent species together with those of 3FPY- H^{18}OH species some structural parameters were fitted with STRFIT program,^[7] in particular the O-H...N intermolecular bond length and the O-H...N hydrogen bond angle. The obtained values are, respectively, $1.9839(6)\text{\AA}$ and $156.1(1)^\circ$ and the experimental rotational constants are reproduced with an error that falls within unit of MHz. The fitted and derived hydrogen bond parameters are reported in Table 9.4, where they are also compared to the *ab initio* values.

Table 9.4 - r_0 and r_e hydrogen bond parameters of 3FPY-W1.

Fitted parameters		
	$R_{N1H12}/\text{\AA}$	$\angle N1\cdots O13H12/^\circ$
r_0	1.9836(6) ^a	156.1(1)
r_e	1.9785	157.5
Derived parameters		
	$R_{O13H11}/\text{\AA}$	$\angle N1\cdots O13C6/^\circ$
r_0	2.8074(6)	94.8(1)
r_e	2.8092	94.7

^aUncertainties (in parentheses) are expressed in units of the last digit.

The derived experimental structural parameters involved in the intermolecular interaction of the observed 3FPY-W1 conformer can be compared with the ones obtained in the rotational spectroscopy studies, already cited in the previous chapter, between diazines and a molecule of water.^[8-10] The behavior of the hydrogen bond lengths in these systems is in general to decrease when the distance between the two heterocyclic nitrogen atoms increases; in fact going from the pyridazine-water complex to the pyrimidine and to the pyrazine ones, the corresponding values are 2.04 Å, 1.98 Å and 1.94 Å. The value obtained for 3FPY-W1 corresponds to the one of the pyrimidine-water and this fact could be linked to the similarity between the positions of the atom inserted: the second nitrogen atom of the diazine on the pyridine ring and the fluorine atom introduced in the *meta* position of the pyridine ring. Regarding instead the O-H...N angle the ones obtained in the diazines complexes are: 166° for pyridazine-water, 165° for pyrimidine-water and 152° for pyrazine-water system. This last value is the closest the one fitted for the 3FPY-W1 complex (O-H...N angle 156(1)°) and a consideration that could be made is that the electron density distribution on both the systems is quite similar to produce a smaller O-H...N angle and a more distorted structure, in order to obtain in this fluorinated complex a second weak interaction between the oxygen of the water and the hydrogen opposite to the fluorine inserted.

9.4 Dissociation Energy

The intermolecular stretching motion can be, in a first approximation, well isolated from the other low-frequency motions and for an asymmetric top complex in which the stretching motion between

the two subunits is almost parallel to the *a*-axis of the complex, the stretching force constant (k_s) can be roughly estimated using a pseudo-diatomic approximation, as explained previously in Chapter 1. According to this procedure, the value obtained for 3FPY-W1 is $k_s = 17.42 \text{ N}\cdot\text{m}^{-1}$ which is comparable with the ones obtained for two of the diazine-water systems ($k_s = 13.8 \text{ N}\cdot\text{m}^{-1}$ for pyrimidine-water and $k_s = 13.1 \text{ N}\cdot\text{m}^{-1}$ for pyridazine-water adduct, see ref. 9 and 10 respectively). Instead it can be noted the difference with the experimental k_s values of fluorobenzene derivatives water complexes presented by Brendel and co-workers (see ref. 11), where the smaller values are in accord with the weaker nature of the O-H...F and C-H...O hydrogen bonds with respect with the O-H...N intermolecular hydrogen bond exhibited in 3FPY-W adduct which turns out to be a stronger and stabilizing interaction.

The dissociation energy (E_D) of the 3FPY-W1 complex was evaluated to be $30.19 \text{ kJ}\cdot\text{mol}^{-1}$ by assuming a Lennard-Jones potential function, according to:^[12] $E_D=1/72k_sR_{CM}^2$ (see Chapter 1 for more details). The value obtained is quite similar to the ones estimated by the calculations: $E_D=29.25 \text{ kJ mol}^{-1}$; $E_{0D}=21.78 \text{ kJ mol}^{-1}$; $E_D^{BSSE}= 23.60 \text{ kJ mol}^{-1}$; $E_{0D}^{BSSE}=16.44 \text{ kJ mol}^{-1}$. The trend of the calculated values is the one expected when the zero point energy contribution and the correction for BSSE using the counterpoint procedure are considered. Even though all the values are affected by different type of approximations, the experimental E_D and the theoretical ones are comparable with each other and are related to the nature and strength of the O-H...N interaction.

9.5 Conclusions

The analysis of the rotational spectrum of the 3FPY-W complex represents one of the first high resolution spectroscopy works about microsolvation effect on fluorinated pyridine rings. The rotational constants and fourth order centrifugal distortion constants for the most stable conformation were obtained analyzing the rotational spectra of the parent species and its water isotopologues in the 6-18.5 GHz frequency region. From rotational constants, partial r_0 and r_s structures were determined and information about the orientation of the water subunit with respect to the 3FPY ring was obtained.

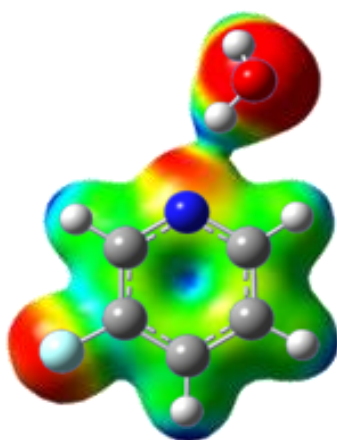


Figure 9.3 - Picture of the observed 3FPY-W1 conformation, where the electronic distribution surface colored by the electrostatic potential is also displayed. The red areas identify the most electronegative regions and the blue ones the most electropositive areas.

The results point out the water preference to create an intermolecular O-H•••N hydrogen bond instead of other type of weaker linkages. This behavior can be related to the small effect produced on the geometry of the pyridine ring by fluorination in *meta* position, which leaves the nitrogen atom to be the preferred site for intermolecular hydrogen bond because it presents the highest electronic density (see Figure 9.3). This fact is further evidenced by the relatively high value of the dissociation energy, that confirms the relatively high strength of this intermolecular interaction.

9.6 References

- [1] C. W. van Dijk, M. Sun, J. van Wijngaarden, *J. Phys. Chem. A*, 116, 4082-4088, **2012**, and refs. within.
- [2] P. Boopalachandran, J. Laane, *Spectrochimica Acta A*, 79, 1191-1195, **2011**.
- [3] S. F. Boys, F. Bernardi, *Mol. Phys.*, 19, 553, **1970**.
- [4] M. J. Frisch, G. W. Trucks, H. B. Schlegel, G. E. Scuseria, M. A. Robb, J. R. Cheeseman, G. Scalmani, V. Barone, B. Mennucci, G. A. Petersson, H. Nakatsuji, M. L. Caricato, X.; Hratchian, H. P.; Izmaylov, A. F.; Bloino, J.; Zheng, G.; Sonnenberg, J. L.; Hada, M.; Ehara, M.; Toyota, K.; Fukuda, R.; Hasegawa, J.; Ishida, M.; Nakajima, T.; Honda, Y.; Kitao, O.; Nakai, H.; Vreven, T.; Montgomery, J. A.; J. E. J. Peralta, F. B. Ogliaro, M.; Heyd, J. J.; Brothers, E.; Kudin, K. N.; Staroverov, V. N.; Kobayashi, R.; Normand, J.; Raghavachari, K.; Rendell, A.; Burant, J. C.; Iyengar, S. S.; Tomasi, J.; Cossi, M.; Rega, N.; Millam, J. M.; Klene, M.; Knox, J. E.; J. B. Cross, V. A. Bakken, C.; Jaramillo, J.; Gomperts, R.; Stratmann, R. E.; Yazyev, O.; Austin, A. J.; Cammi, R.; Pomelli, C.; Ochterski, J. W.; Martin, R. L.; Morokuma, K.; Zakrzewski, V. G.; Voth, G. A.; Salvador, P.; Dannenberg, J. J.; Dapprich, S.; A. D. Daniels, Ö. F. Farkas, J. B.; Ortiz, J. V.; Cioslowski, J.; Fox, D. J., Gaussian, Inc., Wallingford CT, **2009**.
- [5] J. K. G. Watson, "Vibrational spectra and structure", Vol. 6, Elsevier, Amsterdam, Oxford & New York, **1977**.
- [6] J. Kraitchman, *Am. J. Phys.*, 21, **1953**.
- [7] Kisiel, Z. PROSPE - Programs for Rotational SPECTroscopy
<http://www.ifpan.edu.pl/~kisiel/prospe.htm>
- [8] W. Caminati, L. B. Favero, P. G. Favero, A. Maris, S. Melandri, *Angew. Chem. Int. Ed.*, 37, 6, **1998**.
- [9] S. Melandri, M. E. Sanz, W. Caminati, P. G. Favero, Z. Kisiel, *J. Am. Chem. Soc.*, 120, 11504-11509, **1998**.
- [10] W. Caminati, P. Moreschini, P. G. Favero, *J. Phys. Chem. A*, 102, 8097-8100, **1998**.
- [11] K. Brendel, H. Mäder, Y. Xu, W. Jäger, *J. Mol. Spectr.*, 268, 47-52, **2011**.
- [12] S. E. Novick, S. J. Harris, K. C. Janda, W. Klemperer, *Can. J. Phys.*, 53, 2007-2015, **1975**.

9.7 Appendix

Table 9.5 - Measured frequencies (MHz) for the transitions observed for the parent species of 3FPY-W1 conformation.

J'	Ka'	Kc'	F'	J''	Ka''	Kc''	F''	$\nu_{\text{OBS}}/\text{MHz}$	$\Delta\nu_{\text{OBS-CALC}}/\text{kHz}$
4	0	4	5	3	0	3	4	7540.9593	2.1
			4				3	7540.8596	-2.4
			3				2	7540.8778	-0.2
4	1	4	5	3	1	3	4	7194.8991	1.0
			4				3	7194.7454	-1.2
			3				2	7194.8132	0.3
4	1	3	5	3	1	2	4	8058.8505	-2.2
			4				3	8058.7235	0.0
			3				2	8058.8678	3.3
4	2	3	5	3	2	2	4	7640.2478	1.2
			4				3	7639.8171	-0.3
			3				2	7640.3566	-0.2
4	2	2	5	3	2	1	4	7748.1029	2.1
			4				3	7747.7417	-1.8
			3				2	7748.1996	-1.2
4	3	2	5	3	3	1	4	7669.5841	2.1
			4				3	7668.6849	3.8
			3				2	7669.9347	0.5
4	3	1	5	3	3	0	4	7671.6634	4.7
			4				3	7670.7626	2.1
			3				2	7672.0112	0.9
5	0	5	6	4	0	4	5	9349.9368	0.4
			5				4	9349.8315	-2.9
			4				3	9349.8909	-1.5
5	1	5	6	4	1	4	5	8975.2801	-0.8
			5				4	8975.1841	-0.7
			4				3	8975.2178	-3.1
5	1	4	6	4	1	3	5	10050.5741	-0.8
			4				3	10050.5741	1.1
			5				4	10050.4895	-0.7
5	2	4	6	4	2	3	5	9536.5350	1.9
			5				4	9536.2973	-2.1
			4				3	9536.5545	-3.2
5	2	3	6	4	2	2	5	9747.5028	-1.0
			4				3	9747.5028	-16.8
			5				4	9747.3564	0.6
5	3	3	6	4	3	2	5	9594.8088	-2.3
			5				4	9594.3499	0.5
			4				3	9594.9324	6.2

Chapter 9 - 3-FLUOROPYRIDINE•••WATER

J'	Ka'	Kc'	F'	J''	Ka''	Kc''	F''	ν_{OBS}/MHz	$\Delta\nu_{OBS-CALC}/kHz$
5	3	2	6	4	3	1	5	9602.0552	0.1
			5				4	9601.5999	0.4
			4				3	9602.1701	0.9
6	0	6	7	5	0	5	6	11117.3036	-1.1
			6				5	11117.1996	0.5
			5				4	11117.2779	1.2
6	1	6	7	5	1	5	6	10745.2082	-0.5
			5				4	10745.1629	-2.5
			6				5	10745.1379	0.2
6	1	5	7	5	1	4	6	12025.0420	-1.3
			5				4	12025.0420	2.5
			6				5	12024.9699	-4.1
6	2	5	7	5	2	4	6	11423.7723	0.0
			5				4	11423.7723	-1.9
			6				5	11423.6249	0.9
6	2	4	7	5	2	3	6	11779.2604	-0.8
			6				5	11779.2044	-2.0
			5				4	11779.2604	4.5
7	0	7	8	6	0	6	7	12846.5797	1.9
			7				6	12846.4746	0.4
			6				5	12846.5558	-1.9
7	1	7	8	6	1	6	7	12504.1539	-1.3
			7				6	12504.0936	-3.8
			6				5	12504.1272	4.4
7	1	6	8	6	1	5	7	13976.9245	0.2
			7				6	13976.8562	-2.2
			6				5	13976.9245	3.3
7	2	6	8	6	2	5	7	13300.2546	0.1
			7				6	13300.1483	-0.5
			6				5	13300.2490	-0.8
7	2	5	8	6	2	4	7	13837.8298	2.7
			7				6	13837.8127	-2.5
			6				5	13837.8127	-4.5
8	1	7	9	7	1	6	8	15900.1120	-2.8
			8				7	15900.0432	-2.9
			7				6	15900.1120	-0.8
8	2	6	9	7	2	5	8	15912.0586	7.0
			8				7	15912.0586	2.4
			7				6	15912.0462	4.1
9	0	9	10	8	0	8	9	16228.9661	4.7
			9				8	16228.8793	2.1
			8				7	16228.9418	-6.0
9	1	9	10	8	1	8	9	15990.0618	0.0
			9				8	15990.0174	-0.1
			8				7	15990.0400	-1.8

Chapter 9 - 3-FLUOROPYRIDINE...WATER

J'	Ka'	Kc'	F'	J''	Ka''	Kc''	F''	ν_{OBS}/MHz	$\Delta\nu_{OBS-CALC}/kHz$
9	1	8	10	8	1	7	9	17788.1022	1.7
			9				8	17788.0268	0.9
			8				7	17788.1022	2.5
9	2	8	10	8	2	7	9	17014.8427	-2.3
			9				8	17014.7778	2.0
			8				7	17014.8427	4.1
9	3	7	10	8	3	6	9	17320.2139	-3.8
			9				8	17320.1382	1.3
			8				7	17320.2139	-4.1
9	3	6	10	8	3	5	9	17470.4489	-4.1
			9				8	17470.4120	3.3
			8				7	17470.4489	-1.3
3	1	3	4	2	0	2	3	8298.3189	1.0
			3				2	8298.0067	-1.1
			2				1	8298.2126	-2.8
3	2	1	4	2	1	2	3	15736.0718	3.6
			3				2	15737.1896	3.0
			2				1	15735.4674	2.3
4	1	4	5	3	0	3	4	9800.1826	2.4
			4				3	9799.8090	-0.5
			3				2	9800.1663	-5.5
5	0	5	6	4	1	4	5	7090.7126	-0.9
			5				4	7090.8878	0.8
			4				3	7090.5984	-0.2
5	1	5	6	4	0	4	5	11234.5003	-3.6
			5				4	11234.1326	0.3
			4				3	11234.5173	2.6
6	0	6	7	5	1	5	6	9232.7351	-2.2
			6				5	9232.9007	-0.5
			5				4	9232.6562	1.8
6	1	6	7	5	0	5	6	12629.7719	-4.2
			6				5	12629.4376	2.1
			5				4	12629.7930	5.3
7	0	7	8	6	1	6	7	11334.1098	3.4
			7				6	11334.2395	1.7
			6				5	11334.0439	-2.8
7	1	7	8	6	0	6	7	14016.6294	2.9
			6				5	14016.6294	-4.5
			7				6	14016.3358	2.0
5	2	3	6	5	1	4	6	8418.5308	3.7
			5				5	8418.5495	-3.3
			4				4	8418.5167	-5.2
5	3	3	6	5	2	4	6	16127.0720	-1.2
			5				5	16127.6690	-0.5
			4				4	16126.9526	0.8

Chapter 9 - 3-FLUOROPYRIDINE...WATER

J'	Ka'	Kc'	F'	J''	Ka''	Kc''	F''	ν_{OBS}/MHz	$\Delta\nu_{OBS-CALC}/kHz$
6	1	5	7	6	0	6	7	6030.0338	-1.7
			6				6	6030.9411	-2.1
			5				5	6029.8807	-1.7
7	1	6	8	7	0	7	8	7160.3846	2.6
			7				7	7161.3280	0.7
			6				6	7160.2431	-2.7

Table 9.6 - Measured frequencies (MHz) for the transitions observed for the isotopologue species H¹⁸OH of 3FPY-W1 conformation.

J'	Ka'	Kc'	F'	J''	Ka''	Kc''	F''	$\nu_{\text{OBS}}/\text{MHz}$	$\Delta\nu_{\text{OBS-CALC}}/\text{kHz}$
4	0	4	5	3	0	3	4	7157.4792	-3.8
			4				3	7157.3976	2.4
			3				2	7157.4055	3.7
4	1	4	5	3	1	3	4	6837.2154	-0.8
			4				3	6837.0671	1.9
			3				2	6837.1268	-4.0
4	1	3	5	3	1	2	4	7616.3904	-4.4
			4				3	7616.2621	-4.5
			3				2	7616.4104	5.1
4	2	3	5	3	2	2	4	7237.5357	-3.7
			4				3	7237.1071	0.4
			3				2	7237.6475	-3.1
4	2	2	5	3	2	1	4	7324.4879	-0.4
			4				3	7324.1160	-3.9
			3				2	7324.5868	-3.5
5	0	5	6	4	0	4	5	8884.6337	0.7
			5				4	8884.5419	2.9
			4				3	8884.5857	-2.0
5	1	5	6	4	1	4	5	8531.5812	0.7
			5				4	8531.4851	-0.7
			4				3	8531.5177	-2.5
5	1	4	6	4	1	3	5	9502.2175	-0.6
			4				3	9502.2175	2.4
			5				4	9502.1321	-3.8
6	0	6	7	5	0	5	6	10576.4647	1.5
			6				5	10576.3646	-0.2
			5				4	10576.4341	-0.4
6	1	6	7	5	1	5	6	10217.2811	1.1
			6				5	10217.2103	-0.5
			5				4	10217.2353	-1.2
6	1	5	7	5	1	4	6	11374.4775	-3.2
			6				5	11374.4168	1.5
			5				4	11374.4725	-3.4
7	0	7	8	6	0	6	7	12234.2413	-0.8
			7				6	12234.1450	1.3
			6				5	12234.2257	3.8
7	1	7	8	6	1	6	7	11893.7296	-2.6
			7				6	11893.6750	-1.3
			6				5	11893.7046	5.0
7	1	6	8	6	1	5	7	13229.0998	2.4
			7				6	13229.0384	1.6
			6				5	13229.0998	5.7

Chapter 9 - 3-FLUOROPYRIDINE•••WATER

J'	Ka'	Kc'	F'	J''	Ka''	Kc''	F''	ν_{OBS}/MHz	$\Delta\nu_{OBS-CALC}/kHz$
8	0	8	9	7	0	7	8	13863.8155	-6.0
			8				7	13863.7247	0.4
			7				6	13863.7974	-0.5
8	1	8	9	7	1	7	8	13560.8399	-2.7
			8				7	13560.7918	-2.8
			7				6	13560.8138	-3.6
3	1	3	4	2	0	2	3	8094.1085	-0.4
			3				2	8093.8026	-1.4
			2				1	8093.9947	-8.5
4	1	4	5	3	0	3	4	9533.0450	0.6
			4				3	9532.6761	2.3
			3				2	9533.0450	9.1
5	1	5	6	4	0	4	5	10907.1433	1.5
			5				4	10906.7666	2.2
			4				3	10907.1582	3.9
6	0	6	7	5	1	5	6	8553.9513	-3.1
			6				5	8554.1425	3.1
			5				4	8553.8702	2.3
6	1	6	7	5	0	5	6	12239.7953	6.4
			6				5	12239.4380	1.8
			5				4	12239.7953	-7.8
7	0	7	8	6	1	6	7	10570.9193	2.9
			7				6	10571.0785	6.2
			6				5	10570.8538	0.5

Table 9.7 - Measured frequencies (MHz) for the transitions observed for the DOH monodeuterated isotopologue species of 3FPY-W1 conformation.

J'	Ka'	Kc'	F'	J''	Ka''	Kc''	F''	$\nu_{\text{OBS}}/\text{MHz}$	$\Delta\nu_{\text{OBS-CALC}}/\text{kHz}$
5	0	5	6	4	0	4	5	9217.5441	0.0
			5				4	9217.4450	-1.0
			4				3	9217.5005	0.0
5	1	5	6	4	1	4	5	8848.5688	1.3
			5				4	8848.4670	-6.6
			4				3	8848.5152	6.5
5	1	4	6	4	1	3	5	9899.5720	0.8
			4				3	9899.5720	3.2
			5				4	9899.4839	-4.7
6	0	6	7	5	0	5	6	10962.1214	-0.1
			6				5	10962.0199	0.2
			5				4	10962.0938	0.0
6	1	6	7	5	1	5	6	10594.1097	2.5
			6				5	10594.0406	2.6
			5				4	10594.0592	-5.6
6	1	5	7	5	1	4	6	11845.4126	0.0
			6				5	11845.3445	-1.0
			5				4	11845.4126	4.1
7	0	7	8	6	0	6	7	12669.4657	-3.5
			7				6	12669.3674	-1.7
			6				5	12669.4511	1.7
7	1	7	8	6	1	6	7	12329.0337	-0.6
			6				5	12329.0065	4.0
			7				6	12328.9772	-0.9
3	1	3	4	2	0	2	3	8215.8592	-5.1
			3				2	8215.5641	-0.9
			2				1	8215.7653	3.8
4	1	4	5	3	0	3	4	9698.4997	4.9
			4				3	9698.1369	2.1
			3				2	9698.4810	-4.5

Table 9.8 - Measured frequencies (MHz) for the transitions observed for the HOD monodeuterated isotopologue species of 3FPY-W1 conformation.

J'	Ka'	Kc'	F'	J''	Ka''	Kc''	F''	$\nu_{\text{OBS}}/\text{MHz}$	$\Delta\nu_{\text{OBS-CALC}}/\text{kHz}$
5	0	5	6	4	0	4	5	9042.9432	-4.5
			5				4	9042.8462	-2.2
			4				3	9042.9006	-1.8
5	1	5	6	4	1	4	5	8682.4653	2.1
			5				4	8682.3677	1.2
			4				3	8682.4019	-0.3
5	1	4	6	4	1	3	5	9693.0471	1.8
			4				3	9693.0471	4.3
			5				4	9692.9601	-0.7
6	0	6	7	5	0	5	6	10759.2658	-2.4
			6				5	10759.1609	-3.8
			5				4	10759.2353	-4.1
6	1	6	7	5	1	5	6	10396.5013	0.2
			6				5	10396.4352	5.2
			5				4	10396.4555	-1.6
6	1	5	7	5	1	4	6	11600.4342	-1.8
			6				5	11600.3724	4.6
			5				4	11600.4342	2.6
7	0	7	8	6	0	6	7	12439.8689	-8.0
			7				6	12439.7730	-1.4
			6				5	12439.8581	1.6
7	1	7	8	6	1	6	7	12100.5863	0.5
			7				6	12100.5316	3.5
			6				5	12100.5559	3.1
7	1	6	8	6	1	5	7	13488.1681	-1.5
			7				6	13488.1051	-0.5
			6				5	13488.1681	2.2
3	1	3	4	2	0	2	3	8132.7591	-7.6
			3				2	8132.4490	-5.0
			2				1	8132.6564	-4.9
4	1	4	5	3	0	3	4	9592.1799	7.9
			4				3	9591.8002	5.3
			3				2	9592.1697	6.1

Table 9.9 - Measured frequencies (MHz) for the transitions observed for the DOD bi-deuterated isotopologue species of 3FPY-W1 conformation.

J'	Ka'	Kc'	F'	J''	Ka''	Kc''	F''	$\nu_{\text{OBS}}/\text{MHz}$	$\Delta\nu_{\text{OBS-CALC}}/\text{kHz}$
5	0	5	6	4	0	4	5	8921.9049	-1.6
			5				4	8921.8058	-4.8
			4				3	8921.8568	-5.2
5	1	5	6	4	1	4	5	8566.8123	6.8
			5				4	8566.7128	1.7
			4				3	8566.7433	-2.4
5	1	4	6	4	1	3	5	9555.7568	-0.1
			4				3	9555.7568	2.6
			5				4	9555.6700	-4.6
6	0	6	7	5	0	5	6	10617.1824	-5.9
			6				5	10617.0881	-0.1
			5				4	10617.1613	1.3
6	1	6	7	5	1	5	6	10258.5202	1.5
			6				5	10258.4509	1.4
			5				4	10258.4767	1.1
6	1	5	7	5	1	4	6	11436.9840	2.0
			6				5	11436.9161	0.2
			5				4	11436.9840	6.4
7	0	7	8	6	0	6	7	12277.5889	-1.2
			7				6	12277.4893	-1.2
			6				5	12277.5610	-9.1
7	1	7	8	6	1	6	7	11940.6000	2.0
			6				5	11940.5650	-0.7
			7				6	11940.5464	4.5
7	1	6	8	6	1	5	7	13299.3987	0.4
			7				6	13299.3339	-2.7
			6				5	13299.3987	4.1
3	1	3	4	2	0	2	3	8056.2222	-8.2
			3				2	8055.9195	-5.7
			2				1	8056.1242	-2.6
4	1	4	5	3	0	3	4	9498.0092	1.0
			4				3	9497.6476	8.2
			3				2	9498.0092	9.2

PENTAFLUOROPYRIDINE ... WATER

10.1 Introduction

Pursuing the same purposes as described in Chapters 8 and 9, the effects of ring fluorination are further deepened, studying the behavior of the water-probe on a perfluorinated aromatic ring: the rotational spectrum of pentafluoropyridine...water (penta-FPY-W) complex is here analyzed.

As already described, the introduction of fluorine atom(s) into organic molecules causes in general major changes in their physico-chemical properties; most importantly chemical reactivity and biological activity, compared to the non-fluorinated analogues. Whenever included into organic molecular frameworks fluorine atoms bring in novel properties which result useful, sometimes unexpectedly, in many different fields, such as material's and separation science, organic synthesis, *etc.*^[1] Certainly as the number of fluorine atoms increases, this changes in properties are not only enhanced but it is possible to witness a complete transformation of the behavior of the molecular system. The perfluorination effect is well known in supramolecular chemistry as well as in crystal engineering, where the inversed electron density distribution shown by perfluorinated aromatic rings can be combined with the typical π -cloud of the non fluorinated one in order to build new interesting systems, characterized by phenyl-perfluorophenyl interactions.^[2] As reported in ref.2, in spite of the latter phenyl-perfluorophenyl stacking featuring that presents a stabilizing energy of about $30 \text{ kJ}\cdot\text{mol}^{-1}$, other observed contacts involving fluorine atoms are generally weak. Nevertheless, the co-operation of these weak interactions can have a significant influence not only on crystal structures but also on chemical and physical properties, providing stability to these fluorine compounds.

Concerning perfluorinated aromatic compounds, literature is quite poor on gas phase spectroscopic studies in describing their interactions and behavior. Few articles,^[3,4] published several years ago, studied the perfluorination effects with photoelectron spectroscopy. In particular the authors described how the π ionization potentials of planar aromatic systems and their perfluoro derivatives are very nearly equal, whereas the σ ionization potentials in the perfluoro compounds are several electron volts larger than in the perhydro compounds, attesting the perfluorination effect.

Regarding studies on small complexes within this family of compounds or rotational spectroscopy works on analogous molecules, the scenery is also not so copious. As affirmed in both cited reviews,^[1,2] there is still much work needed to understand structural, chemical, physical and biological properties of fluorine compounds for further applications in the life sciences and the materials subject.

Exploring the essential chemical point of view, the analysis of perfluorinated compounds by rotational spectroscopy can lead to point out basic interactions that governs their stability on conformational arrangements. Moreover gas-phase spectroscopic studies of microsolvated aromatics compounds are particularly relevant to evaluate the forces that drive the conformational preferences and describe the adduct' properties in the presence of solvent molecules.

For all of the above reasons, together with the absence of this kind of studies in the scientific literature, it seemed interesting to move from fluoro-monosubstitution to perfluoro-substitution on the pyridine ring in order to evaluate the changes in presence of the water probe.

We expect for a perfluorinated compound, that the centre of the ring will present a positive charge and therefore the water moiety will lie above the penta-FPyr with the oxygen lone pairs pointed towards the aromatic ring. This behavior is mentioned also by Brendel *et al.* in the previously cited fluorobenzene•••water and p-difluorobenzene•••water dimers rotational spectroscopic study.^[5] In fact, comparing their planar arrangements observed for both clusters with other systems, they reported the case of hexafluorobenzene•••water complex, analyzed in the K. Brendel Ph.D. Thesis,^[6] where the hydrogen atoms of the water point away from the aromatic ring. This system presents an inverse arrangement respect to the benzene•••water complex,^[7] where the hydrogen atoms of the water are oriented towards the ring plane.

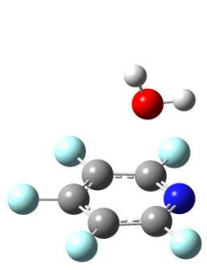
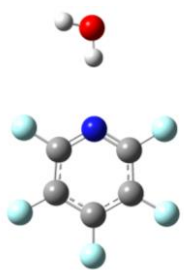
To give more information about perfluorinated compounds and to evaluate the behavior of the pyridine ring in comparison between the other monosubstituted species already described before, the penta-FPY-W complex is here analyzed by rotational spectroscopy.

10.2 Theoretical calculations

As reported in previous chapters, the *ab initio* methods used to characterize the conformational arrangements of this type of complexes were proved to be appropriate for spectroscopic purposes. In particular regarding the penta-FPY-W complex, geometry optimizations of different structures have been performed using the MP2 method with the 6-311++G** basis set, using also the counterpoise procedure with basis set superposition error (BSSE).^[8] Vibrational frequency calculations of all the optimized structures are carried out in the harmonic approximation to check

whether all of those are real minima. The Gaussian 09 program package was used to carry out all the calculations.^[9]

Table 10.1 - Spectroscopic parameters, relative energies and shape of the two possible conformations for pentafluoropyridine...water complex, calculated with MP2/6-311++G** and BSSE correction.

	penta-FPY-W1	penta-FPY-W2
		
MP2/6-311++G** BSSE		
<i>A</i> /MHz	1003	1064
<i>B</i> /MHz	819	698
<i>C</i> /MHz	608	423
μ_a /D	-0.01	-2.81
μ_b /D	-0.57	-1.55
μ_c /D	2.25	-0.68
μ_{TOT} /D	2.32	3.29
<i>D_J</i> /kHz	0.22	0.53
<i>D_{JK}</i> /kHz	0.43	-1.30
<i>D_K</i> /kHz	-0.40	3.04
<i>d₁</i> /kHz	-0.02	-0.14
<i>d₂</i> /kHz	0.07	-0.04
χ_{aa} /MHz	2.37	-4.60
χ_{bb} /MHz	-4.51	2.36
χ_{cc} /MHz	2.15	2.24
ΔE_0 /kJ•mol ⁻¹	0 ^a	4.94

^a Absolute zero point corrected energy: -819.186593Hartrees.

As shown in Table 10.1, the penta-FPY-W complex can give rise to two different arrangements: the water moiety can lie above the penta-FPY ring with the oxygen lone pairs oriented towards the positive π -cloud (penta-FPYr-W1), or in a planar disposition with one hydrogen of the water pointing towards the nitrogen of the penta-FPY unit (penta-FPY-W2). The optimizations of both geometries with MP2-BSSE corrected method give the spectroscopic parameters and the relative ZPE-corrected energy reported in Table 10.1. In particular the global

minimum is predicted to be the penta-FPY-W1 conformation, more stable than the penta-FPY-W2 of $4.94 \text{ kJ}\cdot\text{mol}^{-1}$. Only the MP2-BSSE corrected data are reported because the simple MP2 method was unable to minimize the penta-FPY-W2 arrangements that presented a negative vibrational frequency value.

Concerning predicted dipole moments components, it can be noted that for the penta-FPY-W1 conformation, μ_c represents the highest value while for penta-FPyr-W2 conformer the highest value is the μ_a component.

Considering the relative energy results together with the predicted values of the dipole moments components, the search was conducted in order to reveal the presence of the penta-FPY-W1 conformation in the jet, starting search μ_c -type rotational transitions.

10.3 Experimental Results and Analysis

The rotational spectrum in the 6-18.5 GHz frequency region of penta-FPY-W complex was recorded using the COBRA-type PJ-FTMW spectrometer at the University of Bologna, already described in Chapter 3. Molecular clusters were generated in a supersonic expansion, under conditions optimized for the molecular adduct formation.

penta-FPY (99%) was purchased from Alfa Aesar and used without further purification. The measurements were carried out using helium as the carrier gas at a stagnation pressure of $\sim 0.4 \text{ MPa}$ passed over the samples of water and penta-FPY (at 0°C), in two separated containers, and expanded through a solenoid valve (General Valve, Series 9, nozzle diameter 0.5 mm) into the Fabry-Perot cavity. The spectral line positions were determined after Fourier transformation of the time domain signal with 8k data points, recorded with 100 ns sample intervals. Each rotational transition displays a Doppler splitting, enhanced by the coaxial arrangement of the spectrometer. The rest frequency was calculated as the arithmetic mean of the frequencies of the two Doppler components. The estimated accuracy of the frequency measurements is better than 3 kHz, resolution is better than 7 kHz.

Preliminary trial predictions of the rotational spectra were based on the rotational constants reported in Table 10.1. It was possible to assign only one spectrum, that of the species penta-FPY-W1 and according to the theoretical values of the dipole moment components, the first search has been targeted to the μ_c -R band. The $J = 5 \leftarrow 4$ was observed first (see Figure 10.1) and then the assignment was extended to other rotational transitions with rotational quantum number J ranging from $J = 4$ up to $J = 8$. Because of the overall low intensity of the spectrum, it was not possible to

measure any μ_b -type transitions and this result is in agreement with the small values predicted by calculation ($\mu_b = -0.57$ Debye).

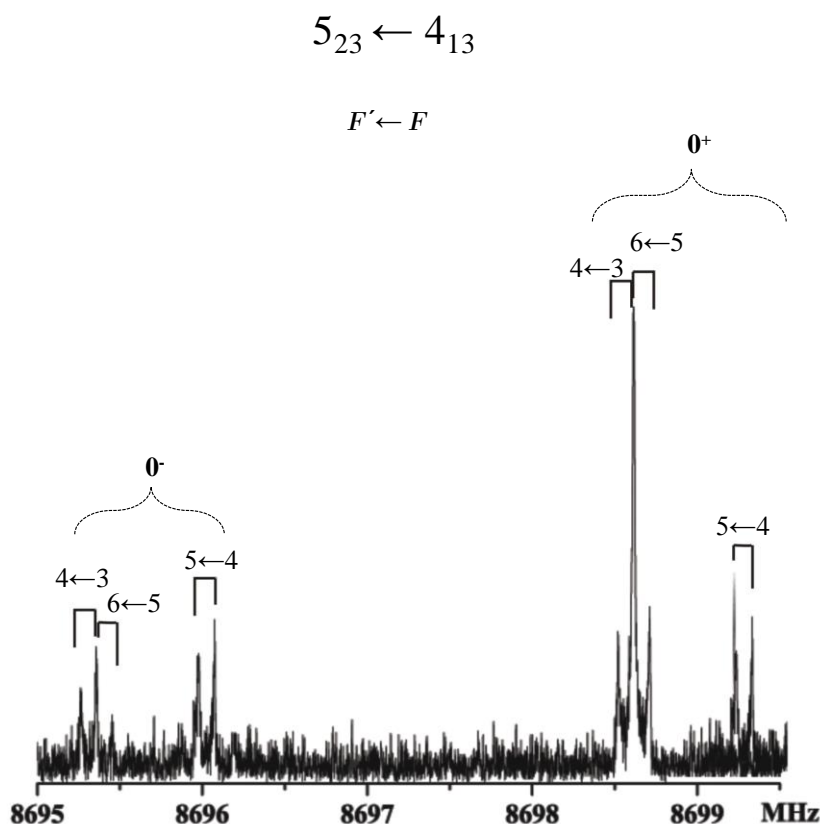


Figure 10.1 - $5_{23} \leftarrow 4_{13}$ transition of the observed penta-FPY-W1 conformation. Each rotational line is split by Doppler effect and the nuclear quadrupole hyperfine effect (quantum numbers $F' \leftarrow F$ are shown). Moreover the two vibrational state 0^+ and 0^- are shown with the statistical weight 3:1 due to the internal rotation of the water moiety.

All the measured transitions showed a nuclear-quadrupole hyperfine structure due to the presence of the nitrogen ^{14}N nucleus. Moreover, all the assigned rotational transitions were formed by doublets with splitting varying from 0.16 to 5.10 MHz. All doublets consist of a stronger high frequency component and a weaker low frequency component (as shown in Figure 10.1), with the same intensity ratios for all observed doublets. Both states have been treated independently as asymmetric rotor states for what concerns rotational constants and centrifugal distortion constants, instead the quadrupole coupling constants were fitted in common. The S -reduction of Watson's semirigid rotational Hamiltonian in the I' representation^[10] was used to fit the experimental frequencies, giving the spectroscopic constants for both states reported in Table 10.2. All the observed frequencies are listed in Table 10.5.

Table 10.2 - Experimental spectroscopic constants of the observed penta-FPY-W1 conformation for both vibrational states 0^+ and 0^- .

	penta-FPY-W1	
	0^+	0^-
A/MHz	1009.0860(1) ^a	1008.8572(1)
B/MHz	819.3550(2)	819.6669(2)
C/MHz	614.1098(7)	613.6164(7)
D_J/kHz	0.292(2)	0.285(2)
D_{JK}/kHz	0.52(1)	0.52(1)
D_K/kHz	-0.566(8)	-0.548(8)
d_2/kHz	0.0839(3)	0.0828(3)
χ_{aa}/MHz	1.964(6)	
χ_{bb}/MHz	-3.720(5)	
χ_{cc}/MHz	1.756(5)	
N^b	116	114
σ^c/kHz	3	

^a Error in parentheses in units of the last digit.

^b Number of lines in the fit.

^c Root-mean-square deviation of the fit.

To explain the double structure observed in the microwave spectrum, a consideration of internal rotation motion in penta-FPY-W1 is required. As already discussed in Chapter 1, internal rotation leads to a splitting of the ground state torsional eigenvalues, that in this system can be caused by the rotation of H₂O molecule about its C₂ axis. Since this motion involves the two equivalent hydrogen atoms of the water moiety, all the lines were split by their interchange. Since the hydrogen atoms are fermions and the exchange of one pair of hydrogen atoms demands for an antisymmetric total wave function, a statistical weight of 3 to 1 is originated due to spin functions. Thus, the ground state of this torsional motion is split into two levels, named 0^+ and 0^- , with different spin statistical weights due to the internal rotation of the water molecule. For this reason two sets of rotational constants were obtained (see Table 10.2). A similar internal motion due to the water moiety was observed also in the phenol•••water complex by rotational spectroscopy.^[11] The stable structure obtained for this cluster revealed a *trans*-linear hydrogen bonding arrangement with the hydrogen atoms of the water moiety lying above and below the aromatic plane.

This type of motion is confirmed also by the investigation of some water isotopologues species. These species were generated by adding D₂O or H₂¹⁸O to the system and observing the rotational spectrum in the same conditions as for the normal species. In particular regarding monodeuterated isotopologues (penta-FPY-DOH and penta-FPY-HOD, where the first hydrogen is

number 13 and the second one is referred to the hydrogen 14 (depicted in Figure 10.2 where the complete numbering used for the observed complex is reported), the splitting is not observed because the two hydrogen atoms are not equivalent anymore. Instead concerning penta-FPY- $H^{18}OH$, the splitting still appears in the rotational spectrum, as expected. All the spectroscopic parameter for these isotopologues are reported in Table 10.3 and the measured frequencies are listed in Tables 10.6, 10.7 and 10.8. The intensity of the rotational spectrum of the bi-deuterated species was too low to allow observation.

Table 10.3 - Experimental spectroscopic constants of the observed water's isotopologues of penta-FPY-W1 conformation.

penta-FPY-W1	$H^{18}OH$ 0^+	$H^{18}OH$ 0^-	DOH	HOD
A /MHz	979.8040(3) ^a	979.5771(5)	984.9340(3)	988.7861(4)
B /MHz	802.5616(3)	802.9166(5)	805.4598(4)	812.9364(5)
C /MHz	612.625(1)	612.101(3)	612.784(1)	609.986(2)
D_J /kHz	0.300(6)	0.30(1)	0.289(4)	0.262(6)
D_{JK} /kHz	0.59(2)	0.60(4)	[0.59] ^d	[0.59] ^d
D_K /kHz	-0.63(2)	-0.63(4)	[-0.63] ^d	[-0.63] ^d
d_2 /kHz	0.0822(9)	0.081(1)	[0.0822] ^d	[0.0822] ^d
χ_{aa} -N/MHz	1.97(1)		2.00(1)	2.07(4)
χ_{bb} -N/MHz	-3.675(4)		-3.706(6)	-3.74(1)
χ_{cc} -N/MHz	1.701(4)		1.706(6)	1.66(1)
χ_{aa} -D/MHz	.	.	-0.09(1)	-0.12(2)
χ_{bb} -D/MHz	.	.	-0.123(4)	0.208(7)
χ_{cc} -D/MHz	.	.	0.209(4)	-0.088(7)
N^b	57	57	71	49
σ^c /kHz		3	4	5

^a Error in parentheses in units of the last digit.

^b Number of lines in the fit.

^c Root-mean-square deviation of the fit.

^d Values fixed to the ones of the parent species.

Concerning the monodeuterated species, looking the Table 10.3, it can be noted that it was possible to measure also the hyperfine structure due to the deuterium atom and thus the quadrupole coupling constants for this atom were also obtained.

From the experimental rotational constants obtained for the different species of the global minimum penta-FPY-W1 and using Kraitchman's substitution method^[12] a partial experimental r_s -structure was determined. Such analysis leads to the determination of the absolute values of the principal axis coordinates of the substituted atom from the changes in principal moments of inertia

resulting from a single isotopic substitution. In Table 10.4 the coordinates of the oxygen atom and the two hydrogen atoms of the water molecule obtained from this procedure are reported. Looking at this table, it can be noted that, regarding the oxygen atom, the set of a , b and c has two values obtained from the two vibrational state 0^+ and 0^- which characterized its rotational spectrum, instead for the hydrogen coordinates the values of the coordinates were obtained considering only the 0^+ state.

These r_s coordinates can be compared with the calculated ones (r_e) and the ones obtained from the r_0 structure. In fact, to extract information about the structure of the global minimum observed, a partial r_0 -structure analysis was done starting from the calculated geometry and adjusting some structural parameters to reproduce the observed rotational constants. In this analysis the experimental rotational constant of the parent species together with those of the observed isotopologues (H^{18}OH , DOH and HOD) were used to fit a few significant structural parameters with the STRFIT program.^[13] In this analysis the rotational constants of the 0^+ of the parent state were taken into account for what concerns the parent species and the H^{18}OH one. The structural parameters fitted are the distance between the oxygen atom and the center of mass (c.m.) of the complex and the relative angle with the nitrogen atom, as shown in Figure 10.2. The obtained values are: O-c.m. = 2.994(8) Å and O-c.m.-N = 84.2(5)° which can be compared to the starting *ab initio* ones that were O-c.m. = 3.025 Å and O-c.m.-N = 81.380°: the distance between the oxygen and the center of mass decreases by about 0.03 Å and the angle increases of about 3°. Using these fitted values the experimental rotational constants are reproduced with an error that falls just above unit of MHz.

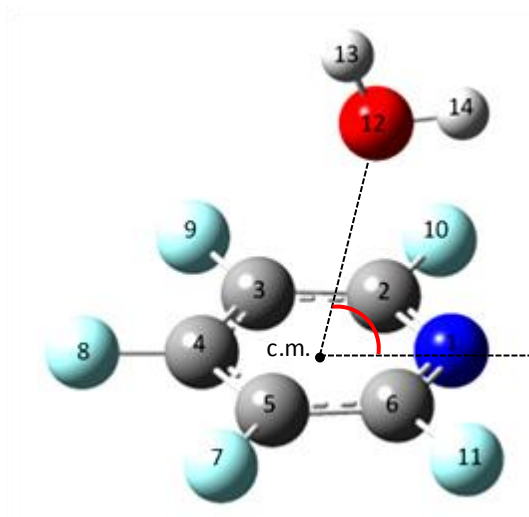


Figure 10.2 - Image of the observed conformation of penta-FPY-W1 with the atom numbering used in the text. It is also shown the center of mass (c.m.) of the complex and the values obtained from the partial structural fit are: O-c.m.= 2.994(8) Å and O-c.m.-N = 84.2(5)°.

Table 10.4 - Values of the coordinates (Å) relating to the isotopic substitutions (r_s), obtained from computational data (r_e) and derived from the effective structure (r_0) for the penta-FPY-W1 conformation.

	r_e	r_s	r_0
O			
a	0.006612 ^a	[0] [°]	0.00217(2)
b	-1.103816	±0.979(2)/ ±0.990(2) *	-0.87(4)
c	2.535486	±2.5669(6)/ ±2.5630(6)	2.58(1)
H₁₃			
a	0.008	±0.258(6)	0.00535(2)
b	-0.913	±1.274(1)	-0.62(5)
c	3.476	±3.2636(5)	3.503(8)
H₁₄			
a	-0.003	±0.266(6)	0.00180(2)
b	-2.064	±2.3149(8)	-1.83(4)
c	2.499	±2.2178(8)	2.61(2)

^a Error expressed in units of the last decimal digit.

[°] Slightly imaginary values: set to zero.

* The first coordinate value is obtained from the 0 state while the second one is obtained considering the 1 state.

Looking Table 10.4, it can be noted that the coordinates of the hydrogen atoms are not satisfactorily reproduced, probably due to the motion that affects the molecule of water with respect to penta-FPY.

As already mentioned in the introduction, not many microwave studies are reported with the same kind of interaction that is here observed, but a comparison with the chlorotrifluoroethylene...water^[14] complex can be done. In fact in this work the most stable conformation is established by a lp... π interaction between the oxygen of the water and the carbon-carbon double bond and that can be explained in terms of an electron-withdrawing effect from the π -electronic system towards the halogen atoms (especially the F atoms) generating a positive potential above the carbon atom linked to the two fluorine atoms. The distance between the two interacting atoms (O and C₁) is derived to be 2.947 Å. Even if the system is completely different to the one analyzed here, the distances that characterized the intermolecular interaction are quite similar. As affirmed by authors, this kind of lp... π interactions that is in competition with hydrogen bonds and halogen bonds, takes place when water is interacting with perhalogenated alkenes. But from this study, it is clear how perfluorinated aromatic systems are also involved to create the same kind of interactions, that are not observed in the perhydrogenated analogues, (see benzene...water complex, ref. 7).

10.4 Conclusions

The analysis of the rotational spectrum in the 6-18.5 GHz frequency region, of the pentaFPY-W complex represents the first high resolution spectroscopy work about microsolvation effect on the perfluorinated pyridine ring. The rotational constants, fourth order centrifugal distortion constants and the quadrupole coupling constants for the most stable conformation were obtained analyzing the rotational spectra of the parent species and its water isotopologues. The fully rotationally resolved cluster spectra of the type presented here are perhaps the most direct approach to an understanding of the structural and energetic implications of weak intermolecular forces at the two-body level.

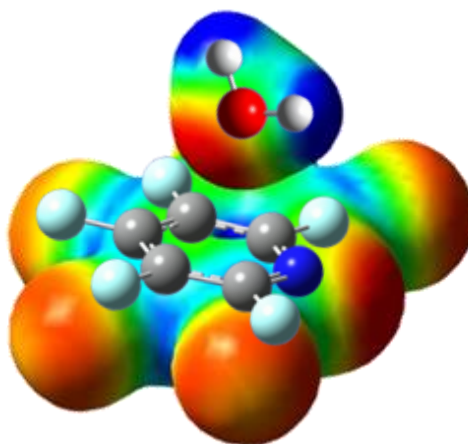


Figure 10.3 - Picture of the observed penta-FPY-W1 conformation, where the electronic distribution surface colored by the electrostatic potential is also displayed. The red areas identify the most electronegative regions and the blue ones the most electropositive areas and it can be noted the complete inverse electron density distribution of the perfluorinated aromatic ring.

In particular in this work, the direct observation of perfluorination effect was here firstly detected between the pyridine ring and the water molecules. As shown in Figure 10.3, the complete inversed electron density distribution of the penta-FPY unit allows the water molecule to arrange above the ring in the more stable conformation characterized by a $lp\cdots\pi$ interaction.

10.5 References

- [1] M. Cametti, B. Crousse, P. Metrangolo, R. Milani, G. Resnati, *Chem. Soc. Rev.*, 41, 31-42, **2012**.
- [2] K. Reichenbacher, H. I. Süss, Jürg Hulliger, *Chem. Soc. Rev.*, 34, 22-30, **2005**.
- [3] C. R. Brundle, M. B. Robin, N. A. Kuebler, and H. Basch, *J. Amer. Chem. Soc.*, 94, 1451, **1972**.
- [4] C. R. Brundle, M. B. Robin, N. A. Kuebler, *J. Amer. Chem. Soc.*, 94, 1466, **1972**.
- [5] K. Brendel, H. Mäder, Y. Xu, W. Jäger, *J. Mol. Spectr.*, 268, 47–52, **2011**.
- [6] K. Brendel, Ph.D. Thesis, Kiel, **2004**.
- [7] S. Suzuki, P.G. Green, R.E. Bumgarner, S. Dasgupta, W.A. Goddard III, G.A. Blake, *Science*, 257, 942–945, **1992**.
- [8] S. F. Boys, F. Bernardi, *Mol. Phys.*, 19, 553, **1970**.
- [9] M. J. Frisch, G. W. Trucks, H. B. Schlegel, G. E. Scuseria, M. A. Robb, J. R. Cheeseman, G. Scalmani, V. Barone, B. Mennucci, G. A. Petersson, H. Nakatsuji, M. L. Caricato, X.; Hratchian, H. P.; Izmaylov, A. F.; Bloino, J.; Zheng, G.; Sonnenberg, J. L.; Hada, M.; Ehara, M.; Toyota, K.; Fukuda, R.; Hasegawa, J.; Ishida, M.; Nakajima, T.; Honda, Y.; Kitao, O.; Nakai, H.; Vreven, T.; Montgomery, J. A.; J. E. J. Peralta, F. B. Ogliaro, M.; Heyd, J. J.; Brothers, E.; Kudin, K. N.; Staroverov, V. N.; Kobayashi, R.; Normand, J.; Raghavachari, K.; Rendell, A.; Burant, J. C.; Iyengar, S. S.; Tomasi, J.; Cossi, M.; Rega, N.; Millam, J. M.; Klene, M.; Knox, J. E.; J. B. Cross, V. A. Bakken, C.; Jaramillo, J.; Gomperts, R.; Stratmann, R. E.; Yazyev, O.; Austin, A. J.; Cammi, R.; Pomelli, C.; Ochterski, J. W.; Martin, R. L.; Morokuma, K.; Zakrzewski, V. G.; Voth, G. A.; Salvador, P.; Dannenberg, J. J.; Dapprich, S.; A. D. Daniels, Ö. F. Farkas, J. B.; Ortiz, J. V.; Cioslowski, J.; Fox, D. J., Gaussian, Inc., Wallingford CT, **2009**.
- [10] J. K. G. Watson, “Vibrational spectra and structure”, Vol. 6, Elsevier, Amsterdam, Oxford & New York, **1977**.
- [11] M. Gerhards, M. Schmitt, K. Kleiner, W. Stahl, *J. Chem. Phys.*, 104 (3), **1996**.
- [12] J. Kraitchman, *Am. J. Phys.*, 21, **1953**.
- [13] Kisiel, Z. PROSPE - Programs for Rotational SPECTroscopy
<http://www.ifpan.edu.pl/~kisiel/prospe.htm>
- [14] Q. Gou, G. Feng, L. Evangelisti, W. Caminati, *Angew. Chem. Int. Ed.*, 52, 11888 –11891, **2013**.

10.6 Appendix

Table 10.5 - Measured frequencies (MHz) for the transitions observed for both vibrational state 0^+ and 0^- of the parent species of penta-FPY-W1 conformation.

J'	Ka'	Kc'	F'	J''	Ka''	Kc''	F''	$\nu_{\text{OBS}}/\text{MHz}$ 0^+	$\Delta\nu_{\text{OBS-CALC}}/\text{MHz}$ 0^+	$\nu_{\text{OBS}}/\text{MHz}$ 0^-	$\Delta\nu_{\text{OBS-CALC}}/\text{MHz}$ 0^-
4	4	0	5	3	3	0	4	7785.1268	-0.0013	7783.4572	-0.0025
			4				3	7784.8792	-0.0005	7783.2101	-0.0005
			3				2	7785.1498	0.0016	7783.4810	0.0007
4	4	1	5	3	3	1	4	7809.8832	-0.0023	7808.4751	-0.0032
			4				3	7809.7766	-0.0030	7808.3709	-0.0017
			3				2	7809.8553	0.0037	7808.4452	0.0009
4	3	1	5	3	2	1	4	7183.2818	-0.0025	7182.6973	0.0034
			4				3	7182.8671	-0.0009	7182.2777	-0.0021
			3				2	7183.4928	0.0007	7182.9001	-0.0010
4	3	2	5	3	2	2	4	7382.2946	-0.0017	7382.1321	0.0028
			4				3	7382.3828	0.0042	7382.2147	0.0024
			3				2	7382.2708	-0.0042	7382.1058	-0.0019
5	1	4	6	4	0	4	5	8910.2943	0.0008	8912.7024	0.0017
			5				4	8911.1248	0.0016	8913.5259	-0.0019
			4				3	8910.0904	0.0007	8912.4974	0.0000
5	2	4	6	4	1	4	5	8958.1930	-0.0004	8959.8531	0.0002
			5				4	8958.8824	0.0003	8960.5391	-0.0015
			4				3	8958.0186	0.0019	8959.6736	-0.0025
5	2	3	6	4	1	3	5	8695.4077	0.0029	8698.6646	0.0030
			5				4	8696.0240	-0.0005	8699.2819	-0.0002
			4				3	8695.3087	-0.0019	8698.5665	-0.0004
5	3	2	6	4	2	2	5	8703.1730	0.0000	8704.0750	-0.0002
			5				4	8703.0888	-0.0003	8703.9947	0.0004
			4				3	8703.2668	0.0035	8704.1661	0.0013
5	3	3	6	4	2	3	5	9024.4399	-0.0010	9025.2114	0.0013
			5				4	9024.6948	-0.0023	9025.4675	0.0004
			4				3	9024.3937	0.0000	9025.1582	-0.0043
5	4	2	6	4	3	2	5	9325.5917	-0.0002	9324.7708	0.0004
			5				4	9325.4999	-0.0027	9324.6833	0.0015
			4				3	9325.6078	-0.0066	9324.7898	-0.0029
5	4	1	6	4	3	1	5	9201.7128	0.0000	9199.9621	0.0041
			5				4	9201.2721	0.0005	9199.5148	-0.0020
			4				3	9201.8374	-0.0007	9200.0824	-0.0012
5	5	0	6	4	4	0	5	9812.4169	0.0005	9810.3629	0.0024
			5				4	9812.2782	-0.0008	9810.2266	0.0039
			4				3	9812.4169	0.0109	9810.3472	-0.0029
5	5	1	6	4	4	1	5	9819.7949	0.0000	9817.8542	-0.0007
			5				4	9819.6932	-0.0007	9817.7570	0.0029
			4				3	9819.7792	0.0047	9817.8333	-0.0012

Chapter 10 - PENTAFLUOROPYRIDINE...WATER

J'	Ka'	Kc'	F'	J''	Ka''	Kc''	F''	ν_{OBS}/MHz 0^+	$\Delta\nu_{OBS-CALC}/MHz$ 0^+	ν_{OBS}/MHz 0^-	$\Delta\nu_{OBS-CALC}/MHz$ 0^-
6	1	5	7	5	0	5	6	10730.6026	0.0033	10733.0586	-0.0008
			6				5	10731.2859	0.0000	10733.7448	0.0004
			5				4	10730.4569	0.0004	10732.9181	0.0011
6	2	5	7	5	1	5	6	10744.7254	-0.0010	10746.8932	0.0001
			6				5	10745.3710	-0.0012	10747.5349	-0.0029
			5				4	10744.5913	0.0009	10746.7593	0.0021
6	2	4	7	5	1	4	6	10563.8141	0.0057	10567.8325	-0.0038
			6				5	10564.4637	-0.0040	10568.4933	-0.0005
			5				4	10563.7003	-0.0029	10567.7309	-0.0005
6	3	3	7	5	2	3	6	10358.0250	-0.0018	10360.9672	0.0025
			5				4				
			6				5	10358.2642	0.0009	10361.2087	0.0043
6	3	4	7	5	2	4	6	10735.6937	-0.0016	10737.4559	-0.0034
			6				5	10736.0690	0.0002	10737.8320	-0.0009
			5				4	10735.6378	0.0052	10737.3986	0.0022
6	4	2	7	5	3	2	6	10615.4444	0.0025	10614.5957	-0.0076
			6				5	10615.1081	-0.0012	10614.2749	0.0013
			5				4	10615.5431	0.0003	10614.7094	0.0056
6	4	3	7	5	3	3	6	10899.6650	0.0015	x	x
			6				5	10899.7004	0.0009	x	x
			5				4	10899.6650	-0.0045	x	x
6	5	1	7	5	4	1	6	11252.8992	0.0003	11250.6356	0.0012
			6				5	11252.5960	-0.0013	11250.3328	0.0011
			5				4	11252.9552	-0.0023	11250.6905	-0.0029
6	5	2	7	5	4	2	6	11306.3023	0.0000	11304.7660	0.0013
			6				5	11306.1640	0.0029	11304.6231	-0.0006
			5				4	11306.3225	-0.0033	11304.7858	-0.0023
6	6	1	7	5	5	1	6	11835.4810	-0.0039	11833.0494	-0.0023
			6				5	11835.4046	0.0006	11832.9728	0.0020
			5				4	11835.4730	0.0046	11833.0403	0.0050
6	6	0	7	5	5	0	6	11833.5477	-0.0006	11831.0769	0.0019
			6				5	11833.4617	0.0026	11830.9867	0.0011
			5				4	11833.5335	0.0000	11831.0564	-0.0038
7	1	6	8	6	0	6	7	12536.8185	0.0033	12539.4726	0.0043
			7				6	12537.4137	-0.0005	12540.0661	0.0000
			6				5	12536.7088	0.0009	12539.3623	0.0011
7	2	6	8	6	1	6	7	12540.5049	-0.0020	12543.0661	0.0010
			7				6	12541.0941	-0.0018	12543.6534	0.0003
			6				5	12540.3972	-0.0039	12542.9553	-0.0040
7	2	5	8	6	1	5	7	12429.6186	0.0015	12433.4962	-0.0005
			7				6	12430.1658	-0.0026	12434.0460	0.0001
			6				5	12429.5374	0.0019	12433.4147	-0.0007
7	3	5	8	6	2	5	7	12496.6431	-0.0005	12499.2418	0.0009
			7				6	12497.0672	0.0020	12499.6601	-0.0019
			6				5	12496.5787	-0.0009	12499.1769	0.0000

Chapter 10 - PENTAFLUOROPYRIDINE...WATER

J'	Ka'	Kc'	F'	J''	Ka''	Kc''	F''	ν_{OBS}/MHz 0^+	$\Delta\nu_{OBS-CALC}/MHz$ 0^+	ν_{OBS}/MHz 0^-	$\Delta\nu_{OBS-CALC}/MHz$ 0^-
7	3	4	8	6	2	4	7	12159.6470	-0.0025	12164.7370	-0.0034
			7				6	12160.1242	0.0004	12165.2257	0.0096
			6				5	12159.6015	-0.0002	12164.6850	-0.0074
7	4	4	8	6	3	4	7	12545.2442	-0.0015	12546.6379	-0.0003
			7				6	12545.4151	0.0031	12546.8094	0.0039
			6				5	x	x	12546.6261	0.0026
7	4	3	8	6	3	3	7	12127.4902	0.0058	12128.8897	-0.0010
			7				6	12127.4151	-0.0051	12128.8296	-0.0007
			6				5	12127.5283	-0.0012	12128.9334	-0.0019
7	5	3	8	6	4	3	7	12826.8003	0.0000	12826.0744	-0.0007
			7				6	12826.7210	0.0011	12825.9945	-0.0011
			6				5	12826.8261	0.0046	12826.1024	0.0062
7	5	2	8	6	4	2	7	12645.1208	0.0030	12642.6415	-0.0009
			7				6	12644.7298	0.0001	12642.2530	-0.0015
			6				5	12645.1946	-0.0024	12642.7220	0.0001
7	6	2	8	6	5	2	7	13309.4896	0.0013	13307.3043	-0.0041
			7				6	13309.3459	-0.0023	13307.1647	-0.0038
			6				5	13309.4985	-0.0062	13307.3252	0.0001
7	6	1	8	6	5	1	7	13291.3155	0.0014	13288.7876	0.0027
			7				6	13291.1243	0.0031	13288.5914	0.0003
			6				5	13291.3400	0.0000	13288.8122	0.0012
7	7	1	8	6	6	1	7	13852.9492	0.0010	13850.0469	0.0031
			7				6	13852.8829	-0.0020	13849.9837	0.0031
			6				5	13852.9280	-0.0059	13850.0267	-0.0029
7	7	0	8	6	6	0	7	13852.4770	0.0007	13849.5617	0.0019
			7				6	13852.4121	0.0008	13849.4954	0.0006
			6				5	13852.4555	-0.0068	13849.5401	-0.0058
8	8	0	9	7	7	0	8	15870.7279	0.0001	15867.3595	0.0023
			8				7	15870.6782	0.0006	15867.3099	0.0030
			7				6	15870.7191	0.0034	15867.3428	-0.0022
8	8	1	9	7	7	1	8	15870.8370	-0.0002	15867.4698	-0.0002
			8				7	15870.7860	-0.0013	15867.4213	0.0012
			7				6	15870.8275	0.0024	15867.4530	-0.0048

Table 10.6 - Measured frequencies (MHz) for the transitions observed for both vibrational state 0^+ and 0^- of the isotopologue species $H^{18}OH$ of penta-FPY-W1 conformation.

J'	Ka'	Kc'	F'	J''	Ka''	Kc''	F''	ν_{OBS}/MHz 0^+	$\Delta\nu_{OBS-CALC}/MHz$ 0^+	ν_{OBS}/MHz 0^-	$\Delta\nu_{OBS-CALC}/MHz$ 0^-
4	4	0	5	3	3	0	4	7570.6428	-0.0021	7568.9943	-0.0023
			4				3	7570.4012	0.0023	7568.7512	0.0014
			3				2	7570.6682	0.0049	7569.0195	0.0040
4	4	1	5	3	3	1	4	7593.3450	0.0012	7591.9771	-0.0004
			4				3	7593.2405	0.0037	7591.8701	-0.0007
			3				2	7593.3072	-0.0021	7591.9423	-0.0008
5	1	4	6	4	0	4	5	8693.4020	-0.0039	8696.2166	-0.0024
			5				4	8694.2176	-0.0027	8697.0302	-0.0003
			4				3	8693.2104	0.0037	8696.0233	0.0030
5	2	4	6	4	1	4	5	8738.9594	-0.0003	8740.9470	-0.0011
			5				4	8739.6302	-0.0019	8741.6199	0.0002
			4				3	8738.7810	-0.0066	8740.7731	-0.0030
5	2	3	6	4	1	3	5	8492.3842	0.0024	8496.0969	0.0038
			5				4	8492.9909	0.0024	8496.7018	0.0009
			4				3	8492.2920	0.0014	8495.9984	-0.0030
5	3	2	6	4	2	2	5	8502.6930	0.0020	8503.8205	-0.0021
			5				4	8502.6008	-0.0010	8503.7365	-0.0004
			4				3	8502.7846	0.0032	8503.9122	0.0000
5	3	3	6	4	2	3	5	8801.7701	-0.0014	8802.7854	0.0005
			5				4	8802.0188	0.0003	8803.0327	0.0000
			4				3	8801.7263	-0.0001	8802.7390	-0.0006
5	4	2	6	4	3	2	5	9084.0648	0.0097	9083.3490	0.0022
			5				4	9083.9592	-0.0033	9083.2554	0.0001
			4				3	9084.0736	-0.0041	9083.3722	0.0027
5	4	1	6	4	3	1	0	8969.9994	-0.0027	8968.2815	0.0059
			5				4	8969.5684	0.0042	8967.8348	-0.0026
			4				3	8970.1199	-0.0059	8968.3984	-0.0010
5	5	0	6	4	4	0	5	9538.6337	0.0007	9536.6071	0.0007
			5				4	9538.4939	-0.0026	9536.4679	-0.0015
			4				3	9538.6172	-0.0045	9536.5890	-0.0063
5	5	1	6	4	4	1	5	9545.3482	-0.0016	9543.4460	-0.0015
			5				4	9545.2434	-0.0054	9543.3431	-0.0033
			4				3	9545.3380	0.0089	9543.4333	0.0065
6	2	5	7	5	1	5	6	10481.7577	-0.0028	10484.3373	-0.0009
			6				5	10482.3894	-0.0024	10484.9691	0.0006
			5				4	10481.6305	0.0026	10484.2055	-0.0003
6	2	4	7	5	1	4	6	10311.0029	0.0022	10315.6134	0.0024
			6				5	x	x	10316.2594	0.0013
			5				4	10310.8972	-0.0004	10315.5057	-0.0025
6	3	3	7	5	2	3	6	10120.9959	0.0002	10124.3673	-0.0007
			5				4				
			6				5	10121.2233	0.0009	10124.5991	0.0006

Chapter 10 - PENTAFLUOROPYRIDINE...WATER

J'	Ka'	Kc'	F'	J''	Ka''	Kc''	F''	$\nu_{\text{OBS}}/\text{MHz}$ 0^+	$\Delta\nu_{\text{OBS-CALC}}/\text{MHz}$ 0^+	$\nu_{\text{OBS}}/\text{MHz}$ 0^-	$\Delta\nu_{\text{OBS-CALC}}/\text{MHz}$ 0^-
6	6	1	7	5	5	1	6	11502.6779	-0.0013	11500.2835	0.0002
			6				5	11502.5955	-0.0028	11500.1994	-0.0029
			5				4	11502.6649	0.0025	11500.2690	0.0025
6	6	0	7	5	5	0	6	11500.9258	-0.0024	11498.4906	0.0009
			6				5	11500.8405	0.0011	11498.4054	0.0048
			5				4	11500.9169	0.0038	11498.4704	-0.0041
7	3	5	8	6	2	5	7	12192.4615	0.0006	12195.5333	-0.0013
			7				6	12192.8806	0.0080	12195.9459	0.0000
			6				5	12192.4004	0.0018	12195.4768	0.0044
7	3	4	8	6	2	4	7	11875.6905	-0.0001	11881.4529	-0.0012
			7				6	11876.1516	-0.0031	11881.9192	-0.0005
			6				5	11875.6419	-0.0025	11881.4091	0.0015
7	4	4	8	6	3	4	7	12239.2703	0.0039	12241.0186	0.0036
			6				5	12239.2501	-0.0025	12241.1743	-0.0012
			7				6	12239.4210	-0.0048	12240.9953	-0.0057

Table 10.7 - Measured frequencies (MHz) for the transitions observed for the DOH monodeuterated isotopologue species of penta-FPY-W1 conformation.

J'	Ka'	Kc'	F'_N	F'_D	J''	Ka''	Kc''	F''_N	F''_D	$\nu_{\text{OBS}}/\text{MHz}$	$\Delta\nu_{\text{OBS-CALC}}/\text{MHz}$
4	4	0	4	5	3	3	0	3	4	7607.9065	-0.0011
			4	3				3	2		
			4	4				3	3		
			5	6				4	5		
			5	4				4	3		
			5	5				4	4		
			3	4				2	3		
4	4	1	3	2	3	3	1	2	2	7631.1357	0.0015
			4	5				3	4		
			4	3				3	2		
			4	4				3	3		
			3	4				2	3		
			3	2				2	1		
			3	3				2	2		
5	2	3	4	3	4	1	3	3	2	8527.5362	-0.0038
			4	5				3	4		
			4	4				3	3		
			6	7				5	6		
			6	6				5	5		
			5	4				4	3		
			5	6				4	5		
5	3	2	5	4	4	2	2	4	3	8537.3987	-0.0054
			5	6				4	5		
			5	5				4	4		
			6	5				5	4		
			6	7				5	6		
			6	6				5	5		
			4	3				3	2		
5	1	4	4	5	4	0	4	3	4	8730.9337	-0.0009
			4	4				3	3		
			6	5				5	4		
			6	7				5	6		
5	1	4	4	5	4	0	4	3	4	8730.9879	-0.0011
			6	5				5	4		
			6	7				5	6		
			6	6				5	5		

Chapter 10 - PENTAFLUOROPYRIDINE•••WATER

<i>J'</i>	<i>Ka'</i>	<i>Kc'</i>	<i>F'_N</i>	<i>F'_D</i>	<i>J''</i>	<i>Ka''</i>	<i>Kc''</i>	<i>F''_N</i>	<i>F''_D</i>	<i>v</i> _{OBS} /MHz	Δv _{OBS-CALC} /MHz
			5	4				4	3	8731.9406	0.0015
			5	6				4	5	8731.9592	0.0055
			5	5				4	4	8732.0079	-0.0002
5	2	4	4	3	4	1	4	3	2	8776.9067	-0.0075
			5	5				3	4	8776.9329	0.0039
			4	5				3	4	8777.0840	-0.0094
			6	5				5	4	8777.1053	0.0006
			6	7				5	6	8777.1593	-0.0021
			6	6				5	5	8777.7640	-0.0063
			5	4				4	3	8777.7841	0.0001
			5	6				4	5	8777.8269	-0.0016
			5	5				4	4	8777.8539	0.0025
			4	5				4	4		
			6	5				4	4		
5	3	3	4	3	4	2	3	3	2	8840.4963	0.0067
			4	5				3	4		
			6	5				5	4	8840.5364	0.0015
			6	7				5	6		
			6	6				5	5	8840.5642	-0.0037
			5	4				4	3	8840.7791	-0.0005
			5	6				4	5	8840.7903	0.0041
			5	5				4	4	8840.8152	0.0021
6	3	3	7	6	5	2	3	6	5		
			7	8				6	7	10162.1288	-0.0001
			5	4				4	3		
			5	6				4	5		
			7	7				6	6	10162.1490	0.0020
			5	5				4	4		
			6	5				5	4	10162.3610	0.0034
			6	7				5	6		
			6	6				5	5	10162.3833	0.0077
6	2	4	5	6	5	1	4	4	5	10354.8558	0.0041
			5	5				4	4	10354.8945	0.0042
			7	6				6	5	10354.9460	-0.0012
			7	8				6	7	10354.9579	0.0042
			7	7				6	6	10354.9908	-0.0035
			6	5				5	4	10355.6013	-0.0024
			6	7				5	6		
			6	6				5	5	10355.6439	-0.0010
6	3	4	5	4	5	2	4	4	3	10519.3898	-0.0005
			5	6				4	5		
			5	6				5	5	10519.4151	0.0047
			7	6				6	5	10519.4422	-0.0050
			7	8				6	7		
			7	6				4	5	10519.4555	-0.0014

Chapter 10 - PENTAFLUOROPYRIDINE•••WATER

J'	Ka'	Kc'	F'_N	F'_D	J''	Ka''	Kc''	F''_N	F''_D	ν_{OBS}/MHz	$\Delta\nu_{OBS-CALC}/MHz$
			7	6				5	5	10519.4814	-0.0013
			7	7				6	6		
			6	5				5	4	10519.8218	0.0003
			6	7				5	6		
			6	6				6	5	10519.8218	0.0003
			6	6				4	5	10519.8490	-0.0003
			6	6				5	5		
6	2	5	5	4	5	1	5	4	3	10527.3693	-0.0065
			7	6				4	5	10527.3874	0.0015
			5	6				4	5		
			6	5				4	4	10527.3693	0.0046
			5	5				4	4	10527.4368	-0.0051
			7	6				6	5	10527.5104	-0.0012
			5	6				6	5	10527.5311	0.0088
			7	8				6	7		
			6	7				6	6	10527.5104	-0.0014
			7	7				6	6	10527.5765	0.0000
			6	5				5	4	10528.1560	0.0042
			6	7				5	6		
			5	5				5	4	10528.2243	0.0015
			7	7				5	6		
			6	6				5	5	10528.1909	-0.0161

Table 10.8 - Measured frequencies (MHz) for the transitions observed for the HOD monodeuterated isotopologue species of penta-FPY-W1 conformation.

J'	Ka'	Kc'	F'_N	F'_D	J''	Ka''	Kc''	F''_N	F''_D	$\nu_{\text{OBS}}/\text{MHz}$	$\Delta\nu_{\text{OBS-CALC}}/\text{MHz}$		
4	4	0	4	3	3	3	0	3	2	7637.5053	-0.0024		
			4	5				3	4				
			4	4				3	3			7637.5252	0.0002
			3	2				2	2			7637.7552	0.0015
			5	4				4	3			7637.7770	0.0064
5	6	4	5										
4	4	1	4	5	3	3	1	3	4	7663.6841	-0.0104		
			5	6				4	5	7663.7981	-0.0074		
			5	4				4	3				
5	3	2	5	4	4	2	2	4	3	8595.2136	0.0070		
			5	5				4	4				
			5	6				4	5				
			6	5				5	4			8595.2711	0.0016
			6	7				5	6				
			6	6				5	5				
			4	3				3	2			8595.3538	-0.0010
4	4	3	3										
4	5	3	4										
5	2	3	4	4	4	1	3	3	3	8608.5793	-0.0047		
			4	5				3	4	8608.6144	-0.0056		
			4	3				3	2	8608.6768	-0.0020		
			6	6				5	5	8608.7135	-0.0013		
			6	7				5	6	8609.2901	-0.0074		
			6	5				5	4				
			5	5				4	4	8609.3237	-0.0090		
			5	6				4	5				
5	4	4	3										
5	1	4	4	4	4	0	4	3	3	8804.9960	0.0013		
			4	5				3	4	8805.0406	0.0018		
			4	3				3	2	8805.1906	0.0045		
			6	6				5	5	8805.2347	0.0035		
			6	7				5	6	8805.9708	-0.0027		
			6	5				5	4				
			5	5				4	4	8806.0166	0.0062		
			5	6				4	5	8806.0266	0.0072		
5	4	4	3										
5	2	4	4	4	4	1	4	3	3	8844.2163	0.0057		
			4	5				3	4	8844.2459	-0.0012		
			4	3				3	2	8844.3816	0.0037		
			6	6				5	5				
			6	7				5	6	8844.4190	0.0036		
			6	5				5	4				

Chapter 10 - PENTAFLUOROPYRIDINE•••WATER

J'	Ka'	Kc'	F'_N	F'_D	J''	Ka''	Kc''	F''_N	F''_D	ν_{OBS}/MHz	$\Delta\nu_{OBS-CALC}/MHz$
			5	5				4	4	8845.0441	0.0049
			5	6				4	5		
			5	4				4	3	8845.0735	0.0003
5	3	3	4	4	4	2	3	3	3		
			4	5				3	4	8899.6550	0.0048
			4	3				3	2		
			6	7				5	6		
			6	5				5	4	8899.7002	0.0003
			5	5				4	4	8899.9302	-0.0053
			5	6				4	5		
			5	4				4	3	8899.9498	0.0011
6	3	3	5	5	5	2	3	4	4		
			7	7				6	6	10249.3733	-0.0043
			6	6				5	5	10249.6348	-0.0033
6	3	4	5	5	5	2	4	4	4		
			5	6				4	5		
			5	4				4	3	10597.8755	-0.0068
			7	7				6	6	10597.9179	-0.0046
			7	8				6	7		
			7	6				6	5	10597.9403	-0.0027
			6	6				5	5	10598.2834	-0.0023
			6	7				5	6		
			6	5				5	4	10598.3004	-0.0051
6	1	5	5	6	5	0	5	4	5		
			5	4				4	3	10598.7845	-0.0001
			7	7				6	6	10598.8886	0.0062
			7	8				6	7		
			7	6				6	5	10598.9325	0.0129
			6	6				5	5	10599.5389	0.0047
			6	7				5	6		
			6	5				5	4	10599.5729	0.0039
6	2	5	5	5	5	1	5	4	4		
			5	6				4	5	10609.7400	-0.0022
			5	4				4	3	10609.7778	0.0010
			7	7				6	6	10609.8795	0.0085
			7	8				6	7		
			7	6				6	5	10609.9029	-0.0032

Chapter 11

BENZYLAMINE ... WATER**11.1 Introduction**

Hydrogen-bonded complexes have been deeply studied in recent years because they may serve to understand processes in liquids, conformational structures of biomolecules, and other topics. They also may be used as simple model systems for studying intermolecular interactions and large amplitude motions because quantum chemical calculations of these kind of complexes are still difficult.^[1] In particular recent studies have been reported on the properties of complex formed by water with organic molecules in gas phase supersonic expansion, to get extensive information about hydrogen bonds (see *e. g.* refs. 2, 3 and 4).

As it is well known, the selectivity and role of molecules and bioactive molecules are determined by the shape achieved through covalent interaction and non bonding interactions occurring within molecules, and from the different types of environments. As a result the conformational preferences are a delicate balancing between intra and intermolecular interactions. An understanding of this balance is particularly important for flexible systems. In fact the behaviour of flexible molecules to change their structural arrangements as isolated systems in order to form an optimal interactions with binding partners is nowadays a confirmed expectation.^[5] Therefore the determination of the structural arrangements of compounds in a microsolvation environment by gas-phase spectroscopic studies is particularly relevant to explore the forces that drive to the conformational minimum and describe the adduct' properties in the presence of solvent molecules. The rotational spectrum of benzylamine...water complex (BA-w) is here analyzed in order to determine the stable conformations of this adduct and evaluate the structural changes that the BA molecule exhibits in a complexation state.

The conformational properties of the isolated BA molecule and its derivatives, which form an important class of organic compounds, have long been debated in the literature (see *e. g.* refs. 6 and 7). In particular, a free-jet absorption millimeter-wave study^[8] has characterized the complete conformational surface of BA by means of density functional calculations coupled to rotational spectroscopy. In this work two stable conformers were identified: in the global minimum conformation the amino group is almost perpendicular to the aromatic plane and the aminic

hydrogen atoms are both pointing symmetrically towards the π cloud forming a weak N-H••• π interaction. In the second conformer, the dihedral angle between the amino side chain and the aromatic ring is 42° with the nitrogen electron lone pair pointing towards the hydrogen atom in the *ortho* position. In this latter conformation the effects of a tunneling motion due to the aminic group that connects two of the four equivalent forms, through the lowest potential energy path, was observed in the rotational spectrum. The two equivalent forms can interchange through a low-energy planar transition state with an estimated barrier $B_2 \approx 4.9 \text{ kJ}\cdot\text{mol}^{-1}$. The conformational landscape of BA will be mentioned again in a further section, as a starting point to evaluate the possible conformational minima relevant for the BA-w complex.

Concerning studies on water complexes with partner-compounds similar to BA, with which we can make interesting comparisons to evaluate the exhibited kind of interactions in the presence of a water molecule and the different conformational changes of each partner, we can cite 2-phenylethylamine (PEA) and aniline 1:1 water complexes which have been already analyzed both with rotational spectroscopy^[9,10] and other techniques.^[11,12] These molecules differ from BA with respect to the length of the amino side chain: in particular PEA presents one more carbon in the side chain compared to BA, while in aniline the amino group is directly linked to the aromatic ring, without any alkyl chain between them.

Concerning the PEA•••water complex, Dickinson *et al.* (see ref. 11) used laser induced fluorescence and mass-selected resonant two-photon ionization of the $S_1 \leftarrow S_0$ electronic transition to detect clusters of different stoichiometry. Within a given stoichiometry, the identification of different conformations relies on band contour analysis and calculated energy differences and the authors affirm that the most stable conformers are those in which the methylene chain is folded into a *gauche* structure and the terminal amino hydrogen atoms are oriented toward the aromatic ring, to form weakly hydrogen-bonded structures with binding energies of $\sim 5.5 \text{ kJ}\cdot\text{mol}^{-1}$.

A univocal determination of the water complex's structure is then obtained by rotational spectroscopy by Melandri *et al.* (see ref. 9). In this work the lowest energy conformation is confirmed to be the one with the same interactions already mentioned above where the monomer acts as a base towards water moiety. More precisely, when the water molecule approaches PEA, its hydrogen atom is directed towards the lone pair of the nitrogen atom without disrupting the original conformation of the monomer. In this adduct the complexation with a molecule of water seems not to affect much the structure of the molecule and the main structural parameters of the flexible amino side chain remain basically unaltered.

Regarding the aniline•••water complex, it has been shown by microwave spectroscopy^[10] that, in the ground state, aniline acts as a base with water placed in its symmetry plane above the

aromatic ring connected to the amino group *via* hydrogen bonding. The aniline subunit presents the hydrogen atoms of the amino group on the opposite side of the aromatic ring respect to the binding site of the water moiety. Furthermore, Piani *et al.* (see ref. 12) analyzed the aniline...water cluster by resonance-enhanced multi-photon ionization spectroscopy (REMPI), of the $S_1 \leftarrow S_0$ electronic transition in order to describe the system both in the ground and in the electronic excited state. The structural preferences of water in binding aniline were analyzed and the results shown a weaker interaction in the excited state and a rather large difference in geometry between the ground and the first electronically excited state: a significant elongation of the hydrogen bond upon electronic excitation is evaluated upon analysis with quantum chemical calculation. The authors conclude that the water molecule is only slightly bonded to the aniline molecule in S_1 state. In both these cases the amino group acts as a proton acceptor and the water acts as a proton donor.

The situation is slightly different in other complexes where the water molecule interacts with a hydroxyl group: in the benzyl alcohol...water complex the most stable conformation was evaluated by Mons *et al.*^[13] to be the one where the water binds as a proton acceptor the alcohol group and acts as a weak proton donor to the π -system of the aromatic ring.

In the present work the BA-w millimeter-wave spectrum was recorded and the most stable structural arrangement of the adduct was assigned, as described below.

11.2 Theoretical calculations

As already stated, the conformational surface of BA was studied by rotational spectroscopy,^[8] with which the two most stable conformations were observed. Conformer **I** presents the amino group located about 40° from the aromatic plane with the nitrogen electron lone pair pointing towards the hydrogen atom in the *ortho* position, conformer **II** has the amino group perpendicular to the aromatic plane with the aminic hydrogen atoms pointing towards the π cloud. The undetected conformer **III**, predicted to be higher in energy by about $2.6 \text{ kJ}\cdot\text{mol}^{-1}$, presented a planar framework of the heavy atoms with the aminic hydrogen atoms directed towards the aromatic ring above and below this plane. To be consistent with the monomer's classification, the same numbering is used to describe the structures of the complex BA-w, based on the three minima of BA.

The calculations were performed using both B3LYP and MP2 methods with 6-311++G** basis set, in order to compare the experimental results with two different computational methods. The calculation of the vibrational frequencies in the harmonic approximation for all the optimized structures allowed to check that the stationary points were actual minima. All calculations were performed with the Gaussian03-B.01 program package.^[14]

All the conformations described below are the only minima obtained, other structures of the adduct were optimized but then it was found that were not real minimum or they fell in some other more stable conformations already optimized.

The structure and the relative energy values (ΔE_0) obtained with both methods are shown in Figure 11.1 while all the spectroscopic parameters (rotational constants, centrifugal distortion constants, quadrupole coupling constants, dipole moment components) are listed in Table 11.1.

In particular regarding conformer **I** of BA monomer, three possible arrangements can be achieved for the water adduct :

- BA **I**-w N...HO: where one hydrogen of the water moiety forms a hydrogen bond with the electron lone pair of the nitrogen atom and the other hydrogen atom of water is staggered with respect to the aminic hydrogen atoms;
- BA **I**-w (60°) N...HO: this conformation is similar to the first one, where the water unit acts as a hydrogen donor towards the nitrogen electron lone pair, but in this case the hydrogen of water not involved in the intermolecular interaction is about 60° shifted from the first conformation and it is eclipsed with respect to the hydrogen of the amino group that lies on the other side of the aromatic ring;
- BA **I**-w O...HN: in this conformational minimum the water acts as a proton acceptor and the amino group as a proton donor forming an O...HN intermolecular hydrogen bond with one hydrogen of the water moiety pointing towards the π cloud of the BA ring.

Moving to conformer **II** of BA, the stable conformation obtained for the BA-w complex is the one where the water unit links the BA **II** monomer with a N...HO hydrogen bond, maintaining a perpendicular arrangement.

Concerning conformation **III** of BA, two different structures were found: one is characterized by a N...HO interaction between the water unit and the amino group and a second one where an O...HN hydrogen bond is present in which the amino group acts as a proton donor. The first one, BA **III**-w N...HO, was minimized only with the B3LYP method while the second one, BA **III**-w O...HN, only with the MP2 method.

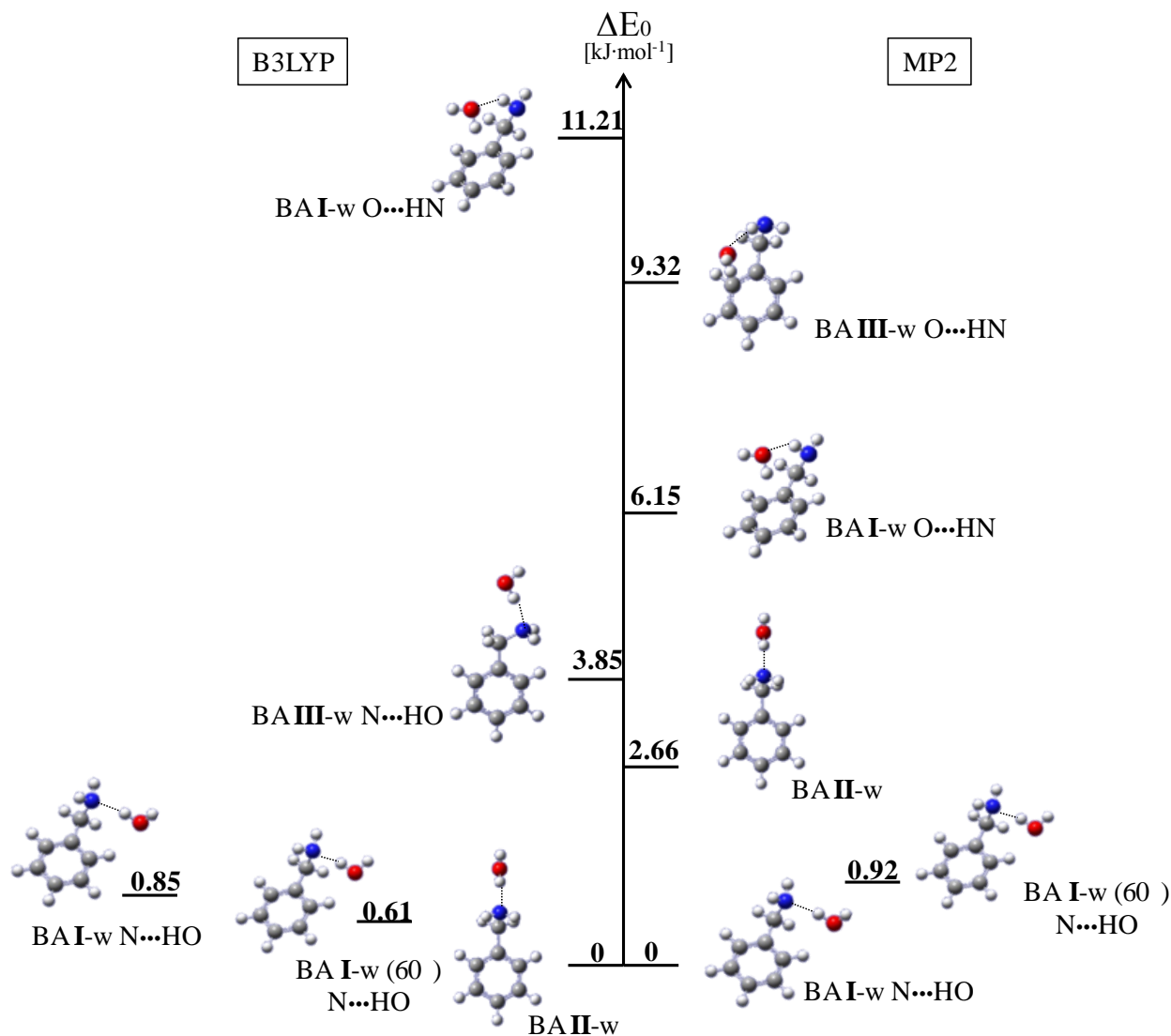


Figure 11.1 - ZPE relative energy values obtained for the different conformations minimized both with B3LYP and MP2 methods at 6-311++G** level of calculations and their shape.

As shown in Figure 11.1, it was possible to optimize five different minima with both methods, but the structures found and also the energy order obtained is quite different.

Regarding the B3LYP method, it can be noted that the global minimum is predicted to be the BA II-w conformer (the same results was obtained for the BA monomer, see ref. 8), but within unit of $\text{kJ}\cdot\text{mol}^{-1}$ other two conformations are predicted: BA I-w (60°) N...HO at $0.61 \text{ kJ}\cdot\text{mol}^{-1}$ and BA I-w N...HO at $0.85 \text{ kJ}\cdot\text{mol}^{-1}$. Then at $3.85 \text{ kJ}\cdot\text{mol}^{-1}$, as already said above, the BA III-w N...HO is found the only minimum for this arrangement of the monomer by B3LYP. The last conformation obtained with this DFT method is the BA I-w O...HN at more than ten $\text{kJ}\cdot\text{mol}^{-1}$.

For what concerns the MP2 method, the global minimum is predicted to be the BA I-w N...HO conformer, which is a different result compared to the one obtained with the B3LYP

method. Then less than one $\text{kJ}\cdot\text{mol}^{-1}$, the BA **I**-w (60°) $\text{N}\cdots\text{HO}$ lies at $0.92 \text{ kJ}\cdot\text{mol}^{-1}$. With the MP2 method the following conformations in order of energy are: BA **II**-w ($2.66 \text{ kJ}\cdot\text{mol}^{-1}$), BA **I**-w $\text{O}\cdots\text{HN}$ ($6.15 \text{ kJ}\cdot\text{mol}^{-1}$) and BA **III**-w $\text{O}\cdots\text{HN}$ ($9.32 \text{ kJ}\cdot\text{mol}^{-1}$), the latter being the only arrangement optimized for the BA **III** structure by MP2 method.

From these results it can be noted that the conformational landscape of BA-w adduct is quite complex and it is not described univocally by different theoretical methods: first the global minima are predicted to be different and then, in general the calculated energies of all the possible conformations present quite different results with the B3LYP and the MP2 methods. Looking at these results, the B3LYP method seems to concentrate different structures at low energy values while the MP2 method distributes the conformations in a wider range of energies.

As a general conclusions we can state that these results point out that when weak intramolecular interactions are the stabilizing driving forces for a monomer, the interaction with other molecules could alter its conformational preferences, which are influenced by the new intermolecular interactions.

Table 11.1 - Calculated spectroscopic parameters and relative energies of BA-w.

6-311++G**	BA I-w N...HO		BA I-w (60°) N...HO		BA I-w O...HN		BA II-w		BA III-w N...HO	BA III-w O...HN
	B3LYP	MP2	B3LYP	MP2	B3LYP	MP2	B3LYP	MP2	B3LYP	MP2
<i>A</i> /MHz	2579	2614	2533	2507	2102	2126	4520	4387	4543	2063
<i>B</i> /MHz	971	991	988	1019	1087	1140	624	648	631	1179
<i>C</i> /MHz	741	759	746	768	957	1037	574	596	558	1013
<i>D_J</i> / kHz	0.261	0.221	0.275	0.335	0.556	0.420	0.102	0.125	0.117	0.403
<i>D_{JK}</i> / kHz	-0.483	-0.357	-0.191	-0.643	2.112	2.018	2.60	3.25	-1.265	2.782
<i>D_K</i> / kHz	3.753	3.46	3.461	3.882	-0.138	-0.373	-0.150	0.193	9.65	-1.025
<i>d₁</i> / kHz	-0.071	-0.057	-0.066	-0.075	-0.012	-0.064	-0.005	-0.005	-0.021	0.007
<i>d₂</i> / kHz	-0.008	-0.006	-0.009	-0.010	-0.022	0.032	-0.0007	0.002	-0.001	-0.022
<i>μ_a</i> /D	0.44	0.06	0.52	0.57	-0.93	-1.09	2.75	-2.44	-2.17	2.99
<i>μ_b</i> /D	-2.45	-2.40	3.18	-3.1	-0.25	-0.10	-0.01	0.00	2.41	0.51
<i>μ_c</i> /D	1.78	1.66	-0.44	-0.44	-1.83	-1.88	2.39	2.36	0.00	-1.26
<i>μ_{TOT}</i> /D	3.06	2.92	3.25	3.18	2.07	2.18	3.64	3.39	3.24	3.29
<i>χ_{aa'}</i> /MHz	1.64	1.29	1.51	1.28	2.20	2.05	-4.37	-4.26	-4.16	-3.41
<i>χ_{bb'}</i> /MHz	-4.12	-3.69	-3.91	-3.65	1.98	1.89	1.95	1.76	2.07	1.61
<i>χ_{cc'}</i> /MHz	2.49	2.40	2.40	2.36	-4.18	-3.94	2.41	2.51	2.08	1.80
<i>ΔE₀</i> /kJ•mol ⁻¹	0.85	0 ^a	0.61	0.92	11.21	6.15	0 ^b	2.66	3.85	9.32

^a Absolute zero point corrected energy: -402.124429 Hartrees.

^b Absolute zero point corrected energy: -403.303193 Hartrees.

11.3 Experimental Results and Analysis

The millimeter-wave (59.6-74.4 GHz) spectrum of BA-w was recorded using the Free-Jet Absorption MilliMeter Wave spectrometer (FJAMMW - VDI setup), of which the basic design has been described previously (see Chapter 3).

BA was purchased from Sigma Aldrich and used without further purification. The complex between BA and water was formed passing a stream of argon saturated with water at room temperature and at a pressure of about 2 bar over a sample of BA heated to about 60 °C at 500 mbar. The gas mixture was then expanded to about 0.005 mbar through a continuous nozzle with diameter of 0.35mm kept at 5 °C above the sample's temperature. Argon was used as the carrier gas for the first searches and the measurements. Some scans were also performed using helium as carrier gas in order to find new transition belonging to other conformations that could have relaxed in the argon jet.

Based on the rotational constants and dipole moments components reported in Table 11.1, a prediction of the rotational spectrum of most stable conformations of BA-w was done and the investigation on rotational transitions was carried on in the frequency range of the spectrometer. The search was very difficult because of the very low intensity of the signal, after the first fast scans some weak lines were detected in the rotational spectrum. To increase the number of transitions and improve the measurements, it was necessary to accumulate many scans of large ranges of frequency in order to increase the signal to noise ratio. After this research, the lines recorded were assigned to a set of coalesced (due to near prolate degeneracy) μ_b and μ_c R-type transitions with high K_a values (from 9 to 14). Only for the $K_a=8$ was possible to distinguish between μ_b and μ_c components line. These results are in agreement with the predicted rotational spectra where the μ_b and μ_c type transitions are the most intense than the μ_a transitions which become weak for the high rotational quantum numbers involved.

As already said, the lines observed for BA-w complex were very weak, the signal to noise ratio (S/N) obtained in the first search with a fast scan was low enough only to detect the most intense lines of the spectra. In Figure 11.2 one of them, namely the $13_{12}-12_{11}$ transition is depicted, recorded in the fast scan (above) and after four steps of accumulation (below). It can be noted that the S/N increase of about three times and it is sufficient to be able to measure precisely the frequency of this transition. No hyperfine quadrupole splitting of the rotational lines was observed because the most intense lines of the frequency range scanned present a not resolvable splitting and the rotational transitions for which the hyperfine splitting was predicted to be observable at the resolution of our spectrometer, were too weak to be measurable.

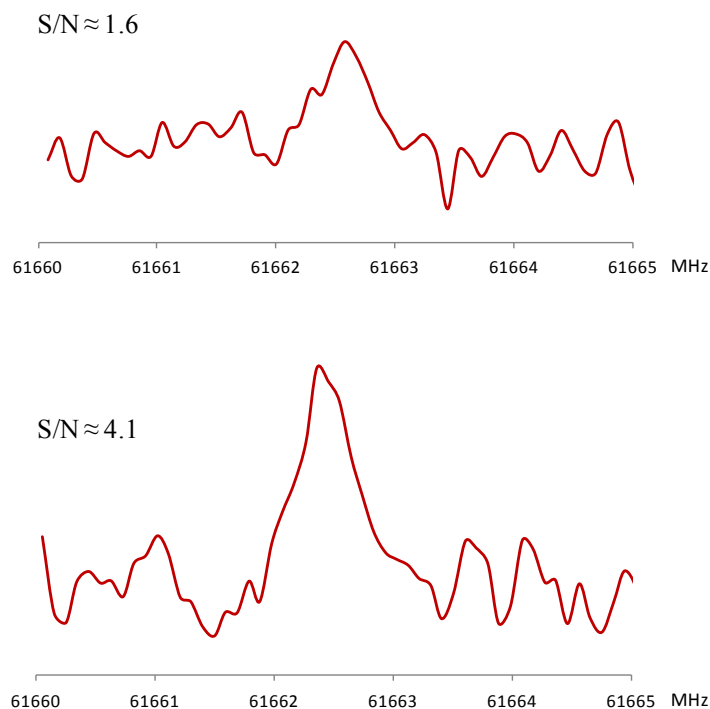


Figure 11.2 - The 13_{12} - 12_{11} coalesced μ_b and μ_c type transition observed for BA I-w N••HO conformation. Above the line in the fast scan mode, with a signal to noise ratio (S/N) of about 1.6 useful for detecting only the most intense transitions. Below the same line after accumulating 4 scans, reaching a S/N of about 4.1, enough to measure precisely the frequency of the transition.

All the rotational constants and centrifugal distortion constants were fitted using Watson's semirigid Hamiltonian in the "S" reduction and F' representation,^[15] and the results are shown in Table 11.2.

Comparing the experimental and calculated rotational constants and considering also the fact that only μ_b and μ_c rotational transitions were observed, it can reliably be concluded that the detected conformer is the BA I-w N••HO one. All the measured transitions are listed in Table 11.3. Extensive searches (also using helium as carrier gas in order to prevent relaxation) have been performed trying to identify other conformers of BA-w. Some lines remain unassigned in the spectrum but an assignment was not possible.

Table 11.2 - Experimental spectroscopic constants of the observed BA I-w N...HO conformer.

BA I-w N...HO	
A/MHz	2569.283(5) ^a
B/MHz	978.66(1)
C/MHz	749.26(1)
D_J/kHz	0.391(5)
D_{JK}/kHz	-1.16(2)
D_K/kHz	6.47(2)
d_2/kHz	0.020(6)
N^b	41
σ^c/MHz	0.04

^a Error in parentheses in units of the last digit.

^b Number of lines in the fit.

^c Root-mean-square deviation of the fit.

Looking at Table 11.1 and 11.2 it can be noted that, even if the MP2 method correctly predicted that the observed conformer (BA I-w N...HO) is the global minimum, the B3LYP method calculated a closer geometry for this conformer as the values of the rotational constants are closer to the experimental ones. In this geometry, the intermolecular N...HO hydrogen bond is calculated to be 1.922 Å and even if it is a predicted value, is quite similar to the one estimated for the effective structure in the PEA-w study ($r_0=1.955(6)$ Å).

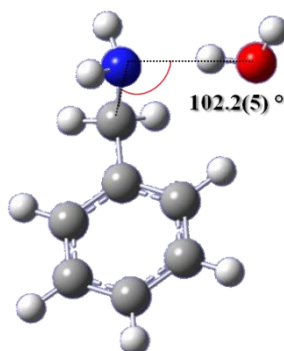


Figure 11.3 - The structure of the observed BA I-w N...HO conformer is shown. Using its experimental rotational constants the angle between the oxygen of the water and the N-C of the amino side chain was fitted. The value obtained is 102.2(5)° while the calculated from B3LYP method was 104.032°.

In this case, since only the rotational constants of the parent species were obtained, a fit of some structural parameter was performed with the STRFIT program,^[16] starting from the B3LYP geometry. The structural parameter that is more significant to reproduce the rotational constants within unit of few MHz, is proved to be the angle between the oxygen of the water and the N-C of the amino side chain: the value fitted is $102.2(5)^\circ$ instead of the calculated 104.032° , (see Figure 11.3).

11.4 Conclusions

In this work the rotational spectra of the most stable conformation of the 1:1 adduct of BA and water was observed. If in the BA monomer the jet plume was populated by two (conformers **I** and **II**) energetically almost-equivalent geometries, the complexation with water leads to the stabilization of one of them (BA **I**) through a N...HO intermolecular interaction. The *gauche* conformation for the monomer becomes the favorite arrangement and, even if the presence of other conformations in the jet cannot be excluded, reliably this one can be consider the global minimum. The behavior of water to act as a proton donor toward the amino group is here confirmed for the BA-w complex. The possibility to continue the research in order to find other conformations is still opened because of the not perfect instrumental conditions, in particular the sensitivity, in which this investigation was performed.

11.5 References

- [1] M. Haeckel, W. Stahl, *J. Mol. Spectr.*, 198, 263–277, **1999**.
- [2] W. Caminati, J.-U. Grabow, “Microwave Spectroscopy in Molecular Systems” in “Frontiers of Molecular Spectroscopy”, *J. Laane Ed.*, Elsevier, **2009**.
- [3] K. Müller-Dethlefs, O. Dopfer, T.G. Wright, *Chem. Rev.*, 94, 1845, **1994**.
- [4] B. Brutschy, *Chem. Rev.*, 100, 3891, **2000**.
- [5] W. L. Jorgensen, *Science*, 254, 954-955, **1991**.
- [6] S. Li, E. R. Bernstein, J. I. Seeman, *J. Phys. Chem.*, 96, 8808-8813, **1992**.
- [7] S. M. Melikova, A. Koll, A. Karpfen, P. Wolschann, *J. Mol. Struct.*, 523, 223-239, **2000**.
- [8] S. Melandri, A. Maris, P. G. Favero, W. Caminati, *ChemPhysChem.*, 3, 172-177, **2001**.
- [9] S. Melandri, A. Maris, B. M. Giuliano, L. B. Favero, W. Caminati, *Phys. Chem. Chem. Phys.*, 12, 10210-10214, **2010**.
- [10] U. Spoerel, W. Stahl, *J. Mol. Spectr.*, 190, 278-289, **1998**.
- [11] J. A. Dickinson, M. R. Hockridge, R. T. Kroemer, E. G. Robertson, J. P. Simons, J. McCombie, M. Walker, *J. Am. Chem. Soc.*, 120, 2622-2632, **1998**.
- [12] G. Piani, M. Pasquini, I. López-Tocón, G. Pietraperzia, M. Becucci, E. Castellucci, *Chem. Phys.*, 330, 138-145, **2006**.
- [13] M. Mons, E. G. Robertson, J. P. Simons, *J. Phys. Chem. A*, 104, 1430-1437, **2000**.
- [14] M. J. T. Frisch, G. W.; Schlegel, H. B.; Scuseria, G. E.; Robb, M. A.; Cheeseman, J. R.; Montgomery, Jr., J. A.; Vreven, T.; Kudin, K. N.; Burant, J. C.; Millam, J. M.; Iyengar, S. S.; Tomasi, J.; Barone, V.; Mennucci, B.; Cossi, M.; Scalmani, G.; Rega, N.; Petersson, G. A.; Nakatsuji, H.; Hada, M.; Ehara, M.; Toyota, K.; Fukuda, R.; Hasegawa, J.; Ishida, M.; Nakajima, T.; Honda, Y.; Kitao, O.; Nakai, H.; Klene, M.; Li, X.; Knox, J. E.; Hratchian, H. P.; Cross, J. B.; Adamo, C.; Jaramillo, J.; Gomperts, R.; Stratmann, R. E.; Yazyev, O.; Austin, A. J.; Cammi, R.; Pomelli, C.; Ochterski, J. W.; Ayala, P. Y.; Morokuma, K.; Voth, G. A.; Salvador, P.; Dannenberg, J. J.; Zakrzewski, V. G.; Dapprich, S.; Daniels, A. D.; Strain, M. C.; Farkas, O.; Malick, D. K.; Rabuck, A. D.; Raghavachari, K.; Foresman, J. B.; Ortiz, J. V.; Cui, Q.; Baboul, A. G.; Clifford, S.; Cioslowski, J.; Stefanov, B. B.; Liu, G.; Liashenko, A.; Piskorz, P.; Komaromi, I.; Martin, R. L.; Fox, D. J.; Keith, T.; Al-Laham, M. A.; Peng, C. Y.; Nanayakkara, A.; Challacombe, M.; Gill, P. M. W.; Johnson, B.; Chen, W.; Wong, M. W.; Gonzalez, C.; Pople, J. A. , Gaussian 03 (Revision B.01) ed., Gaussian, Inc., Pittsburgh PA, **2003**.
- [15] J. K. G. Watson, “Vibrational spectra and structure”, Vol. 6, Elsevier, Amsterdam, Oxford & New York, **1977**.
- [16] Kisiel, Z. PROSPE - Programs for Rotational SPECTroscopy
<http://www.ifpan.edu.pl/~kisiel/prospe.htm>

11.6 Appendix

Table 11.4 - Measured frequencies in MHz for the transitions observed for conformer BA I-w N...HO of BA-w.

J'	Ka'	Kc'	J''	Ka''	Kc''	$\nu_{\text{OBS}}/\text{MHz}$	$\Delta\nu_{\text{OBS-CALC}}/\text{MHz}$
14	14		13	13 ^a		70182.45	0.00
15	14		14	13		71918.32	-0.06
14	13		13	12		66791.33	0.05
15	13		14	12		68526.84	0.04
16	13		15	12		70261.81	0.06
12	12		11	11		59926.70	0.00
13	12		12	11		61662.47	-0.01
14	12		13	11		63397.82	-0.05
16	12		15	11		66866.41	0.00
17	12		16	11		68598.98	0.01
18	12		17	11		70329.90	-0.02
19	12		18	11		72058.83	-0.03
14	11		13	10		60001.75	-0.06
15	11		14	10		61735.18	0.03
16	11		15	10		63466.94	-0.02
18	11		17	10		66924.26	0.08
20	11		19	10		70369.22	-0.02
21	11		20	10		72085.63	-0.02
16	10		15	9		60061.34	0.08

J'	Ka'	Kc'	J''	Ka''	Kc''	$\nu_{\text{OBS}}/\text{MHz}$	$\Delta\nu_{\text{OBS-CALC}}/\text{MHz}$
17	10		16	9		61786.38	-0.04
18	10		17	9		63507.69	-0.02
20	10		19	9		66935.28	-0.03
22	10	13	21	9	12	70335.79	0.05
		12			12		
		12			13	70336.69	-0.03
		13			13		
23	10	14	22	9	13	72022.69	0.05
		13			14	72024.97	0.04
18	9	10	17	8	9	60071.69	0.05
		9			10	60072.22	-0.01
19	9	11	18	8	10	61774.06	0.05
		10			11	61775.46	-0.07
20	9	11	19	8	12	63470.31	-0.01
		14	21	8	13	66812.09	-0.01
22	9	13	21	8	14	66830.56	0.05
21	8	14	20	7	13	61508.47	0.06
		13			14	61636.39	-0.01
		14			14	61620.05	0.00
		13			13	61524.73	-0.03
22	8	14	21	7	15	63310.61	0.04
		15			15	63276.61	-0.07
		14			14	63097.75	0.02
		15			14	63063.81	-0.03

^aDoubly overlapped transitions due to near prolate degeneracy of the involved levels: only K_a is given.

ACRYLIC ACID ... WATER

12.1 Introduction

The nature of acids in an aqueous environment is fundamental to many aspects of chemistry.^[1] The distinctive behavior of an acid is to transfer a proton to water but this process can be influenced by the solvation environment. Concerning acid monohydrates, the interaction occurs *via* formation of a hydrogen bond with the acid acting as the hydrogen donor and the water oxygen as the acceptor. If an electronegative center is present in the acid, another usually weaker hydrogen bond may be formed between this center, that acts as the hydrogen acceptor and the second hydrogen atom of water. This characteristic ring-like structure formed by two hydrogen bonds in the 1:1 acid...water complexes have been observed in many microwave spectroscopy studies: see for example works on nitric acid,^[2] sulfuric acid,^[3] formic acid,^[4] acetic acid^[5] and benzoic acid^[6] monohydrates complexes.

Acrylic acid ($\text{CH}_2=\text{CH}-\text{COOH}$, 2-propenoic acid), indicated hereafter as AA, is the smallest unsaturated carboxylic acid. Conformational isomerism arises from the presence of the carbon-carbon double bond, forming two different rotamers: *s-cis* and *s-trans*.^[7] The AA monomer traditionally forms the material basis of high-molecular compounds chemistry. Polycarboxylic acids and polymers based on its derivatives are large-tonnage products.^[8] The study of the interactions between AA and water could be interesting in order to evaluate the structural arrangement occurring between these two molecules. In fact, even if the preferred geometries in monohydrates acids seems quite confirmed (see refs. 1-6), to the best of the authors' knowledge the behavior of an unsaturated carboxylic acid in the presence of a water molecule is not yet analyzed. A rotational spectroscopic study of this monohydrated acid complex can give high resolved data that can help to understand geometries, interactions and motions occurring in this system.

Regarding AA, the dimer, which presents the two allyl groups in a *zusammen* orientation, was observed by rotational spectroscopy thanks to the presence of a permanent value of the μ_b dipole moment component.^[9] This dimer showed a tunneling splitting, originating from the concerted proton transfer of the two carboxylic hydrogen atoms and its observation allowed the determination of the ΔE_{01} barrier of 880.6(6) MHz for the proton transfer motion.

Concerning the 1:1 acid-water adducts, splittings of rotational transitions were observed in all the already mentioned papers. This effect was attributed to large amplitude motions between equivalent minima on the potential energy surface although the treatment to understand this motion is quite complicate. The contemplated ways to describe the path of the tunneling motion are not univocal and many times the presence of very small splitting does not allow to obtain enough information to determine barrier heights from the spectroscopic data, (see for example refs. 2 and 10). Regarding the latest work published on the benzoic acid...water complex,^[6] the authors, based also on the previous studies, hypothesize four different motions to describe the tunneling pathway: (i) wagging of the unbound hydrogen atom of water through the mirror plane of the acid moiety; (ii) rotation of water about the lone pair hydrogen-bonded to the benzoic acid; (iii) rotation of water around its C₂ axis and (iv) exchange of the two hydrogen-bonded protons. As it can be noted, the analysis of the motions that characterize the interactions between carboxylic acids and water is quite complicated.

In this work, the complex between AA and water (AA-w) has been studied by means of PJ-FTMW spectroscopy. *Ab initio* calculations were used to predict the geometry and obtain the spectroscopic parameters useful to guide the experimental research. Moreover the rotational spectra of different isotopologues were observed and analyzed in order to obtain more structural information on this adduct: in particular all the isotopologues of water (AA...H₂¹⁸O, CH₂CHCOOH...HOD, CH₂CHCOOH...DOH, CH₂CHCOOH...D₂O) and the deuterated hydroxyl group species of AA were also analyzed (CH₂CHCOOD...H₂O, CH₂CHCOOD...D₂O, CH₂CHCOOD...DOH and CH₂CHCOOD...HOD).

12.2 Theoretical calculations

Before starting the spectral search, theoretical calculations (MP2/aug-cc-pVTZ) were performed to estimate the relative energies of the different stable conformations of the complex and to predict the values of the spectroscopic parameters. Since the AA monomer presents two rotamers *s-cis* and *s-trans*, the complexation with a molecule of water gives rise to two different conformations. The shape of the two minimized conformers is shown in Figure 12.1 and the numerical results are reported in Table 12.1. Both conformers present the typical ring-like structure where the water acts as a proton acceptor towards the hydrogen atom of the hydroxyl group of AA and as a proton donor with a secondary interaction towards the carboxylic oxygen. As known, AA is a planar molecule and in both optimized structures the complex is calculated to be almost planar.

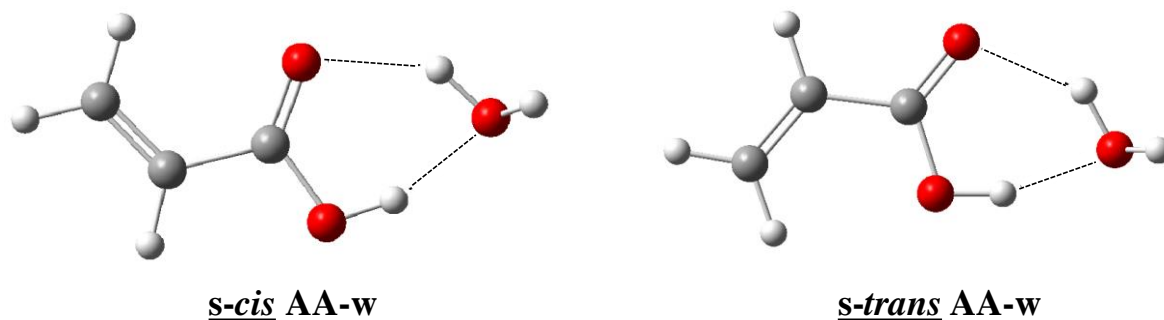


Figure 12.1 - The two most stable conformations of the adduct between acrylic acid and water.

In particular the water's atoms that participate in the intermolecular interaction lie approximately in the same plane of the AA monomer while the "free" hydrogen atom of water is predicted to be out of the *ab* inertial plane of about 0.65\AA in both the *s-cis* and the *s-trans* AA-w conformations. All the other nuclei of the complex do not deviate by more than 0.06\AA from the *ab*-plane, as can be also evaluated looking the small values of the planar moment of inertia P_{cc} reported in Table 12.1. The unbounded hydrogen of water is expected to be involved in an inversion motion between the two equivalent mirror images of the complex.

The ΔE and ΔE_0 reported in Table 12.1, are the energy values with and without zero point correction, and D_e is the dissociation energy value estimated by the calculations. The counterpoise method was also run on the optimized geometries in order to obtain the basis-set superposition error (BSSE) correction,^[11] and the relative $D_{e-B SSE}$ are also reported in the same table. From these relative energy data it can be observed that the two conformers of the complex are quite close in energy and that the energy difference between them is maintained at about the same value as the one obtained for the AA monomer: *s-cis* conformation of AA-W is evaluated to be the most stable one by about $0.74\text{ kJ}\cdot\text{mol}^{-1}$ (AA monomer $0.7(2)\text{ kJ}\cdot\text{mol}^{-1}$ from ref. 7).

The Gaussian 09 program package was used to carry out all the calculations.^[11]

Table 12.1 - Spectroscopic parameters and relative energies of the two conformations for AA-w complex, calculated with MP2/aug-cc-pVTZ.

MP2/aug-cc-pVTZ		
	<i>s-cis</i> AA-w	<i>s-trans</i> AA-w
<i>A</i> /MHz	9380	9014
<i>B</i> /MHz	1738	1771
<i>C</i> /MHz	1470	1485
μ_a /D	0.61	-0.66
μ_b /D	-0.04	-0.48
μ_c /D	1.22	1.22
μ_{TOT} /D	1.36	1.47
<i>D_J</i> /kHz	0.377	0.368
<i>D_{JK}</i> /kHz	-0.394	0.254
<i>D_K</i> /kHz	14.036	14.717
<i>d₁</i> /kHz	-0.070	-0.069
<i>d₂</i> /kHz	-0.006	-0.006
<i>P_{aa}</i> /uÅ ²	290.31	284.84
<i>P_{bb}</i> /uÅ ²	53.37	55.56
<i>P_{cc}</i> /uÅ ²	0.50	0.51
ΔE /kJ•mol ⁻¹	0 ^a	0.74
ΔE_0 /kJ•mol ⁻¹	0 ^b	0.83
ΔE_{BSSSE} /kJ•mol ⁻¹	0 ^c	0.80
$\Delta E_{0-BSSSE}$ /kJ•mol ⁻¹	0 ^d	0.87
<i>D_e</i> /kJ•mol ⁻¹	45.04	45.27
<i>D_{e-BSSSE}</i> /kJ•mol ⁻¹	41.09	41.27

^a Absolute zero point corrected energy: -343.066354 Hartrees.

^b Absolute zero point corrected energy: -342.973686 Hartrees.

^c Absolute zero point corrected energy: -343.064850 Hartrees.

^d Absolute zero point corrected energy: -342.972182 Hartrees.

12.3 Experimental Results and Analysis

The rotational spectrum of AA-w complex in the 6-18.5 GHz frequency region was recorded using the COBRA-type PJ-FTMW spectrometer at the University of Bologna, already described in Chapter 3. Molecular clusters were generated in a supersonic expansion, under conditions optimized for the 1:1 molecular adduct formation.

A commercial sample of AA was supplied by Aldrich and used without further purification. The measurements were carried out using helium as carrier gas at a stagnation pressure of ~0.3 MPa passed over a mixture of AA and water (1:1) and expanded through a solenoid valve (General

Valve, Series 9, nozzle diameter 0.5 mm) into the Fabry–Perot cavity. The spectral line positions were determined after Fourier transformation of the time domain signal with 8k data points, recorded with 100 ns sample intervals. Each rotational transition displays a Doppler splitting, enhanced by the coaxial arrangement of the spectrometer. The rest frequency was calculated as the arithmetic mean of the frequencies of the two Doppler components. The estimated accuracy of the frequency measurements is better than 3 kHz, resolution is better than 7 kHz.

The search for transitions of AA-w began using the rotational constants and dipole moment components from MP2 calculations, shown in Table 12.1. Since the μ_a components are predicted with equal values for both *s-cis* and *s-trans* AA-w conformations, and the μ_b component is notable only in the *s-trans* AA-w conformer, the first search was targeted to μ_b -R-branch transitions for the *s-trans* species in order to assign first this conformer. The first set of rotational transitions observed was the one with $K_a=1$ starting from $J=1$ and going up to $J=4$. Then the measurements continued to μ_a -R-branch transitions ($K_a=0$ and 1 with J from 3 up to 6) and also some μ_b -Q-branch transitions were observed, see Table 12.10 for the list of all the measured transitions.

Regarding the *s-cis* conformer, the search of its rotational spectrum was focused on μ_a -R-branch transitions because the predicted μ_b dipole moment component is almost zero. The first searched transition was the $4_{04}\leftarrow 3_{03}$ that was found to be far from the prediction of about 210 MHz. Then the measurements continued to other J and K_a values: in particular J from 3 up to 6 were measured, with K_a values of 0, 1 and 2. Next, some very weak μ_b -R and Q-branch transitions were measured, see Table 12.10 for the list of all the measured rotational transitions.

The search for μ_c -type transitions was performed, but no lines were observed, although the μ_c dipole moment component is predicted to be above one Debye unit. It can be concluded that all *c*-type transitions were not found due to the splitting related to the large amplitude motion of the unbound hydrogen of the water molecule across the *ab* plane. This observation is consistent with previous studies of other carboxylic acid•••water complexes,^[6,13] and a full-length discussion on the possible tunneling motions of the unbound hydrogen can be found in reference 10.

Representative μ_a and μ_b -R-branch transitions for both conformers are reported in Figure 12.2. As it can be noted, the μ_a rotational transitions are not split while μ_b ones appear split in doublets. The *S*-reduction of Watson's semirigid rotational Hamiltonian in the I' representation^[14] was used to fit the experimental frequencies, giving the spectroscopic constants for both conformers reported in Table 12.2. The observed splitting in the μ_b rotational transitions was fitted separating the rotational constants A in two values: A_{0^+} and A_{0^-} for the 0^+ and 0^- states, respectively.

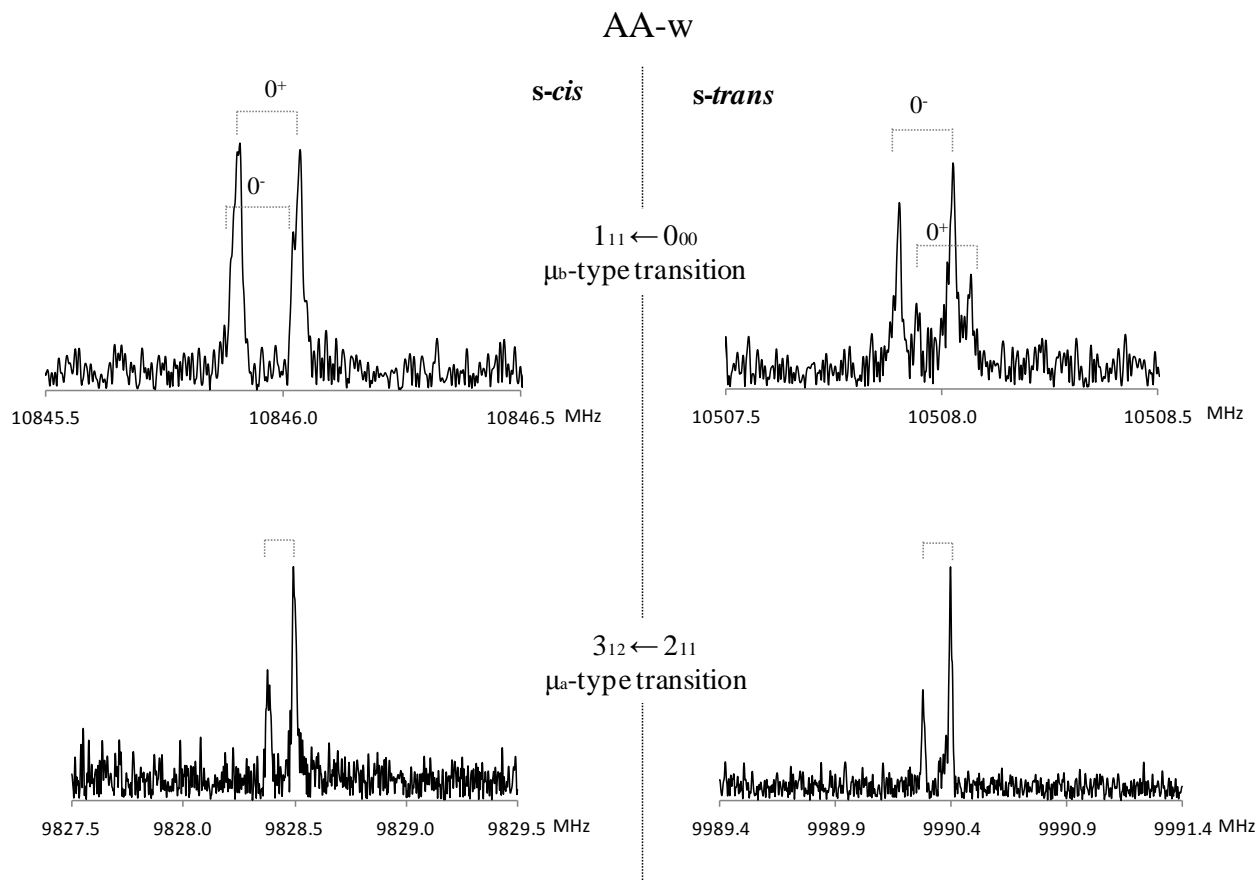


Figure 12.2 - Representative μ_b - and μ_a -type transitions for the *s-cis* and *s-trans* conformation of AA-w adduct. The $1_{11} \leftarrow 0_{00}$ shows the typical tunnelling splitting observed for all the μ_b -type rotational transitions of both conformers. The different size of the splitting for the two conformers is here clearly observable. The Doppler splitting is also observable.

The small splitting observed on the rotational transitions, which is related to the tunneling motion of the water moiety, presents a nuclear spin statistical weight. The statistical weight of a state is determined by the symmetry of the state with respect to the interchange of identical hydrogen atoms. Because the hydrogen nuclei are fermions, the symmetric tunneling wavefunctions can only combine with asymmetric nuclear spin functions, while the asymmetric ones can only combine with the symmetric nuclear spin functions, to make the overall wavefunction asymmetric. For this reason, the two observed states present a nuclear spin statistics $I=3$ and $I=1$ as can be observed looking at the intensities of the μ_b rotational transitions, reported in Figure 12.2. As it can be seen, the overall intensity of the measured lines is very low and the lack of *c*-type transitions and the lower number of *b*-type ones, does not allow to determine the *A* rotational constants with an accuracy similar to that of the *B* and *C* rotational constants. Moreover, the values obtained for the D_K centrifugal distortion constants cannot be determined as no *b*- or *c*-type transitions with $K_a \geq 2$

were recorded (the only *b*-type rotational transition detected for the *s*-cis AA-w rotamer is not enough for its determination).

Table 12.2 - Experimental spectroscopic constants of the *s*-cis and *s*-trans AA-w (H₂O and H₂¹⁸O) molecular complexes.

	<i>s</i> -cis AA...H ₂ O	<i>s</i> -cis AA...H ₂ ¹⁸ O	<i>s</i> -trans AA...H ₂ O	<i>s</i> -trans AA...H ₂ ¹⁸ O
A_0^- /MHz	9400.7045 (24) ^a	9380.8926 (36)	9048.8360 (20)	9014.4048 (26)
A_0^+ /MHz	9400.7250 (24)	9380.9062 (36)	9048.8818 (20)	9014.4457 (26)
B /MHz	1703.2562 (8)	1617.2838 (9)	1734.7897 (9)	1647.2527 (8)
C /MHz	1445.2530 (4)	1382.4819 (6)	1459.1237 (4)	1395.9042 (4)
D_J^b /kHz	0.440 (9)		0.415 (13)	
d_1 /kHz	-0.091 (8)		-0.071 (8)	
σ^c /kHz	4		3	
N^d	23	12	24	14

^a Errors in parentheses are expressed in units of the last digit quoted.

^b The quartic centrifugal distortion constants are set to a common value for the AA...H₂O and AA...H₂¹⁸O complexes.

^c Root-mean-square deviation of the fit.

^d Number of transitions in the fit.

Some evidence regarding the nature of the tunneling motions involving the water moiety was gained by the analysis of the rotational spectra of some isotopic species. In particular all the rotational spectra of the AA-w isotopologues at the water unit were observed substituting D₂O or H¹⁸OH to water and observing the rotational spectrum in the same conditions as for the normal species. Also the spectra related to the species containing the deuterated hydroxyl group of the AA monomer was studied allowing the exchange between the acidic hydrogen and deuterium to occur in a deuterated environment. This was done adding an excess of deuterated water to the monomer and then degassing the water from the AA sample before starting the experiment. The species that were analyzed are named in the tables as follow: AA...H₂O, AA...H₂¹⁸O, CH₂CHCOOH...D₂O, CH₂CHCOOD...H₂O, CH₂CHCOOD...D₂O, CH₂CHCOOH...DOH, CH₂CHCOOH...HOD, CH₂CHCOOD...DOH and CH₂CHCOOD...HOD. All the spectroscopic parameter fitted for these isotopic species are reported in Table 12.2 (AA...H₂O and AA...H₂¹⁸O) and Table 12.3 (the seven deuterated species) and the measured frequencies are listed in Tables 12.10 and 12.11.

Table 12.3 - Experimental rotational constants of seven deuterated forms of the *s-cis* and *s-trans* AA-w molecular complexes. NOTE: the centrifugal distortion constants D_J and d_I were fixed to the values obtained for the normal species (see table 12.2) as they are undetermined from the fit.

		<i>s-cis</i> AA-w	<i>s-trans</i> AA-w
CH ₂ CHCOOH...D ₂ O	A/MHz	9162.46 (96) ^a	8931.08 (82)
	B/MHz	1612.8191 (8)	1635.3482 (8)
	C/MHz	1377.1633 (8)	1388.1750 (8)
	σ^b /kHz	4	1
	N ^c	6	6
CH ₂ CHCOOD...H ₂ O	A/MHz	9259.20 (81)	8894.74 (63)
	B/MHz	1690.9528 (8)	1726.9157 (8)
	C/MHz	1433.0568 (8)	1449.5274 (8)
	σ /kHz	4	2
	N	6	6
CH ₂ CHCOOD...D ₂ O	A/MHz	9018.90 (92)	8779.33 (77)
	B/MHz	1602.7946 (8)	1629.0851 (8)
	C/MHz	1366.5927 (8)	1379.9827 (8)
	σ /kHz	6	2
	N	6	6
CH ₂ CHCOOH...DOH	A/MHz	9238.89 (64)	9010.06 (60)
	B/MHz	1679.2511 (8)	1702.9038 (10)
	C/MHz	1424.3095 (8)	1435.6737 (8)
	σ /kHz	4	3
	N	6	5
CH ₂ CHCOOH...HOD	A/MHz	9317.26 (97)	8977.14 (78)
	B/MHz	1634.0261 (8)	1663.3698 (8)
	C/MHz	1395.8177 (8)	1409.1137 (8)
	σ /kHz	4	5
	N	6	6
CH ₂ CHCOOD...DOH	A/MHz	9094.43 (79)	8852.96 (67)
	B/MHz	1667.7692 (8)	1695.7213 (8)
	C/MHz	1412.6268 (8)	1426.5477 (8)
	σ /kHz	5	3
	N	6	6
CH ₂ CHCOOD...HOD	A/MHz	9175.92 (93)	8826.76 (74)
	B/MHz	1623.3142 (8)	1656.5286 (8)
	C/MHz	1384.8088 (8)	1400.5205 (8)
	σ /kHz	4	3
	N	6	6

^a Errors in parentheses are expressed in units of the last digit quoted.

^b Root mean square of the errors.

^c Number of lines included in the fit.

The nature of the internal motion is verified by observations that in these spectra the splitting is not observed in the deuterated isotopologues while it persists in the spectrum of the AA...H₂¹⁸O species. The reason for this is that the insertion of deuterium atoms in the nuclei involved in the intermolecular interactions breaks the symmetry since the hydrogen atoms are not equivalent anymore. This interpretation is in agreement with the results obtained for all the mixed hydrogen-deuterium species, but it is not consistent with the unsplit lines observed in the CH₂CHCOOD...DOH species and in the complete deuterated isotopomer CH₂CHCOOD...D₂O. In fact, in these cases the symmetry in the system is still present, all the atoms involved in the intermolecular interactions are deuterium atoms. As it is well known, in this case the result can be attributed to the increase of the mass involved in a motions which causes a reduction of the splitting. Since in this system the splitting observed is already very small (see Table 12.4 for a summary of the observed splittings), in these deuterated species it could collapsed in a not detectable value.

Table 12.4 - Summary of the observed splittings (kHz) in the *s-cis* and *s-trans* AA-w (AA...H₂O and AA...H₂¹⁸O) molecular complexes.

	<i>s-cis</i> AA...H ₂ O	<i>s-cis</i> AA...H ₂ ¹⁸ O	<i>s-trans</i> AA...H ₂ O	<i>s-trans</i> AA...H ₂ ¹⁸ O
ΔA / kHz	20(5) ^a	14(7)	46(4)	41(5)
Q-branch μ_b -type				
1 (1, 1) - 0 (0, 0)	22		38	40
2 (1, 2) - 1 (0, 1)	17	13	40	41
3 (1, 3) - 2 (0, 2)			37	40
R-branch μ_b -type				
1 (1, 0) - 1 (0, 1)	15		45	
2 (1, 1) - 2 (0, 2)	17	14	49	
3 (1, 2) - 3 (0, 3)	32		56	43
4 (1, 3) - 4 (0, 4)			55	

^a Errors in parentheses are expressed in units of the last digit quoted.

Moreover, from Table 12.4, it can be pointed out as the splitting of the *s-trans* species is greater than the *s-cis* one. This effect can be due to the different masses involved in the motion that produce distinct energy barrier, but its origin is not described conclusively and no data about difference on splitting values for two rotamers is reported in literature for the same kind of complexes.

Besides the rotational constants, the planar moment of inertia ($P_{cc} = (I_{aa} + I_{bb} - I_{cc})/2$, see Chapter 1 for more details), can act as an index to test the precision of the *ab initio* calculations. In the case of the AA monomer and its complex with water, the magnitude of P_{cc} reflects the distribution of the masses out of the *ab* inertial plane, where the carboxylic group and all the hydrogen bonds are lying. In Table 12.5 the P_{cc} values for all the observed species are reported together with the P_{aa} and P_{bb} to complete information. Focusing on the P_{cc} experimental value for the parent species, it can be noted as reasonable agreement exists with the *ab initio* one: the $\Delta P_{cc, OBS-CALC}$ obtained is about $-0.01 \text{ u}\text{\AA}^2$. Concerning the studied isotopic species, looking Table 12.5 it can be noted, that, as expected, the higher values of P_{cc} are related to the species which present the deuterium atom in “free” position, thus lying out of the *ab* plane ($\text{CH}_2\text{CHCOOH}\cdots\text{D}_2\text{O}$, $\text{CH}_2\text{CHCOOH}\cdots\text{HOD}$, $\text{CH}_2\text{CHCOOD}\cdots\text{D}_2\text{O}$, $\text{CH}_2\text{CHCOOD}\cdots\text{HOD}$). The complexation with a molecule of water in AA causes a distortion from the planar arrangement that instead characterized both monomers and also the dimer observed for this carboxylic acid.^[7,9]

Table 12.5 - Planar moments of inertia expressed in $\text{u}\text{\AA}^2$, of several observed isotopologues of the *s-cis* and *s-trans* AA-w molecular complexes.

	<i>s-cis</i> AA-w			<i>s-trans</i> AA-w		
	P_{aa}	P_{bb}	P_{cc}	P_{aa}	P_{bb}	P_{cc}
AA...H ₂ O	296.32	53.36	0.40	290.91	55.44	0.41
AA...H ₂ ¹⁸ O	312.09	53.47	0.40	306.39	55.65	0.41
CH ₂ CHCOOH...D ₂ O	312.58	54.39	0.77	308.25	55.81	0.78
CH ₂ CHCOOH...DOH	300.54	54.29	0.42	296.35	55.67	0.43
CH ₂ CHCOOH...HOD	308.56	53.51	0.73	303.09	55.56	0.74
CH ₂ CHCOOD...H ₂ O	298.47	54.18	0.40	292.24	56.41	0.41
CH ₂ CHCOOD...D ₂ O	314.54	55.27	0.77	309.44	56.78	0.78
CH ₂ CHCOOD...DOH	302.61	55.15	0.42	297.61	56.66	0.43
CH ₂ CHCOOD...HOD	310.60	54.35	0.73	304.34	56.51	0.74

Using all the rotational constants obtained from the fits, a partial experimental r_s -structure using Kraitchman’s substitution method was determined.^[15] Such analysis leads to the determination of the absolute values of the principal axis coordinates of the substituted atom from the changes in principal moments of inertia resulting from a single isotopic substitution. As reported in Tables 12.6 and 12.7 for the *s-cis* and *s-trans* AA-w conformations respectively, these coordinates for the oxygen atom of the water moiety, for the hydrogen atom of the hydroxyl group

of the AA (named H_{acid}), and for the two hydrogen atoms of the water molecule (named H_{bound} and H_{free}) were obtained.

The calculation can be performed considering a single substitution, so different combinations can be done from all the species observed (in Tables 12.6 and 12.7 the initial and final species used for each monosubstitution are reported).

To extract more information about the relative orientation of the two subunits, a partial r_0 -structure analysis for the observed complex was done starting from the MP2 structure and adjusting some structural parameters to reproduce the observed rotational constants. Using the experimental rotational constants of the parent species together with those of all the isotopic species observed, some structural parameters were fitted with STRFIT program.^[16] In particular, all the bond lengths and bond angles fitted are reported in Figure 12.3 (r_0 -structure for *s-cis* AA-w) and in Figure 12.4 (r_0 -structure for *s-trans* AA-W) and with these data the experimental rotational constants are reproduced with an error that falls within unit of MHz.

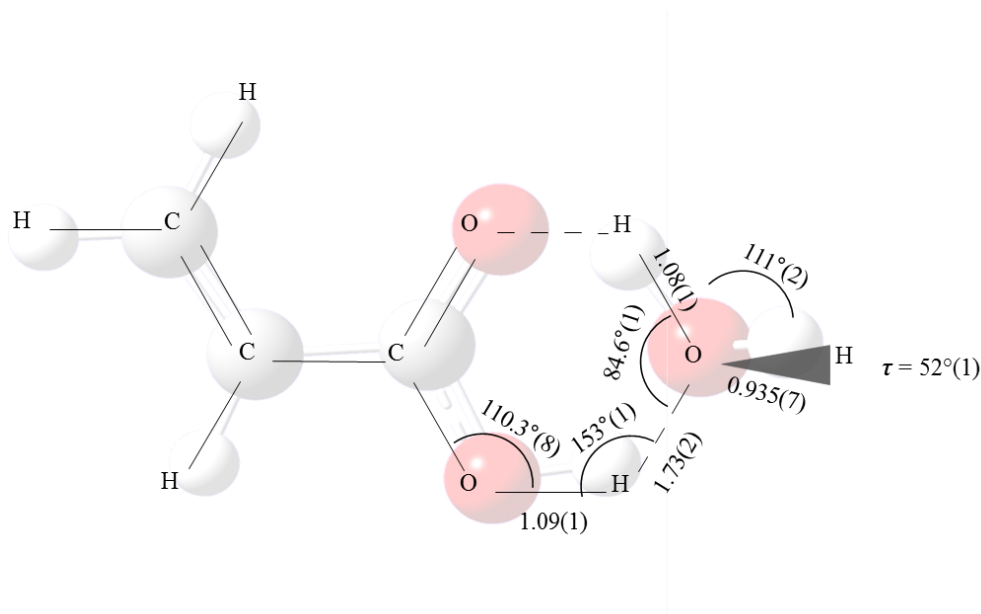


Figure 12.3 - Molecular structure of the *s-cis* conformation of AA-w adduct derived from structural fit. The bond lengths are expressed in unit of Å and the bond angles in degrees. The dihedral angle τ represents how much the hydrogen atom of the water not involved in intermolecular interactions lies above the *ab* plane.

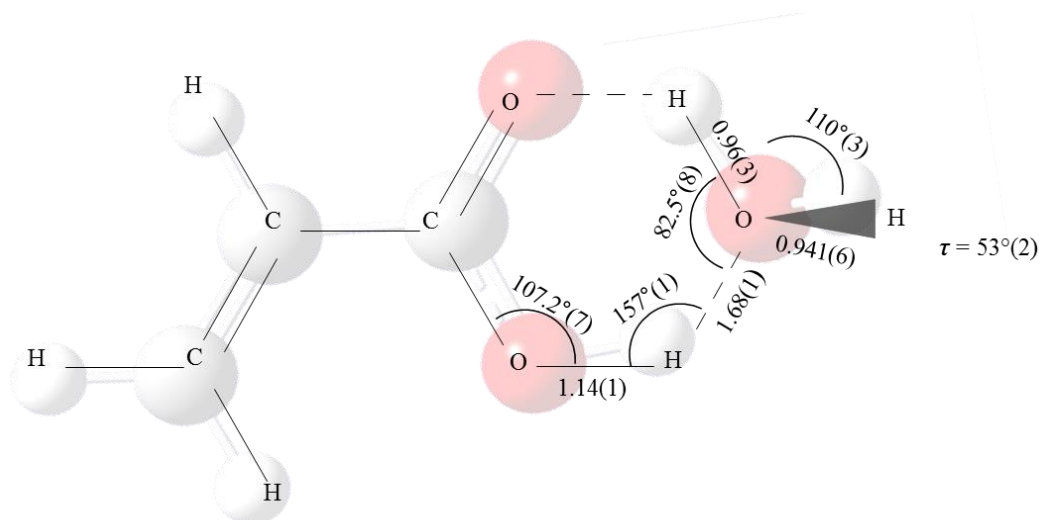


Figure 12.4 - Molecular structure of the *s-trans* conformation of AA-w adduct derived from structural fit. The bond lengths are expressed in unit of Å and the bond angles in degrees. The dihedral angle τ represents how much the hydrogen atom of the water not involved in intermolecular interactions lies above the *ab* plane.

Focusing on the intermolecular hydrogen bond length between the acidic hydrogen of the AA and the oxygen atom of the water, the values obtained are 1.73(2) Å and 1.68(1) Å for the *s-cis* and the *s-trans* AA-w respectively. Comparing these values with the *ab initio* ones (1.77 Å for both conformers), a decrease in the length of this intermolecular hydrogen bond is clearly noticeable, indicating a stronger interaction between the two units. Regarding the r_0 -structure of other monohydrate acid complexes, few data are present in the literature. In fact for the majority of the complexes already mentioned, the *ab initio* values were considered. The values obtained for this R-COOH•••OH₂ interaction in the AA-w adduct appear close to the calculated one for trifluoroacetic acid water complex (1.75 Å) and benzoic acid water complex (1.76 Å).^[6,10] Concerning the formic acid•••water complex, Priem *et al.* described the molecular structure based on the experimental moments of inertia and on dipole moments components: the same R-COOH•••OH₂ intermolecular hydrogen bond is reported to be 1.810 Å, quite larger than the ones obtained for the system here reported.^[4] This value is more consistent with the one obtained for the propanoic acid water complex, reported by Ouyang *et al.* to be 1.838 Å,^[13] indicating as the double carbon-carbon bond present in AA changes the electron distribution of the molecule causing a reduction of the intermolecular distances. Another structural parameter obtained for the two rotamers is the dihedral angle τ that indicates how much the unbounded hydrogen bond of the water lies above the *ab* plane. The values are quite similar for both the *s-cis* and *s-trans* conformations ($\tau=52^\circ(1)$ and $\tau=53^\circ(2)$ respectively) confirming the non planar structure of the adducts. The very similar geometries

achieved for the two conformers of AA during the complexation with the water molecule indicate that the position of the double carbon-carbon bond is not involved in the structural determination of the adduct.

Table 12.6 - Values of the coordinates (\AA) relating to the isotopic substitutions (r_s) for the *s-cis* AA-w conformer. NOTE: H_{acid} refers to the hydrogen of the carboxylic functional group, H_{bound} refers to the water hydrogen involved in the intermolecular interaction and H_{free} refers to the water hydrogen unbound.

<i>s-cis</i> AA-w		r_s		
	SINGLE SUBSTITUTION	a	b	c
O	AA...H ₂ O → AA...H ₂ ¹⁸ O	±2.8353(5) ^a	±0.243(6)	±0.05(3)
H_{acid}	AA...H ₂ O → CH ₂ CHCOOD...H ₂ O	±1.4696(13)	±0.911(2)	±0.05(4)
	CH ₂ CHCOOH...HOD → CH ₂ CHCOOD...HOD	±1.4300(17)	±0.920(3)	[0] ^b
	CH ₂ CHCOOH...DOH → CH ₂ CHCOOD...DOH	±1.4392(15)	±0.937(2)	±0.06(4)
H_{bound}	AA...H ₂ O → CH ₂ CHCOOH...DOH	±2.0555(9)	±0.970(2)	±0.15(1)
	CH ₂ CHCOOD...H ₂ O → CH ₂ CHCOOD...DOH	±2.0337(8)	±0.994(2)	±0.15(2)
	CH ₂ CHCOOD...D ₂ O → CH ₂ CHCOOD...HOD	±1.9730(13)	±0.943(3)	±0.20(1)
	CH ₂ CHCOOH...D ₂ O → CH ₂ CHCOOH...HOD	±1.9931(13)	±0.922(3)	±0.19(1)
H_{free}	AA...H ₂ O → CH ₂ CHCOOH...HOD	±3.5036(6)	±0.393(5)	±0.592(4)
	CH ₂ CHCOOD...H ₂ O → CH ₂ CHCOOD...HOD	±3.4869(7)	±0.415(6)	±0.589(4)
	CH ₂ CHCOOD...D ₂ O → CH ₂ CHCOOD...DOH	±3.4279(7)	±0.331(7)	±0.574(4)
	CH ₂ CHCOOH...D ₂ O → CH ₂ CHCOOH...DOH	±3.4432(7)	±0.313(7)	±0.577(4)

^a Error expressed in units of the last decimal digit.

^b Slightly imaginary values: set to zero.

Table 12.7 - Values of the coordinates (\AA) relating to the isotopic substitutions (r_s) for the *s-trans* AA-w conformer. NOTE: H_{acid} refers to the hydrogen of the carboxylic functional group, H_{bound} refers to the water hydrogen involved in the intermolecular interaction and H_{free} refers to the water hydrogen unbound.

<i>s-trans</i> AA-w		r_s		
SINGLE SUBSTITUTION		a	b	c
O	AA...H ₂ O → AA...H ₂ ¹⁸ O	±2.8084(5) ^a	±0.337(4)	±0.05(3)
H_{acid}	AA...H ₂ O → CH ₂ CHCOOD...H ₂ O	±1.1523(16)	±0.988(2)	[0] ^b
	CH ₂ CHCOOH...HOD → CH ₂ CHCOOD...HOD	±1.1177(20)	±0.981(2)	±0.08(3)
	CH ₂ CHCOOH...DOH → CH ₂ CHCOOD...DOH	±1.1214(19)	±1.003(2)	[0] ^b
H_{bound}	AA...H ₂ O → CH ₂ CHCOOH...DOH	±2.3360(8)	±0.477(4)	±0.14(1)
	CH ₂ CHCOOD...H ₂ O → CH ₂ CHCOOD...DOH	±2.3206(9)	±0.507(4)	±0.13(2)
	CH ₂ CHCOOD...D ₂ O → CH ₂ CHCOOD...HOD	±2.2405(10)	±0.510(4)	±0.19(1)
	CH ₂ CHCOOH...D ₂ O → CH ₂ CHCOOH...HOD	±2.2539(1)	±0.488(4)	±0.20(1)
H_{free}	AA...H ₂ O → CH ₂ CHCOOH...HOD	±3.4952(6)	±0.348(6)	±0.589(3)
	CH ₂ CHCOOD...H ₂ O → CH ₂ CHCOOD...HOD	±3.4838(6)	±0.326(7)	±0.594(4)
	CH ₂ CHCOOD...D ₂ O → CH ₂ CHCOOD...DOH	±3.4134(7)	±0.338(6)	±0.581(4)
	CH ₂ CHCOOH...D ₂ O → CH ₂ CHCOOH...DOH	±3.4235(6)	±0.364(6)	±0.579(4)

^a Error expressed in units of the last decimal digit.

^b Slightly imaginary values: set to zero.

From the structural fit, the coordinates relative to the oxygen atom of the water and the hydrogen atoms (H_{acid} , H_{bonded} and H_{free}) are also obtained and their values are reported in Tables 12.8 and 12.9 together with the calculated ones (r_e). All the coordinates obtained from the r_s , the r_e and the r_0 structure can be compared looking Tables 12.6 and 12.8 for the *s-cis* form and 12.7 and 12.9 for the *s-trans* form.

Table 12.8 - Values of the coordinates (\AA) obtained from computational data (r_e) and derived from the effective structure (r_0) for the *s-cis* AA-w conformation.

<i>s-cis</i> AA-w	r_e			r_0		
	a	b	c	a	b	c
O	-2.808	-0.251	0.063	-2.852(1)	-0.210(3)	0.084(1)
H_{acid}	-1.460	0.901	-0.017	-1.556(9)	0.934(15)	-0.017(2)
H_{bound}	-2.098	-0.916	-0.001	-2.070(7)	-0.950(15)	0.006(1)
H_{free}	-3.417	-0.444	-0.654	-3.520(4)	-0.348(38)	-0.555(9)

Table 12.9 - Values of the coordinates (\AA) obtained from computational data (r_e) and derived from the effective structure (r_0) for the *s-trans* AA-w conformation.

<i>s-trans</i> AA-w	r_e			r_0		
	a	b	c	a	b	c
O	-2.781	-0.340	0.063	-2.822(1)	-0.329(3)	0.081(1)
H_{acid}	-1.137	-0.988	-0.024	-1.277(11)	-0.989(14)	-0.015(3)
H_{bound}	-2.327	0.521	0.004	-2.336(6)	0.500(28)	0.014(2)
H_{free}	-3.420	-0.351	-0.655	-3.504(4)	-0.362(40)	-0.567(8)

12.4 Dissociation Energy

The intermolecular stretching motion can be, in a first approximation, well isolated from the other low-frequency motions and for an asymmetric top complex in which the stretching motion between the two subunits is almost parallel to the *a*-axis of the complex, the stretching force constant (k_s) can be roughly estimated using a pseudo-diatomic approximation, as already explained in Chapter 1.

Accordingly to this procedure, the value obtained for AA-w is $k_s = 17.2 \text{ N}\cdot\text{m}^{-1}$ for *s-cis* adduct and $k_s = 19.1 \text{ N}\cdot\text{m}^{-1}$ for *s-trans* adduct. These values are of the same order of magnitude of the one reported by Schnitzler *et al.* for benzoic acid•••water complex: $k_s = 13.2 \text{ N}\cdot\text{m}^{-1}$, another monohydrated acid complex.^[6]

The dissociation energy (E_D) of the AA-w complex was evaluated to be $17.8 \text{ kJ}\cdot\text{mol}^{-1}$ for the *s-cis* adduct and $19.7 \text{ kJ}\cdot\text{mol}^{-1}$ for the *s-trans* adduct by assuming a Lennard–Jones potential function, according to:^[17] $E_D = 1/72 k_s R_{CM}^2$ (see Chapter 1 for more details). The value obtained is quite small compared to those predicted by calculations (see Table 12.1). Certainly, this simplified model is not as accurate as the MP2 calculation, which yielded a dissociation energy of $45 \text{ kJ}\cdot\text{mol}^{-1}$ and $41 \text{ kJ}\cdot\text{mol}^{-1}$ with and without the BSSE correction. Even if you consider an overestimated error on the calculation of about 25%, the obtained values are still far from the ones estimated by the Lennard-Jones potential. The considered approximation in this case is too strong to describe this system and maybe the calculated value approaches better the real one.

Comparing the calculated values of the dissociation energies for the AA-w complex with the one predicted for the AA dimer (about $50\text{--}60 \text{ kJ}\cdot\text{mol}^{-1}$, see ref. 9), these higher values seem to reflect the strength between the two acid units instead of the weaker interaction between the acid and the water unit here analyzed.

12.5 Conclusions

This is the first experimental investigation of the structure of AA-w, where both rotamers *s-cis* and *s-trans* structures complexed with a molecule of water were observed. The 1:1 water adduct of the simplest unsaturated carboxylic acid presents a six-membered ring geometry for both its rotamers that characterized their stability. Also for this monohydrated acid adduct, the water moiety undergoes complex internal dynamics. In particular a proton interchange motion is established by an observed spectral doubling which disappears in the water deuterated complexes. A second type of large-amplitude motion is inferred from the absence of rigid rotor *c*-type transitions, even in the

DOH species where the proton interchange is quenched. This latter motion is interpreted in terms of large amplitude wagging of the “free” hydrogen of the water moiety.

12.6 References

- [1] K. R. Leopold, *Annu. Rev. Phys. Chem.*, 62, 327-349, **2011**.
- [2] M. Canagaratna, J. A. Phillips, M. E. Ott, K. R. Leopold, *J. Phys. Chem. A*, 102, 1489, **1998**.
- [3] D. L. Fiacco, S. W. Hunt, K. R. Leopold, *J. Am. Chem. Soc.*, 124, 4504, **2002**.
- [4] D. Priem, T.-K. Ha, A. Bauder, *J. Chem. Phys.*, 113, 169, **2000**.
- [5] B. Ouyang, B. J. Howard, *Phys. Chem. Chem. Phys.*, 11, 366-373, **2009**.
- [6] E. G. Schnitzler, W. Jäger, *Phys. Chem. Chem. Phys.*, 16, 2305, **2014**.
- [7] C. Calabrese, A. Vigorito, G. Feng, L. B. Favero, A. Maris, S. Melandri, W.D. Geppert, W. Caminati, *J. Mol. Spectr.*, 295, 37-43, **2014**, and refs. within.
- [8] A.D. Pomogailo *et al.*, *Macromolecular Metal Carboxylates and Their Nanocomposites*, Springer Series in Materials Science 138, 2010, Chapter 2.
- [9] G. Feng, L. B. Favero, A. Maris, A. Vigorito, W. Caminati, R. Meyer, *J. Am. Chem. Soc.*, 134, 19281, **2012**.
- [10] B. Ouyang, T. G. Starkey, B. J. Howard, *J. Phys. Chem. A*, 111, 6165-6175, **2007**.
- [11] S. F. Boys, F. Bernardi, *Mol. Phys.*, 19, 553, **1970**.
- [12] M. J. Frisch, G. W. Trucks, H. B. Schlegel, G. E. Scuseria, M. A. Robb, J. R. Cheeseman, G. Scalmani, V. Barone, B. Mennucci, G. A. Petersson, H. Nakatsuji, M. L. Caricato, X.; Hratchian, H. P.; Izmaylov, A. F.; Bloino, J.; Zheng, G.; Sonnenberg, J. L.; Hada, M.; Ehara, M.; Toyota, K.; Fukuda, R.; Hasegawa, J.; Ishida, M.; Nakajima, T.; Honda, Y.; Kitao, O.; Nakai, H.; Vreven, T.; Montgomery, J. A.; J. E. J. Peralta, F. B. Ogliaro, M.; Heyd, J. J.; Brothers, E.; Kudin, K. N.; Staroverov, V. N.; Kobayashi, R.; Normand, J.; Raghavachari, K.; Rendell, A.; Burant, J. C.; Iyengar, S. S.; Tomasi, J.; Cossi, M.; Rega, N.; Millam, J. M.; Klene, M.; Knox, J. E.; J. B. Cross, V. A. Bakken, C.; Jaramillo, J.; Gomperts, R.; Stratmann, R. E.; Yazyev, O.; Austin, A. J.; Cammi, R.; Pomelli, C.; Ochterski, J. W.; Martin, R. L.; Morokuma, K.; Zakrzewski, V. G.; Voth, G. A.; Salvador, P.; Dannenberg, J. J.; Dapprich, S.; A. D. Daniels, Ö. F. Farkas, J. B.; Ortiz, J. V.; Cioslowski, J.; Fox, D. J., Gaussian, Inc., Wallingford CT, **2009**.
- [13] B. Ouyang, B. J. Howard, *J. Phys. Chem. A*, 112, 8208-8214, **2008**.
- [14] J. K. G. Watson, "Vibrational spectra and structure", Vol. 6, Elsevier, Amsterdam, Oxford & New York, **1977**.
- [15] J. Kraitchman, *Am. J. Phys.*, 21, **1953**.
- [16] Kisiel, Z. PROSPE - Programs for Rotational SPEctroscopy
<http://www.ifpan.edu.pl/~kisiel/prospe.htm>
- [17] S. E. Novick, S. J. Harris, K. C. Janda, W. Klemperer, *Can. J. Phys.*, 53, 2007-2015, **1975**.

12.7 Appendix

Table 12.10 - Measured frequencies (MHz) for the transitions observed for the species AA...H₂O and AA...H₂¹⁸O of the *s-cis* and *s-trans* conformations

$J(K_a', K_c') - J''(K_a'', K_c'')$	<i>s-cis</i> AA...H ₂ O		<i>s-cis</i> AA...H ₂ ¹⁸ O		<i>s-trans</i> AA...H ₂ O		<i>s-trans</i> AA...H ₂ ¹⁸ O	
	$\nu_{\text{OBS}}/\text{MHz}$	$\Delta\nu_{\text{OBS-CALC}}$	$\nu_{\text{OBS}}/\text{MHz}$	$\Delta\nu_{\text{OBS-CALC}}$	$\nu_{\text{OBS}}/\text{MHz}$	$\Delta\nu_{\text{OBS-CALC}}$	$\nu_{\text{OBS}}/\text{MHz}$	$\Delta\nu_{\text{OBS-CALC}}$
Q-branch μ_b -type								
1 (1, 0) - 1 (0, 1)	0 ⁻	7955.4523	0.0012			7589.7141	0.0021	
	0 ⁺	7955.4674	-0.0042			7589.7590	0.0012	
2 (1, 1) - 2 (0, 2)	0 ⁻	8219.8285	-0.0004	8238.4558	0.0008	7873.0195	-0.0025	
	0 ⁺	8219.8455	-0.0039	8238.4700	0.0014	7873.0686	0.0008	
3 (1, 2) - 3 (0, 3)	0 ⁻	8628.2672	-0.0039			8312.2056	-0.0061	8274.4411 -0.0023
	0 ⁺	8628.2994	0.0079			8312.2613	0.0040	8274.4841 -0.0001
R-branch μ_b -type								
1 (1, 1) - 0 (0, 0)	0 ⁻	10845.9522	-0.0040			10507.9624	0.0041	10410.3111 0.0035
	0 ⁺	10845.9742	-0.0024			10508.0006	-0.0035	10410.3514 0.0029
2 (1, 2) - 1 (0, 1)	0 ⁻	13736.4560	0.0032	13528.3268	-0.0008	13426.2024	0.0061	13202.1063 -0.0003
	0 ⁺	13736.4733	0.0000	13528.3398	-0.0014	13426.2426	0.0005	13202.1470 -0.0005
3 (1, 3) - 2 (0, 2)	0 ⁻	16500.3847	0.0113			16209.5195	0.0008	15870.6353 -0.0010
	0 ⁺	16500.3847	-0.0092			16209.5563	-0.0082	15870.6748 -0.0024
4 (1, 3) - 4 (0, 4)	0 ⁻					8923.9309	-0.0045	
	0 ⁺					8923.9860	0.0054	
R-branch μ_a -type								
3 (0, 3) - 2 (0, 2)		9419.9903	-0.0064	8978.2792	-0.0057	9551.1512	0.0008	9104.1641 0.0002
3 (1, 3) - 2 (1, 2)		9054.5527	0.0052	8643.8142	0.0002	9163.4902	0.0004	8748.5080 0.0002
3 (1, 2) - 2 (1, 1)		9828.4391	0.0003	9348.1258	-0.0011	9990.3399	-0.0001	9502.4346 -0.0039
3 (2, 2) - 2 (2, 1)		9445.4888	0.0086					
4 (0, 4) - 3 (0, 3)		12530.3812	-0.0054	11946.6494	-0.0045	12699.4423	0.0011	12109.5443 0.0027
4 (1, 4) - 3 (1, 3)		12065.4824	0.0049	11519.0950	-0.0004	12209.3310	-0.0009	11657.4903 -0.0012
4 (1, 3) - 3 (1, 2)		13096.8554	0.0027	12457.8197	0.0025	13311.1647	0.0000	12662.2553 0.0025
5 (0, 5) - 4 (0, 4)		15615.9438	-0.0082			15818.2002	0.0033	
5 (1, 5) - 4 (1, 4)		15070.4854	0.0039			15248.1467	0.0016	
5 (1, 4) - 4 (1, 3)		16358.3403	0.0007			16623.6217	-0.0025	
6 (0, 6) - 5 (0, 5)				17817.4752	0.0031			
6 (1, 6) - 5 (1, 5)		18068.4279	-0.0038	17253.9425	0.0025	18278.6432	-0.0012	

Table 12.11 - Measured frequencies in MHz for the transitions observed for seven deuterated forms of the *s-cis* and *s-trans* AA-w conformations.

$J'(K_a', K_c') - J''(K_a'', K_c'')$	<i>s-cis</i> AA-w		<i>s-trans</i> AA-w	
	$\nu_{\text{obs}}/\text{MHz}$	$\Delta\nu_{\text{OBS-CALC}}$	$\nu_{\text{obs}}/\text{MHz}$	$\Delta\nu_{\text{OBS-CALC}}$
CH₂CHCOOH...D₂O				
3 (0, 3) - 2 (0, 2)	8948.1939	-0.0039	9045.8513	-0.0019
3 (1, 3) - 2 (1, 2)	8613.0644	-0.0069	8695.9595	-0.0012
3 (1, 2) - 2 (1, 1)	9319.9368	-0.0054	9437.3669	-0.0024
4 (0, 4) - 3 (0, 3)	11905.6827	-0.0041	12032.4751	-0.0007
4 (1, 4) - 3 (1, 3)	11477.9026	0.0022	11587.5951	0.0010
4 (1, 3) - 3 (1, 2)	12420.0082	-0.0014	12575.6735	0.0002
CH₂CHCOOD...H₂O				
3 (0, 3) - 2 (0, 2)	9346.0906	-0.0046	9497.7437	-0.0005
3 (1, 3) - 2 (1, 2)	8981.1448	-0.0046	9108.3402	-0.0029
3 (1, 2) - 2 (1, 1)	9754.7127	-0.0045	9940.3488	-0.0043
4 (0, 4) - 3 (0, 3)	12431.3834	-0.0035	12627.0920	-0.0016
4 (1, 4) - 3 (1, 3)	11967.5025	0.0003	12135.5319	0.0022
4 (1, 3) - 3 (1, 2)	12998.4287	-0.0022	13244.2066	0.0015
CH₂CHCOOD...D₂O				
3 (0, 3) - 2 (0, 2)	8885.9204	-0.0069	9001.6039	-0.0005
3 (1, 3) - 2 (1, 2)	8550.3842	-0.0086	8649.5628	-0.0026
3 (1, 2) - 2 (1, 1)	9258.8921	-0.0064	9396.7534	-0.0021
4 (0, 4) - 3 (0, 3)	11822.0977	-0.0035	11972.4620	-0.0013
4 (1, 4) - 3 (1, 3)	11394.1989	0.0042	11525.4916	0.0018
4 (1, 3) - 3 (1, 2)	12338.4682	0.0001	12521.2483	-0.0003
CH₂CHCOOH...DOH				
3 (0, 3) - 2 (0, 2)	9285.2993	-0.0046	9386.9393	-0.0004
3 (1, 3) - 2 (1, 2)	8924.3211	0.0019	9010.4122	-0.0030
3 (1, 2) - 2 (1, 1)	9689.0219	-0.0053		
4 (0, 4) - 3 (0, 3)	12350.9700	-0.0030	12482.5579	-0.0009
4 (1, 4) - 3 (1, 3)	11891.8790	-0.0048	12005.7252	-0.0059
4 (1, 3) - 3 (1, 2)	12911.0124	-0.0019	13073.8836	-0.0016
CH₂CHCOOH...HOD				
3 (0, 3) - 2 (0, 2)	9067.6870	-0.0054	9191.3820	0.0045
3 (1, 3) - 2 (1, 2)	8728.8107	-0.0021	8832.0123	0.0034
3 (1, 2) - 2 (1, 1)	9443.3339	-0.0075	9594.6632	0.0048
4 (0, 4) - 3 (0, 3)	12064.9038	-0.0034	12224.9422	-0.0014
4 (1, 4) - 3 (1, 3)	11632.1946	-0.0013	11768.6087	-0.0045
4 (1, 3) - 3 (1, 2)	12584.5165	0.0003	12784.9695	-0.0073
CH₂CHCOOD...DOH				
3 (0, 3) - 2 (0, 2)	9215.3186	-0.0064	9337.0028	0.0026
3 (1, 3) - 2 (1, 2)	8854.4556	0.0058	8958.4122	-0.0039
3 (1, 2) - 2 (1, 1)	9619.7524	-0.0042	9765.7892	-0.0044
4 (0, 4) - 3 (0, 3)	12257.1099	-0.0019	12414.8102	-0.0026
4 (1, 4) - 3 (1, 3)	11798.5837	-0.0076	11936.1227	0.0023
4 (1, 3) - 3 (1, 2)	12818.5002	-0.0025	13012.0075	0.0009
CH₂CHCOOD...HOD				
3 (0, 3) - 2 (0, 2)	9002.1003	-0.0046	9144.1999	-0.0002
3 (1, 3) - 2 (1, 2)	8663.1366	-0.0029	8782.9476	0.0041
3 (1, 2) - 2 (1, 1)	9378.5487	-0.0078	9550.8440	0.0013
4 (0, 4) - 3 (0, 3)	11976.9644	-0.0038	12161.0370	-0.0003
4 (1, 4) - 3 (1, 3)	11544.5132	-0.0008	11702.9477	-0.0039
4 (1, 3) - 3 (1, 2)	12498.0054	0.0004	12726.2814	-0.0035

CONCLUSION

Rotational spectroscopy is an important tool to evaluate the conformational attitude of molecules, to define their structure and to characterize the large amplitude vibrational modes that can be present. Information about the structure of a molecule are fundamental to define its physical-chemical role that is determined by the conformational arrangement achieved through covalent interactions and non bonding interactions occurring within the molecules and different types of environments. An understanding of the forces that drive the stabilization of this conformational arrangement is essential to increase the knowledge on chemical and biological processes.

This dissertation presents results of rotational spectra and theoretical modeling on different selected molecular systems in order to deepen the contribution of non-covalent interactions and electronic effects on their conformational landscape.

The capability to detect hyperfine structures of internal motions and quadrupole coupling effects by rotational spectroscopic technique, allows to describe in details all the features that characterize different molecular systems. The series of investigations of selected medium-size molecules and complexes show how different instrumental setups can be used to obtain a variety of results on molecular properties. These properties are not only useful in the field of molecular physics or chemistry but are also relevant to other scientific areas, like material science, biochemistry and astronomical searches.

In addition, this dissertation shows how precise experimental results can be complemented by theoretical calculations and how they can also be used to benchmark the results of the theoretical approaches, since they are obtained in the same isolated conditions. The studies reported here reveal that great care must be taken in the theoretical characterization of flexible molecules, tautomeric equilibria and molecular complexes in which weak intermolecular interactions are present. Certainly the calculations are a valuable aid to guide and rationalize experiments but they cannot yet replace the experimental structural characterization which is essential to give the final answer.

Finally, the results of these investigations highlight how complexation through non-covalent interactions and halogen substitution cause changes on the conformational landscape of the selected molecules. In particular, this changes on the monomer' structure are quite smooth when the halogenation is partial, but as the number of halogen atoms increases, the system involved starts to behave as a completely novel species. The halogen substitution is also explored in tautomeric systems where it is shown how the position of the halogen atom inserted affects the prototropic equilibrium.

PUBLICATIONS

- C. Calabrese, A. Maris, L. Evangelisti, L. B. Favero, S. Melandri, W. Caminati. “Keto-Enol Tautomerism and Conformational Landscape of 1,3-Cyclohexanedione from Its Free Jet Millimeter-Wave Absorption Spectrum”. *J. Phys. Chem. A.*, 117, 50, 13712-13718, **2013**. DOI: 10.1021/jp4078097
- C. Calabrese, A. Vigorito, G. Feng, L. B. Favero, A. Maris, S. Melandri, W. D. Geppert, W. Caminati. “Laboratory rotational spectrum of acrylic acid and its isotopologues in the 6–18.5 GHz and 52-74.4 GHz frequency ranges”. *J. Mol. Spectrosc.*, 295, 37-43, **2014**. DOI: 10.1016/j.jms.2013.11.003
- S. Kumar, S. K. Singh, C. Calabrese, A. Maris, S. Melandri, A. Das. “Structure of saligenin: Microwave, UV and IR spectroscopy studies in a supersonic jet combined with quantum chemistry calculations”. *Phys. Chem. Chem. Phys.*, 16, 17163, **2014**. DOI: 10.1039/c4cp01693a
- A. Maris, C. Calabrese, S. Melandri, S. Blanco. “Accurate spectroscopy of polycyclic aromatic compounds: from the rotational spectrum of fluoren-9-one in the millimeter wave region to its infrared spectrum”. *J. Chem. Phys.*, 142, 024317, **2015**. DOI: 10.1063/1.4905134
- C. Calabrese, A. Maris, L. Dore, W. D. Geppert, P. Fathi, S. Melandri. “Acrylic acid (CH₂CHCOOH): the rotational spectrum in the millimeter range up to 397 GHz”. *Mol. Phys.*, accepted. DOI: 10.1080/00268976.2015.1025879

ACADEMIC CONGRESSES

- IMAMPC2012 - International Meeting on Atomic and Molecular Physics and Chemistry, 12-14 September 2012, Scuola Normale Superiore, Pisa, Italy. I presented an oral contribution on “*ROTATIONAL SPECTROSCOPY: A SPECIFIC TOOL TO INVESTIGATE THE CONFORMATIONAL PREFERENCES OF MOLECULES*”.
- Theory, Experiments And Modeling Of Chemical Processes, Dynamics And Molecular Interactions (International Conference), 29 November 2012, Sala Ulisse, Accademia delle Scienze, Bologna, Italy. I presented an oral contribution on “*INTERNAL MOTIONS AND COMPLEX CONFORMATIONAL SURFACES IN FLEXIBLE ORGANIC MOLECULES*”.
- XII Giornata della Chimica dell’Emilia Romagna, 17 December 2012, Sala Acquario, Polo Chimico Bio Medico, Università di Ferrara, Ferrara, Italy. I presented a poster contribution titled “*THE ROTATIONAL STUDY OF A FLEXIBLE MOLECULE: 2(N)-METHYLAMINOETHANOL. A CHALLENGE FOR ROTATIONAL SPECTROSCOPY*”.
- XIII Giornata della Chimica dell’Emilia Romagna, 18 December 2013, Area della Ricerca, CNR - Centro Nazionale delle Ricerche, Bologna, Italy. I presented a poster contribution titled “*THE EFFECT OF RING FLUORINATION AND WATER COMPLEXATION ON MOLECULAR FLEXIBILITY AND TUNNELING PATHWAYS: THE ROTATIONAL SPECTRUM OF 2-FLUOROBENZYLAMINE AND BENZYLAMINE-WATER*”.
- HRMS2014 - The 23rd International Conference on High Resolution Molecular Spectroscopy, 2-6 September 2014, Università di Bologna, Bologna, Italy. I presented an oral contribution on “*HALOGEN SUBSTITUTION EFFECTS ON THE TAUTOMERIC AND CONFORMATIONAL EQUILIBRIA OF MOLECULES AND MOLECULAR COMPLEXES: A ROTATIONAL STUDY*”.
- XI Simposio de Investigadores Jóvenes, Real Sociedad Española de Química - Sigma Aldrich, 4-7 November 2014, Universidad del País Vasco, Bilbao, Spain. I presented an oral contribution on “*RING FLUORINATION EFFECTS ON MOLECULAR WATER CLUSTERS: THE CASES OF 2-FLUOROPYRIDINE, 3-FLUOROPYRIDINE AND PENTA-FLUOROPYRIDINE. A ROTATIONAL SPECTROSCOPY STUDY*”.

ACKNOWLEDGEMENTS

I would like to thank my supervisor Prof. Sonia Melandri for having shared with me her expertise, for her moral attitude and for showing me complete confidence during these three years.

I would like to express also my gratitude to Dr. Assimo Maris for her willingness to help me in various aspects of my investigation, she is a thorough researcher.

I also thank Prof. Walther Caminati for always making available his endless knowledge on rotational spectroscopy and for his natural generosity.

I want also extend my thanks to every colleague who is or was working with me in this group, Luca Evangelisti, Qian Gou, Gang Feng, Michela B. Giuliano, Laura B. Favero, Biagio Velino, Lorenzo Spada, Annalisa Vigorito and Montserrat Vallejo-López for all their kindness, help and good company.

I would also like to thank all the helps and suggestions from the other groups, professors and researchers with whom I collaborated.

I would remember Eraldo Sbarbati, a precious man who taught me a lot on both the technical and human aspects. Also thanks to him it has started the collaboration with Sergio Mariotti, too modest to define him as just a technician, a fundamental point of reference and assistance in improving our setups.

Last but for sure not least, many thanks to all the Spectroscopy Group of Bilbao, in particular to Dr. Emilio J. Cocinero for his willingness and support in my entire stay and more, I found a second home.

